

AMTRAK/KNORR DISC BRAKE STUDY VOLUME I FINAL REPORT



SEPTEMBER 1980

Document is available to the public through the
National Technical Information Service,
Springfield, Virginia 22161.

REPRODUCED BY
NATIONAL TECHNICAL
INFORMATION SERVICE
U.S. DEPARTMENT OF COMMERCE
SPRINGFIELD, VA 22161

Prepared for

**U.S. DEPARTMENT OF TRANSPORTATION
FEDERAL RAILROAD ADMINISTRATION
OFFICE OF PASSENGER SYSTEMS (RRD-21)
WASHINGTON, D.C. 20590**

**AMTRAK
400 NORTH CAPITOL STREET N.W.
WASHINGTON, D.C. 20001**

NOTICE

This document is disseminated under the sponsorship of the Department of Transportation in the interest of information exchange. The United States Government assumes no liability for its contents or use thereof.

NOTICE

The United States Government does not endorse products or manufacturers. Trade or manufacturers' names appear herein solely because they are considered essential to the object of this report.

1. Report No. FRA/ORD-80/62.1		2. Government Accession No.		3. Recipient's Catalog No. PB81 109837	
4. Title and Subtitle Amtrak/Knorr Disc Brake Study Volume I Final Report				5. Report Date September 1980	
				6. Performing Organization Code	
7. Author(s) R. Scofield and R. Avant				8. Performing Organization Report No. ENSCO-DOT-FR-80-12 - /	
9. Performing Organization Name and Address Rail Transportation Engineering Division ENSCO, Inc. 2560 Huntington Avenue Alexandria, VA 22303				10. Work Unit No. (TRAIS)	
				11. Contract or Grant No. DOT-FR-64113/WHS-9043-007	
12. Sponsoring Agency Name and Address U.S. DEPARTMENT OF TRANSPORTATION Federal Railroad Administration (RRD-12) 400 Seventh Street, S.W. Washington, DC 20590				13. Type of Report and Period Covered Final Report February-July 1979	
				14. Sponsoring Agency Code RRD-21	
15. Supplementary Notes Co-sponsor - AMTRAK, 400 North Capitol St., N.W., Washington, DC 20001 Volume II - Appendices A through I					
16. Abstract This report describes the Amtrak/Knorr Disc Brake Study which was developed: (1) To evaluate candidate replacement disc brakes for the Knorr disc brakes presently in use on Amfleet and Turboliner cars. (2) To explain the cause of the loosening of the attaching pins and the excessive wear experienced by the disc-brake friction ring on the Knorr disc brakes. (3) To find out why the disc brake failure rate was much higher when the outside temperature was below 32 degrees Fahrenheit. This report covers the first six months of a three-year controlled revenue service test, an over-the-road test, and laboratory tests to correlate over-the-road test results to pin wear.					
17. Key Words Wheel/rail inputs, RMS g-level analysis, RMS spectral analysis, Brake forces, Exceedence analysis			18. Distribution Statement Document is available to the public through the National Technical Information Service, Springfield, VA 22161		
19. Security Classif. (of this report) Unclassified		20. Security Classif. (of this page) Unclassified		21. No. of Pages 208	22. Price

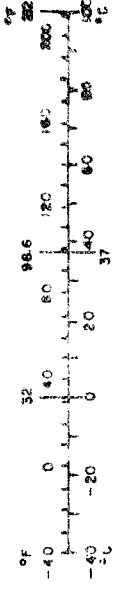
METRIC CONVERSION FACTORS

Approximate Conversions to Metric Measures

Symbol	When You Know	Multiply by	You Find	Symbol
LENGTH				
in	inches	2.5	centimeters	cm
ft	feet	30	centimeters	cm
yd	yards	0.9	meters	m
mi	miles	1.6	kilometers	km
AREA				
sq in	square inches	6.5	square centimeters	cm ²
sq ft	square feet	0.09	square meters	m ²
sq yd	square yards	0.8	square meters	m ²
sq mi	square miles	2.6	square kilometers	km ²
acres	acres	0.4	hectares	ha
MASS (weight)				
oz	ounces	28	grams	g
lb	pounds	0.45	kilograms	kg
	short tons (2000 lb)	0.9	tonnes	t
VOLUME				
tblsp	tablespoons	5	milliliters	ml
teaspoon	teaspoons	15	milliliters	ml
fl oz	fluid ounces	30	milliliters	ml
c	cups	0.24	liters	l
pint	pints	0.47	liters	l
qt	quarts	0.95	liters	l
gal	gallons	3.8	liters	l
cu ft	cubic feet	0.03	cubic meters	m ³
cu yd	cubic yards	0.76	cubic meters	m ³
TEMPERATURE (exact)				
°F	Fahrenheit temperature	5/9 (after subtracting 32)	Celsius temperature	°C

Approximate Conversions from Metric Measures

Symbol	When You Know	Multiply by	You Find	Symbol
LENGTH				
mm	millimeters	0.04	inches	in
cm	centimeters	0.4	inches	in
m	meters	3.3	yards	yd
m	meters	1.1	feet	ft
km	kilometers	0.6	miles	mi
AREA				
sq cm	square centimeters	0.16	square inches	sq in
sq m	square meters	1.2	square yards	sq yd
sq km	square kilometers	0.4	square miles	sq mi
ha	hectares (10,000 m ²)	2.5	acres	acres
MASS (weight)				
g	grams	0.035	ounces	oz
kg	kilograms	2.2	pounds	lb
t	tonnes (1000 kg)	1.1	short tons	short tons
VOLUME				
ml	milliliters	0.03	fluid ounces	fl oz
l	liters	2.1	quarts	qt
l	liters	1.06	gallons	gal
m ³	cubic meters	0.26	cubic feet	cu ft
m ³	cubic meters	35	cubic yards	cu yd
m ³	cubic meters	1.3	short tons	short tons
TEMPERATURE (exact)				
°C	Celsius temperature	9/5 (then add 32)	Fahrenheit temperature	°F



1.0

*1 in 1.254 exactly. For other exact conversions and more detailed tables, see NBS Misc. Publ. 285, Units of Weights and Measures, Price \$2.25, SD Catalog No. C13-10 286.

TABLE OF CONTENTS

<u>Section</u>	<u>Title</u>	<u>Page</u>
	Table of Contents	i
	List of Illustrations	iv
	List of Tables	xi
	Executive Summary	xii
1.0	INTRODUCTION	1-1
	1.1 Purpose	1-1
	1.2 Background	1-2
	1.3 Objectives	1-4
2.0	REVENUE SERVICE TESTING	2-1
	2.1 Introduction	2-1
	2.2 Revenue Service Test	2-3
	2.3 Failure Records Versus Environmental Records for the Disc-Brakes Currently In Use	2-7
3.0	OVER-THE-ROAD TEST	3-1
	3.1 Objective and Approach	3-1
	3.1.1 Wheel/Rail Inputs	3-3
	3.1.2 Brake Inputs	3-4
	3.1.2.1 Strain Transducers	3-4
	3.1.2.2 Pressure Transducers	3-5
	3.1.2.3 Decelostat Angular Velocity	3-7
	3.2 Instrumentation Check-Out and Calibration	3-7
	3.2.1 Accelerometers	3-7
	3.2.2 Accelerometer Filters	3-7
	3.2.3 Strain Transducers	3-7
	3.2.4 Pressure Transducers	3-8
	3.2.5 Tachometer	3-8
	3.2.6 Data Collection System	3-8
	3.3 Instrumentation	3-9
	3.4 Test Procedures	3-9
	3.4.1 Test Consist	3-9
	3.4.2 Shakedown Run	3-13
	3.4.3 Test Runs	3-13
	3.4.4 Data Collection	3-15

TABLE OF CONTENTS (CONT'D)

<u>Section</u>	<u>Title</u>	<u>Page</u>
3.5	Test Results	3-15
	3.5.1 Inertial Forces	3-16
	3.5.1.1 RMS G-Level Analysis	3-16
	3.5.1.2 RMS Spectral Analysis	3-27
	3.5.1.3 Instantaneous Time Histories	3-35
	3.5.1.4 Exceedence Analysis	3-40
	3.5.1.5 Observations	3-55
	3.5.2 The Pioneer III Truck Shock Ring	3-56
	3.5.3 Brake Forces	3-64
4.0	LABORATORY SUBTEST	4-1
4.1	General Requirements	4-1
	4.1.1 General Objectives	4-1
	4.1.2 Technical Objectives and Requirements	4-1
4.2	Static Loading Requirements	4-2
4.3	Dynamic Loading Requirements	4-2
4.4	Instrumentation and Data Collection Apparatus	4-4
4.5	Instrumentation Procedures	4-6
4.6	Post-Test Procedures	4-6
4.7	Modifications to Test Plan	4-8
4.8	Instrumentation Installation	4-8
	4.8.1 Strain Gaged Pins	4-9
	4.8.2 Micro-Slip Detector	4-9
	4.8.3 Coordinate System	4-11
	4.8.4 Accelerometers	4-11
4.9	Static Load Testing Procedures and Results	4-15
4.10	Dynamic Test Procedures and Results	4-17
4.11	Comparison to ORT Data	4-29
4.12	Lateral Impulse Loading Test Observations	4-31
4.13	Conclusions	4-36
4.14	Vertical Impulse Loading (DROP) Test Observations	4-50

TABLE OF CONTENTS (CONT'D)

<u>Section</u>	<u>Title</u>	<u>Page</u>
	4.15 Conclusions	4-50
	4.16 Summary of Laboratory Test Observations	4-52
	4.17 RMS Model	4-65
	4.18 Percent Time Exceedence Model	4-66
	4.19 Spectral Graphs	4-66
5.0	RESULTS AND CONCLUSIONS	5-1
	5.1 Summary of Observations	5-1
	5.2 Conclusions	5-5
	5.3 Recommendations	5-6

LIST OF ILLUSTRATIONS

<u>Figure</u>	<u>Title</u>	<u>Page</u>
1-1	Number of Discs on Cars and Failed Discs	1-3
2-1	WABCO Disc Brake	2-2
2-2	KPI Brake	2-4
2-3	New York Air Brake (BSI) Disc Brake	2-5
2-4	Knorr Disc Brake Design in Use by Amtrak Since 1977	2-8
2-5	Amfleet Disc Brake Failures - 1977	2-9
2-6	Amfleet Disc Brake Failures - 1978	2-10
2-7	Amfleet Disc Brake Failures - 1979	2-11
2-8	Amfleet Disc-Brake Failures During the Winter of 1976/1977	2-13
2-9	Amfleet Disc-Brake Failures During the Winter of 1977/1978	2-14
2-10	Amfleet Disc-Brake Failures During the Winter of 1978/1979	2-15
3-1	Inputs to the Wheelset	3-2
3-2	Brake Rigging Suspension Strips and Strain Bridge Used in the Over-the-Road Test	3-6
3-3	Overall Instrumentation Plan	3-10
3-4	Test Car Instrumentation Layout	3-11
3-5	Test Consist	3-13
3-6	Test Zones for the Over-the-Road Test	3-14
3-7	Vertical Axle Acceleration (V_1) vs Speed (Bandwidth 2.5 Hz to 1000 Hz)	3-18
3-8	Vertical Truck Accelerations (V_2) vs Speed (Bandwidth 2.5 Hz to 1000 Hz)	3-19

LIST OF ILLUSTRATIONS (CONT'D)

<u>Figure</u>	<u>Title</u>	<u>Page</u>
3-9	Lateral Axle Accelerations (L_1) vs Speed (Bandwidth 2.5 Hz to 1000 Hz)	3-20
3-10	Lateral Truck Accelerations (L_2) vs Speed (Bandwidth 2.5 Hz to 1000 Hz)	3-21
3-11	Vertical Axle Accelerations (V_1) vs Speed (Bandwidth 2.5 Hz to 500 Hz)	3-22
3-12	Vertical Truck Accelerations (V_2) vs Speed (Bandwidth 2.5 Hz to 500 Hz)	3-23
3-13	Lateral Axle Accelerations (L_1) vs Speed (Bandwidth 2.5 Hz to 500 Hz)	3-24
3-14	Lateral Axle Accelerations (L_2) vs Speed (Bandwidth 2.5 Hz to 500 Hz)	3-25
3-15	RMS Spectral Graph of Vertical Accelerations at 77 mph	3-28
3-16	RMS Spectral Graphs of Lateral Accelerations at 77 mph	3-29
3-17	Vertical Axle Accelerations (Frozen)	3-30
3-18	Vertical Axle Accelerations (Unfrozen)	3-31
3-19	Lateral Axle Accelerations (Frozen)	3-32
3-20	Lateral Axle Accelerations (Unfrozen)	3-33
3-21	Comparison of Frozen and Unfrozen Vertical Axle Accelerations	3-34
3-22	Instantaneous Vertical Axle Accelerations (V_1) Time Enhanced - 32 Samples from the Boston Run	3-36
3-23	Instantaneous Lateral Axle Accelerations (L_1) Time Enhanced - 32 Samples from the Boston Run	3-37
3-24	Instantaneous Vertical Truck Accelerations (V_2) Time Enhanced - 32 Samples from the Boston Run	3-38

LIST OF ILLUSTRATIONS (CONT'D)

<u>Figure</u>	<u>Title</u>	<u>Page</u>
3-25	Instantaneous Lateral Truck Accelerations (L_2) Time Enhanced - 32 Samples from the Boston Run	3-39
3-26	Probability Density Function (PDF) at Bandwidth 0 to 1000 Hz	3-42
3-27	Cumulative Distribution Function Obtained from the Integration of a PDF	3-43
3-28	Percent Time Exceedence (%tE) of Vertical Axle Accelerations	3-45
3-29	Percent Time Exceedence (%tE) of Lateral Axle Accelerations	3-46
3-30	Exponential Decrease of %tE with G-Level Increase	3-48
3-31	Effect of Speed on %tE	3-49
3-32	Effect of Track Stiffness of %tE	3-50
3-33	Percent Time Exceedence (%E) as a Function of Acceleration (g) Exceedence Level and Train Speed (s)	3-53
3-34	Shock Ring	3-58
3-35	Coherence of Vertical Truck Accelerations (V_2) to Vertical Axle Accelerations (V_1)	3-59
3-36	Transfer Function for Vertical Truck Accelerations (V_2) to Vertical Accelerations (V_1)	3-60
3-37	Transfer Function of Lateral Truck Accelerations (L_2) to Lateral Axle Accelerations (L_1) - Coherence Blanking = 0.8	3-61
3-38	Transfer Function of Vertical Accelerations (V_2) to Vertical Axle Accelerations (V_1)	3-62
3-39	Transfer Function of Lateral Truck Accelerations (L_2) to Lateral Axle Accelerations (L_1)	3-63

LIST OF ILLUSTRATIONS (CONT'D)

<u>Figure</u>	<u>Title</u>	<u>Page</u>
3-40	Illustration of Brake Torque Forces (T) and Brake Normal Forces (N)	3-66
3-41	Brake Force Signals with Slide Control Activity	3-69
3-42	Power Spectrum of Vertical Truck Accelerations (V_2) and Brake Disc Torque Force ($SG_1 + SG_2$)	3-70
3-43	Coherence of Brake Disc Torque Force ($SG_1 + SG_2$) to Vertical Truck Accelerations (V_2)	3-71
3-44	Transfer Function of Brake Disc Torque Force ($SG_1 + SG_2$) to Vertical Truck Accelerations (V_2)	3-72
3-45	Transfer Function of Disc Brake Torque Force ($SG_1 + SG_2$) to Vertical Truck Accelerations (V_2) with Coherence Blanking = 0.8	3-73
3-46	Power Spectrum of Lateral Axle Accelerations (L_1) and Brake Disc Normal Force ($SG_1 + SG_2$)	3-74
3-47	Coherence of Brake Disc Normal Force ($SG_1 - SG_2$) to Lateral Axle Accelerations (L_1)	3-75
3-48	Transfer Function of Brake Disc Normal Force ($SG_1 - SG_2$) to Lateral Axle Accelerations (L_1)	3-76
3-49	Transfer Function of Brake Disc Normal Force ($SG_1 - SG_2$) to Lateral Axle Accelerations (L_1) with Coherence Blanking = 0.8	3-77
4-1	Knorr Disc Brake Assembly--Force Vectors are Indicated in Positive Direction	4-3
4-2(a)	Drop Shock Testing Configuration	4-4
4-2(b)	Pendulous Mass Used to Provide Lateral Impulse Loading on Disc Brake Assembly	4-4
4-3	Wheelset Handling Rack	4-7
4-4	Instrumented Disc Coordinate System as Viewed from No. 5 Wheel Side of Brake Disc Assembly	4-10
4-5	Side View of Instrumented Wheelset	4-11

LIST OF ILLUSTRATIONS (CONT'D)

<u>Figure</u>	<u>Title</u>	<u>Page</u>
4-6	Cross Section of Disc Assembly Showing Strain Gaged Pin and Hub Socket	4-12
4-7	ENSCO Micro-Slip Detector	4-13
4-8	Micro-Slip Detector (MSDT) Installation Diagram	4-14
4-9	Clockwise Tangential Load Test at Zero Degrees (6-18-79)	4-18
4-10	Counterclockwise Tangential Load Test at 180 Degrees (6-15-79)	4-19
4-11	Outboard Lateral Load Test at Zero Degrees (6-18-79)	4-20
4-12	Outboard Lateral Load Test at 180 Degrees (6-18-79)	4-21
4-13	Diametric Load Test at 270 Degrees (6-19-79)	4-22
4-14	Diametric Load Test at Zero Degrees (6-18-79)	4-23
4-15	Micro-Slip of Pin with Lateral Loading	4-24
4-16	Micro-Slip of Pin with 100-Pound Lateral Load	4-25
4-17	Pin Motion with 500-Pound Lateral Load	4-26
4-18	Pin Motion with Impulse Loading	4-27
4-19	Pin Motion with Lateral Load	4-28
4-20	Comparison of 80 mph Over-The-Road Test (OTR) and Laboratory Test rms g-levels versus the Square Root of Bong and Drop Height	4-32
4-21	Comparison of Predicted 120 mph Over-the-Road to Laboratory Tests	4-33
4-22	Lateral Bending Stress on Pins vs. Frequency	4-34
4-23	Lateral Impulse Loading	4-36
4-24	Comparison of Peak Values of LAA, LAR, TBS, LBS and MSDT	4-38

LIST OF ILLUSTRATIONS (CONT'D)

<u>Figure</u>	<u>Title</u>	<u>Page</u>
4-25	Lateral Impulse Loading Data	4-39
4-26	Lateral Impulse Loading Data	4-40
4-27	Lateral Impulse Loading Data	4-41
4-28	Lateral Impulse Loading Data	4-42
4-29	Lateral Impulse Loading Data	4-43
4-30	Lateral Impulse Loading Data (Wheelset on Rails)	4-44
4-31	Lateral Impulse Loading Data (Wheelset on Rails)	4-45
4-32	Lateral Impulse Loading Data	4-46
4-33	Lateral Impulse Loading Data	4-47
4-34	Lateral Impulse Loading Data	4-48
4-35	Lateral Impulse Loading Data	4-49
4-36	Vertical Impulse Loading Data	4-53
4-37	Vertical Impulse Loading Data	4-54
4-38	Vertical Impulse Loading Data	4-55
4-39	Vertical Impulse Loading Data	4-56
4-40	Vertical Impulse Loading Data	4-57
4-41	Vertical Impulse Loading Data	4-58
4-42	Vertical Impulse Loading Data	4-59
4-43	Vertical Impulse Loading Data	4-60
4-44	Vertical Impulse Loading Data	4-61
4-45	Vertical Impulse Loading Data	4-62
4-46	RMS Vertical Accelerations Axle (VAA) and rms Lateral Accelerations Axle (LAA) versus the Square Root of the Height of Wheelset Drop Distance (in.)	4-63

LIST OF ILLUSTRATIONS (CONT'D)

<u>Figure</u>	<u>Title</u>	<u>Page</u>
4-47	Pin Bending Strain, Hub Hole Reaction Strain and Pin-to-Hub Hole Micro-Slip Versus the Square Root of Wheelset Drop Distance	4-64
4-48	Typical Spectral Graph (Bong Test Wheels on Rails)	4-68
4-49	Typical Spectral Graph (Bong Test, Wheels on Rails)	4-69
4-50	Corresponding Data from the Micro-Slip Detector and the Instrumented Strain Gages	4-70
4-51	Typical Spectral Results (Drop Test)	4-72
4-52	Typical Spectral Results (Drop Test)	4-74
4-53	Micro-Slip vs. Frequency	4-76
5-1	Amfleet Disc Brake Failures During the Winter of 1977/1978	5-1
5-2	Amfleet Disc Brake Failures During the Winter of 1978/1979	5-2
5-3	Vertical Axis Acceleration (V_2) vs. Speed (Bandwidth 2.5 to 500 Hz)	5-3
5-4	Lateral Axis Acceleration (L_1) vs. Speed (Bandwidth 2.5 to 500 Hz)	5-4
5-5	Comparison of Frozen and Unfrozen Vertical Axis Accelerations	5-5
5-6	Transfer Function of Vertical Accelerations (V_2) to Vertical Axle Accelerations (V_1)	5-6
5-7	Percent Time Exceedence as a Function of Acceleration Exceedence and Train Speed	5-6
5-8	Lateral Response at Bearings (Axle Side and Truck Side)	5-7

LIST OF TABLES

<u>Table</u>	<u>Title</u>	<u>Page</u>
3-1	Knorr Brake Test	3-12
3-2	%tE for Data from 2.5 to 500 Hz at a Constant Speed of 64 mph and at Constant Track Stiffneww (T)*	3-52
3-3	%tE for Data from 2.5 to 500 Hz at a Constant 10 g and at Constant Track Stiffness (T)	3-52
3-4	Boston Run -- Vertical Axle Acceleration Data	3-54
3-5	Montreal Run -- Vertical Axle Acceleration Data	3-55
3-6	Calculation of the Coefficient at Friction	3-67
4-1	Data Channels	4-3
4-2	Functions To Be Determined	4-8
4-3	Load Configurations	4-15

EXECUTIVE SUMMARY

GENERAL

The Brake Test Program was developed to evaluate candidate replacement disc brakes and to explore the cause of the loosening of the attaching pins on the Knorr disc presently used on Amfleet cars. The disc-brake friction ring on the Knorr brake (used on Amfleet and the Turboliner cars) has been experiencing excessive wear and loosening. Amtrak has studied this problem and has found that the problem reoccurs each winter and that the discs on cars in service on the West Coast have not experienced this failure. Amtrak records clearly show that the failure is related to winter operation on the Northeast Corridor (NEC) and in the Midwest. To overcome this problem, Amtrak has worked with Knorr-Bremse and several other equipment suppliers to develop alternate disc hardware.

REVENUE SERVICE TESTING

The first part of this program was designed to evaluate the candidate discs using a controlled revenue service test. The newest Knorr designs, and discs developed by Westinghouse Air Brake Company (WABCO) and BSI (marketed by New York Air Brake Company) were installed on standard Amcoach cars which were operated in revenue service on the NEC.

The Revenue Service Test developed as part of this test program is scheduled to continue for the next several years. This report includes only the results of the first six months of the test program, which is not long enough to be significant. Amtrak will continue to monitor the cars equipped with the alternate candidate hardware. The results of the Revenue Service Test will be more significant after the candidate

hardware has been in service for two years. Previous failure-history seems to indicate that it takes two years for the pins to fail. Most pins survive the first winter of service, but almost 100 percent of the hardware in Northeast Corridor Service fails during the second winter. In the six months of revenue service testing covered by this report, only one pair of WABCO disc-brakes failed; however, this pair was found to have been installed incorrectly. It is not clear whether the assembly error caused the disc-attachment failure, nonetheless, WABCO has modified their disc to strengthen the tabs which failed.

In conjunction with the Revenue Service Test, the Amtrak records were examined to determine whether the failures are related to environmental factors. The results of this review show clearly that the failure rate increases sharply as soon as the average temperature in the northern cities (Washington, DC, New York, NY and Boston, MA) goes below 32 degrees Fahrenheit.

This pattern was apparent in 1978 and 1979. In 1977 the failure rate did not increase until three weeks later. This delay may have occurred because the system for reporting failures was not well developed. The records also show that when the temperature warmed above 32 degrees Fahrenheit, the failures stopped five weeks later. This pattern was repeated in 1978 and 1979. Temperature appears to be the factor which triggers the "winter factor". Other factors were evaluated, but correlation of the failures to average temperature and particularly to the transition to below freezing temperatures was the only positive result of this review. The failure history shows that the failures occur at the same time each year. Therefore, some factor must cause different inputs to the disc assembly at this time of the year.

OVER-THE-ROAD TEST

The second part was an Over-the-Road test (OTR). The OTR consisted of a shakedown run and two data collection runs. For the shakedown run, the instrumented car was attached to a revenue Metroliner service train (a locomotive and Amfleet cars operating on Metroliner schedules) on route from Washington, DC to New York City and back to Washington, DC. The shakedown run was made on 16 February 1979 which was during very cold weather in all of the northern cities.

The first data run was made on 26 February 1979. The car was operated in an Amfleet train on route from Washington, DC to Boston and back to Washington, DC. Prior to the 26 February test run, the weather in the northern cities had been very cold. Up until 24 February the temperatures were well below freezing. On the 24th, 25th and 26th the temperature went above freezing and the northern cities had a near freezing rain.

The second data run was made on 8 March 1979. The test car was attached to a Montreal-bound train which returned to Washington, DC on 9 March. The temperatures in all cities south of New Haven had been well above freezing for over a week prior to the 8 March run.

The instrumented over-the-road tests clearly documented that the disc is subjected to higher acceleration levels when the temperature is below 32 degrees Fahrenheit. The data collected by the nonrotating instrumentation used in the OTR test were examined to determine which if any inputs change sufficiently to qualify as the "winter factor" message. *The test showed that the accelerations were more than two to one higher on 26 February when the roadbed was partially frozen than on the 8 March test after the temperature had been above freezing for a week. Even higher accelerations were observed during the shakedown run which was made in the middle of the*

severe cold weather period of the 1979 winter. The accelerations experienced during the shakedown run were so large that the instrumentation recorder was saturated. The instrumentation was adjusted to accept the high-level signals but as the weather warmed the journal bearing accelerations diminished. The analysis shows that the wheel assembly including the disc resonate at its fundamental frequency causing attachment-pin wear. When the track was frozen, the accelerometers on the journal bearing indicated that the axle assembly resonated severely at 330, 385 and 580 Hz.

When the track is frozen, defects in the wheel and rail surfaces cause the wheelset to resonate. It appears that even if there were no major defects in the wheel and rail surfaces, this same winter factor reaction would occur but to a lesser degree.

The test did not include any experiments which measured the extent to which the roadbed was frozen, but the weather conditions which prevailed prior to the test runs support the freezing theory suggested by the failure analysis.

LABORATORY TESTING

For the third part, laboratory tests were performed to correlate the OTR test results to pin wear. Analysis performed by MIT metallurgists indicated that the pins fail from fretting corrosion which is produced by high-frequency (200 to 600 Hz) rubbing motion between parts which are pressed tightly together. The pins holding the disc to the hub were instrumented with strain gages and a motion detector. The instrumented axle assembly was shocked by hitting the end with a heavy lead pendulum and by dropping one wheel on a section of rail to

simulate the inputs measured from the over-the-road test. The laboratory test showed that pin stress and motion occur at the same frequencies as observed in the over-the-road test; therefore, the increased accelerations produce the pin wear. The laboratory test also showed that the motion and stress in the pin are both proportional to acceleration so the increased wear can be assumed to be proportional to the observed acceleration squared.

The over-the-road test results indicated that on frozen track the accelerations may increase by more than two to one over unfrozen track. The accelerations observed but not recorded during the shakedown run were three or four times higher than the unfrozen data.

The test shows that the winter pin-wear is at least four times summer wear and may be as much as 16 times more. In terms of damage, the effect can be much worse since the higher level inputs will tend to break the parts free so that wear is accelerated. In the milder dynamic environment, corrosion helps to inhibit motion preventing the wear.

At temperatures below 32 degrees Fahrenheit, freezing of the track and roadbed occurred. Track freezing causes a marked loss of damping which produces an amplification of resonance at the natural frequencies of the wheel/axle system. Interaction between the disc, wheel/axle resonance and the resonant responses of the disc produces micro-slip, causing wear in the pins which secure the disc to the axle assembly. Changes in rail response appear to be the cause of the winter failures.

The results of the disc acceleration measurement were studied and an exceedance analysis was developed. This analysis

provides a tool for extrapolating the results of this test to predict the effect of running at 120-mph as scheduled by the NEC Improvement Program.

From the data, *an increased speed (120 mph) is likely to produce an even more serious situation in which the high failure rate may occur all year instead of only during a 15-week period.* It can be predicted that at higher speeds the winter will have an even greater potential for damaging mechanisms which are mounted on the axle or on unsprung parts of the truck.

1.0 INTRODUCTION

1.1 PURPOSE

Based on service experience, Amtrak has found a high rate-of-attachment pin loosening on disc-brake equipment currently in use on Amcoach and Turbo-Train passenger vehicles. The present loosening rate of these brakes under certain winter conditions is so high that fleet maintenance costs are considered excessive. To determine the cause of this loosening which is considered a failure of the equipment, a series of tests were performed. This report presents the results of these tests.

The test series was divided into the following sections:

- Revenue Service Test--The revenue service tests were conducted on improved Knorr discs, improved Knorr pin designs, and discs designed by Westinghouse Air Brake Company (WABCO), and Bergische Stahl Industries (BSI). (The BSI discs were supplied by New York Air Brake.)
- Non-Rotating, Over-the-Road Test--This dynamic test was designed to assess:
 - Variation-to-truck-input during cold weather.
 - Variation-to-transmissibility of truck primary.
 - Operation of slide control in winter conditions.
- Laboratory Test--An environmental Laboratory test was designed to measure the bending stresses in the pins which secure the disc to the hub and to determine the motion between the pin and disc hub in the Knorr disc-brake assembly.

- High Speed Test--The test was designed to observe thermal effects on the alternate disc-brake designs under high-speed stopping. However, this test was dropped because the same information will be obtained from the Dual-Brake Test.

1.2 BACKGROUND

During the winters of 1977, 1978 and 1979, the pins securing the friction ring to the disc brake in the Knorr design currently in use on the Amfleet and on other passenger vehicles were found to loosen to such a degree that they were frequently "bad ordered" and repaired. The failure rate of these pins was found to occur at approximately the same time each winter. Various theories have been presented for the winter related failures; however, to formulate an accurate theory, an understanding of the winter factor is essential.

The Amfleet and Turboliner vehicles operating in the Northeast and Midwest have experienced severe winter-weather failures. The failure rate during the summer months runs approximately five disc failures per week. This rate rises dramatically around the beginning of February to 100 or more disc failures per week. Figures 1-1 and 1-2 show Amtrak data on these failures.

An extensive test plan, included in Appendix I, for determining the cause of this problem was developed in a joint effort by FRA and Amtrak. However, this plan, called the Rotating Test Series, could not be implemented in time to make use of the winter of 1978/1979. Since the Northeast Corridor Program is scheduled to begin high-speed service in 1981, it was imperative that the testing of the brakes be performed. Therefore, the Non-Rotating Test Series, described in this report, was developed and performed during the winter of 1978/1979.

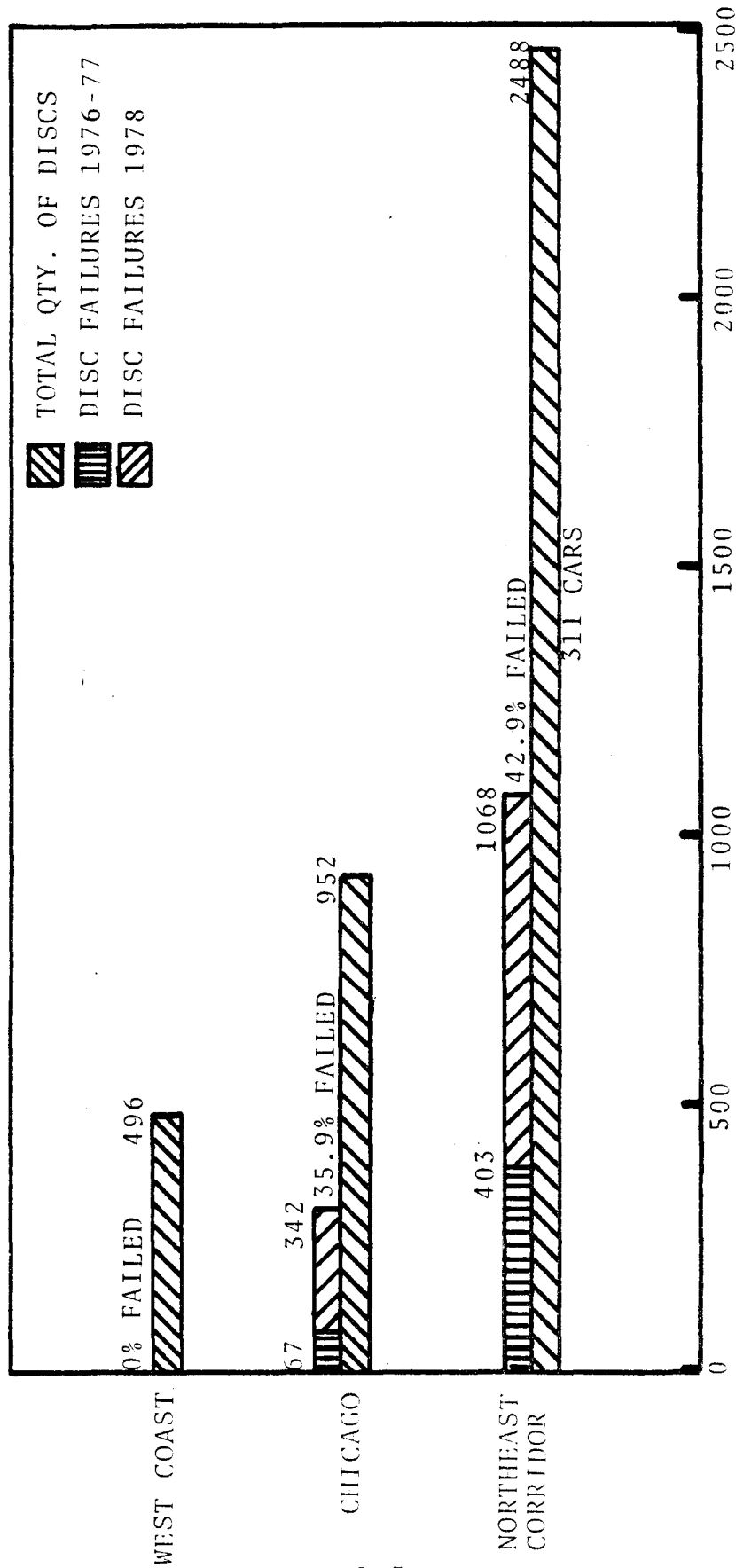


Figure 1-1. Number of Discs on Cars and Failed Discs

1.3 OBJECTIVES

The Non-Rotating Test Series examined the possible causes of the Knorr-disc-brake, retaining-pin-loosening problem and correlated the Northeast Corridor failure rates to these causes. In addition, two improved Knorr disc brakes, a BSI disc brake and a WABCO disc brake were tested in revenue service.

In summary, the test objectives were:

- To investigate the causes of the Knorr pin failure.
- To evaluate the winter factor related to the pin failure.
- To evaluate the performance of alternate brake hardware.

2.0 REVENUE SERVICE TESTING

2.1 INTRODUCTION

Revenue service testing consisted of an actual revenue service test of four new disc-brake designs and a study of disc-brake-failure history correlated with environmental conditions of the Northeast Corridor and the Midwest regions. The revenue service test was designed to test four disc-brake systems.

The first test group of 20 cars was equipped with a disc-brake system manufactured by Westinghouse Air Brake Company (WABCO). Three of these cars had the brakes installed approximately one year prior to this test.

The second group of 20 cars was equipped with a variation of Knorr's basic disc design which used a tapered wedge to expand the split roll pin. This design will be referred to as the KPI design.

The third group of 20 cars was equipped with a new design by Knorr. This design referred to as the KN design has a web to stiffen the hub in the lateral direction and has a heavier interference fit between the hub and the friction ring.

The fourth group was equipped with disc brakes manufactured by BSI and supplied by New York Air Brake. Only three sets of the BSI discs were available which limited this group to three vehicles. A description of the four disc brakes follows.

- WABCO -- The WABCO discs have a steel hub installed on the axle with a heavy press fit. The friction ring is secured to the hub by eight tabs extending inward from the friction ring as shown in Figure 2-1. Spring washers are used on the bolts which

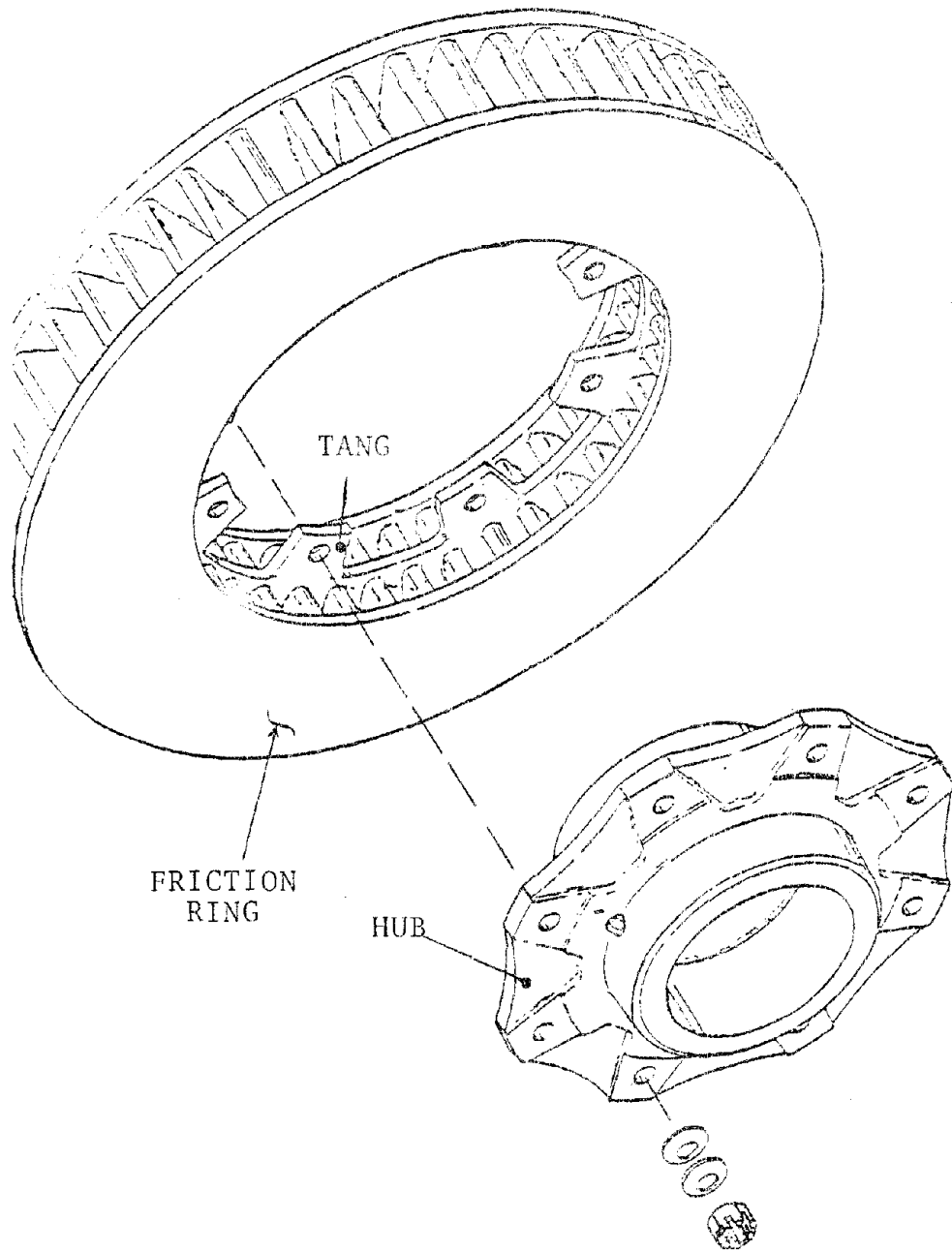


Figure 2-1. WABCO Disc Brake

secure the friction ring to the hub to maintain a tight connection even when the friction ring is hot.

- Knorr KPI -- These discs are standard eight-pin Knorr discs with forged steel hubs and cast iron friction rings. The friction rings are secured with special split pins designed with wedged expansion sleeves which expand so that the pins grip the hub tighter (Figure 2-2).
- Knorr KN -- These discs have a new cast steel hub with web plates in the lateral direction providing increased lateral stiffness. The discs are manufactured with a heavier interference fit between the friction ring and the hub so that at ambient temperatures there is an interference fit between the friction ring and the hub.
- BSI -- The BSI disc has a steel hub installed on the axle similar to the other disc units. The cast iron friction ring has four bars extending inward from the friction ring. The bars fit into slots provided in the friction ring and extend to the hub. The BSI design is shown in Figure 2-3.

2.2 REVENUE SERVICE TEST

The four groups of cars were operated in normal revenue service on the Northeast Corridor. The brake discs were specially marked. Reporting forms were distributed to the maintenance facilities so that disc failures could be reported. The operation of the cars in the control group was monitored from the computerized operational records.

No special procedures for controlling the car movements were used because the operational records from previous years indicated that the average mileage of cars in the Corridor was approximately the same. There were no obvious trends which related disc-brake failures to special regions or usage

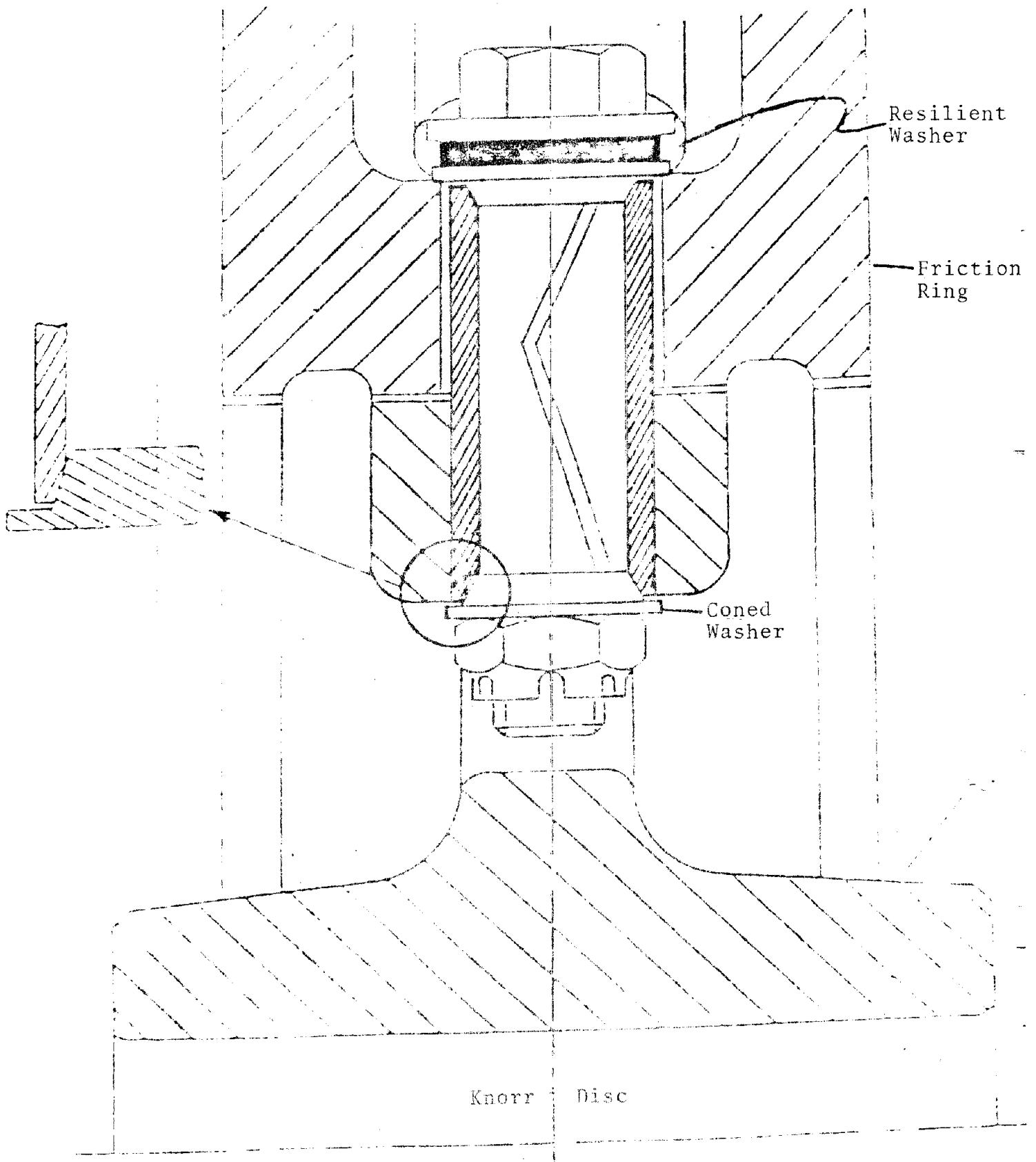


Figure 2-2. KPI Brake

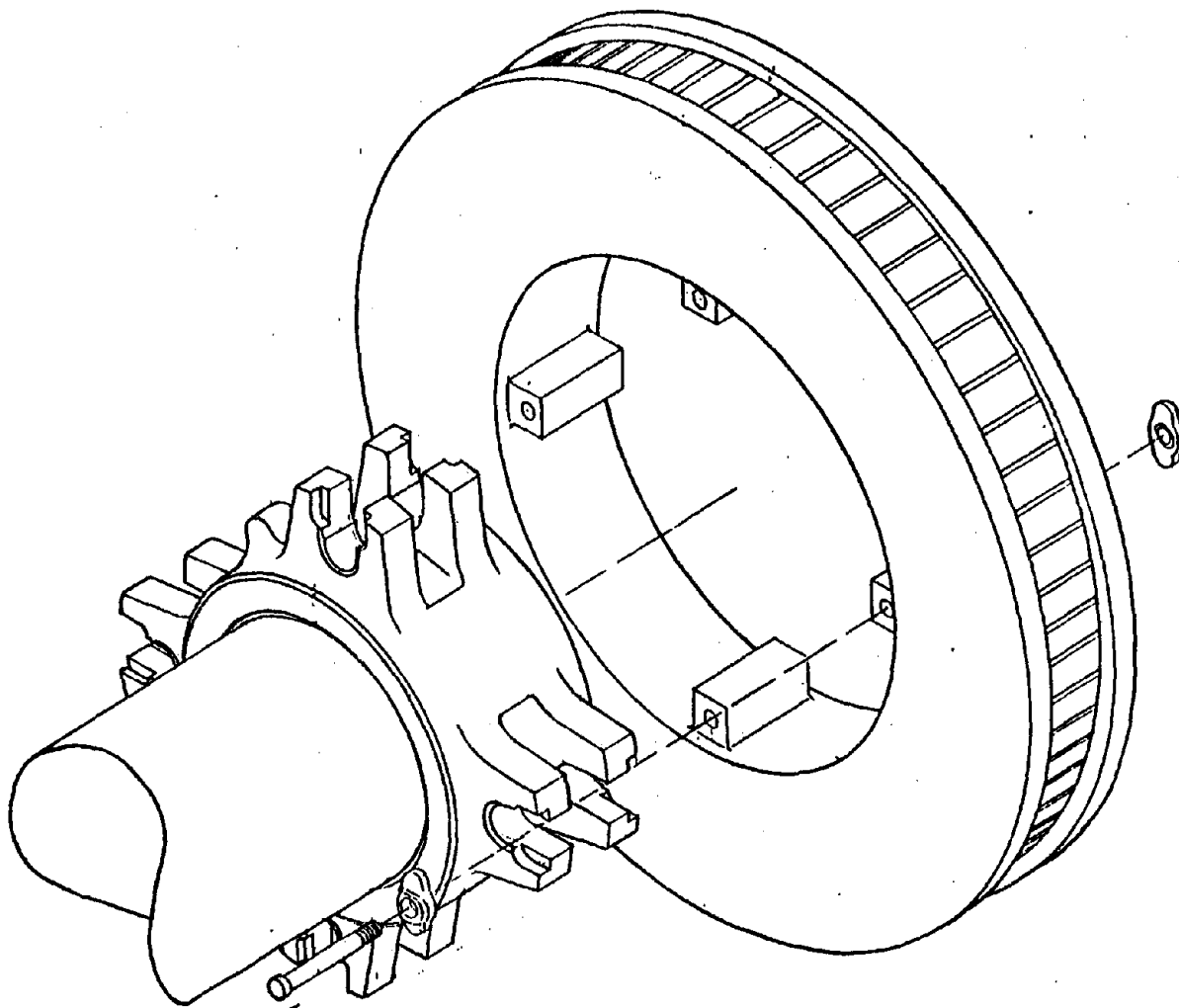


Figure 2-3. New York Air Brake (BSI) Disc Brake

so to keep the test from imposing complicated restrictions on the operation personnel the only rule for the test was that the cars should be kept in service on the Corridor. If the operation reports showed that the cars had been diverted out of the Corridor, Amtrak would reroute the test cars to the Corridor.

After five months of revenue service testing an examination of the disc-brake sample group revealed only one failure. An Amtrak inspection of the test hardware indicated that one of the WABCO discs failed during the five-month period after the start of the revenue service test. The tabs on one disc broke allowing the disc to separate completely from the hub. The tabs on the other disc on the same axle were also found to be cracked. An inspection of the disc unit indicated that the hardware securing the friction ring to the hub remained tight. Metalurgical examinations, performed by WABCO and Massachusetts Institute of Technology (MIT), indicated that the tabs failed from low stress cycle fatigue.

Upon inspection, Amtrak found that the disc had been assembled backwards. However, since the disc is nearly symmetrical, being installed backwards may or may not have caused the disc to be subjected to added loads. By being assembled backwards, the disc was shifted out of place by approximately 0.12 inch. After the one unit failed, Amtrak had the other WABCO discs inspected visually and by a magnetic flux process. The initial reports indicated that the other discs had hairline cracks, but further investigation did not confirm this report. Based on the one incident, however, WABCO has reportedly redesigned the disc friction ring to make the tab thicker and stiffen the tab with gussets extending from the body of the friction ring.

2.3 FAILURE RECORDS VERSUS ENVIRONMENTAL RECORDS FOR THE DISC-BRAKES CURRENTLY IN USE

Data collected by Amtrak for the past three years clearly shows that the failure rate of the Knorr disc brake design (Figure 2-4) in use since 1977, is related to the winter season. For the past two seasons, the maximum failures occurred or were reported in the ninth to the eleventh week of the new year. In the 1977 season the trend was not as clearly defined, but the maximum failures were in the same approximate period. The weekly failure records for the past three years are shown in Figures 2-5, 2-6 and 2-7.

To investigate the cause of the failures, the environmental conditions for the Northeast Corridor were obtained from the Local Climatological Data for Washington, DC; New York, NY; and Boston, MA distributed by the Department of Commerce, National Weather Service. The temperature, precipitation and snow-on-the-ground data for these three Northeast Corridor cities were compared with the failure records and several general trends were observed.

To compare failures and temperature, the failure data were smoothed by averaging the number of failures for a three week period. The averaging showed that the maximum number of failures occur around the tenth week of each year. The temperature data were also smoothed by averaging over a three week period.

A comparison of these data show an interesting correlation between the average temperature and failures. When the average temperature went below 32 degrees F (freezing) the rate of failure started to increase immediately. In 1979 the average temperature in Washington did not fall below 32 degrees F until the fifth week. At this time the average

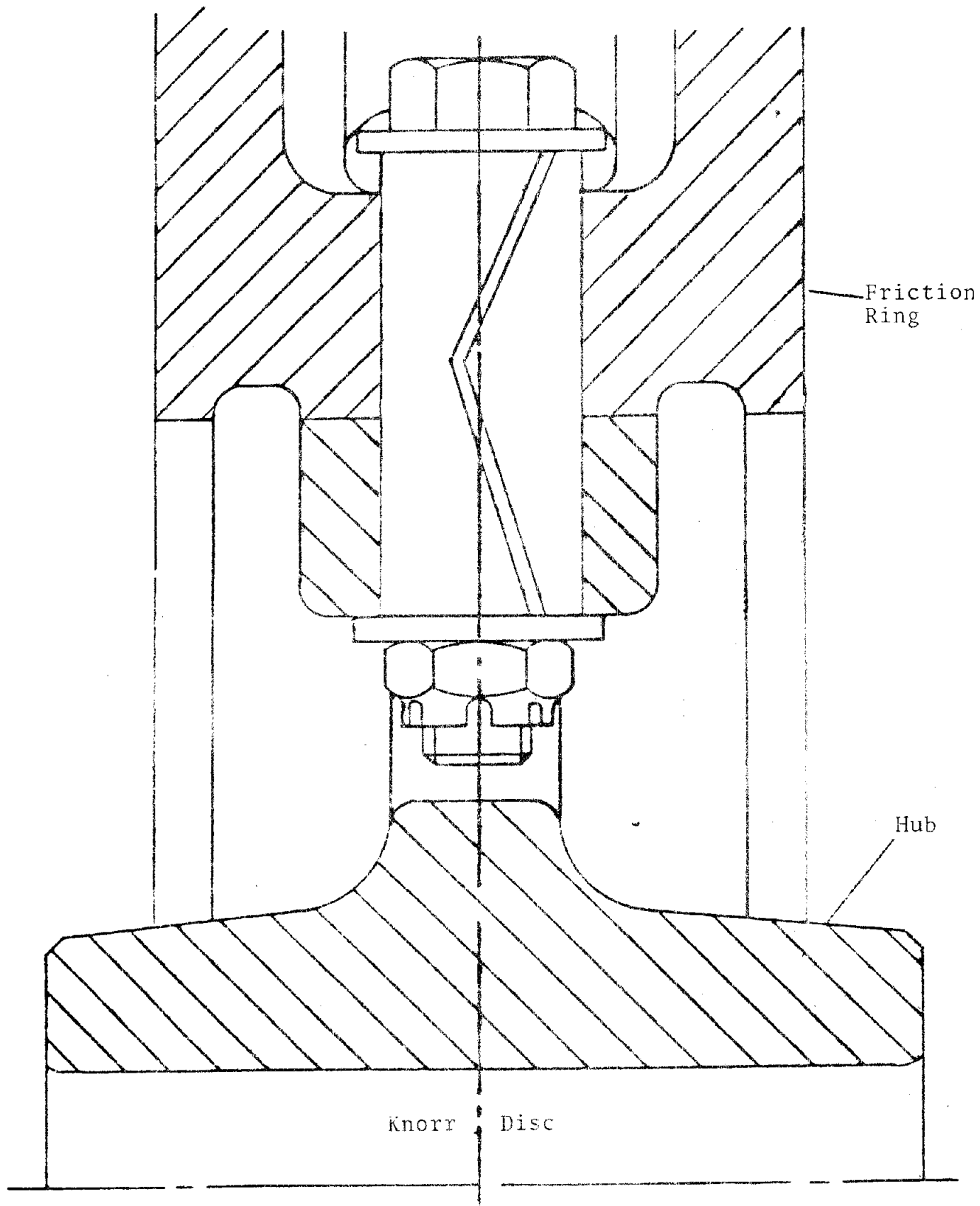


Figure 2-4. Knorr Disc Brake Design in Use by Amtrak Since 1977

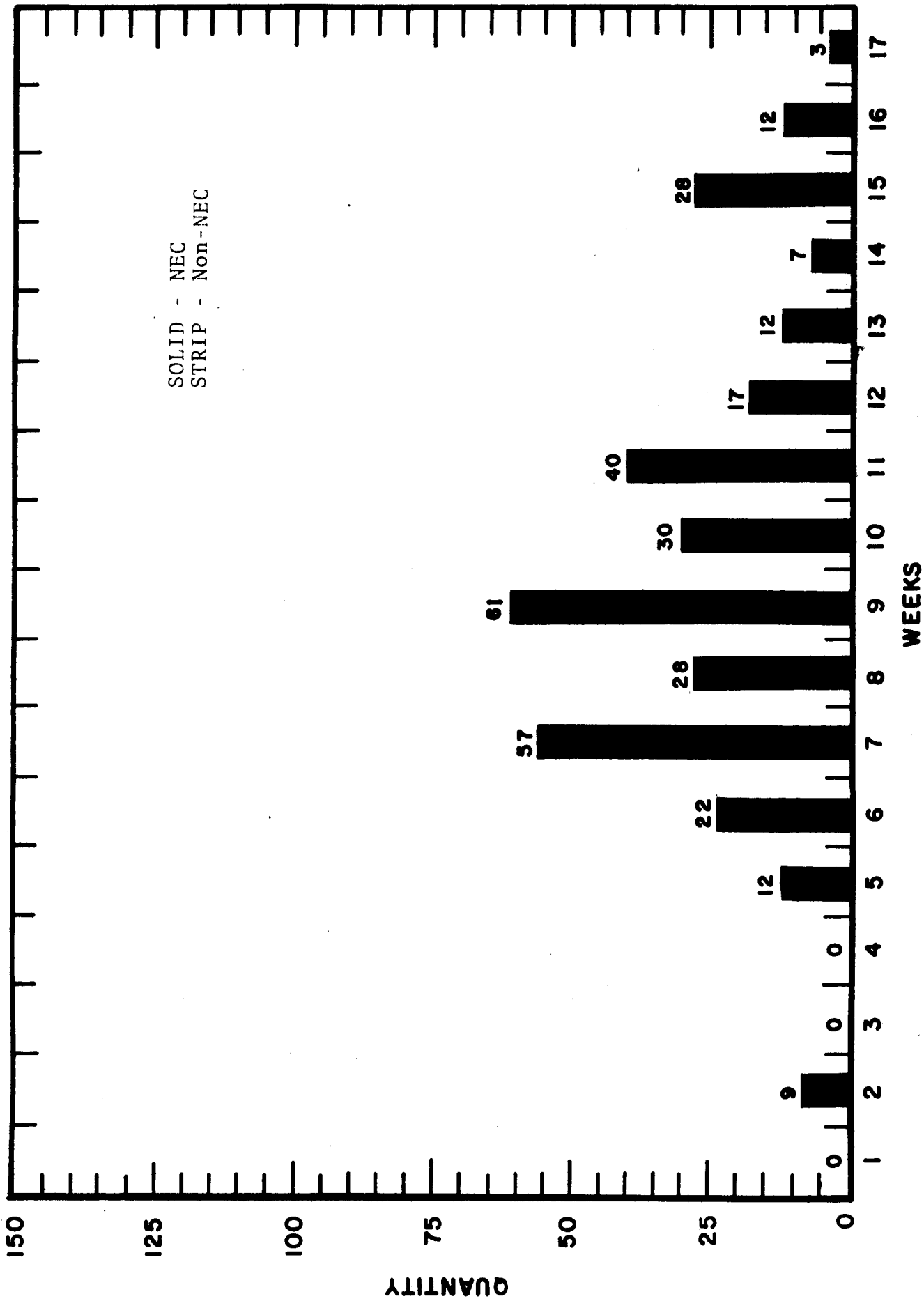


Figure 2-5. Amfleet Disc Brake Failures - 1977

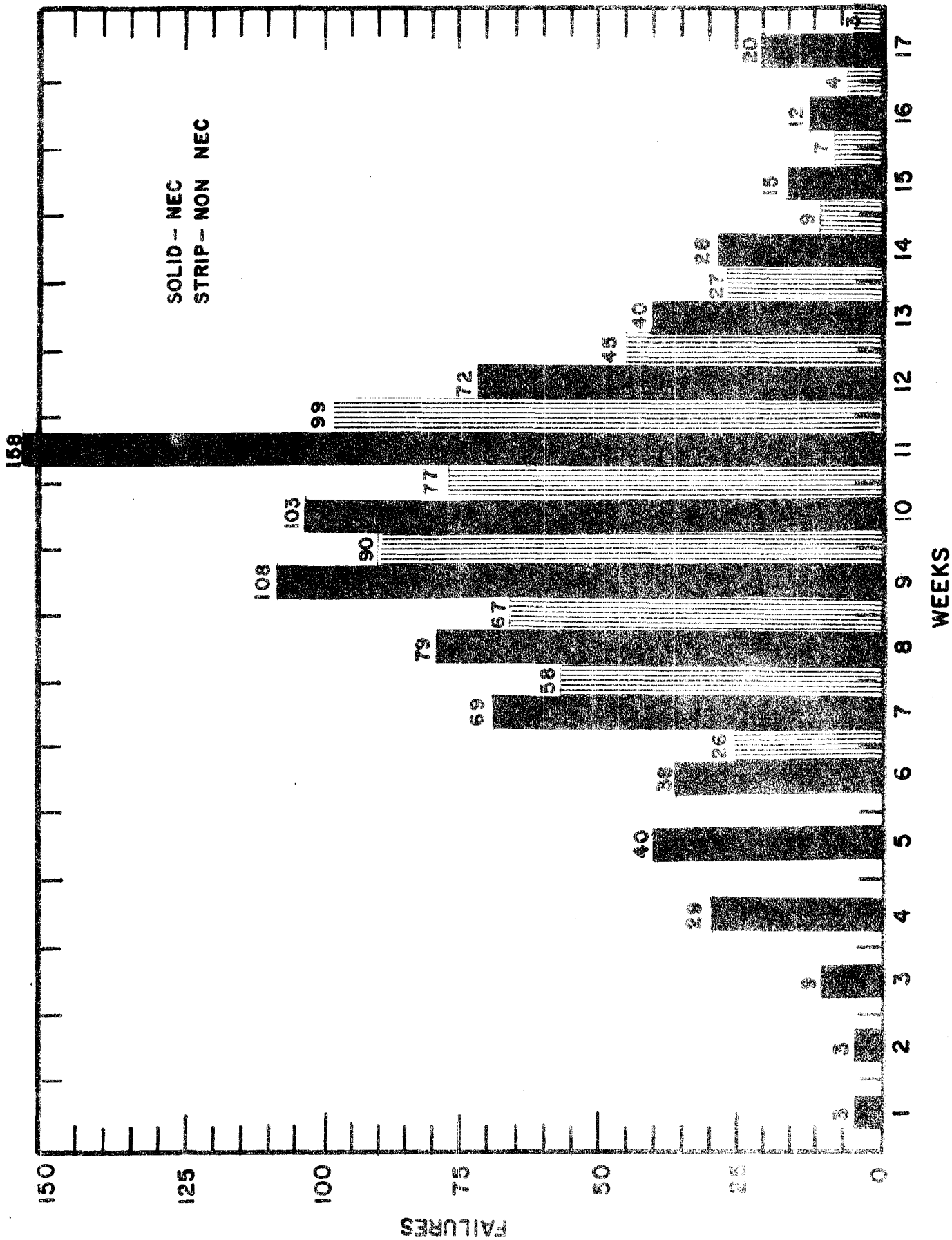


Figure 2-6. Amfleet Disc Brake Failures - 1978

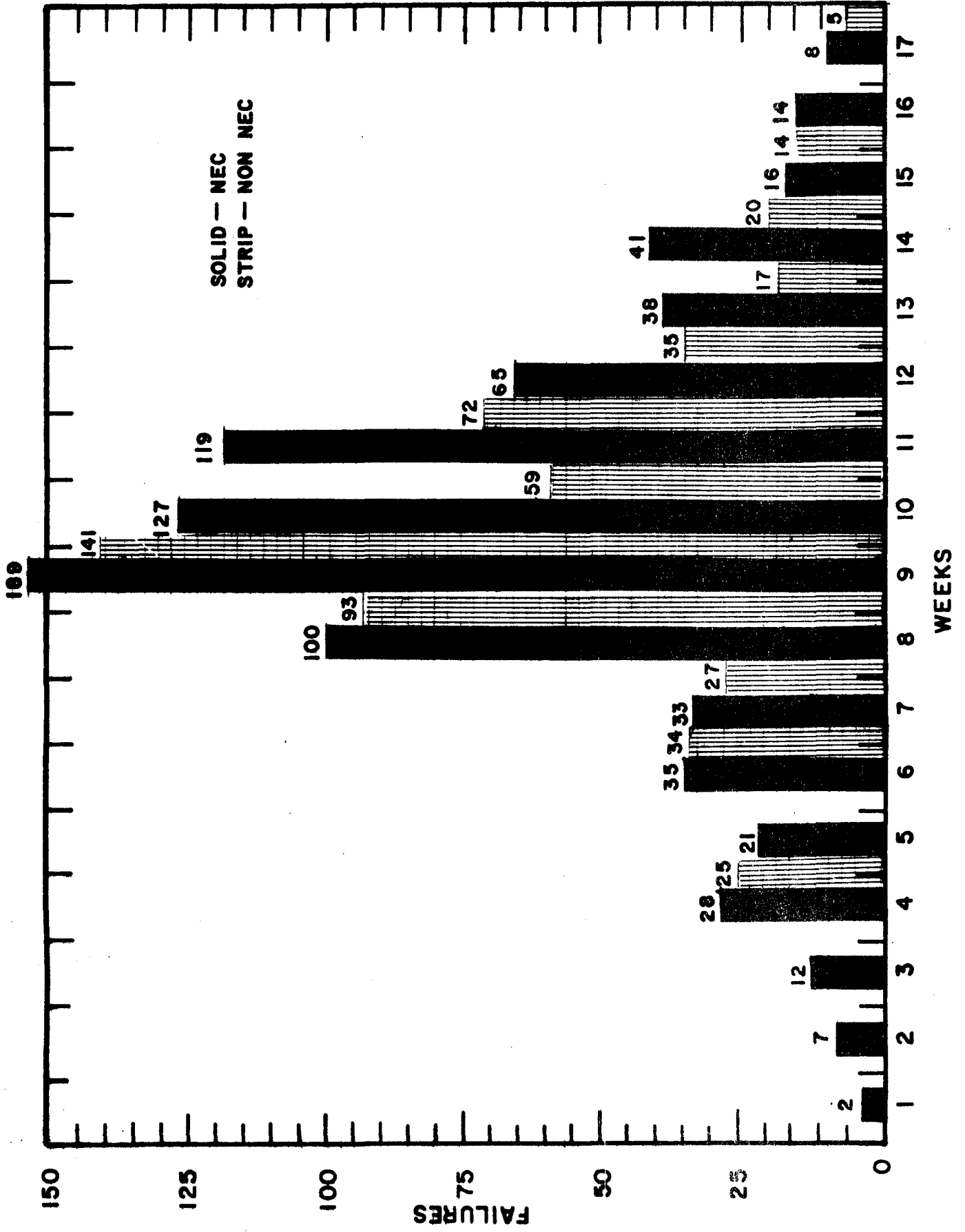


Figure 2-7. Amfleet Disc Brake Failures - 1979

temperature in all regions of the corridor was colder than 32 degrees F and the failure rate increased significantly (Figure 2-10). In 1979, the average temperature in the Northeast Corridor cities remained below 32 degrees F until the ninth week. The failure rate peaked on the tenth week and went down to 30 discs a week by the fourteenth week, five weeks after the temperature warmed above 32 degrees F.

The 1978 and 1977 failure records and average temperatures for the Northeast Corridor cities were compared to determine if the same marked correlation to the onset of freezing existed for the other years. These data are shown in Figures 2-8 and 2-9. In 1978, the correlation to the onset of freezing is similar to 1979. The average temperature exceeded 32 degrees in New York and Boston and one week later the rate of failures started to increase significantly. The average temperature in the Washington area went below 32 degrees F in the third week of 1978 at which time the number of failures increased markedly. In 1978, the temperatures did not warm as suddenly as in 1979. New York and Boston remained below freezing until the eighth and ninth week and four weeks later the failures were down to 30 discs per week.

The 1977 data does not show a relationship to freezing as do the 1978 and 1979 data. In 1977 the average temperature in New York and Boston crossed 32 degrees F in the last weeks of December 1976 and the failure rate was not reported to have increased until the fourth week of 1977. This delay may weaken the argument suggested by the 1978 and 1979 seasons or may represent a delay in reporting these failures. In 1977, the temperatures warmed above 32 degrees F on the seventh week. The disc failures significantly decreased by the twelfth week, five weeks later. The average temperature

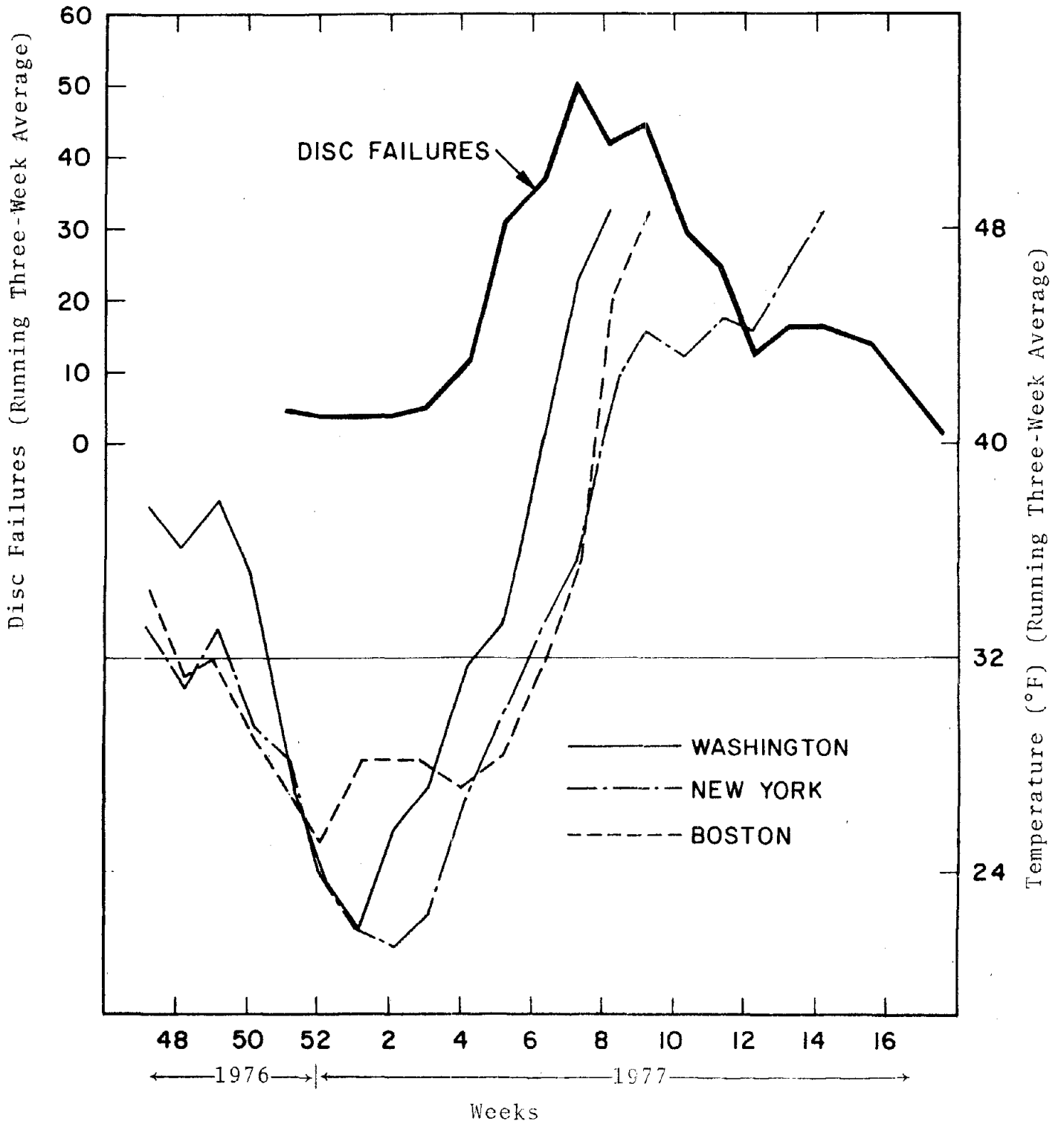


Figure 2-8. Amfleet Disc-Brake Failures During the Winter of 1976/1977.

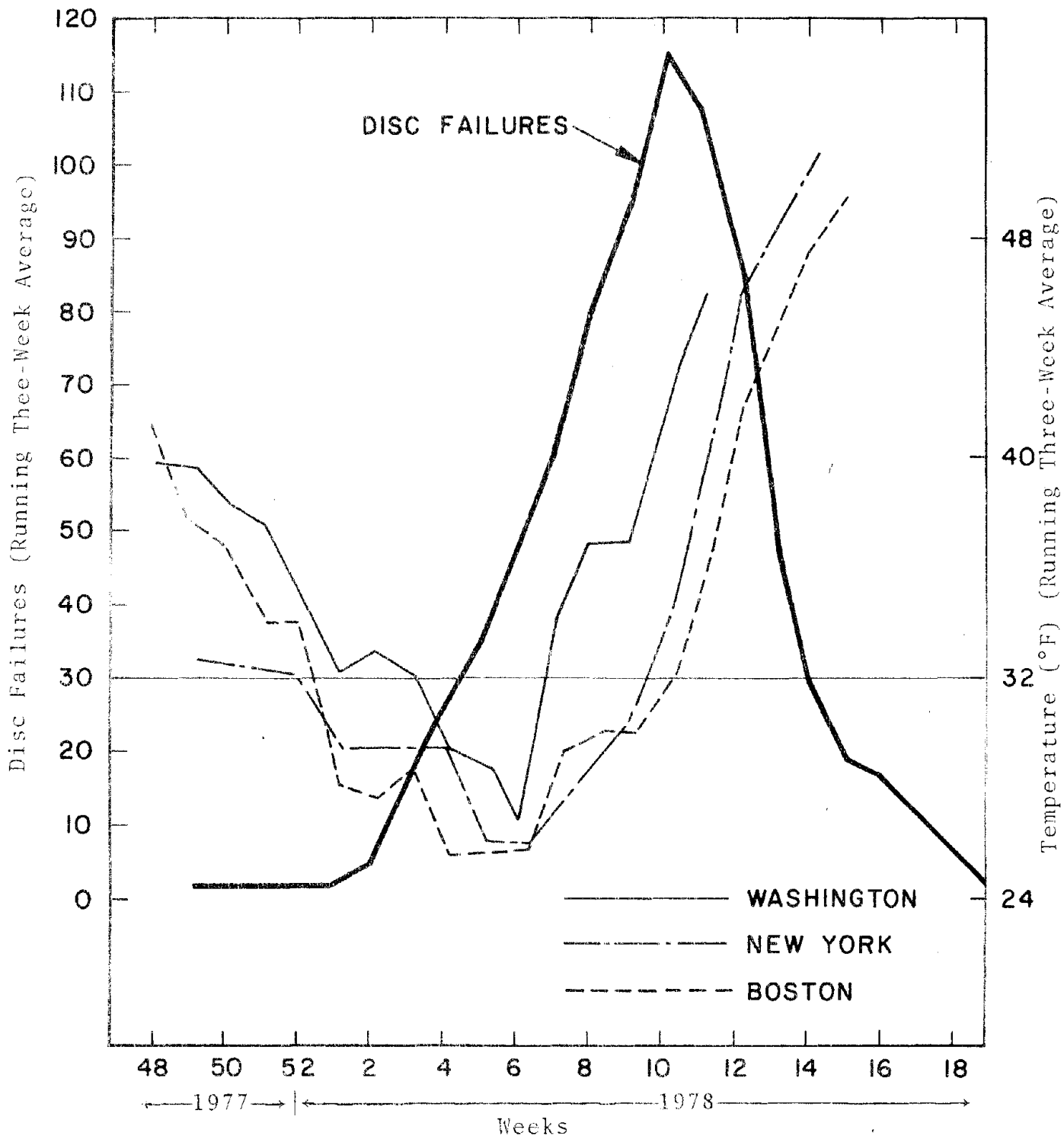


Figure 2-9. Amfleet Disc-Brake Failures During the Winter of 1977/1978

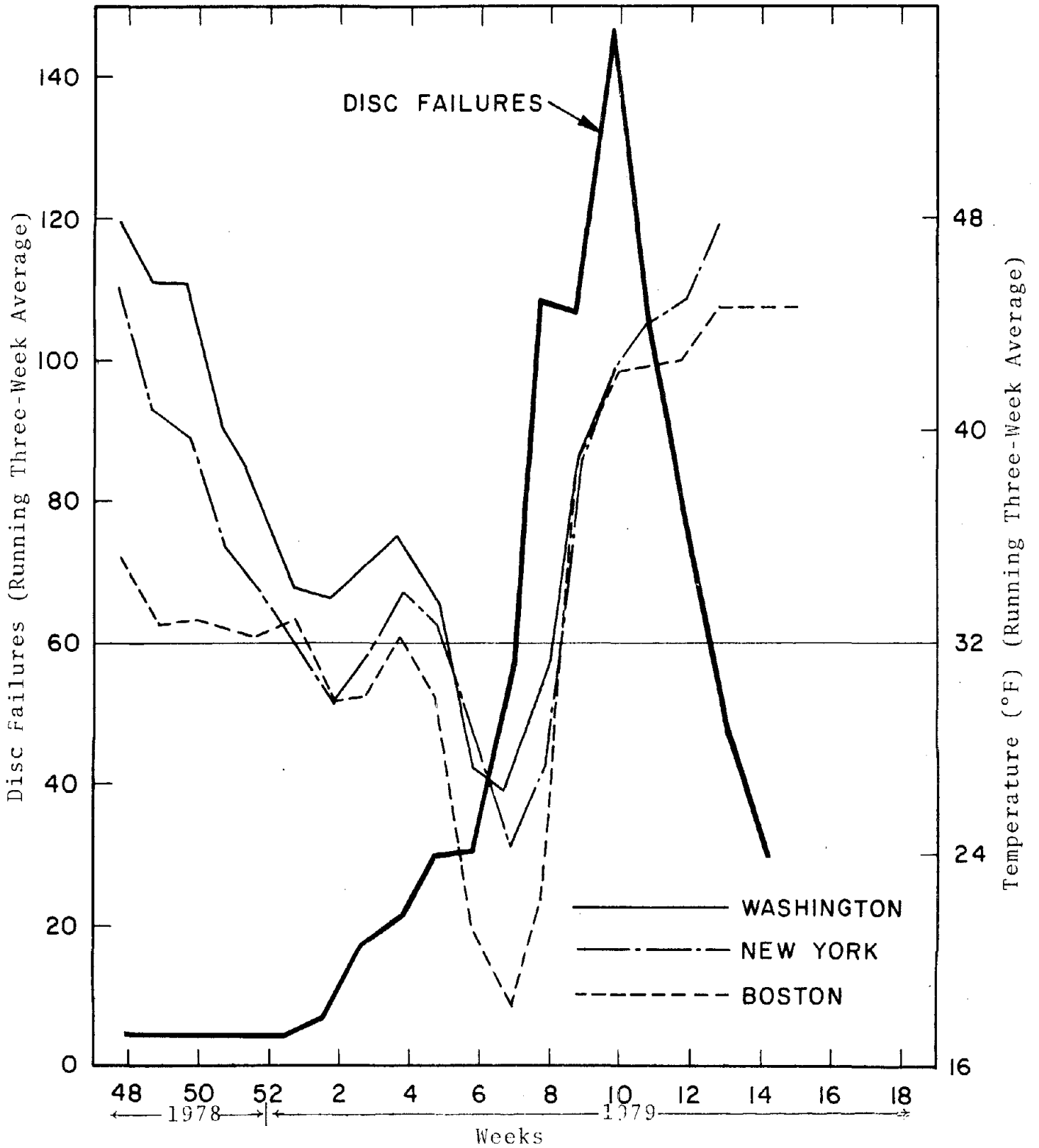


Figure 2-10. Amfleet Disc-Brake Failures During the Winter of 1978/1979

data strongly suggests that the rate of disc failures is related to freezing. The onset of the increasing failure rate seems to start as soon as the average temperature in the northern cities drops below 32 degrees F. The failure rate decreases markedly five weeks after the average temperature warms above 32 degrees F.

Upon comparing precipitation and snow-on-the-ground data to the failure rate, no correlation between the occurrences of loose discs and precipitation or snow-on-the-ground in the Northeast Corridor using Washington, New York and Boston weather data for 1976-77, 1977-78 and 1978-79 were found.

3.0 OVER-THE-ROAD TEST

3.1 OBJECTIVE AND APPROACH

The Non-Rotating, Over-the-Road Test was designed to obtain data on those factors which could be evaluated by using instrumentation mounted on non-rotating portions of the truck assembly. The general objective of this test was to gain an understanding of the effects of the environment on the disc-brakes by looking at the dynamics of the wheelset under different weather conditions.

The approach to the non-rotating test was to isolate the disc and look at the inputs to see if they can be related to the environment or operating conditions. Unless the disc has an inherent sensitivity to the environment, the winter factor has to be contained in the inputs to the disc.

The disc is secured to the hub by a set of split pins. This securing mechanism has a reasonable life on cars operating on the West Coast. Also, very few failures occur on the Northeast Corridor during the summer months; but between the first and twentieth week of each year about 40 percent of the discs in service on the NEC fail (see Section 2.3). The pins that fail are usually in their second year of service. Therefore, a very high percentage of the second year pins fail each winter at exactly the same time of year. This implies that the pins are subjected to something significantly different during this 20 week period of NEC service. The test approach was to monitor and examine the inputs and to uncode the winter factor message.

The major inputs acting on the disc are shown in Figure 3-1. The discs are subjected to force inputs from the wheel/rail interface, from the brake calipers, and from thermodynamic inputs.

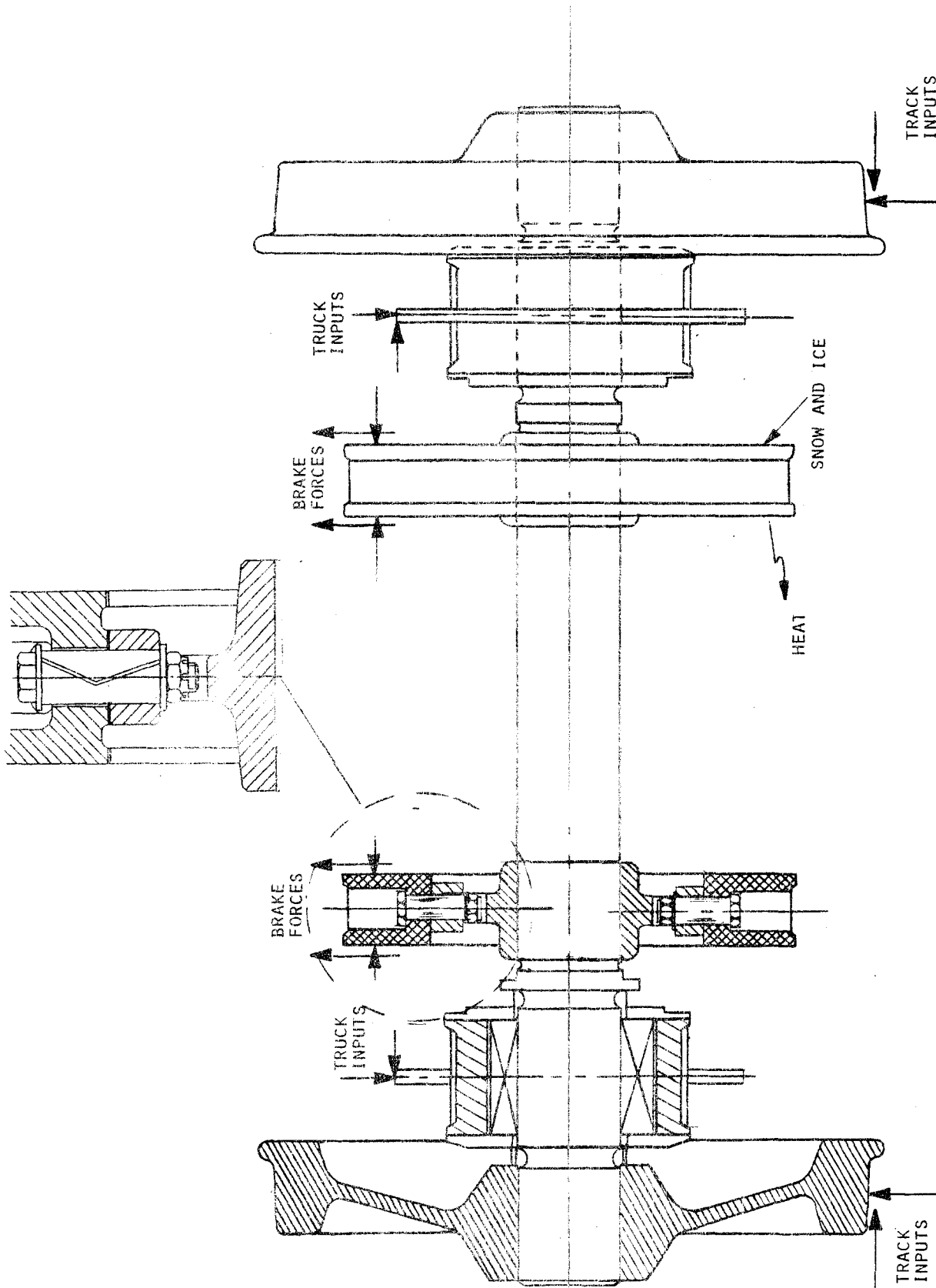


Figure 3-1. Inputs to the Wheelset

To monitor the force input, instrumentation was located on the journal bearing and truck frame. The brake rigging suspension strips were instrumented to monitor inputs from the brake calipers (see Figure 3-2). The inputs to the disc from the truck were detected by the instrumentation located on the outer race of the bearing. To check this path and to measure the stiffness of the shock ring, instrumentation was mounted on the truck-side of the journal bearing shock ring.

The analysis was divided into two phases: a study of journal bearing accelerations caused by impacts at the wheel/rail interface, and a study of the input caused by brake use.

3.1.1 WHEEL/RAIL INPUTS

This phase was designed to monitor inputs from the wheel/rail interface to determine if variations in the track created by temperature changes cause the winter failure problem.

To monitor the wheel/rail inputs, two accelerometers were mounted on the journal bearing housing of the inner axle of the A-truck. Two other accelerometers were mounted on the truck-frame, primary suspension collar of the A-truck to monitor the transmissibility of the primary suspension. The bearing accelerometers were mechanically filtered by mounting them in Benelex blocks to attenuate inputs above two kilohertz which prevented saturation of the accelerometers due to high-frequency elastic body motions.

The accelerometers were oriented to measure the vertical and lateral inputs at each location. The bearing accelerometers were designated V_1 (vertical) and L_1 (lateral). The truck-frame accelerometers were designated V_2 and L_2 . These accelerometers were connected via coaxial cables to an

accelerometer power supply manufactured by PCB Piezotronics, Inc. (PCB). The accelerometer signals were then routed to signal-conditioning attenuator filters where the signals were attenuated by a factor of 0.7 and low-pass filtered at a corner frequency of 185 Hz or 500 Hz*. This nonlinear attenuation system was designed to improve low frequency, low amplitude signals and still be able to record high frequency, high amplitude signals without exceeding the 1.414 volt ac peak input level of the FM tape recorder. The attenuator filter outputs were routed to channels 11 through 14 of the FM analog tape recorder.

Data from these accelerometers were used to evaluate the brake rigging vibration due to wheel/rail inputs. The truck primary was also evaluated because it was believed to stiffen at colder temperature, thereby taking on higher-frequency-pass characteristics which might cause the truck mounted components to receive more energy from short-duration impacts at the wheel/rail interface.

3.1.2 BRAKE INPUTS

To determine brake loads under varying environmental conditions, the brake rigging and decelostat control system were instrumented.

3.1.2.1 Strain Transducers

Torque generated on the disc-brake rotor during braking was measured by connecting strain gages to the suspension strips which connect the brake caliper assembly to the brake rigging support bar. These two suspension strips are directly in line with the center of the brake friction pads and are tangent to the brake assembly rotation. In this position they bear essentially 100 percent of the braking torque.

*The corner frequencies and tape numbers are listed on page 3-6.

Three brake-rigging suspension strips were instrumented with strain bridges as shown in Figure 3-2. Two of the legs of the strain bridges were mounted on each side of the suspension strips. Each leg consisted of a strain gage encapsulated in a glass-fiber reinforced epoxy resin. The gages were installed in a stacked "tee" rosette configuration. The instrumentation was environmentally protected by encasing the suspension strips in rubber. The instrumentation was protected from EMI-induced noise by wrapping the assembly in Aluminum tape. The legs of the strain bridge were mounted to compensate for Poisson effects and temperature variations. The gages were temperature compensated to 250°F which is well above the temperatures experienced by the suspension strips during braking. The strain signals were routed to signal-conditioning amplifiers manufactured by Dynamics Electronics Products, Inc. (Dynamics) from which the strain signals were transmitted through the interface panel to Channels 5 and 6 of the FM analog tape recorder.

3.1.2.2 Pressure Transducers

Two linear-variable-differential-transformer (LVDT)-type pressure transducers were installed at the inlets of one brake cylinder on each truck. These pressure transducers were used to measure decelostat activity for each truck of the instrumented Amcoach. The A-truck transducer was mounted on the brake cylinder of the instrumented brake rigging. The other transducer was mounted on the B-truck. Four-wire, shielded cables carried the pressure signals to the Dynamics amplifiers which were adjusted to provide an attenuated signal of ± 1.414 volts peak to the FM tape recorder (Channels 7 and 8) via the interface.

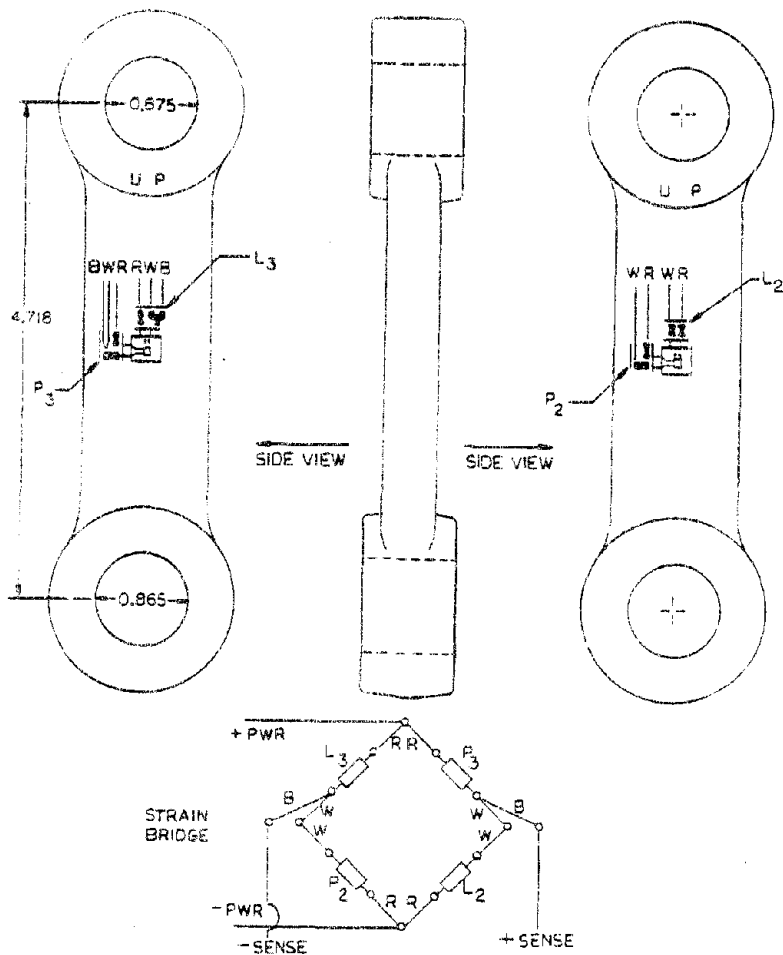


Figure 3-2. Brake Rigging Suspension Strips and Strain Bridge Used in the Over-the-Road Test

LIST OF CORNER FREQUENCIES
AND TAPE NUMBERS

Test	Low-Pass Filter Corner Frequency (in Hertz)	Tape Number
Boston	185	A11
Montreal	185	1, 2, 3 (to CTR 2926)
	500	3 (from CTR 2926) 4, 5 6 (to CTR 1410)
	Open	6 (CTR 1410 to 1423)
	185	6 from CTR 1423)

Data conversion factor = 35 mv/g

3.1.2.3 Decelostat Angular Velocity

High-impedance test probes were used to sample the 100-pulse per revolution, angular-velocity signals used by the decelostat to monitor axle rotation. This information was used to determine consist speed and test axle sliding. The signals from the four axles were routed through Dynamics amplifiers to obtain a ± 1.414 -volt peak signal to Channels 1, 2, 3 and 4 of the FM tape recorder.

3.2 INSTRUMENTATION CHECK-OUT AND CALIBRATION

3.2.1 ACCELEROMETERS

Laboratory tests were conducted to check-out the accelerometers. These tests were performed by using known accelerations which were input to the accelerometer through mountings identical to those used in the operational test.

3.2.2 ACCELEROMETER FILTERS

The accelerometer attenuator filters were calibrated by using a sinusoidal signal input of ± 10 volts peak with a frequency that was increased from 10 to 1,000 Hz in 100-Hz steps. The output amplitude was examined and the attenuation was checked as a function of frequency to ensure an attenuation of 6 dB/decade $\times 0.70$. This attenuation factor was then used during data processing to reconstruct the actual signal amplitudes.

3.2.3 STRAIN TRANSDUCERS

After assembly, the transducers were load tested in a laboratory by subjecting each to a maximum load of 4,000 pounds for at least three cycles. The results of the loading were displayed on an x-y plotter. The calibration was checked by placing a 119,880 ohm precision resistor across one leg of the bridge to simulate a 476-microstrain input to the transducer. Following this, the transducers were mounted in the test assembly and subjected to a known 12-pound weight to

verify that the transducer output was the calculated 2.5-millivolt output.

3.2.4 PRESSURE TRANSDUCERS

After the pressure transducers were installed, they were checked and calibrated by releasing the brake pressure to atmospheric pressure and recording the voltage at zero psig. A dial gage was inserted in the brake line pressure test fitting to measure the applied brake pressure. The pressure was recorded as volts from the pressure transducer and was recorded as psi from the dial gage. Using the values, a scale factor was developed as follows

$$\text{Scale factor (psi/volt)} = \frac{\text{Applied Pressure}}{\text{Volts at applied pressure} - \text{volts at zero pressure}}$$

3.2.5 TACHOMETER

The tachometer was calibrated by using the wheel circumference as measured before and after each test run followed by calculating a pulse frequency based on 100 pulses per wheel revolution. A function generator was then used to produce this pulse frequency which was used to calibrate the speed and distance processor such that 1.414 volts output was equal to 100 mph.

3.2.6 DATA COLLECTION SYSTEM

All active channels of the data collection system were calibrated by using defined inputs (dc, sinusoidal and/or broadband Gaussian noise) from a signal generator.

3.3 INSTRUMENTATION

Figure 3-3 presents the overall instrumentation plan for the test car shown in Figure 3-4. Instrumentation beneath the car consisted of nine sensors mounted on the forward truck and one sensor mounted on the rear truck. The truck mounted sensors monitored the inboard axles of each truck. Four cables were attached to the decelostat control system to monitor tachometer signals developed on each axle by the decelostat system.

The complete instrumentation package was assembled in ENSCO's laboratory in Alexandria, VA. The equipment consisted of PCB accelerometer power supplies, Dynamics signal conditioning amplifiers, attenuator filters, an interface panel, an oscilloscope, a ± 15 -volt ac power supply, function generators, a 10-channel, Honeywell light-pin visicorder, and a digital multimeter. This equipment was mounted in a standard instrumentation rack.

An eight-channel MFE strip chart recorder and a Bell and Howell 14-channel analog tape recorder were also used to record up to 14 channels of data plus a time channel with voice-over simultaneously during each run.

3.4 TEST PROCEDURES

The original test procedures were changed between runs based on reviews following the shakedown run and each subsequent test run. These changes were reviewed by Amtrak prior to implementation. The modifications that were made are reflected in this report.

3.4.1 TEST CONSIST

The test car was an instrumented Amcoach coupled to an Amtrak revenue train. Test car passengers were limited to the train crew, Amtrak, DOT, and contractor personnel. The train make-up for the dynamic tests is shown in Figure 3-5.

Reproduced from
best available copy.

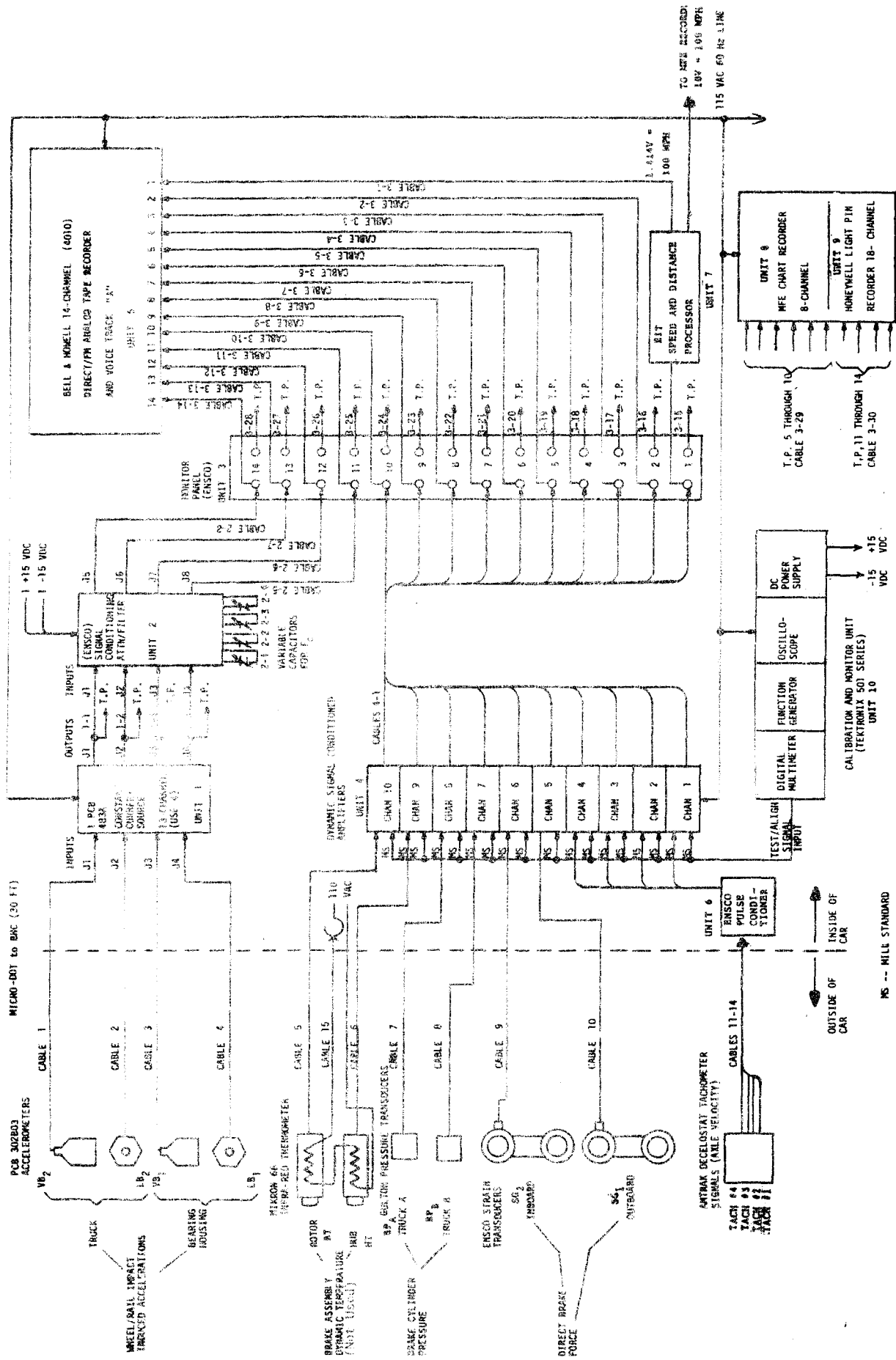
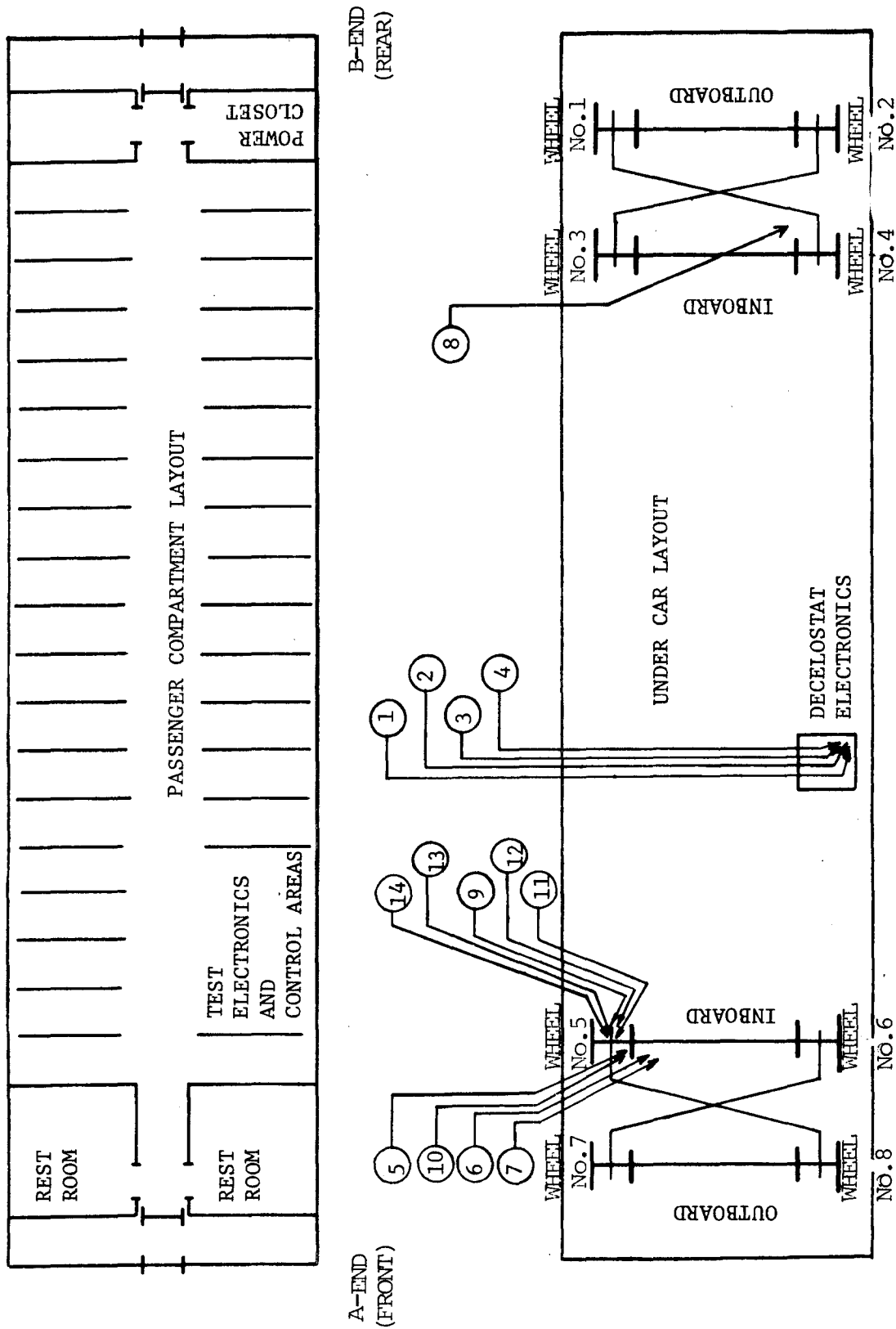


Figure 3-3. Overall Instrumentation Plan



INSTRUMENT LOCATIONS AS SPECIFIED IN TABLE 3-1

Figure 3-4. Test Car Instrumentation Layout

TABLE 5-1

KNORR BRAKE TEST

Systems Channel Monitor Panel and Tape Recorder	Sensor Designator	Sensor Location	Sensor Output (Scale Factor)	Signal Conditioner Type and Channel Assignment	Systems Gain/Atten.	Monitor Panel Output (Full Scale)	MFE Chart Recorder Channel	Visiorder Channel	Sensor Excitation	
1	TACH 1	Truck A OTBD ①	100 PPR .6 to 250 V	DYN-1 4		1.414 Vmax = 100 mph	8			
2	TACH 2	Truck A INBD ②	100 PPR .6 to 250 V	DYN-2 4	X2	100 PPR 1.414 Vmax				
3	TACH 3	Truck B INBD ③	100 PPR .6 to 250 V	DYN-3 4	X2	100 PPR 1.414 Vmax				
4	TACH 4	Truck B OTBD ④	100 PPR .6 to 250 V	DYN-4 4	X2	100 PPR 1.414 Vmax				
5	SG ₁	OTBD Brake Caliper ⑤	.417mv Pound	DYN-5 4	X1K	1.414 Vmax = 33901	1		6 VDC	
6	SG ₂	INBD Brake Caliper ⑥	.417mv Pound	DYN-6 4	X1K	1.414 Vmax = 33901	2		6 VDC	
7	BP B	Truck A ⑦	26.3mv Pound	DYN-7 4	X.672	1.414 Vmax = 801	3		15 VDC	
8	BP A	Truck B ⑧	26.3mv Pound	DYN-8 4	X.672	1.414 Vmax = 801	4		15 VDC	
9	HT	Truck A ⑨	10mv °F	DYN-9 4	X1	1.414 Vmax = 144°F	5		30 VDC (+15 V)	
10	RT	Truck A ⑩	10mv °F	DYN-10 4	X.3535	1.414 Vmax = 400°F	6		30 VDC (+15 V)	
11	L ₁	Bearing Housing ⑪	50mv G	ENSCO-PCB-4 ② ①	X.70 F _C = Var	1.414 Vmax		1		
12	V ₁	Bearing Housing ⑫	50mv G	ENSCO/PCB-3 ② ①	X.70 F _C = Var	1.414 Vmax		2		
13	L ₂	Truck A Frame ⑬	50mv G	ENSCO/PCB-2 ② ①	X.70 F _C = Var	1.414 Vmax		3		
14	V ₂	Truck A Frame ⑭	50mv G	ENSCO/PCB-1 ② ①	X.70 F _C = Var	1.414 Vmax		4		
Voice A		Record position and significant events: milepost, track number, etc.								

NOTE: ○ Indicates transducer location as shown on Figure 3-4.

□ Indicates system unit number as shown on Figure 3-3.

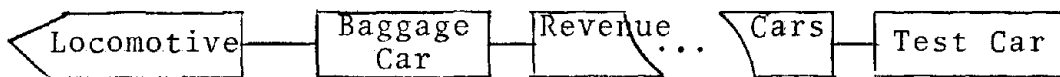


Figure 3-5. Test Consist

The test was confined to one wheelset for all tests runs. This wheelset had a moderately worn profile and slight spalls (within AAR limits) and was selected as being representative of Amfleet conditions.

3.4.2 SHAKEDOWN RUN

The test car was given a pre-operational shakedown run to debug the data channels. Debugging was conducted while underway in a revenue consist on route from Washington, DC to New York City and return.

3.4.3 TEST RUNS

The operational test consisted of two test runs in which the test car was included in a revenue consist. The test route (Figure 3-6) was from Washington, DC to Boston, MA and back for the 26 February test run, and Washington, DC to Montreal, Canada and back for the 10 March test run. Track charts of these areas were reviewed before the tests to determine which sections of track would provide the most information.

The test runs were restricted as much as possible to operation over the same track and at the same speed in that portion between Washington and New Haven. Since this was a difficult criterion to meet, data were collected for a large percentage of each test run and then scanned to obtain data which met the same track and speed criteria so that a comparative analysis could be made.

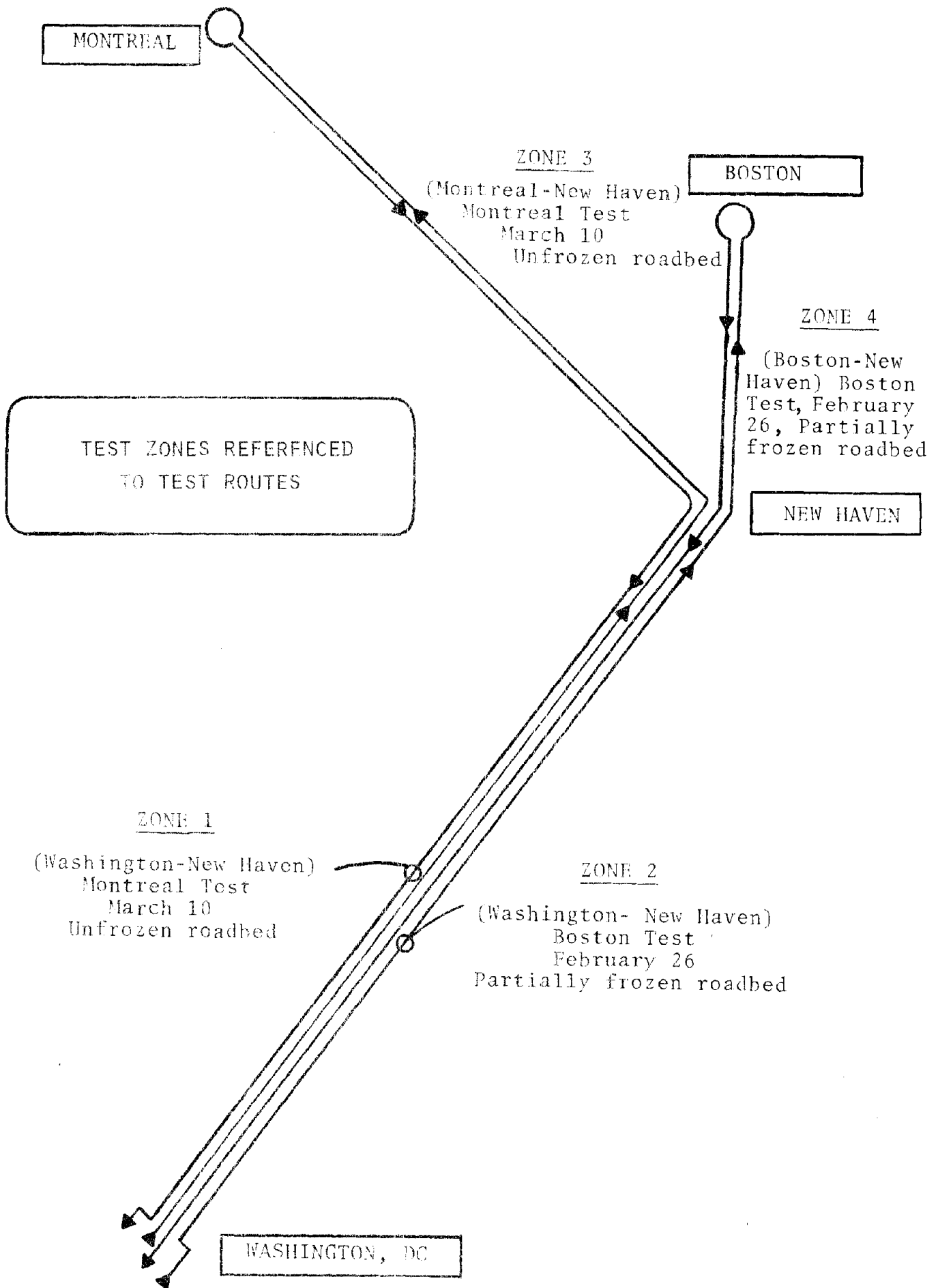


Figure 3-6. Test Zones for the Over-the-Road Test

During the period between test runs, Amtrak removed the test car from service to preserve the wheelset tread condition since the condition of the wheel affects the wheel/rail contact.

3.4.4 DATA COLLECTION

Large portions of the test runs were monitored and recorded using continuous, real-time monitoring devices (oscillographs and oscilloscopes) which were included in the test instrumentation. Cross-reference annotations were inserted on the oscillograph, the magnetic tape and the track charts to ensure correlation of the data during processing. Places of interest, located from the track charts, were documented on the voice-over channel by describing the nature of the data segment and were indicated on the oscillograph display with similar comments.

3.5 TEST RESULTS

The approach used for this phase of the task was to isolate the winter factor by identifying the possible inputs to the disc assembly and monitoring these inputs during similar test runs made under different ambient conditions. The instrumentation was designed to measure these inputs and to collect data which could be used to isolate the winter factor.

The inputs to the brake assembly are:

- Inertial forces. Acceleration amplitudes and frequencies were measured by the instrumentation mounted on the wheelset journal bearing.
- Brake forces. The forces due to the application of the brake caliper mechanism to the friction ring were measured by strain gaging the suspension strips used to transmit brake loads to the truck frame.

- Primary shock ring transfer characteristics. The P-111 primary shock ring was examined to determine if any change in transmissibility occurs during cold weather. This was determined by mounting accelerometers on both the axle and the truck side of the primary shock ring.

3.5.1 INERTIAL FORCES

The accelerations measured by instrumentation mounted on the journal bearing are the best indication of the inertial forces which act on the disc. The principle source of these accelerations is the wheel/rail interface* due to wheel surface defects, track surface defects, and track and roadbed perturbations. These sources of acceleration are present in both winter and summer; however, increased stiffness when the roadbed becomes frozen may cause the amplitude or frequency of the inputs to increase. The journal bearing acceleration data were processed as described in the following paragraphs to determine whether the winter factor is apparent at this point on the axle assembly

3.5.1.1 RMS G-Level Analysis

Acceleration data were collected over extensive sections of track in the Northeast Corridor and sections of the New Haven to Montreal routes (Section 3.4.3). The root-mean-squared (rms) amplitude of three acceleration data was calculated for a large number of points at various locations and speeds.

*Although the impacting at the wheel/rail interface is the prime source of inertial forces on the wheelset (disc brake assembly), the major portion of what is actually sensed by the accelerometers is the wheelset's elastic body responses (ringing) which may exceed the rigid body accelerations in magnitude and may be sustained in amplitude for an extended period of time depending on the amount of damping present.

The test data were processed by a filter network to recover the attenuation used when the data were recorded before reduction. To reduce the acceleration data a Nicolay Scientific 660 spectrum analyzer was used. The analyzer took a series of 16 samples of the test data and digitally processed the data samples to compute the rms values over selected bandwidths. The rms was determined for the acceleration data in the 2.5 to 1,000 Hz band and in the 2.5 to 500 Hz band in both the lateral and vertical directions at various train speeds. This processing was used for data from both runs. The data points were grouped according to bandwidth, zone (refer to Figure 3-6) and test run, then, plotted with amplitude versus speed in Figures 3-7 through 3-14. Curve fitting techniques were then employed to determine a continuous function to describe any trend indicated by the data. A power curve of the form $G_{\text{rms}}(s) = AS^B$ provided the best fit curves using the least-mean-squares method of fitting the curves.

The 2.5 to 500 Hz data are shown in Figures 3-11 through 3-14. These graphs clearly show a significant difference between both vertical and lateral accelerations experienced during the two runs. On 26 February the temperature was approximately 35°F, but prior to this date the temperature was well below freezing. The temperature in the south end of the Corridor (which was used for the comparison) was in the mid-fifties on the 8 March test. This area had been well above freezing for several weeks prior to the 8 March test run.

The acceleration levels and supporting temperature history strongly suggest that track freezing causes a significant increase in the acceleration resulting from wheel-to-rail impacts.

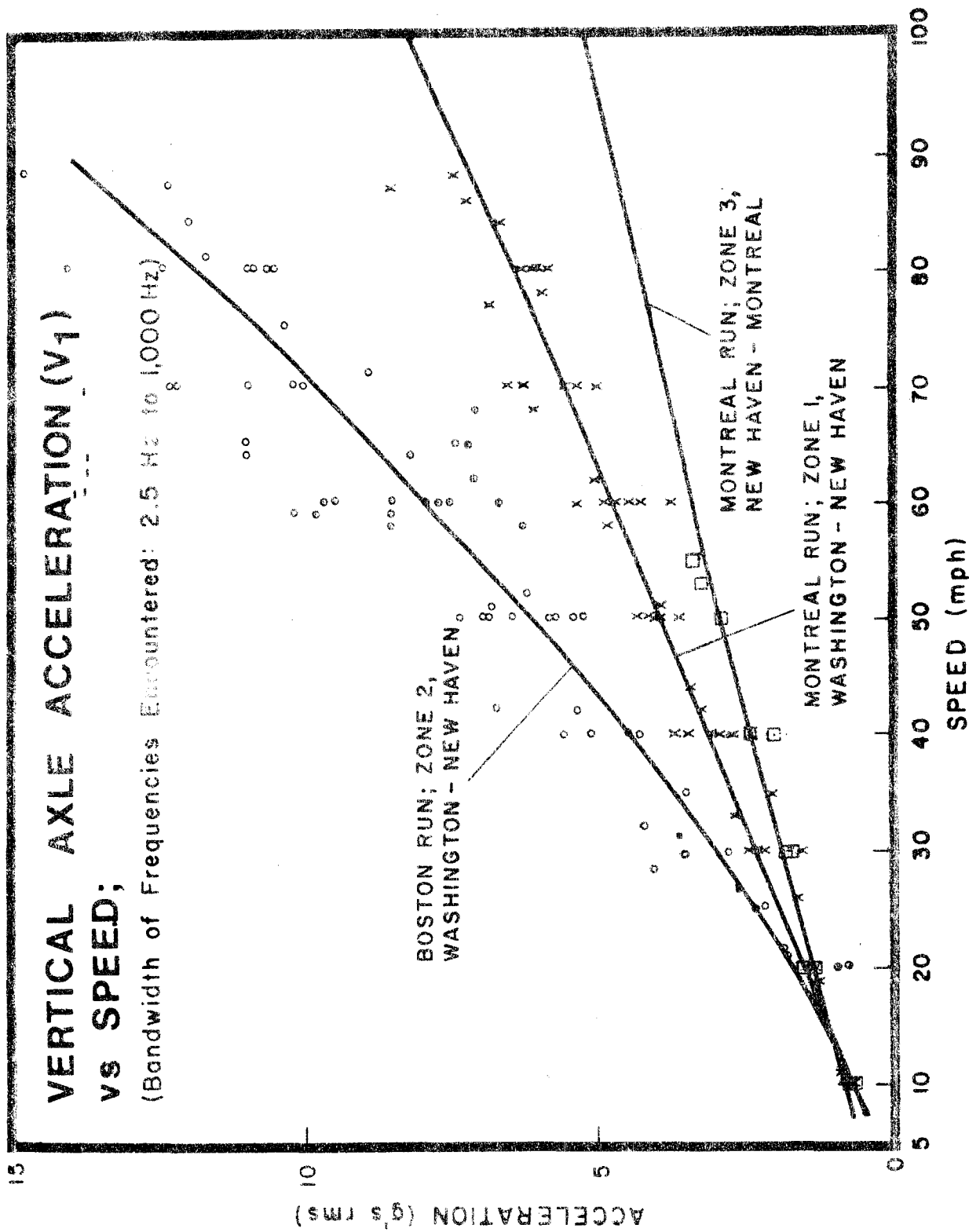


Figure 3-7. Vertical Axle Acceleration (V_1) vs Speed
(Bandwidth 2.5 Hz to 1000 Hz)

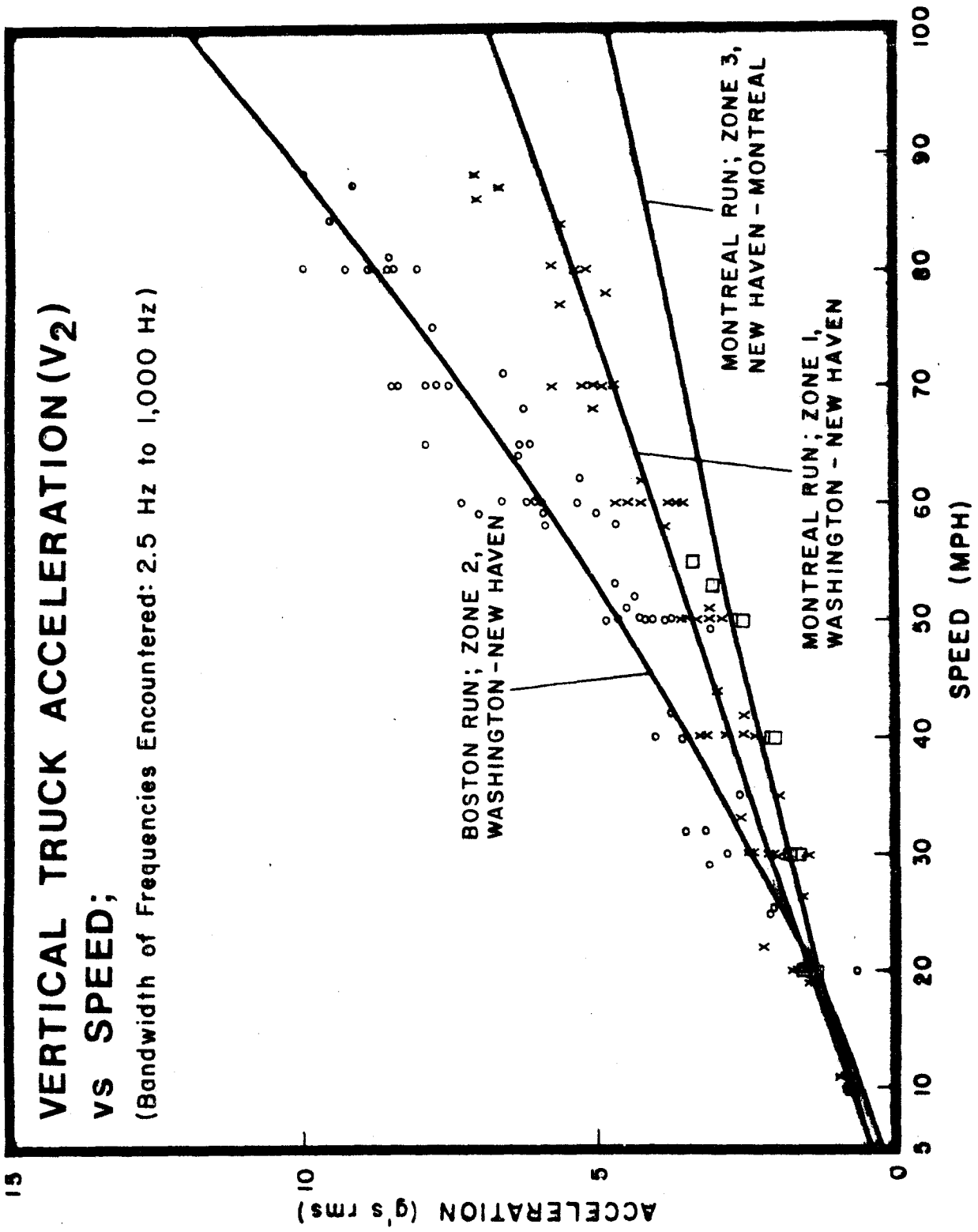


Figure 3-8. Vertical Truck Accelerations (V₂) vs Speed (Bandwidth 2.5 Hz to 1000 Hz)

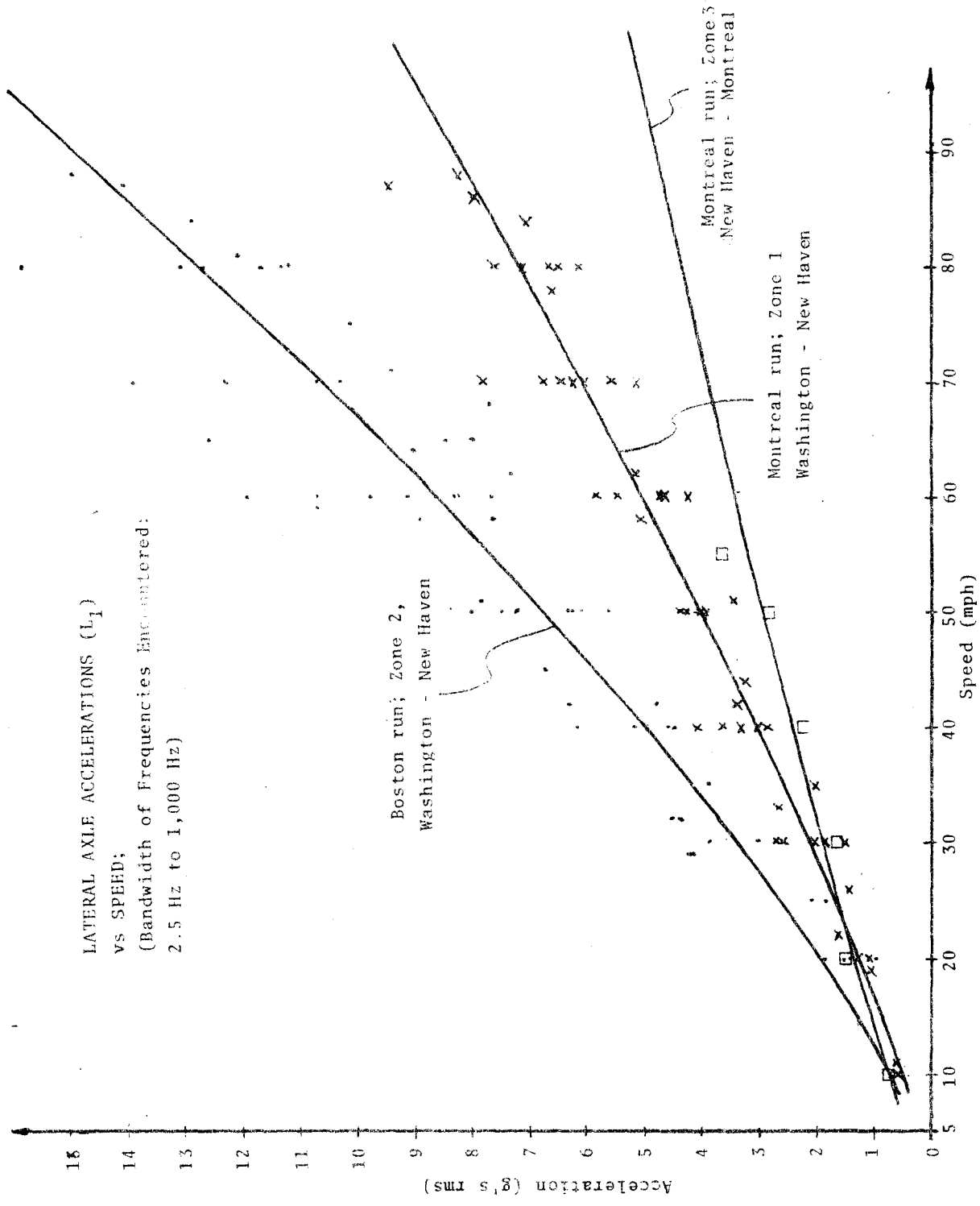


Figure 3-9. Lateral Axle Accelerations (L_1) vs Speed
 (Bandwidth 2.5 Hz to 1000 Hz)

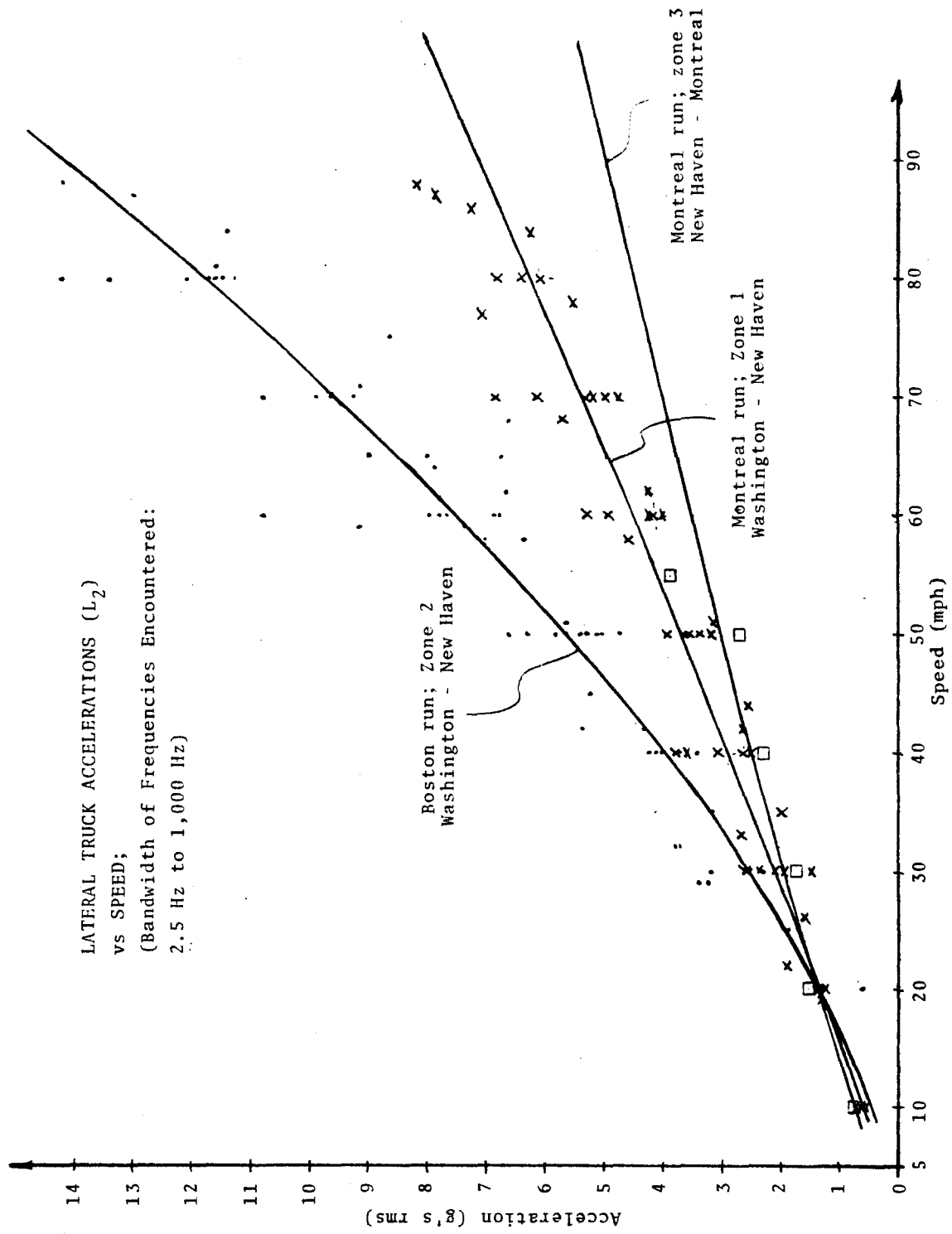


Figure 3-10. Lateral Truck Accelerations (L_2) vs Speed
(Bandwidth 2.5 Hz to 1000 Hz)

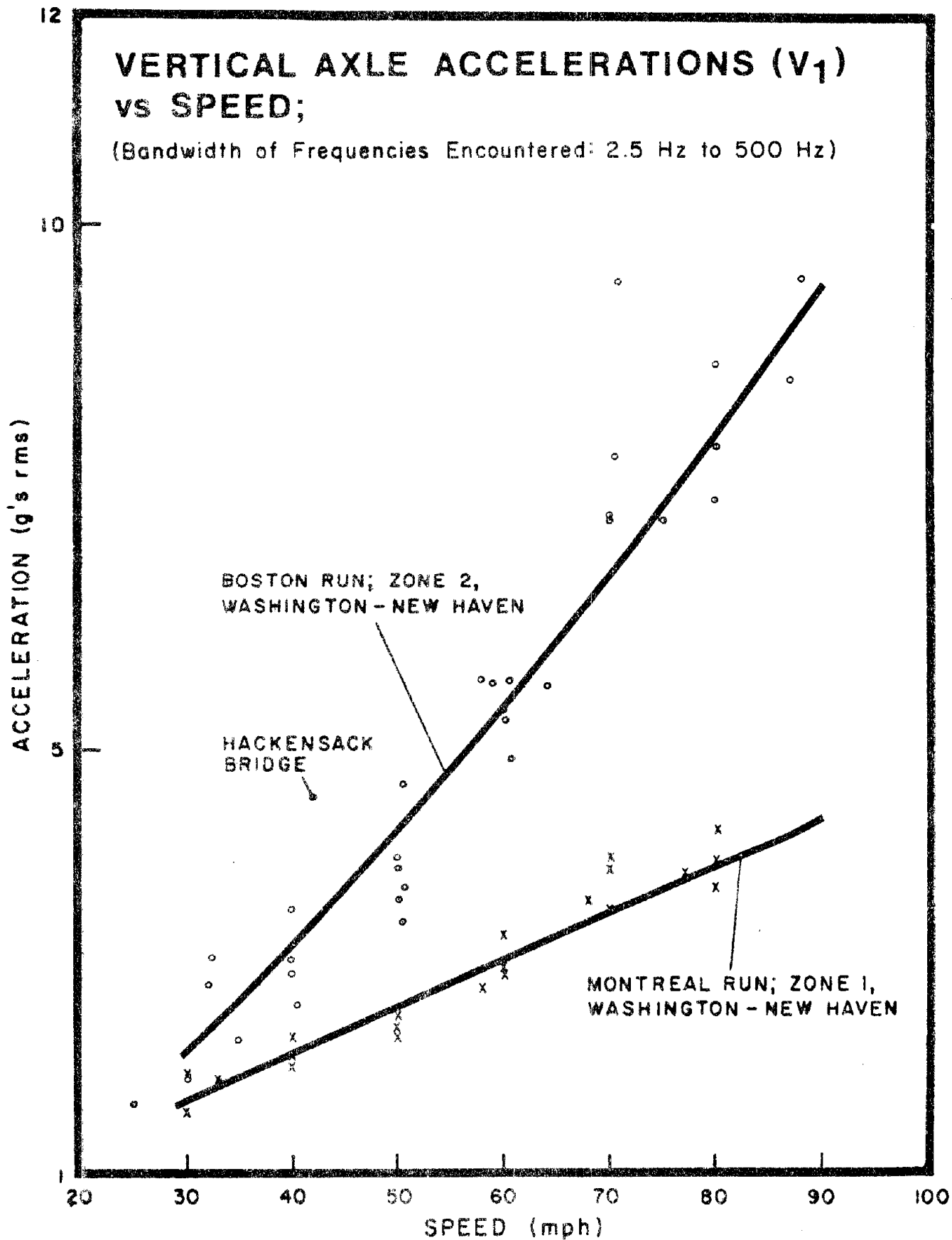


Figure 3-11. Vertical Axle Accelerations (V_1) vs Speed
(Bandwidth 2.5 Hz to 500 Hz)

VERTICAL TRUCK ACCELERATIONS (V_2) vs SPEED;

(Bandwidth of Frequencies Encountered: 2.5 Hz to 500 Hz)

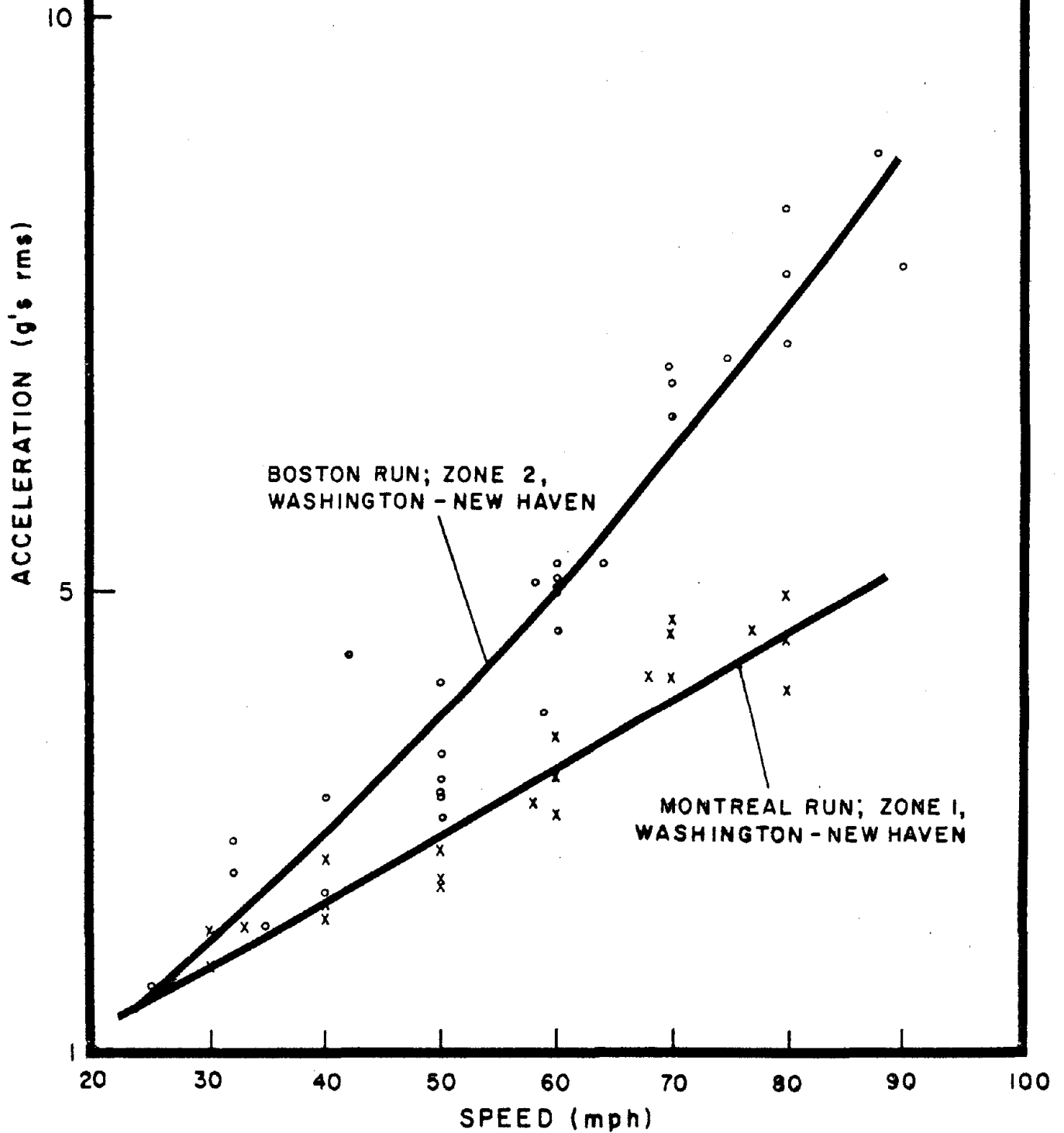


Figure 3-12. Vertical Truck Accelerations (V_2) vs Speed (Bandwidth 2.5 Hz to 500 Hz)

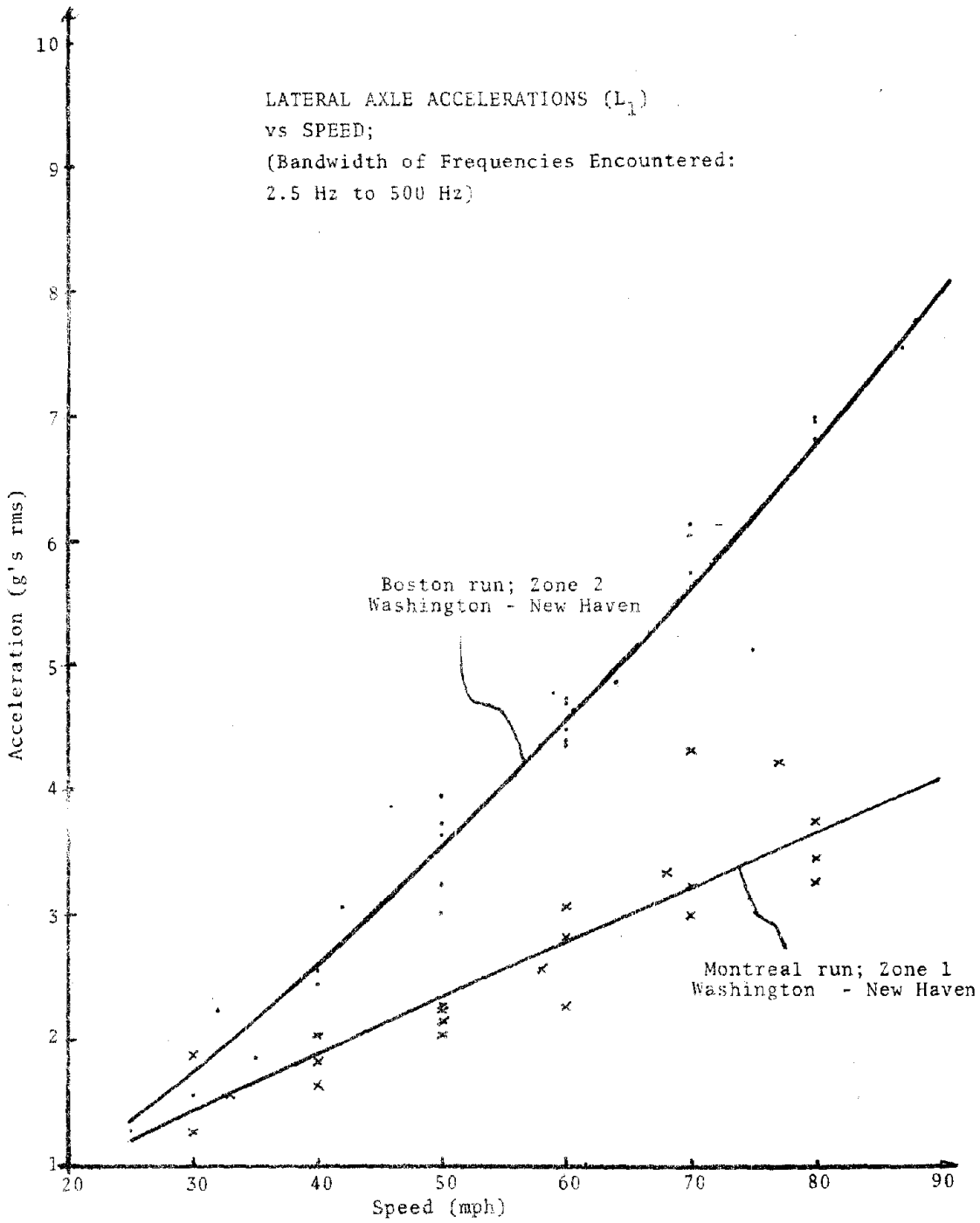


Figure 3-13. Lateral Axle Accelerations (L_1) vs Speed (Bandwidth 2.5 Hz to 500 Hz)

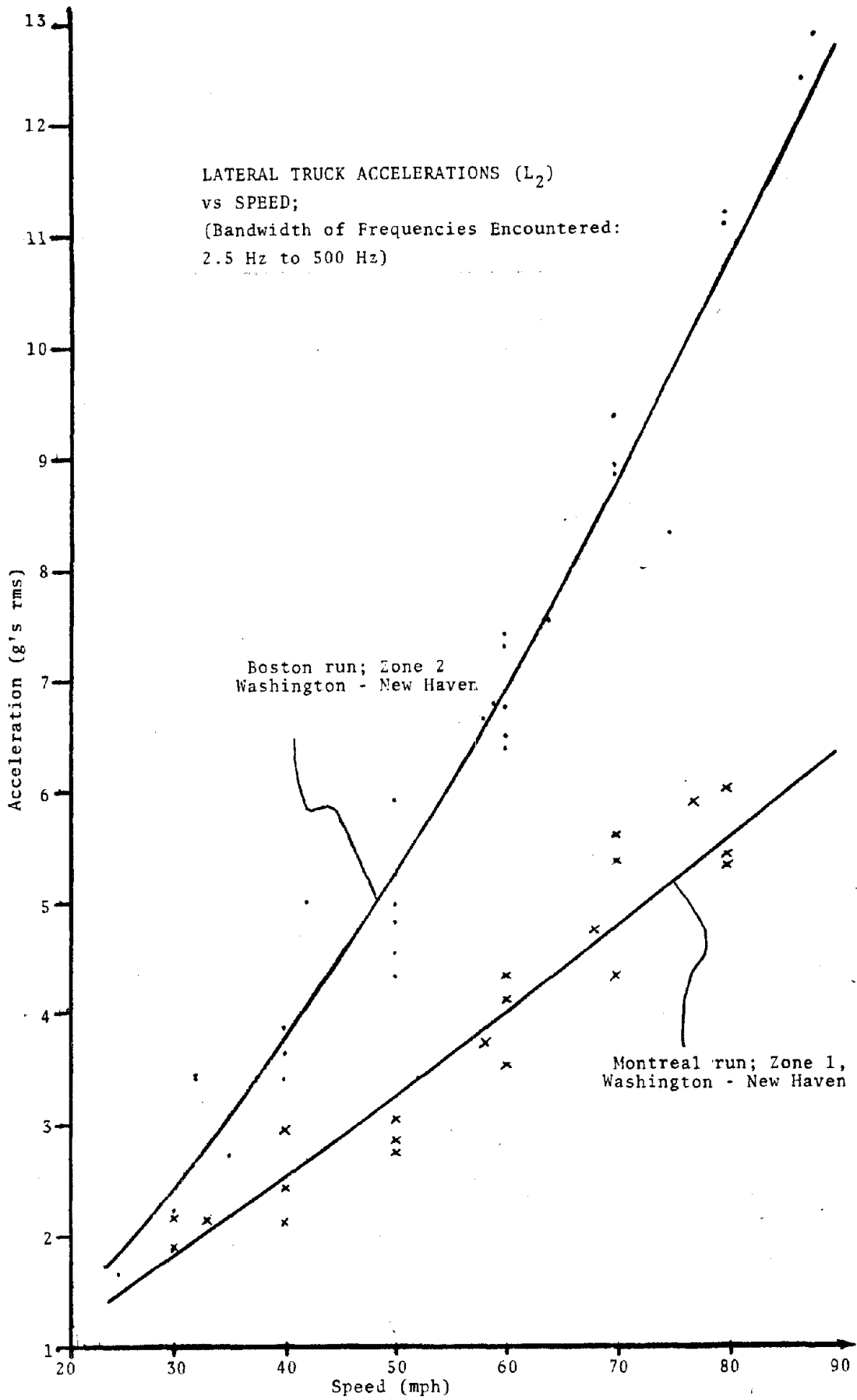


Figure 3-14. Lateral Accelerations (L_2) vs Speed
(Bandwidth 2.5 Hz to 500 Hz)

To further evaluate the significance of this finding, the data were reprocessed to determine the rms of acceleration levels for all frequencies between 2.5 and 500 Hz. This was done using the bandwidth of 0 to 500 Hz instead of 0 to 1,000 Hz to evaluate whether a significant change had occurred in the band of frequencies which are most likely to force vibration of the brake assembly. The results of the 0 to 500 Hz analysis are shown in Figures 3-11 through 3-14. These graphs show that the same trend exists and that the spread between frozen and unfrozen track is even greater when the data are restricted to the lower frequencies.

Figures 3-13 and 3-14 show that the lateral accelerations were greater on the truck than on the axle. The lateral accelerations were significantly reduced when the bandwidth was restricted to 500 Hz. This occurred because the lateral acceleration data contained a significant component at 600 Hz which was eliminated by the restricted bandwidth.

Some data from Zone 3 of the Montreal run were processed in addition to the primary zones used for comparison. These data from New Haven to Montreal are shown in Figures 3-7 through 3-10. The lateral and vertical accelerations from 0 to 1000 Hz appear to have a definite trend which showed that the accelerations in this zone were lower than the data from the other zones.

This same zone was not surveyed on any other occasion so the acceleration level cannot be correlated to temperature. Zone 3 is constructed from much lighter rail than the other test sections (90 pound versus 130/140 pound). This difference is considered to be the reason for the difference in acceleration levels.

3.5.1.2 RMS Spectral Analysis

Acceleration data were analyzed for significant frequency content at various locations and speeds. Typical spectral graphs are shown in Figures 3-15 and 3-16. These rms spectral graphs show a comparison between the accelerations measured on the axle and the truck. At frequencies below 500 Hz, the results are nearly identical. Around 800 to 900 Hz, the axle accelerometer levels are significantly higher than the truck in both the vertical and lateral data. This difference is caused by the journal bearing shock ring which is discussed in Section 3.5.

The patterns of these spectral graphs suggest that the system has some characteristic resonant frequencies and modes which are being driven by a repetitive impulse which occurs at approximately 12 cycles/sec. The data, taken at 77 mph when the wheels were rotating at about 12 revolutions/sec, indicate that wheel defects force the system to resonate at its natural frequencies as illustrated by Figures 3-15 and 3-16.

A comparison of the spectral graphs (Figures 3-17 thru 3-20) for 26 February with those for 8 March show a significant difference in the system response for frozen and unfrozen track. The spectrums from the 8 March (unfrozen) run are shown in Figure 3-18. Even at the higher speeds, it is difficult to pick out marked system frequencies except at 880 Hz. Figure 3-17 shows the spectral graphs from the frozen track (26 February run). This graph is markedly different. As seen from these two figures, the axle accelerations are similar below 275 Hz; however, the resonance response is much larger for the 26 February run. To further show this difference the acceleration data for the two runs are plotted together in Figure 3-21. This graph shows that there were two major differences between the frozen and unfrozen conditions.

RMS SPECTRAL GRAPH 77 MPH
OF VERTICAL ACCELERATIONS

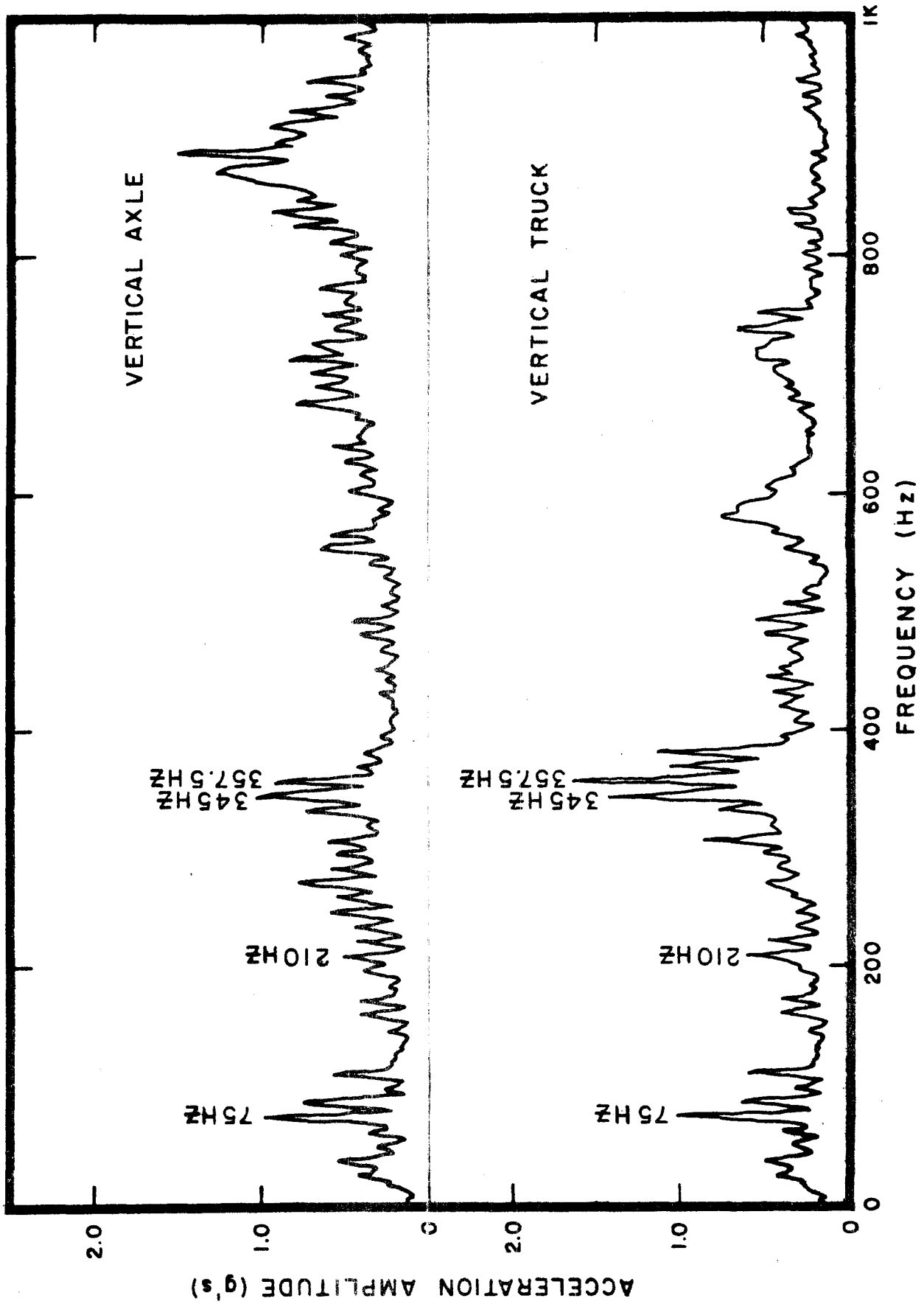


Figure 3-15. RMS Spectral Graph of Vertical Accelerations at 77 mph

RMS SPECTRAL GRAPH 77 MPH
OF LATERAL ACCELERATIONS

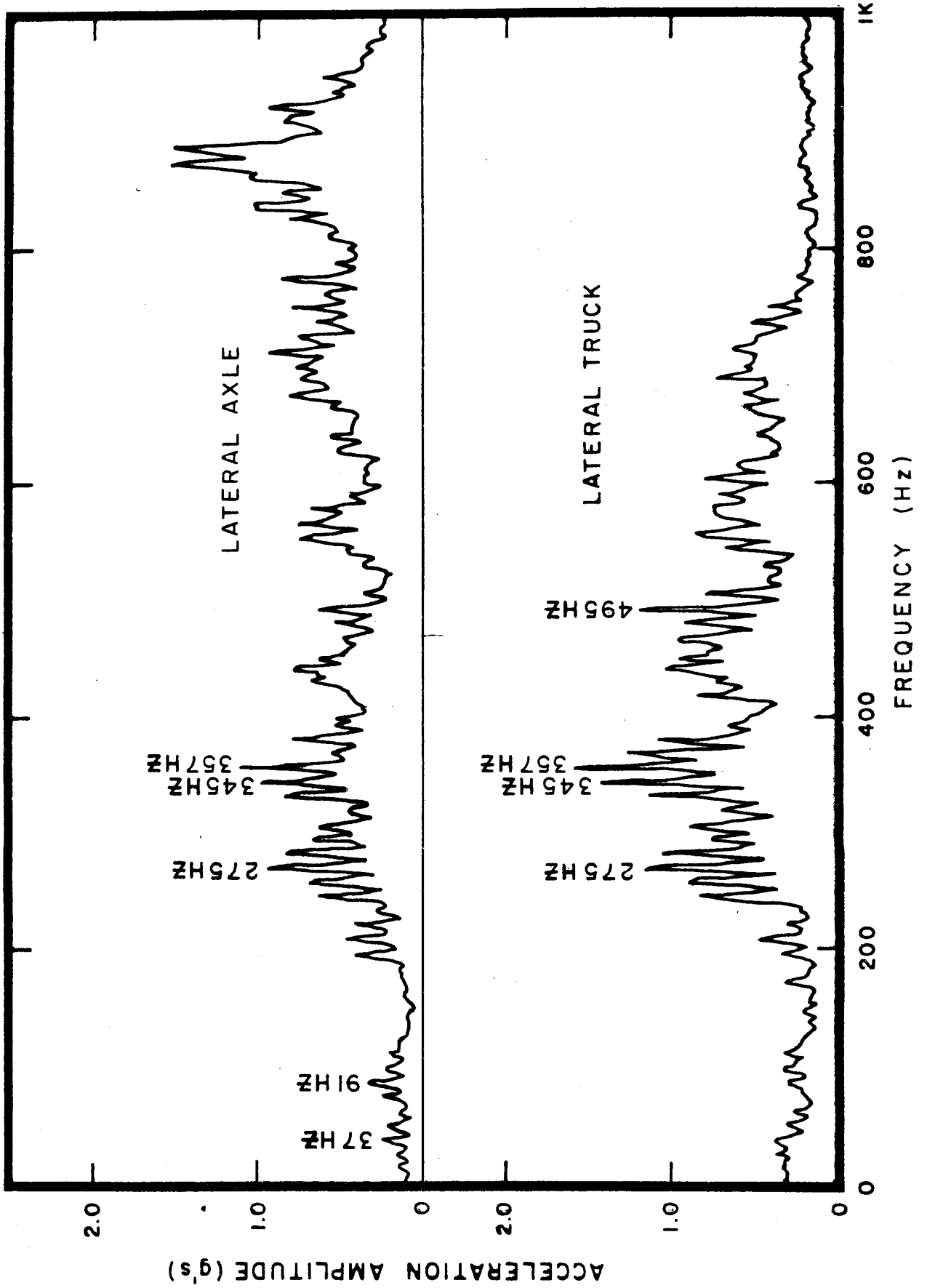
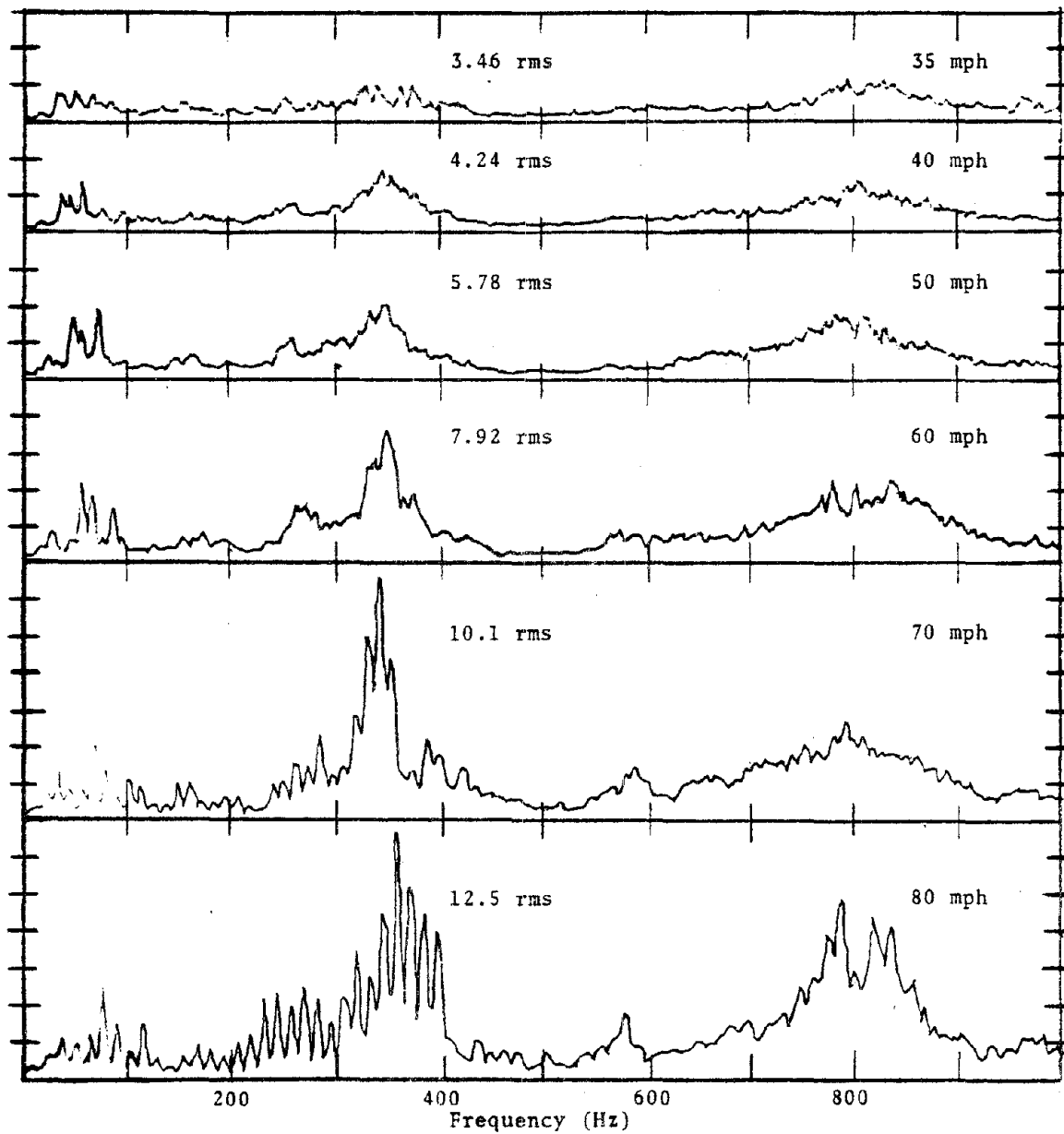
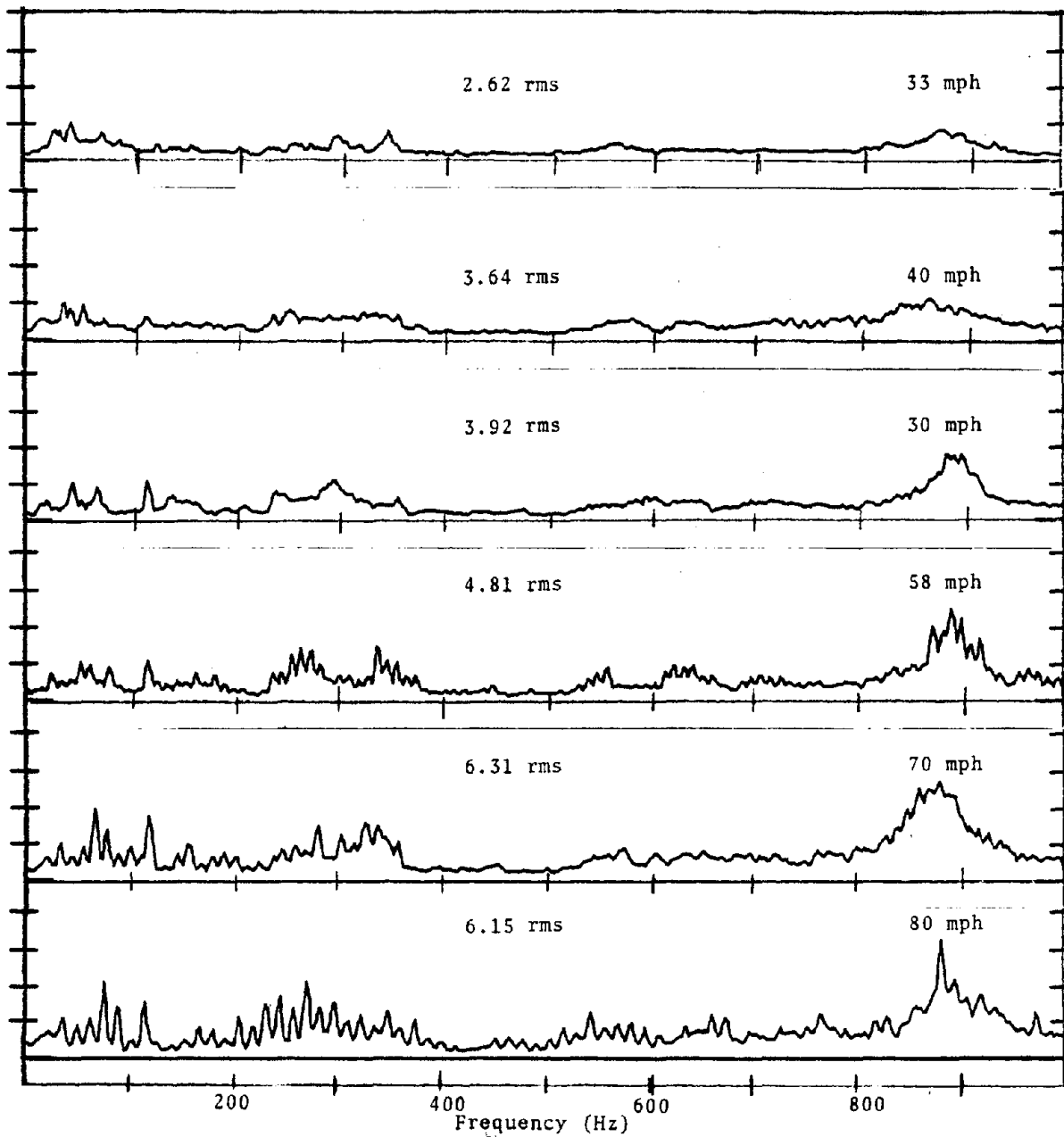


Figure 3-16. RMS Spectral Graphs of Lateral Accelerations at 77 mph



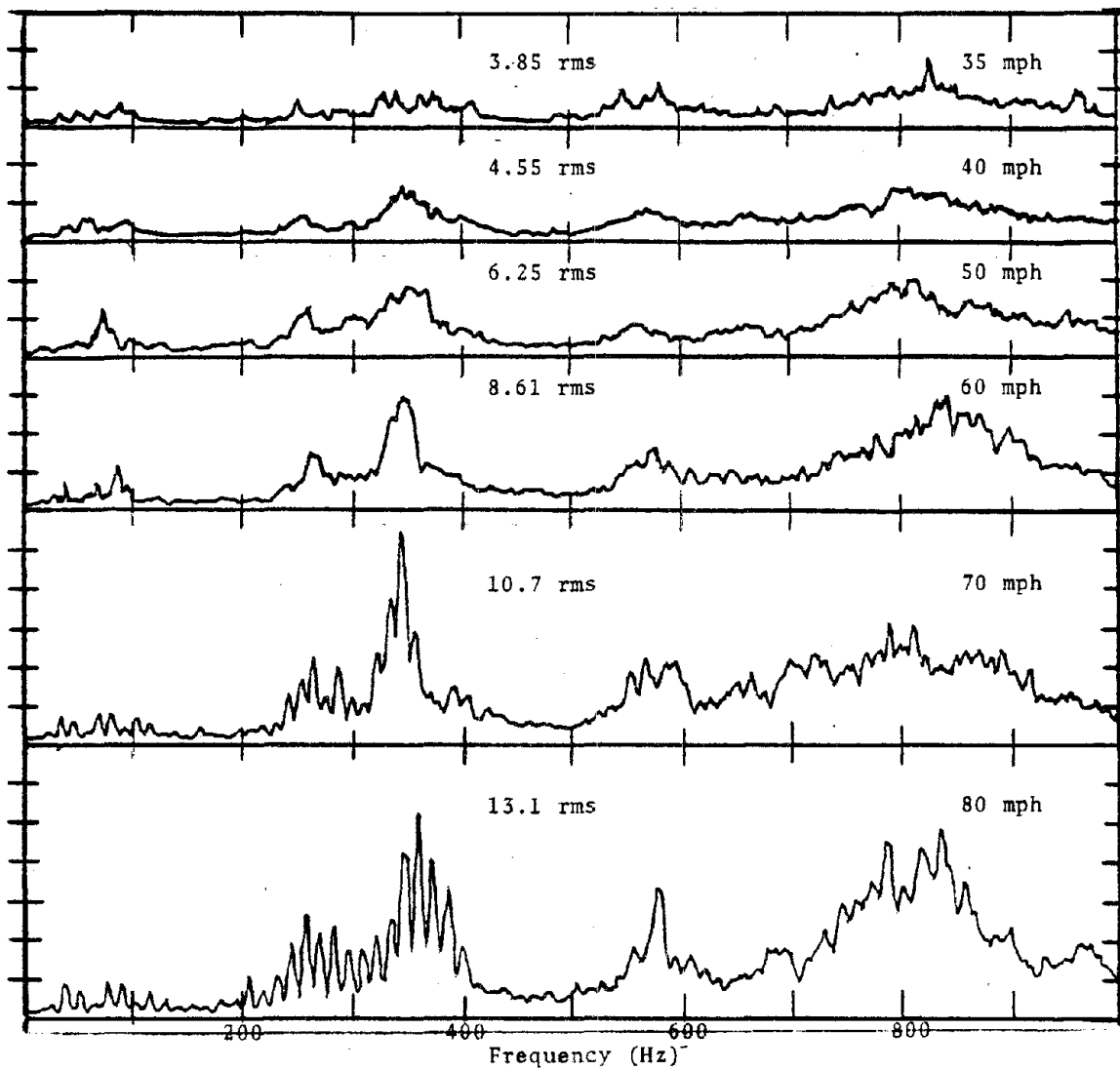
Vertical Axle Accelerations
 Amp = 0.5 g/div
 Boston Run (26 February 1979)
 Chesaco Park (MP 89.0) to Middle River (MP 86.3)

Figure 3-17. Vertical Axle Accelerations (Frozen)



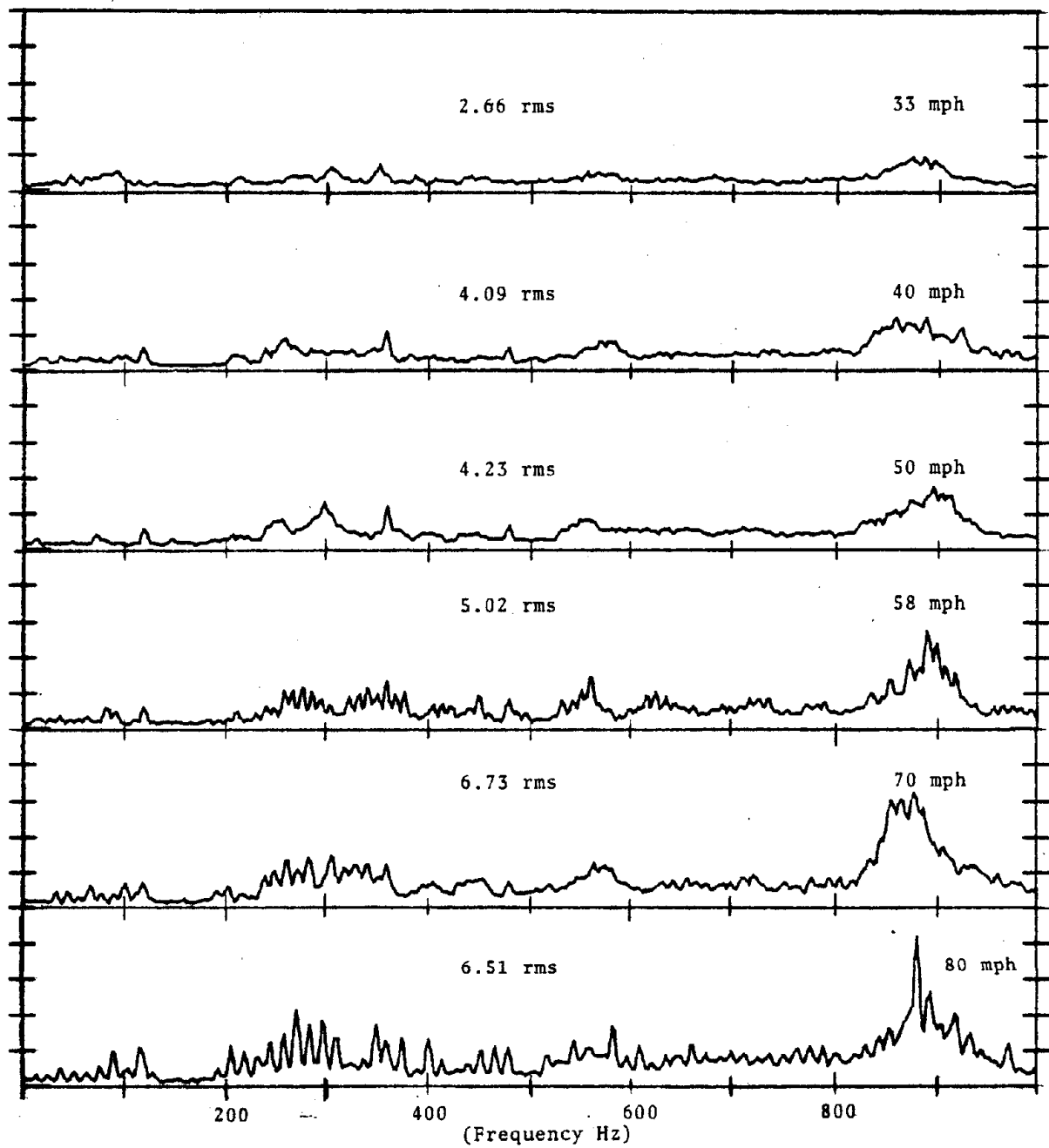
Vertical Axle Accelerations
 Amp = 0.5 g/div
 Montreal Run (8 March 1979)
 Marcus Hook (MP 17.4) to Lynne (MP 11.9)

Figure 3-18. Vertical Axle Accelerations (Unfrozen)



Lateral Axle Accelerations
 Amp = 0.5 g/div
 Boston Run (26 February 1979)
 Chesaco Park (MP 89.0) to Middle River (MP 86.3)

Figure 3-19. Lateral Axle Accelerations (Frozen)



Lateral Axle Accelerations
 Amp = 0.5 g/div
 Montreal Run (8 March 1979)
 Marcus Hook (MP 17.4) to Lynne (MP 11.9)

Figure 3-20. Lateral Axle Accelerations (Unfrozen)

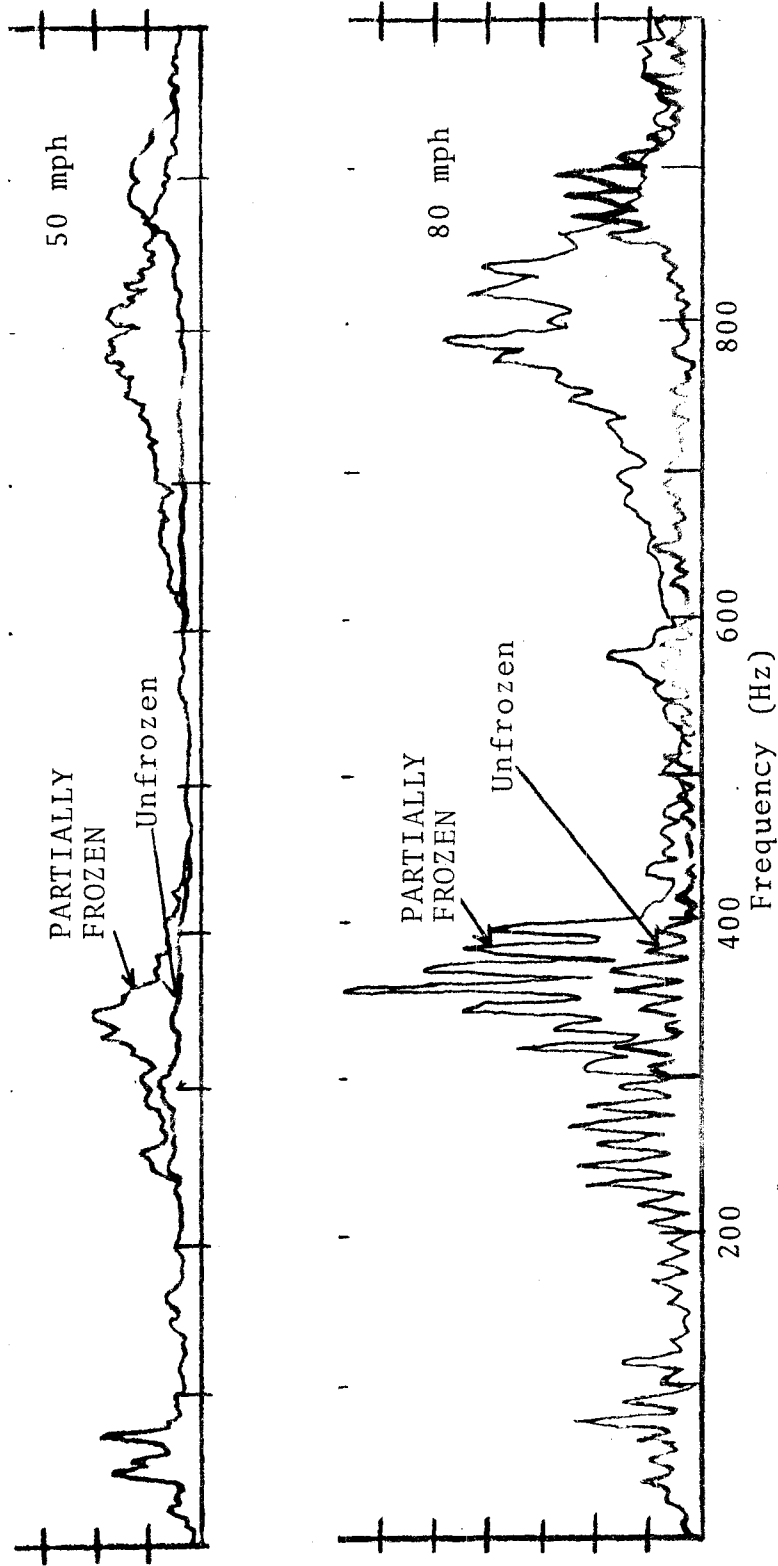


Figure 3-21. Comparison of Frozen and Unfrozen Vertical Axle Accelerations

- The high frequency resonant characteristics appear to have shifted frequency. The resonance peaks are at 880 Hz on the unfrozen run and 800 Hz on the frozen run.
- Resonant response at 800 to 900 Hz and at 300 to 400 Hz bands was significantly higher during the frozen run.
- Significant resonant response at 300 to 400 Hz and 600 Hz was seen in the axle lateral data for the frozen run.

3.5.1.3 Instantaneous Time Histories

Instantaneous time-enhanced graphs were produced from the journal bearing acceleration data. The plots of the vertical and lateral axle accelerations, and of the vertical and lateral truck accelerations are shown in Figures 3-22 through 3-25. These plots were generated by summing 32 data samples using the spectrum analyzer in the instantaneous time sampling mode. In this mode the collection of the data samples is triggered and occurs at a set time after a peak is sensed which exceeds a set threshold.

Through this method, periodic events are emphasized while random events are attenuated. As such the time-enhanced plots show a repetitive or periodic signature for the acceleration data. An examination of the plots (Figures 3-22 through 3-25) shows that the same peaks occurred on each revolution of the wheel. These plots show that the defects in the wheel are input to the system and that even minor defects cause significant acceleration inputs.

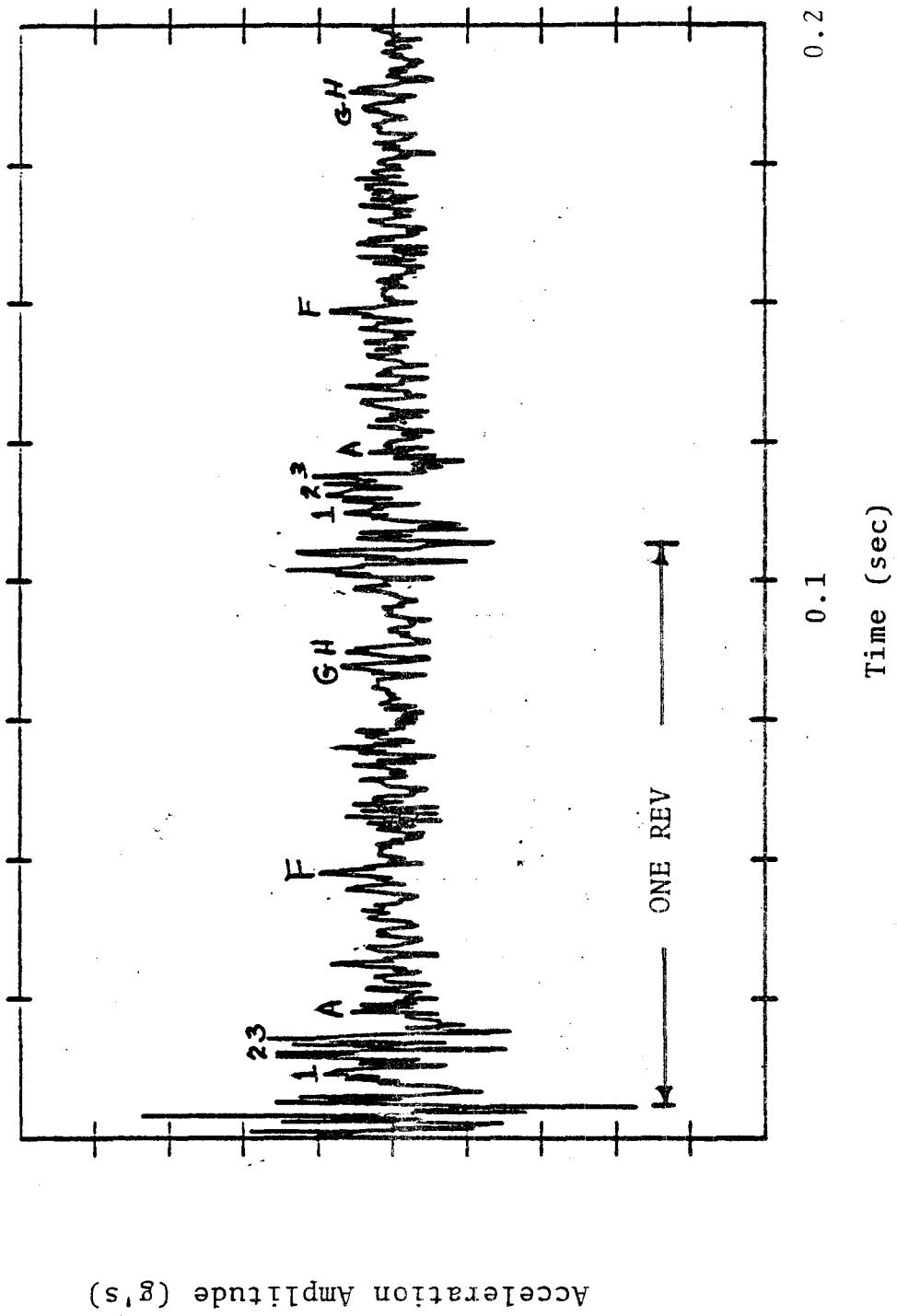


Figure 3-22. Instantaneous Vertical Axle Accelerations (V₁)
Time Enhanced - 32 Samples from the Boston Run

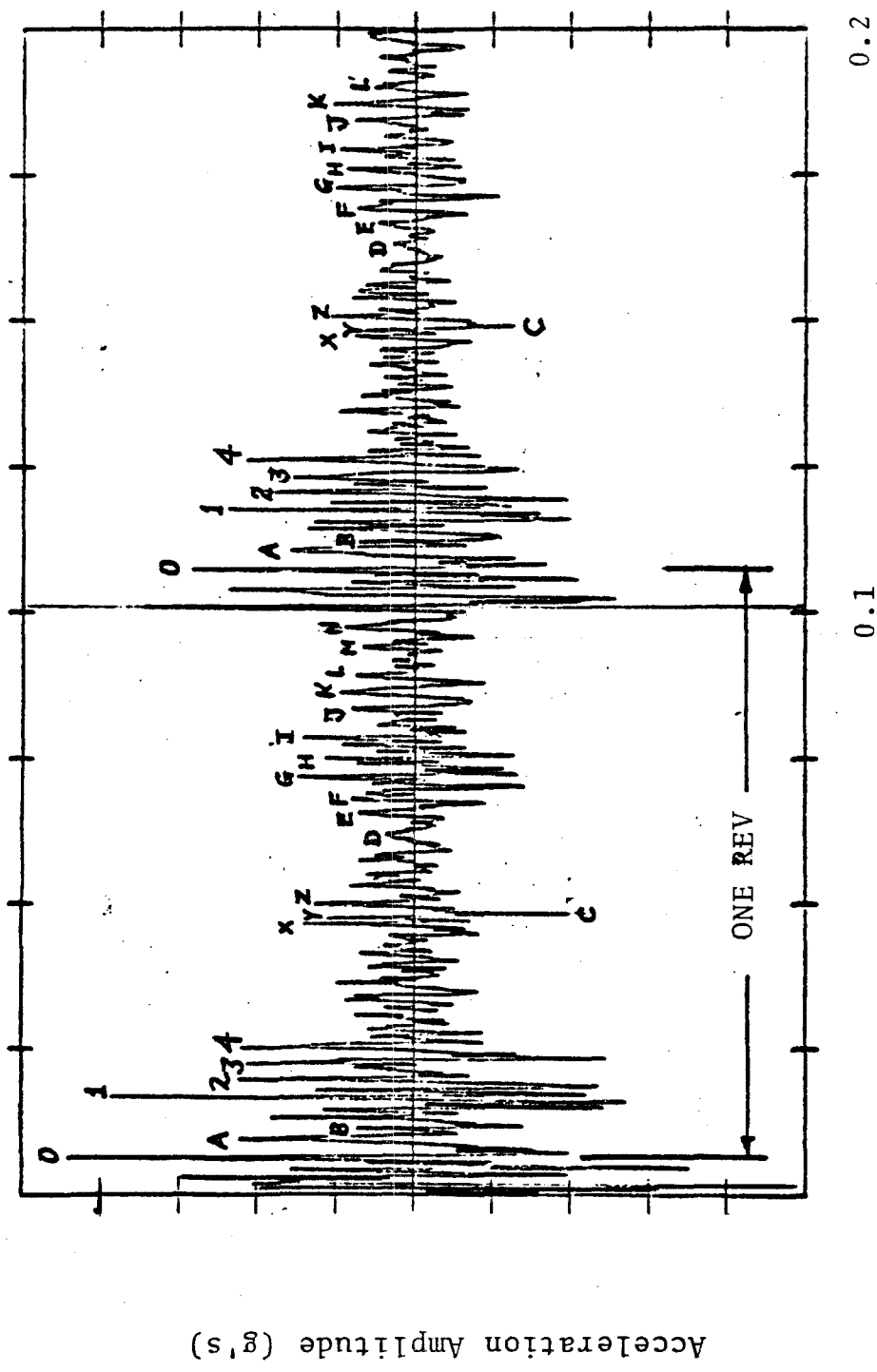


Figure 3-23. Instantaneous Lateral Axle Accelerations (L₁)
 Time Enhanced - 32 Samples from the Boston Run

Acceleration Amplitude (g's)

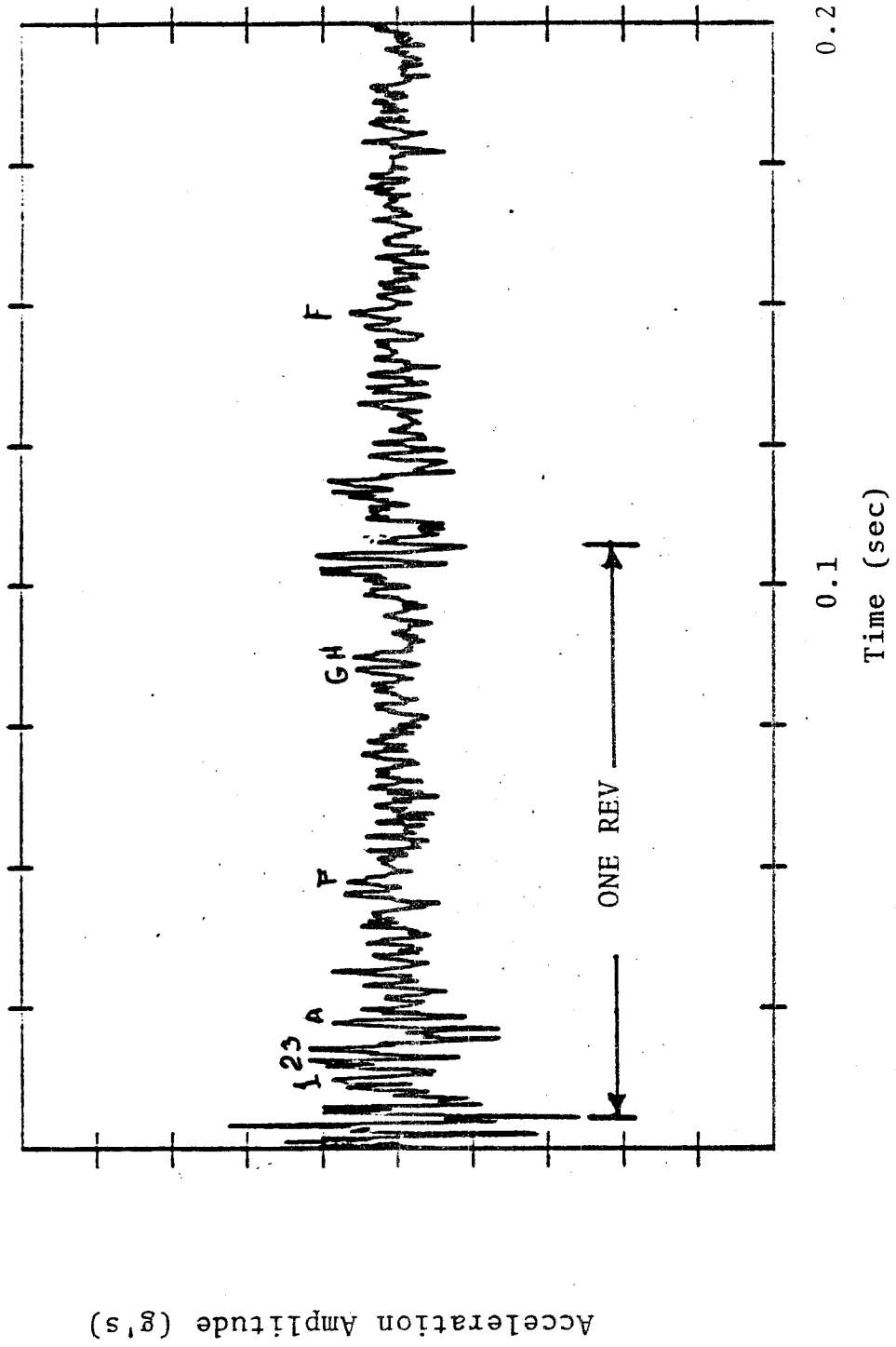


Figure 3-24. Instantaneous Vertical Truck Accelerations (V₂)
 Time Enhanced - 32 Samples from the Boston Run

Acceleration Amplitude (g's)

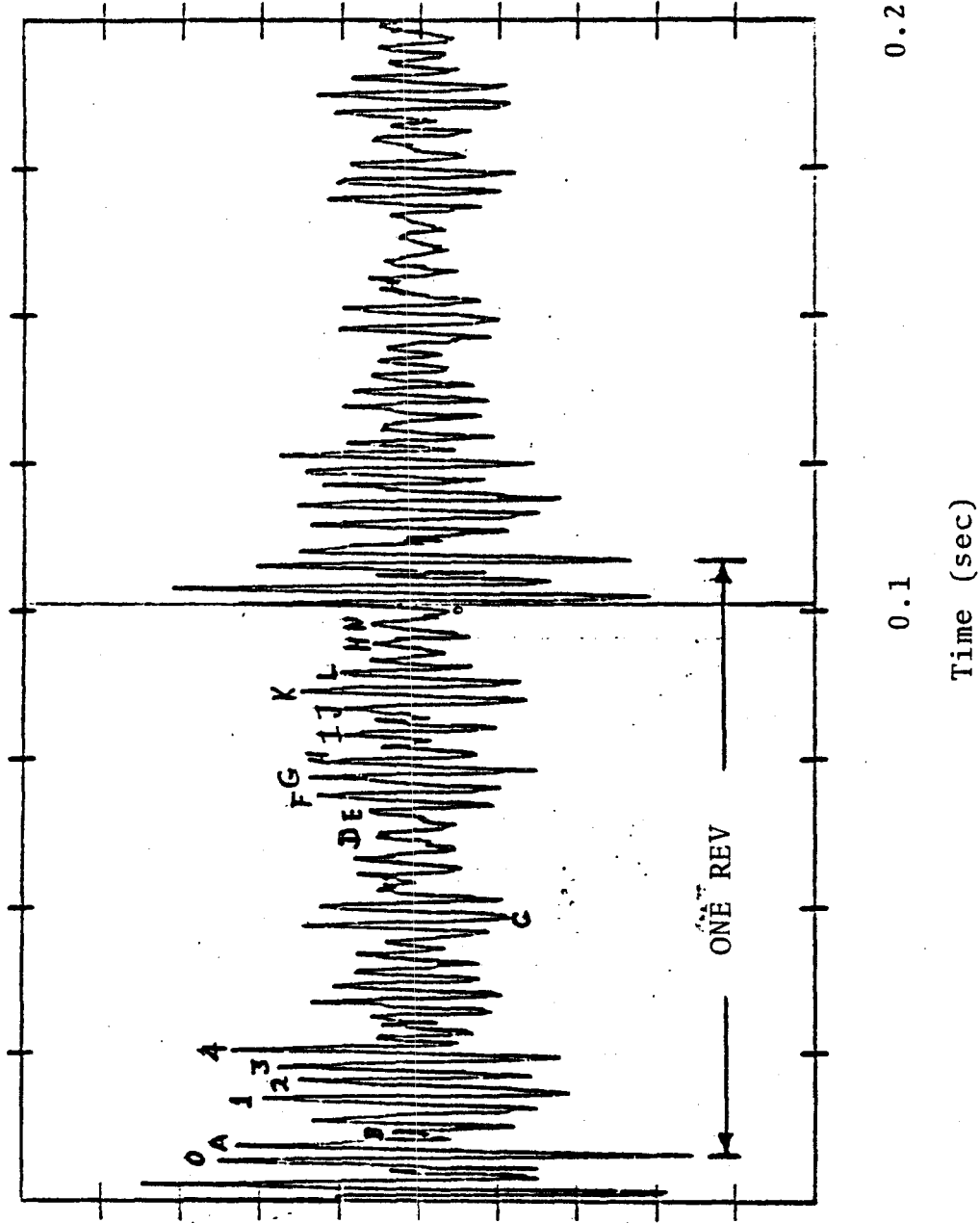


Figure 3-25. Instantaneous Lateral Truck Accelerations (L2)
Time Enhanced - 32 Samples from the Boston Run

A correlation between the time enhanced accelerations and wheel defects can be developed by studying the wheel maps in Appendix A. The wheel maps show the actual defects which were found on the wheels after the test run. Starting with the most severe defect, the defect pattern can be compared with the time-enhanced plots to show that the defects are only one type of input to the resonance system. However, the runs and the spectral analyzer plots show that the wheel defects account for only one-third of the driving force and that the severity of the response is determined more by damping than by the defects. This is substantiated by an analysis of the data from the frozen and unfrozen runs. From this analysis, the most severe accelerations were observed during the frozen run even though the defects were larger during the unfrozen run. These defects became significantly worse between the frozen (26 February) and the unfrozen (8 March) runs, while the acceleration levels were smaller by a factor of over two to one.

In addition, even the smallest defects in the wheel tread cause major accelerations to the wheel/axle system. For this test, the most severe defect in the wheelsets were not beyond the condemning limits. However, even minor flakes on the surface of the wheel caused severe acceleration inputs.

3.5.1.4 Exceedence Analysis

Exceedence analysis was used to determine the extent to which the disc brake assembly is subjected to accelerations which may result in significant inertial forces on the assembly. This analysis is confined to frequencies below 1,000 Hz since higher frequencies do not generate sufficient displacements to significantly contribute to the Knorr disc-brake, resilient-pin failure problem. In other words, an acceleration must occur at a sufficient amplitude and for a sufficient length of

time to cause movement and/or deformation of the disc brake components.

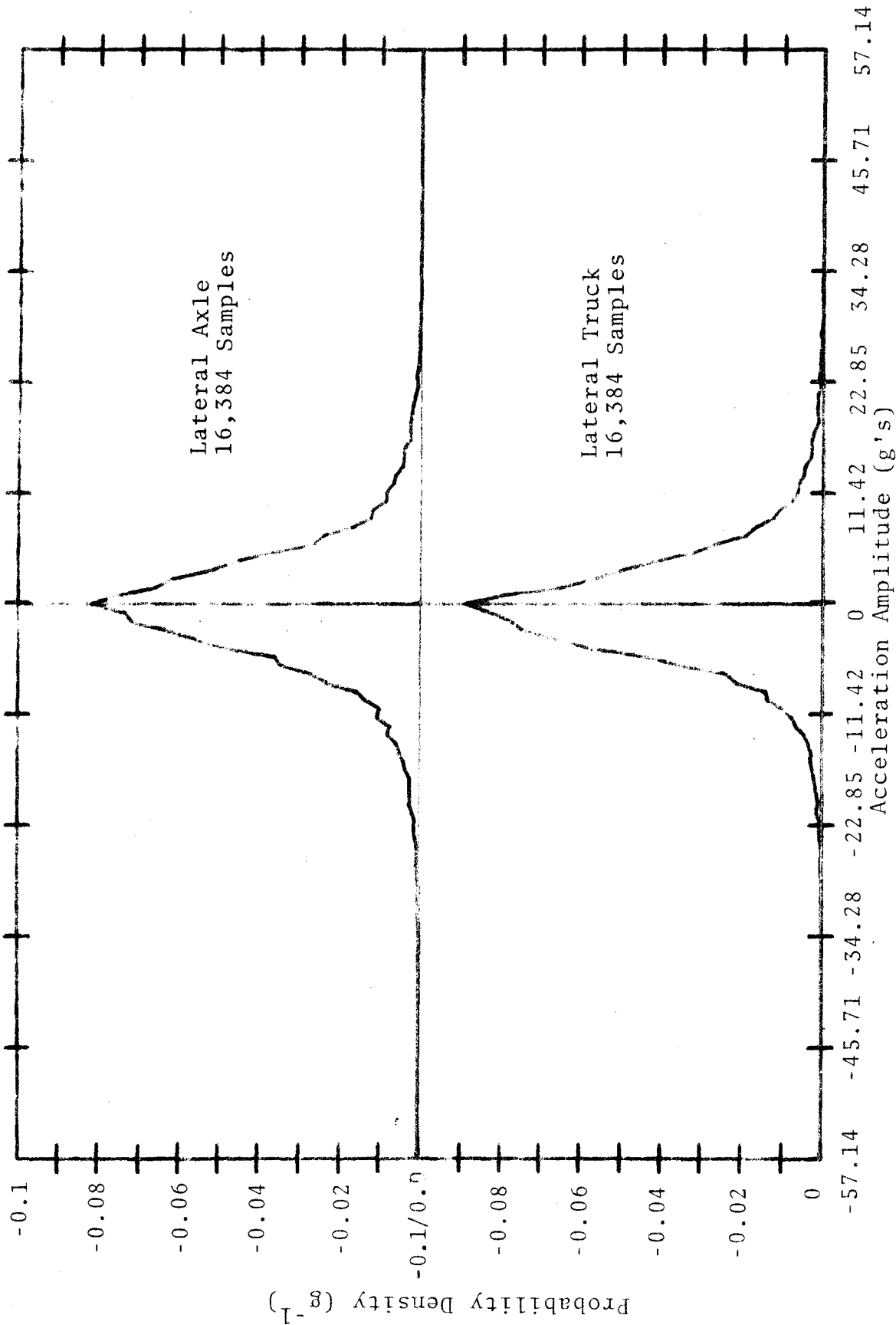
Analysis began by measuring the instantaneous amplitude of a large number of the accelerations sensed in one of the four positions monitored. From this large sample, the probability density function as illustrated in Figure 3-26 was developed. The probability that accelerations will have an amplitude between any two discrete levels is determined by integrating the value of the probability density function (PDF) between the two levels.

$$P \{g_1 < g < g_2\} = \int_{g_1}^{g_2} \text{PDF}(g) dg \quad (3.1)$$

Inspection of the curve shape of the PDF provides information concerning the extent to which the data trends are subject to analysis by standard statistical methods. Figure 3-26 indicates that the lateral axle acceleration data follows the trend of a standard normal distribution described by

$$\text{PDF}(g) = 0.817e^{-g^2/47.62} \quad (3.2)$$

Subsequent integration of the PDF leads to the cumulative distribution function (CDF) of Figure 3-27. The left axis of the CDF, normally shown with values of zero to one, has been multiplied by 100 percent to convert the data interpretation to percent time exceedence. This is reasonable since the initial data sample was collected from accelerations whose amplitude was time variant. The amplitude samples were acquired by measuring the average acceleration amplitude during very short increments of time. From the CDF in Figure



Probability Density Function 0 - 1000 Hz Bandwidth
 Boston Run (26 February 1979)
 North of Susquehanna River (MP 57.0)
 Speed 64 mph, Tape 3 - CTR 3351

Figure 3-26. Probability Density Function (PDF) at Bandwidth 0 to 1000 Hz

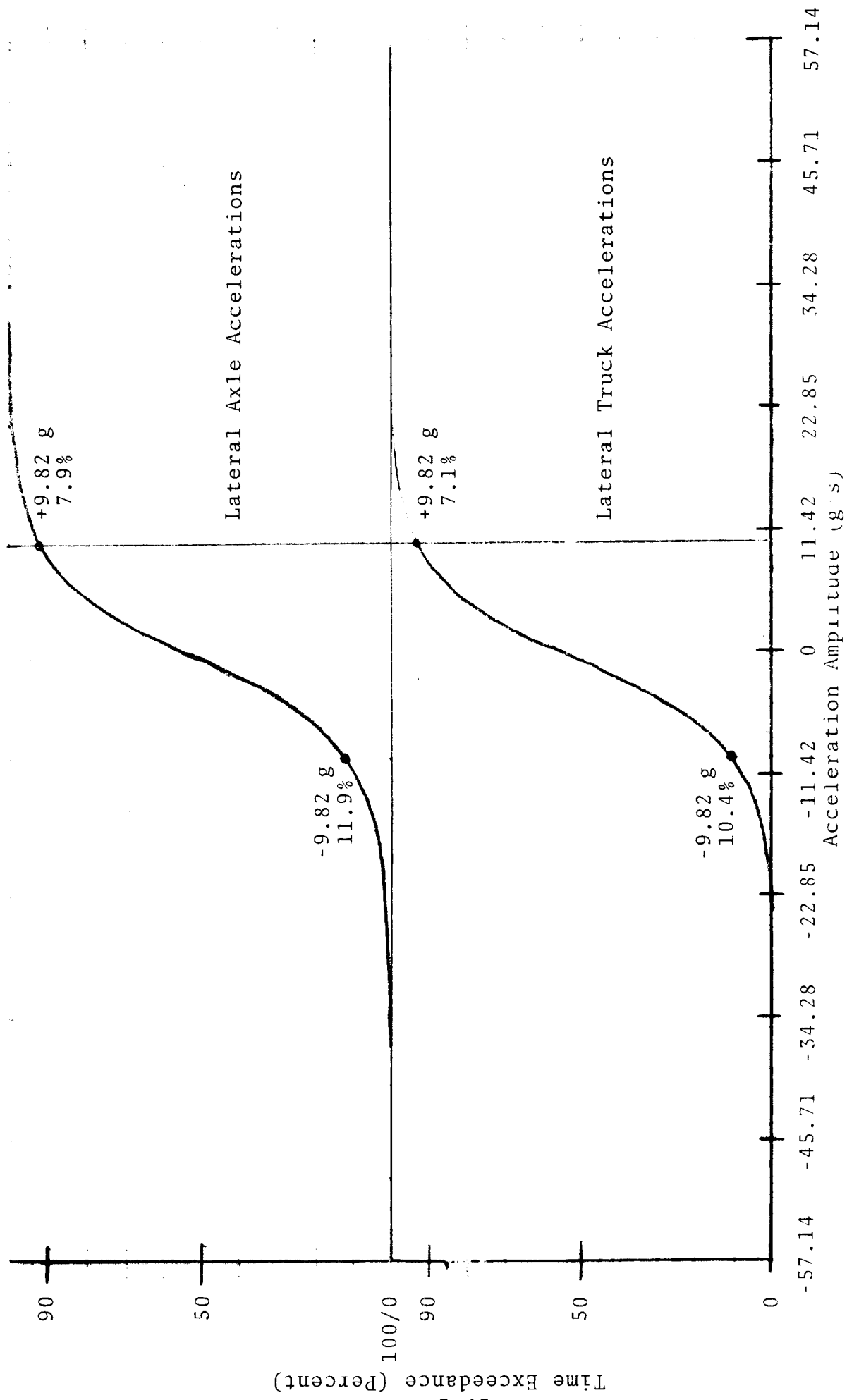


Figure 3-27. Cumulative Distribution Function Obtained from the Integration of a PDF

3-27, the percent time that acceleration levels exceed some selected threshold value (as illustrated by the vertical lines drawn through -9.82 g's and +9.82 g's) can be determined by summing the percent time that amplitudes are more negative than -9.82 g's with the percent time that amplitudes are more positive than +9.82 g's. The acceleration data for this example were filtered to allow only those accelerations with frequencies between zero and 1,000 cycles per second to be present in the sample. Percent time exceedence (%tE) for the 1,000 Hz band-limited data at the 5 g, 10 g, 15 g and 20 g exceedence levels has been calculated from this CDF and plotted in Figure 3-28.

The entire procedure is repeated by filtering the acceleration data so that the highest frequency in the data is successively reduced to 500 Hz, 200 Hz and 100 Hz.

Data points describing each of the exceedence levels are then joined by a trend curve. This is done for vertical axle accelerations in Figure 3-28 and lateral axle accelerations in Figure 3-29.

These curves indicate that the larger %tE is associated with the higher frequencies. An example of the use of %tE is described in the next section.

Percent time exceedence provides an indication of the proportion of running time that the wheelset is subjected to accelerations which exceed a specified g value. In this study percent time exceedence (%tE) was assumed to be a function of three independent variables:

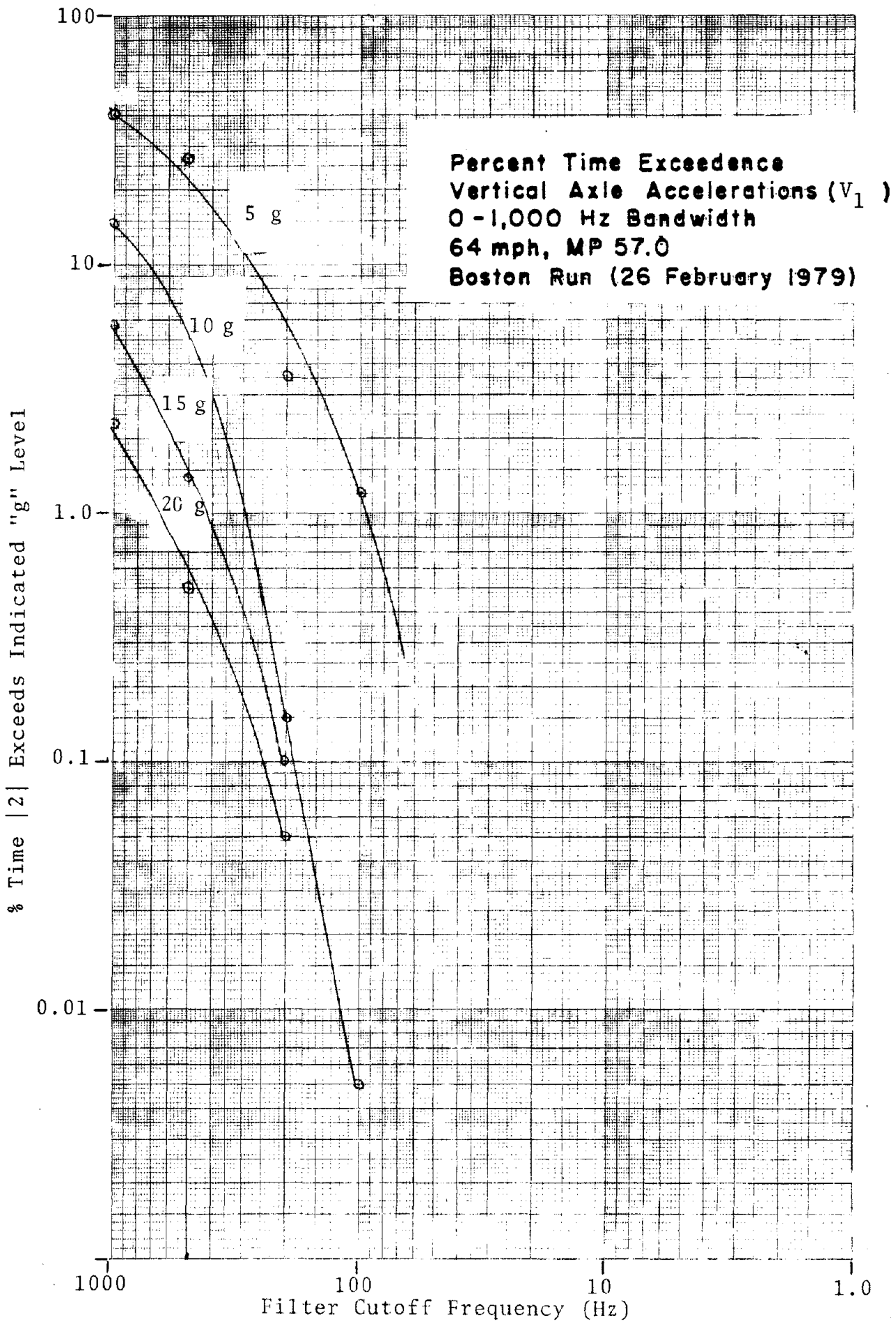


Figure 3-28. Percent Time Exceedance (%tE) of Vertical Axle Accelerations

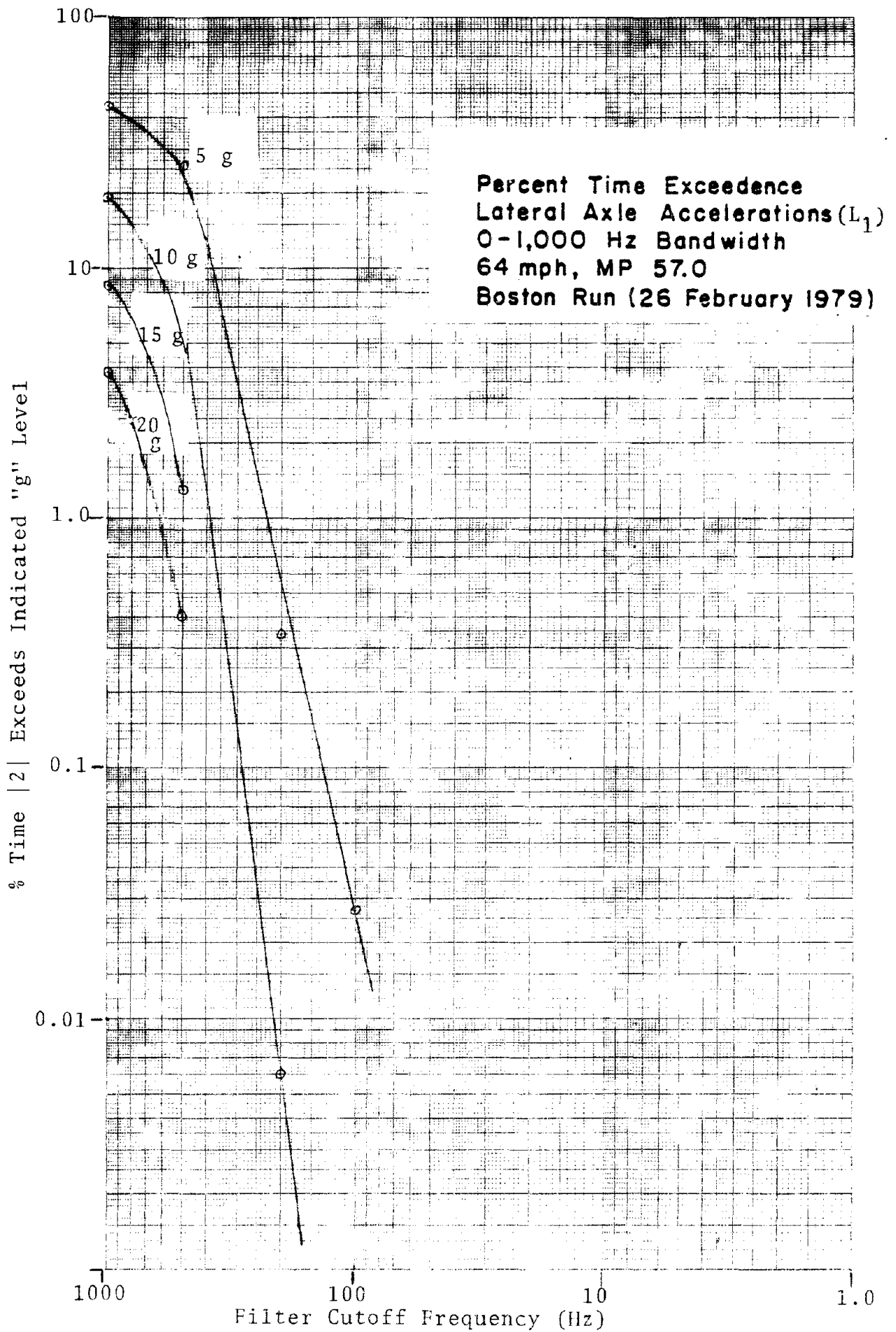


Figure 3-29. Percent Time Exceedance (%tE) of Lateral Axle Accelerations

- g - the specified g level.
- s - the train speed.
- T - roadbed stiffness (a function of temperature).

as such

$$\%tE = f(g,s,T) \quad (3.3)$$

An example analysis was performed which deals with the vertical axle accelerations shown graphically in Figure 3-28. The numerical evaluation will be confined to accelerations having frequencies between zero and 500 Hertz.

From the data shown in Figures 3-28 and 3-29, the %tE is observed to decrease exponentially as the specified g-level increases (Figure 3-30). Although not shown by the family of curves in Figure 3-31, whenever the wheelset is in motion, the %tE for zero g's will be essentially 100 percent.

The effect of speed is such that at zero speed, no accelerations exist, i.e., %tE = 0, but the instant speed becomes greater than zero, then a step function occurs in which %tE steps to 100 percent for zero g-levels. Now the rate of exponential decrease of the %tE as the specified g-level increases will be dependent on the speed at which the wheelset is traveling. Greater speed will in effect result in a greater %tE for a given g-level and vice versa as illustrated in Figure 3-31.

The third factor, roadbed stiffness, will affect %tE similarly to wheelset speed such that increased stiffness will result in higher %tE for a specified g-level and vice versa as illustrated in Figure 3-32, combining the properties exhibited by g, s and T it is observed that:

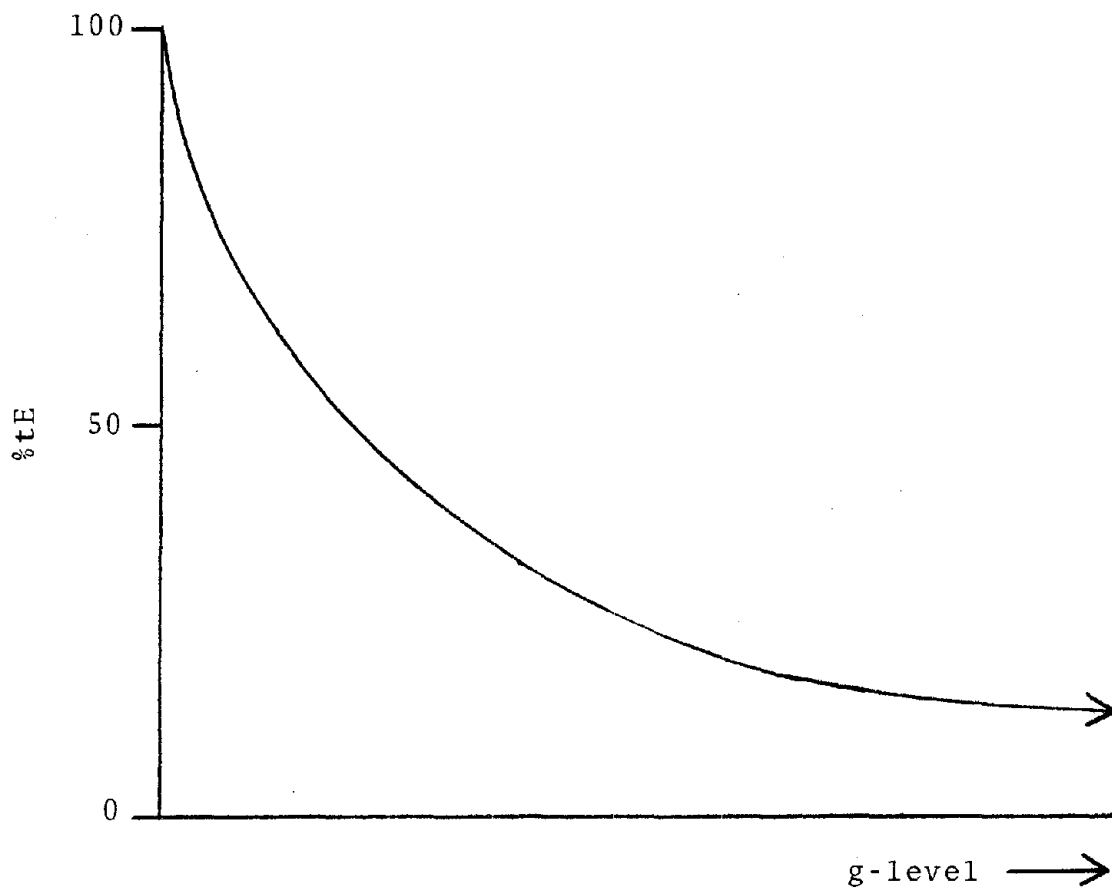


Figure 3-30. Exponential Decrease of %tE with g-Level Increase

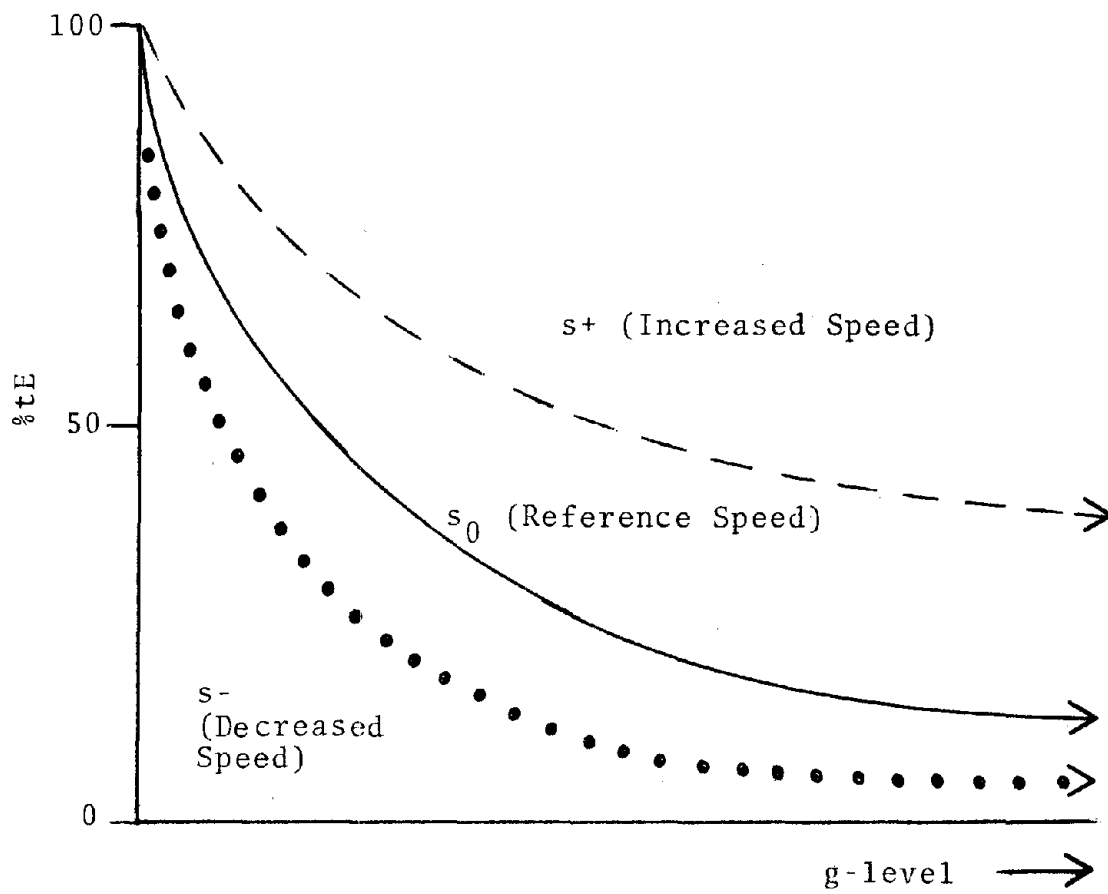


Figure 3-31. Effect of Speed on %tE

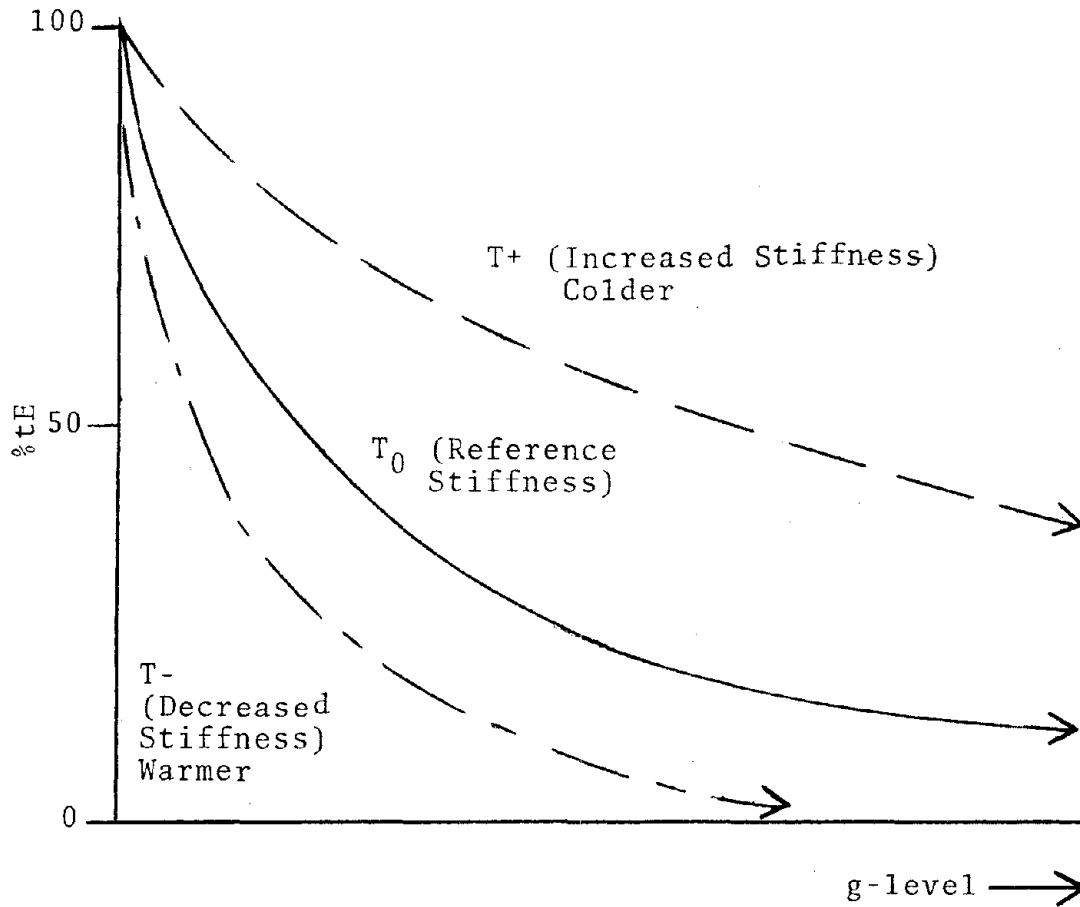


Figure 3-32. Effect of Track Stiffness on %tE

$$\%tE = ke^{-\alpha g/Ts^2} \quad (3.4)$$

where k = initial value constant
 α = exponential argument constant

Equation 3.4 provides a suitable equation of a form which satisfies the previously observed properties and the dimensional analysis requirement which demands that the exponential argument be dimensionless.

From the data collected in the instrumented non-rotating test, Tables 3-2 and 3-3 were developed.

The data collected for the example were taken from a moderately frozen roadbed, hence the value of T would represent a relatively stiff track. Equation 3.4 was modified to make T , which is held constant, part of the exponential argument constant. As such, Equation 3.4 becomes:

$$\%tE = ke^{-\beta g/s^2} \quad (3.5)$$

where $\beta = \alpha/T$
 $k = 100.0$

The data points are listed in Table 3-4.

Using digital curve fitting techniques, the curve shown in Figure 3-33 is fit to the values in Table 3-4. The curve is described by Equation 3.5 with $k = 100$ and $\beta = -865$. This expression may then be used to predict the $\%tE$ for the 100-g acceleration level at 120 mph which is 0.25 percent. This means that a wheelset operating on the Northeast Corridor at 120 mph might be expected to encounter a vertical acceleration occurring at 500 Hz and exceeding 100 g's approximately 60

TABLE 3-2

%tE FOR DATA FROM 2.5 TO 500 Hz AT A CONSTANT SPEED OF 64 MPH AND AT CONSTANT TRACK STIFFNESS (T)*

g's	Percent Exceedence (%tE)
5	26.8
10	5.5
15	1.4
20	0.5

TABLE 3-3

%tE FOR DATA FROM 2.5 TO 500 Hz AT A CONSTANT 10 g AND AT CONSTANT TRACK STIFFNESS (T)*

mph	Percent Exceedence (%tE)
40	2.1
55	4.7
64	5.5
70	19.1

*It was beyond the scope of this study to assign values to T.

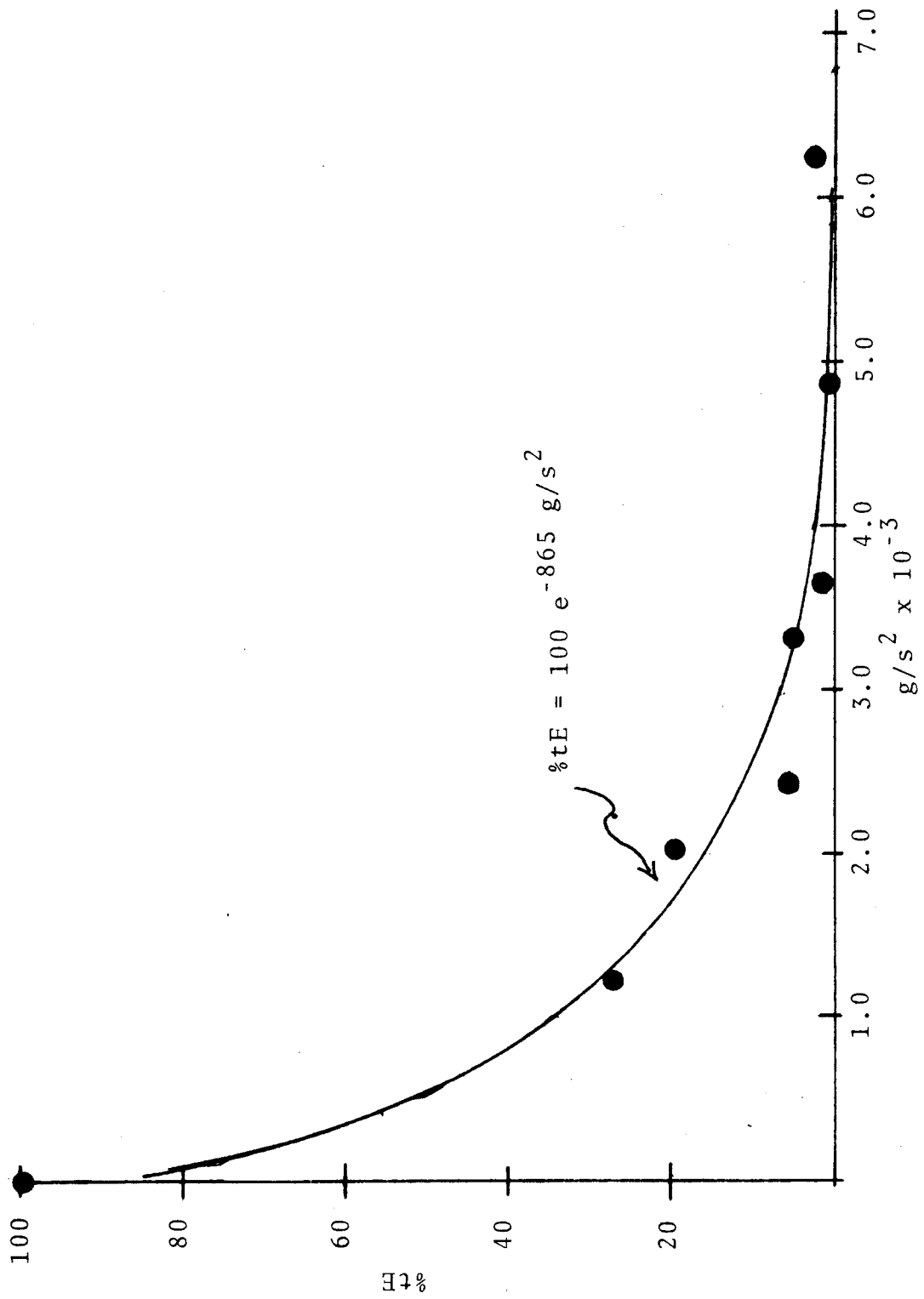


Figure 3-33. Percent Time Exceedence (%E) as a Function of Acceleration (g) Exceedence Level and Train Speed (s)

TABLE 3-4
 BOSTON RUN
 VERTICAL AXLE ACCELERATION DATA

%tE	g-Level	Speed	g/s ²
26.8	5	64	0.00122
5.5	10	64	0.00244
1.4	15	64	0.00366
0.5	20	64	0.00488
2.1	10	40	0.00625
4.7	10	55	0.00331
5.5	10	64	0.00244
19.1	10	70	0.00204
100.0	0	>0	0.00000

times per mile. An Amcoach having service requirements of 8,000 miles per month could incur 480,000 accelerations of greater than 100 g's per month during winter service on the Northeast Corridor.

A second curve can be obtained from the data in Table 3-5. The values for k and β are 100 and -2246 respectively. A comparison of the equation of %tE obtained from the Boston data (Table 3-4) with the equation of %tE obtained from the Montreal data (Table 3-5) yields a ratio of g-levels as follows

$$\frac{g - \text{level Boston}}{g - \text{level Montreal}} = \frac{2246}{865} = 2.6$$

TABLE 3-5
MONTREAL RUN
VERTICAL AXLE ACCELERATION DATA

%tE	g-level	Speed	g/s ²
58.4	4.46	80	0.00069
1.82	13.4	80	0.00209
0.1	22.3	80	0.00348
59.1	4.46	80	0.00069
2.42	13.4	80	0.00209
0.1244	22.3	80	0.00348
100.0	0	>0	0.00000

3.5.1.5 Observations

These observations were made from the material presented in Section 3.5.1.

- RMS levels of vertical acceleration on the journal bearing when partially frozen (see Note 1) (26 February data) are approximately two times the rms levels of vertical acceleration when not frozen (see Note 2) (8 March data).
 - Note 1. The ambient temperature on 26 February was approximately 35°F. It had been in the mid-teens for the previous month with substantial snowfall. The warming trend began two days before the test run with the first above freezing temperatures on 24 February accompanied by extensive rain. Under these conditions the roadbed was considered to have been frozen with slight thawing in process.
 - Note 2. The ambient temperature for the 8 March test runs was in the mid-fifties in Zones 1 and 2 with average temperatures above 40°F since the 26 February run. On this basis, the roadbed condition was classified as unfrozen.

- Cold weather data taken on 26 February indicate that concrete ties exhibit lower than average rms g-levels at 84 mph. Refer to Figure 3-7 through 3-10.
- RMS levels measured on the recently renewed track south of Trenton, NJ were lower than average by approximately one standard deviation from the average predicted by the curve. Refer to Figures 3-7 and 3-9.
- RMS levels measured on bridges showed no significant trend; however, the level for the Hackensack Bridge (refer to Figure 3-11) was significantly greater than the average for 40 mph.
- The winter factor is even more apparent when the data band is limited to 500 Hz. This is significant since inertial forces having frequencies below 500 Hz are prime suspects when examining causes of disc-brake pin loosening.
- RMS levels measured in curves showed that lateral accelerations tend to be above average, but no significant effect was observed in vertical accelerations.
- RMS levels measured in the New York to New Haven area where there is large particle or rock substrate, were typically higher than average while those measured in the Philadelphia, PA to Wilmington, DE area where there is small particle or sand substrate were usually lower than average.
- RMS of g-levels measured on the 90-pound rail of Zone 3 tended to be substantially lower than rms g-levels measured on the 130 to 140-pound rail of Zones 1 and 2. Refer to Figures 3-7 through 3-10.
- RMS g-levels for speeds above 80 mph were very close to the mean predicted by the curve.
- No trend was observed for level track versus track with a grade.

3.5.2 THE PIONEER III TRUCK SHOCK RING

The Amfleet cars were equipped with Pioneer III trucks developed by the Budd Company. This truck has a rubber,

donut-shaped ring as a primary spring. The shock ring is made of Neoprene rubber secured to the truck frame as shown in Figure 3-34.

The shock ring was examined as a winter factor candidate since rubber of the type used for the shock ring does exhibit a dramatic change in stiffness as a function of temperature. Therefore, to act as an effective filter at low frequencies, the shock ring would have to be relatively compliant over the temperature range of the NEC. However, a dramatic change in the stiffness constant (K) at lower temperatures could produce a shock path to the disc brake not present during warm weather.

To determine what occurs, accelerometers were mounted laterally and vertically on the axle side and truck side of the shock ring. Acceleration data were analyzed by determining the coherence and transfer functions of the vertical truck (V_2) to verticle axle (V_1) accelerations and lateral truck (L_2) to lateral axle (L_1). The results of these calculations are illustrated in Figures 3-35 thru 3-39.

The following significant observations can be made:

- Both 26 February and 8 March data indicate high coherence between axle and truck accelerations at frequencies below 500 Hz.
- 26 February (Boston run) data (Figures 3-36 and 3-37) show both vertical and lateral transfer functions having general trends resembling a classical second order mechanical filter system with the roll-off frequency at approximately 450 Hz.

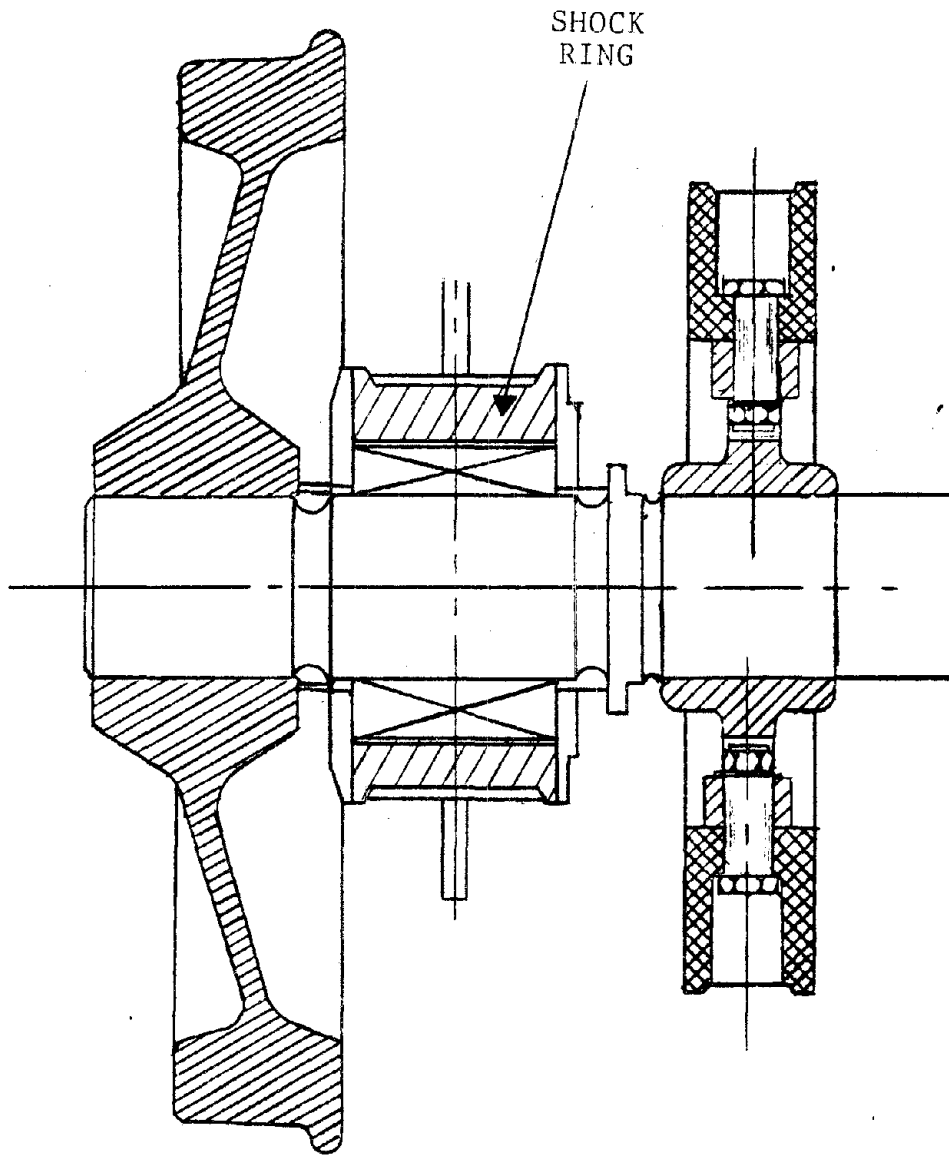


Figure 3-34. Shock Ring

BOSTON RUN - MP 55 - 58 MPH

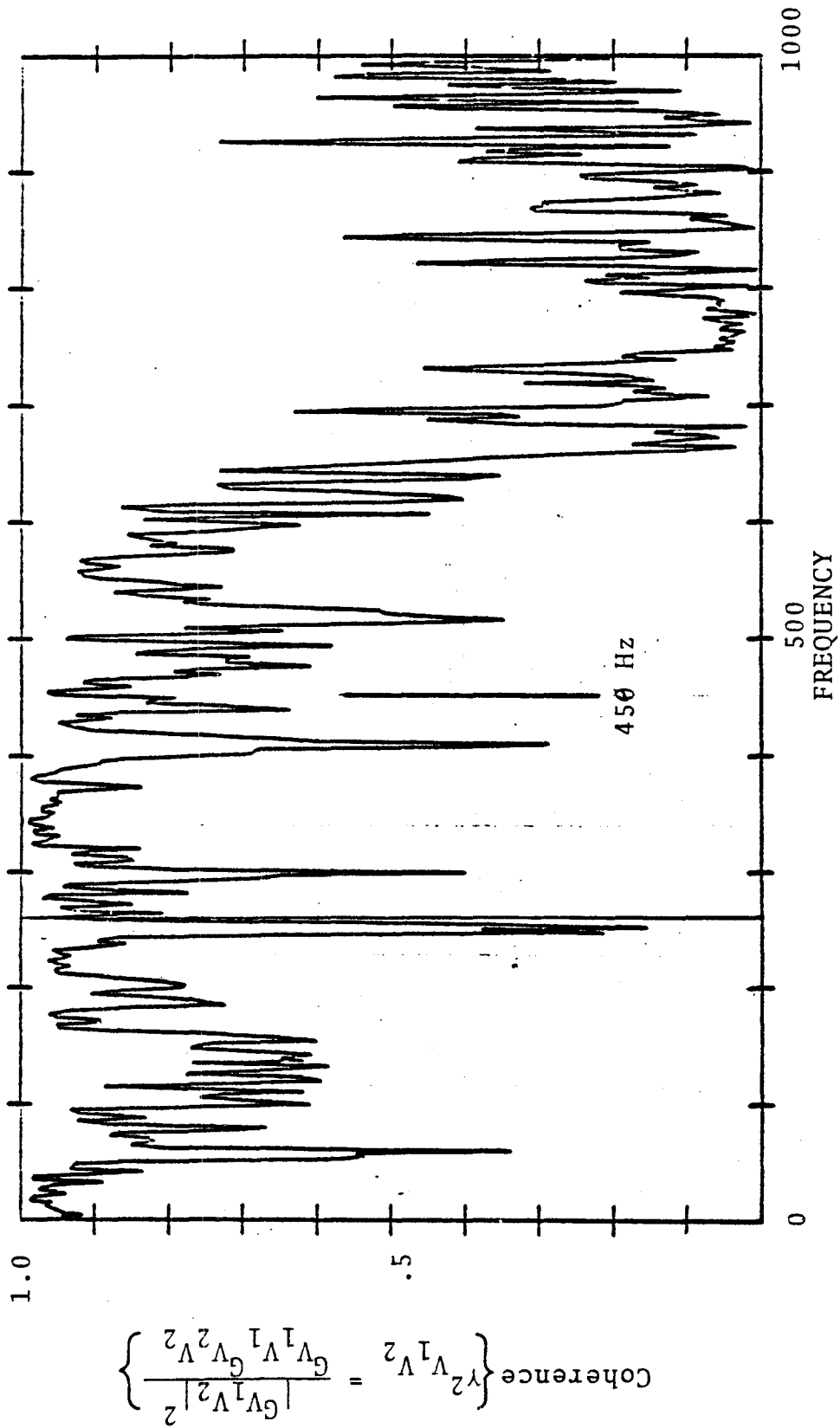


Figure 3-35. Coherence of Vertical Truck Accelerations (V_2) To Vertical Axle Accelerations (V_1)

$$\text{Coherence} \left\{ \begin{matrix} V_2 \\ V_1 \end{matrix} \right\} = \frac{|G_{V_1 V_2}|^2}{G_{V_1} G_{V_2}}$$

BOSTON RUN - MP55 - 58 MPH

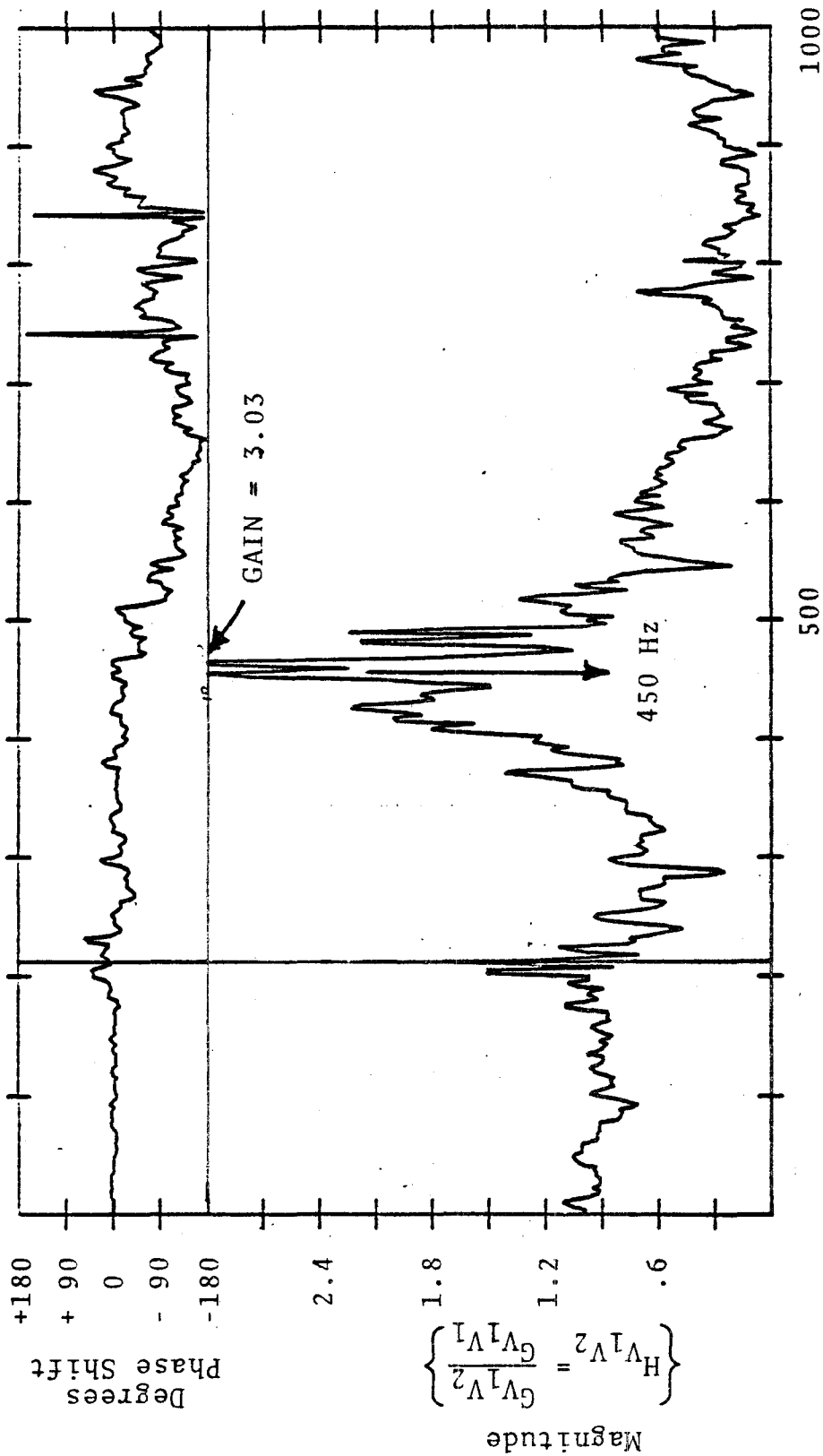


Figure 3-36. Transfer Function for Vertical Truck Accelerations (V_2) To Vertical Accelerations (V_1)

BOSTON RUN - MP55 - 58 MPH

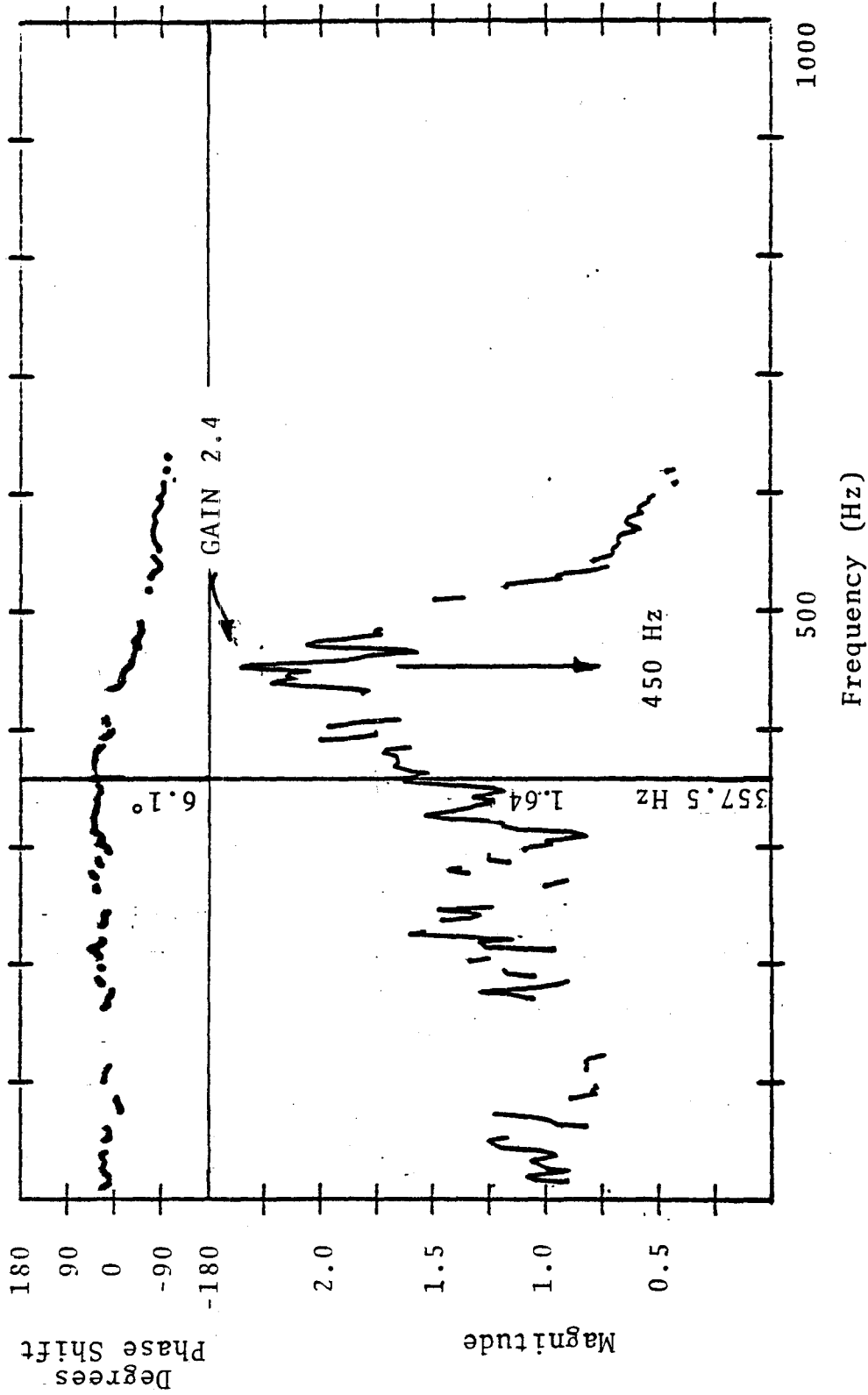


Figure 3-37. Transfer Function of Lateral Truck Accelerations (L_2) To Lateral Axle Accelerations (L_1) - Coherence Blanking = 0.8

MONTREAL RUN - NEAR ST. ALBANS, VT - 60 MPH

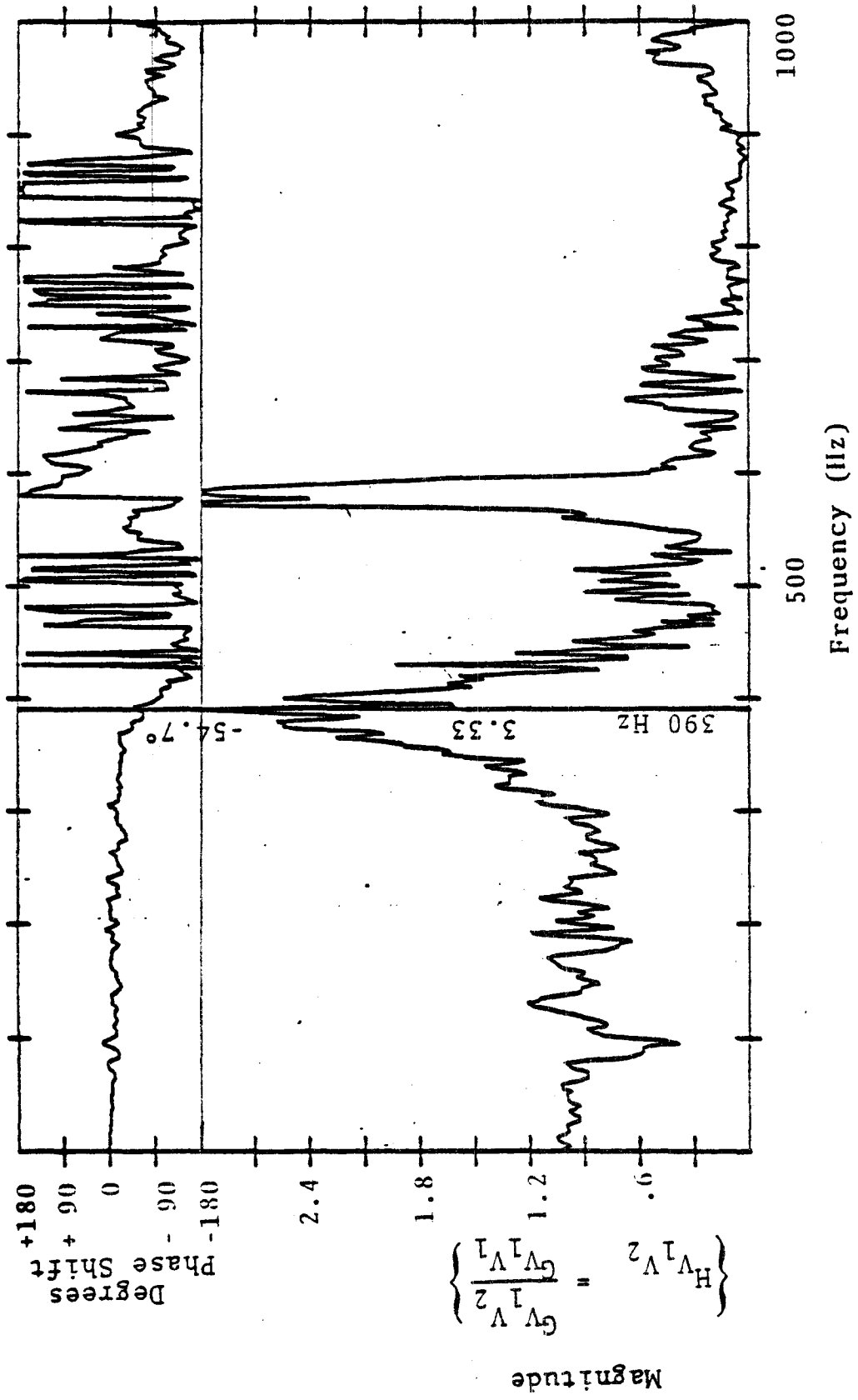


Figure 3-38. Transfer Function of Vertical Accelerations (V_2) To Vertical Axle Accelerations (V_1)

MONTREAL RUN - NEAR ST ALBANS, VT - 60 MPH

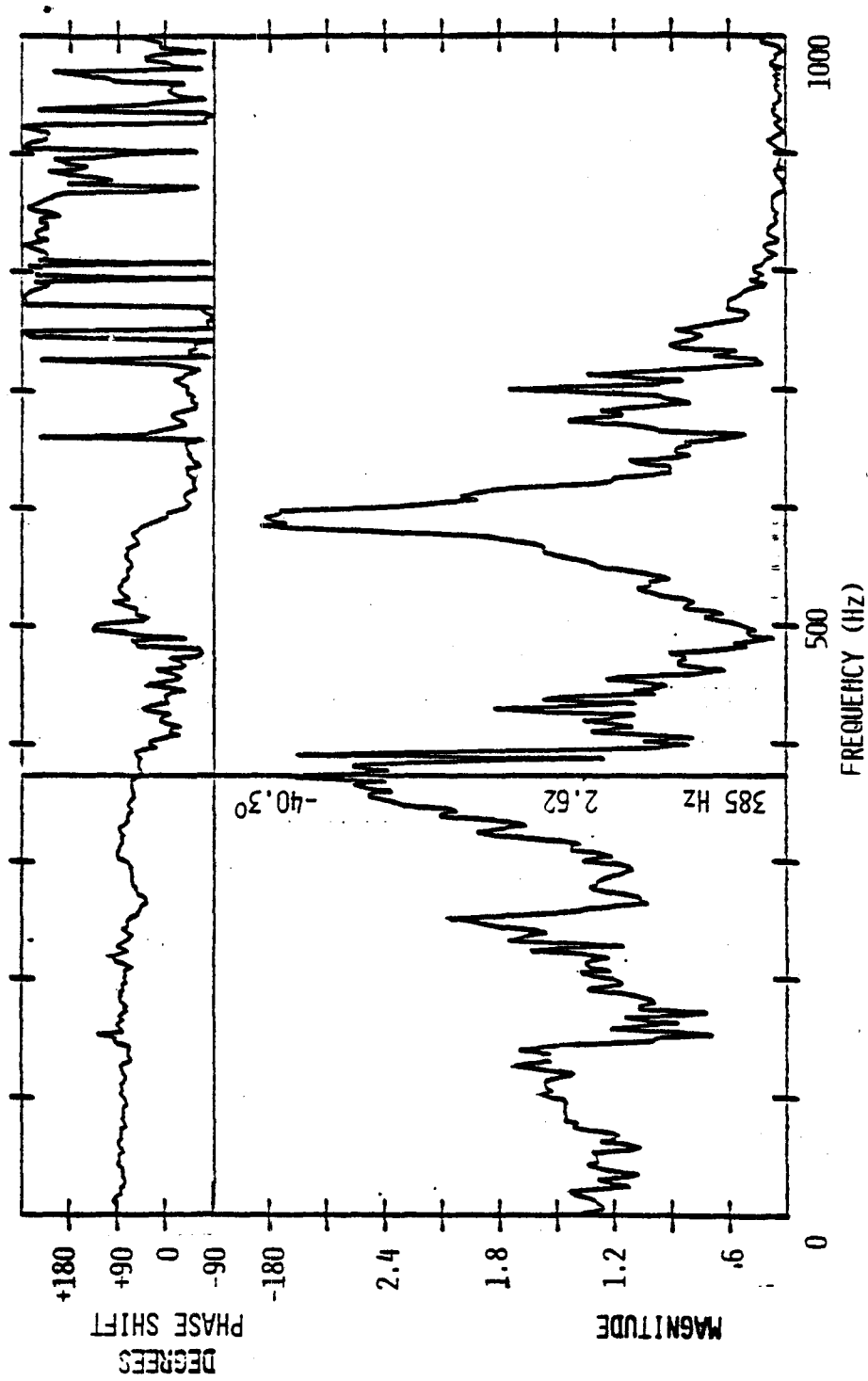


Figure 3-39. Transfer Function of Lateral Truck Accelerations (L₂) to Lateral Axle Accelerations (L₁)

- 8 March (Montreal run) data (Figures 3-38 and 3-39) show essentially the same trend with the roll-off frequency at 390 Hz.
- 8 March data show a second coherent resonance response at 580 Hz.

From these observations the following conclusions can be drawn:

- The rubber element does not act solely as the primary suspension element of the Pioneer III truck.
- The resonant frequency of the shock ring is between 385 and 450 Hz.
- The resonance frequency appears to change with temperature. The frequency was observed to be 450 Hz on 26 February and 385 Hz on 8 March. The ambient temperatures corresponding to these days were 37°F and 50°F respectively.
- Since the results clearly show that the shock ring is not a major contributor of inputs to the truck primary, the indicated frequency shift does not explain the winter factor.
- The truck mass is distributed so that the entire truck mass does not act on the shock ring.

3.5.3 BRAKE FORCES

Another input to the disc brake assembly is from the disc calipers during braking. To monitor this input the brake suspension strips were strain gaged as described in Section 3.1.3.1. The data from the strips provided a good indication of the forces applied to the discs during braking. The results for the warm and cold weather runs were compared to determine whether the brake forces were significantly different. The results indicate that the brake forces are essentially the same under different temperatures. During the second test run on 8 March, the decelostat system developed a malfunction which caused the system to repeatedly release the brakes on one truck but the resulting forces did not exceed the normal forces.

To evaluate the brake forces the coefficient of friction was determined. For speeds between 40 and 80 mph, the coefficient of friction was found to be essentially the same for the environmental conditions of 26 February (Boston run) and 8 March (Montreal run). This conclusion is based on experimental determinations using random samples of data from each test run to calculate the coefficient of friction based on the mechanical assembly given in the Amcoach Maintenance Manual.

The calculation of the coefficient of friction (μ) for the 26 February (Boston) run and the 8 March (Montreal) run was as follows (Figure 3-40):

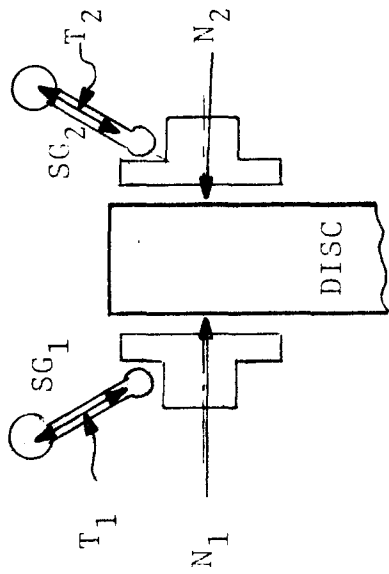
$$\mu = \frac{SG_1 + SG_2}{2AP_{adj}R}$$

$$\mu = .0086 \frac{SG_1 + SG_2}{P_{adj}}$$

where μ = Coefficient of friction
 SG_1 = Inboard gage tension in pounds
 SG_2 = Outboard gage tension in pounds
 P_{adj} = Brake pressure minus six psi compensation for the cylinder return spring.
 A = Brake cylinder piston area in pounds per square inch
 R = Caliper ratio

The results of this evaluation (as shown in Table 3-6) are consistent with the 0.3 to 0.6 range of values for the coefficient of friction of dry asbestos on steel.

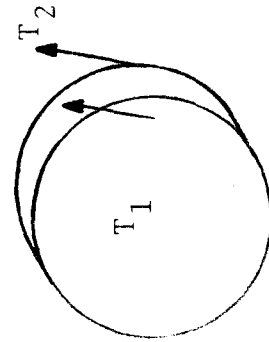
BRAKE MEASUREMENTS ARE IN FORCE UNITS



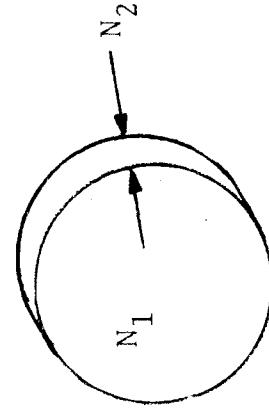
$$N \approx T/\mu$$

$$\mu \approx 0.45 \text{ (COEFFICIENT OF FRICTION)}$$

SIGNIFICANT QUANTITIES



$T_1 + T_2$ TENDS TO BEND SLEEVES IN TANGENT PLANE



$N_1 - N_2$ TENDS TO BEND SLEEVES IN LATERAL PLANE

Figure 3-40. Illustration of Brake Torque Forces (T) And Brake Normal Forces (N)

TABLE 3-6

CALCULATIONS OF THE COEFFICIENT OF FRICTION

Boston Run

Inboard Tension Forces (SG_1) (pounds)	Outboard Tension Forces (SG_2) (pounds)	Combined Tension Force ($SG_1 + SG_2$) (pounds)	Measured Pressure (P) (psi)	Adjusted Pressure ($P_{adj} = P - 6$) (psi)	Coefficient of Friction (μ)
770	952	1722	42.0	36.0	0.41
680	680	1360	33.0	37.0	0.43
680	861	1581	37.5	31.5	0.43
498	498	996	30.0	24.0	0.36
805	635	1440	34.5	28.5	0.43
748	612	1360	39.0	33.0	0.35
μ AVERAGE					0.41

Montreal Run

Inboard Tension Forces (SG_1) (pounds)	Outboard Tension Forces (SG_2) (pounds)	Combined Tension Force ($SG_1 + SG_2$) (pounds)	Measured Pressure (P) (psi)	Adjusted Pressure ($P_{adj} = P - 6$) (psi)	Coefficient of Friction (μ)
460	460	920	22.5	16.5	0.48
680	460	1140	25.0	19.0	0.52
680	460	1140	29.0	23.0	0.43
317	725	1042	27.0	21.0	0.43
362	589	951	27.0	21.0	0.39
544	634	1178	28.0	22.0	0.46
μ AVERAGE					0.45

In addition to measuring the brake forces, the decelostat activity was monitored continuously during testing. Normal activity, defined as decelostat activity due to wheel slip, was essentially the same for each of the test runs with the rate of brake release and reapplication approximately the same. A typical example of decelostat activity is shown in Figure 3-41. During the return run from Montreal on 8 March, decelostat activity was excessive. Post-test examination of the decelostat magnetic sensor cable revealed a faulty cable to the No. 3 axle.

The brake data does contain high cyclic variations in both brake torque forces and brake normal forces. Figure 3-42 shows a spectral plot of the brake force and a similar plot of the truck journal bearing accelerations. In the range of 300 to 500 Hz, brake torque ($T_1 + T_2$ of Figure 3-40 is the same as $SG_1 + SG_2$ of Figure 3-42) appeared very similar to the spectral graph of vertical truck accelerations as shown by Figure 3-43. The coherence between these was greater than 0.8 in this frequency band. The amplitude of the variations were ± 50 percent of the average total torque during braking applications (i.e., brake torque force may vary from 500 to 1500 pounds about an average torque force of 1000 pounds). The transfer functions between total brake torque and vertical truck accelerations (Figures 3-44 and 3-45) show a transfer function of 104 lbs/g. Similar results were observed from a comparison of disc-brake normal force and lateral axle accelerations. Figures 3-46 thru 3-49 illustrate this observation. The observed transfer function of disc-brake normal forces to lateral axle accelerations was 24.1 lbs/g at 412 Hz.

This shows that the brake force data are subject to high frequency oscillations of substantial magnitude both in the tangential (torque) mode and the normal (sideways to disc) mode.

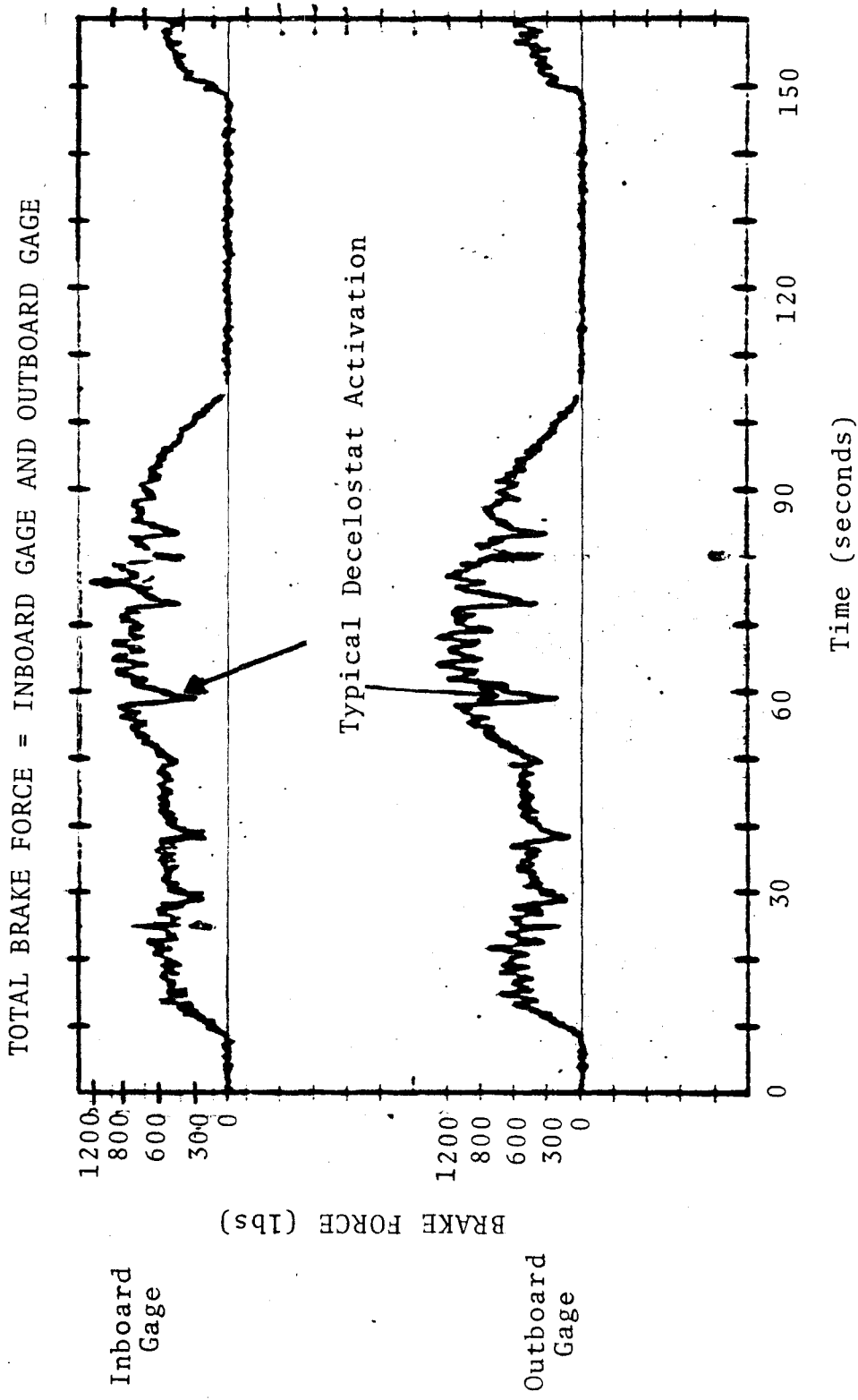


Figure 3-41. Brake Force Signals With Slide Control Activity.

BOSTON RUN, TRENTON, NJ

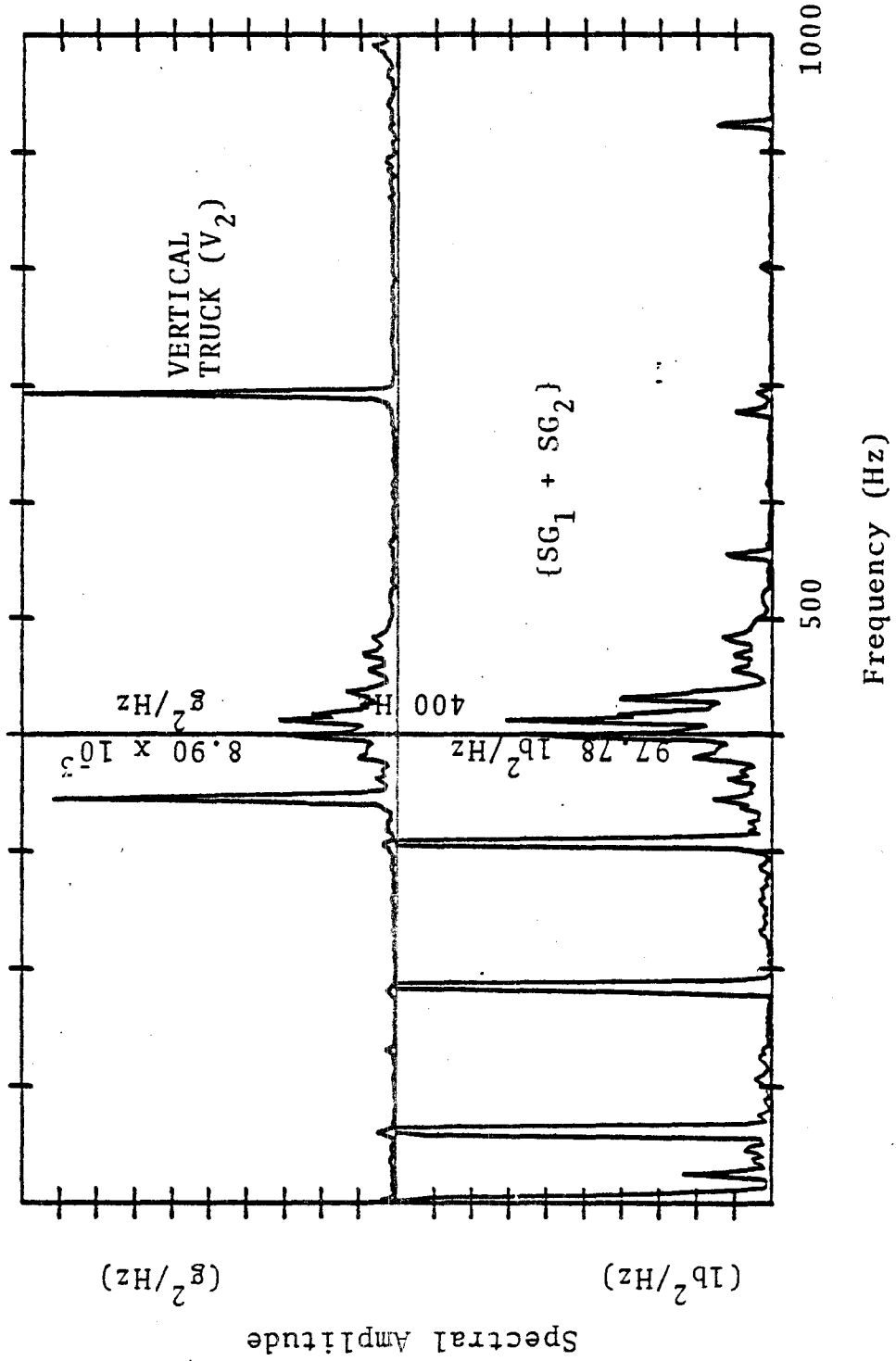


Figure 3-42. Power Spectrum of Vertical Truck Acceleration (V₂) and Brake Disc Torque Force (SG₁ + SG₂)

BOSTON RIJN, TRENTON, NJ

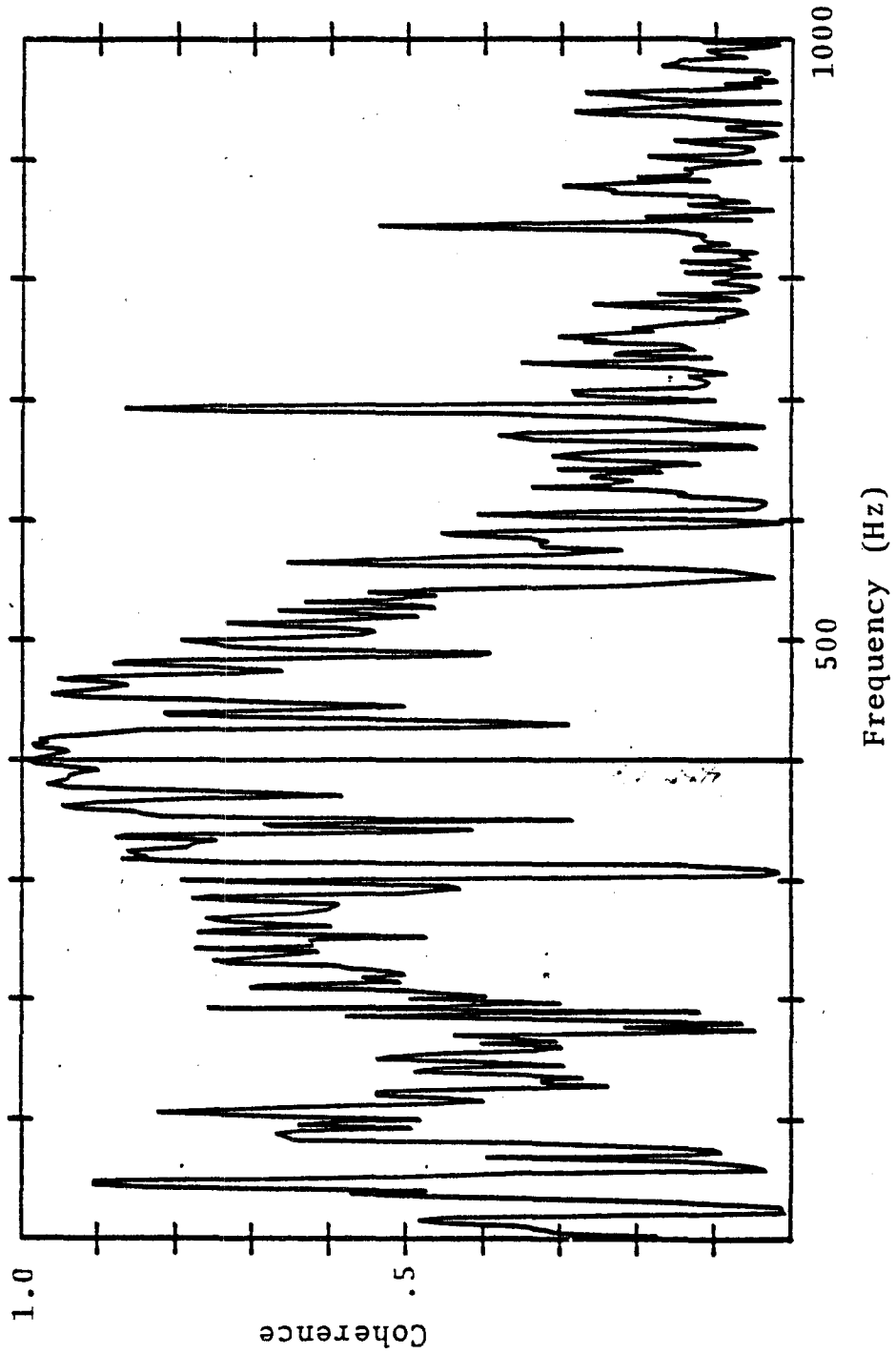


Figure 3-43. Coherence of Brake Disc Torque Force ($SG_1 + SG_2$) To Vertical Truck Accelerations (V_2)

BOSTON RUN, TRENTON, NJ

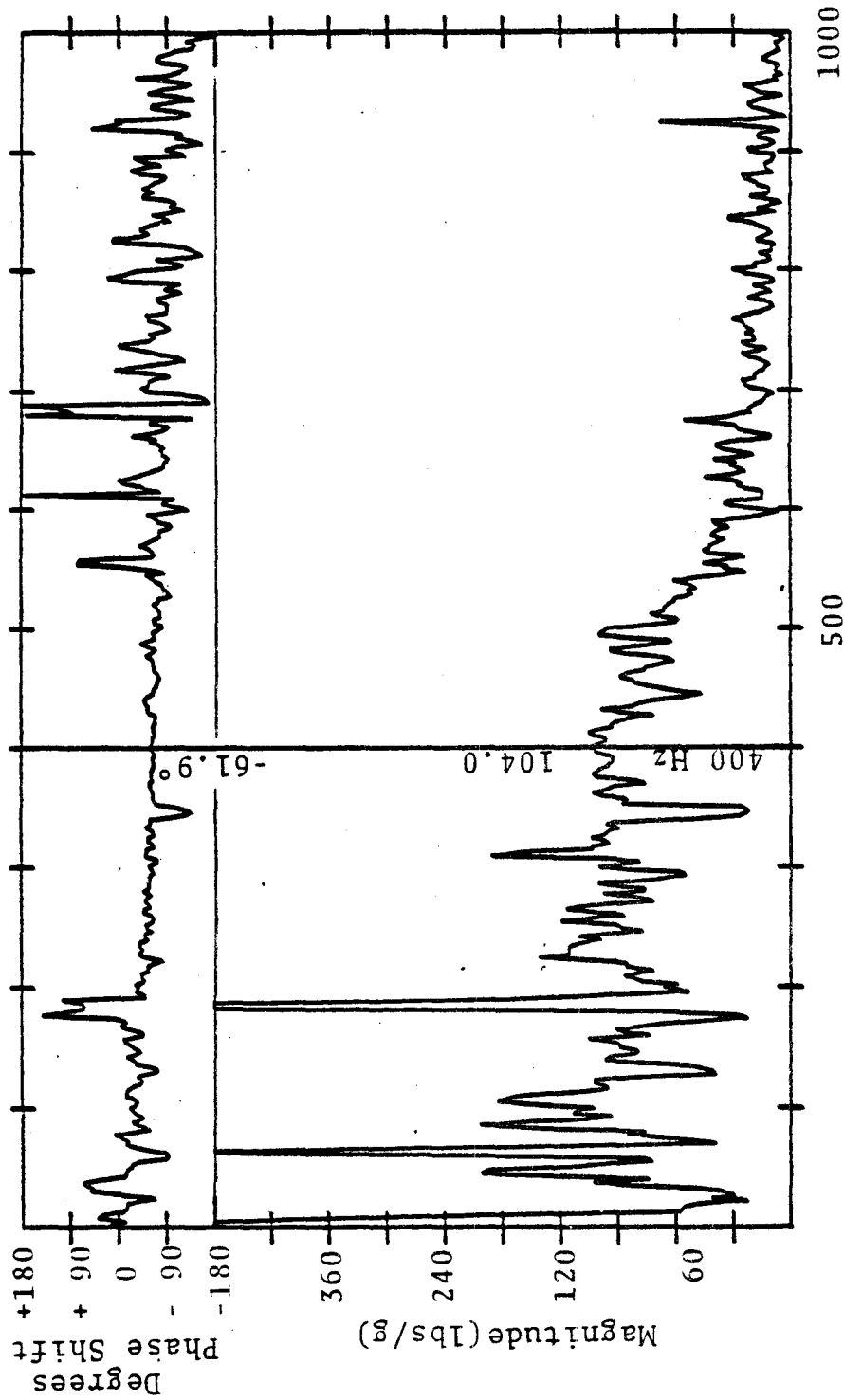


Figure 3-44. Transfer Function of Brake Disc Torque Force ($SG_1 + SG_2$) To Vertical Truck Accelerations (V_2)

BOSTON RUN, TRENTON, NJ

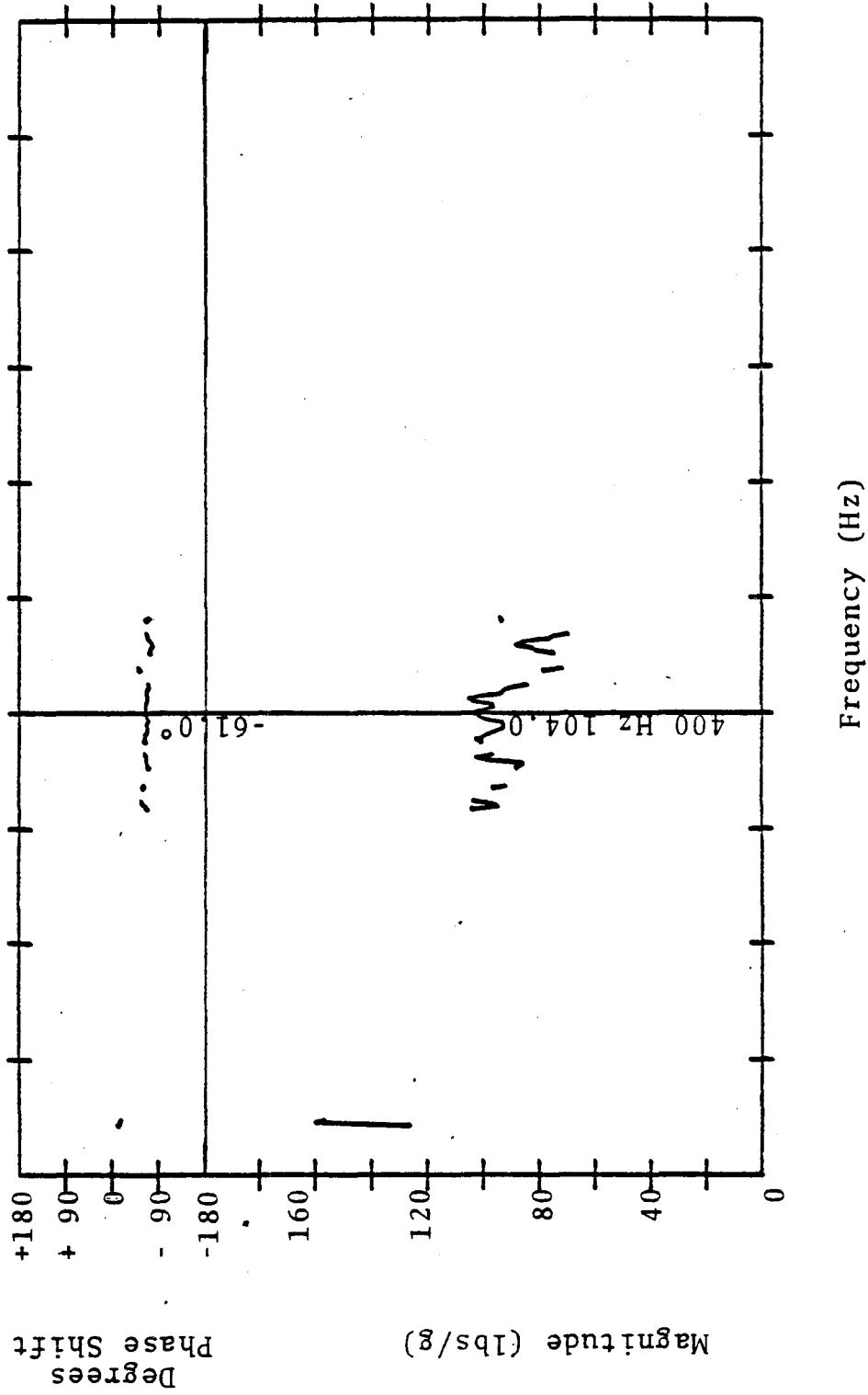


Figure 3-45. Transfer Function of Disc Brake Torque Force ($SG_1 + SG_2$) To Vertical Truck Accelerations (V_2) With Coherence Blanking = 0.8

BOSTON RUN, TRENTON, NJ

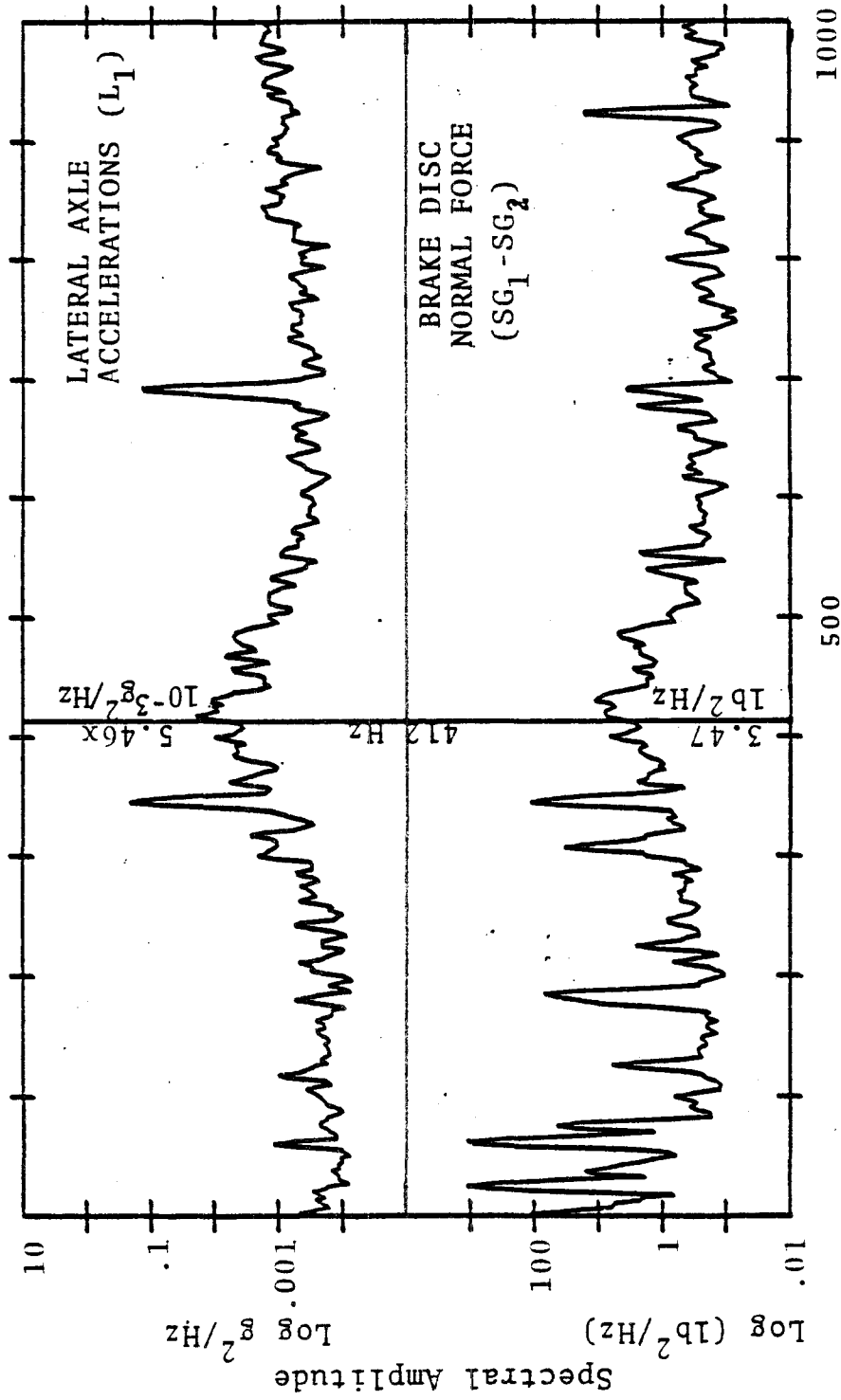


Figure 3-46. Power Spectrum of Lateral Axle Accelerations (L₁) and Brake Disc Normal Force (SG₁-SG₂)

BOSTON RUN, TRENTON, NJ

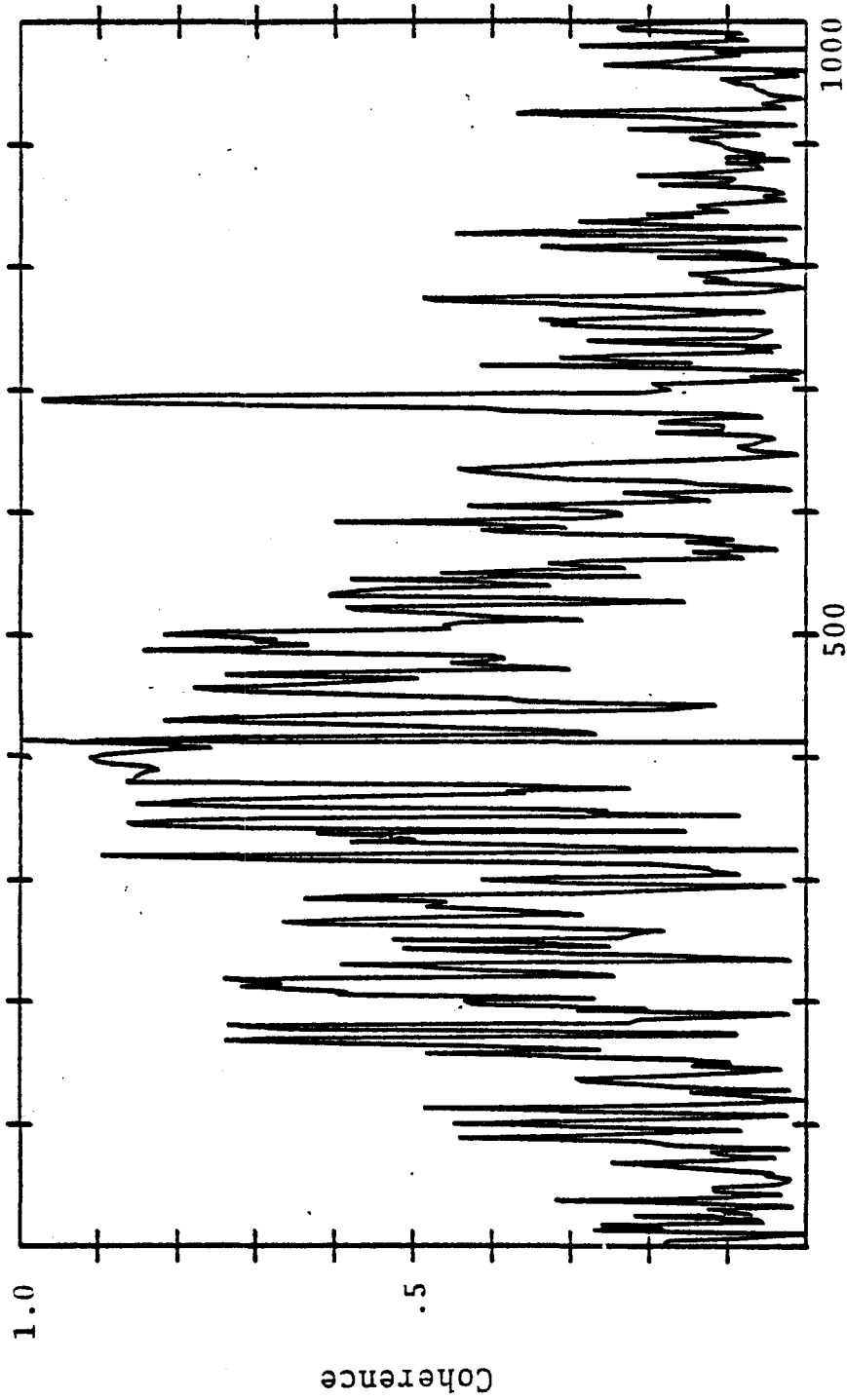


Figure 3-47. Coherence of Brake Disc Normal Force (SG_1-SG_2) To Lateral Axle Accelerations (L_1)

BOSTON RUN, TRENTON, NJ

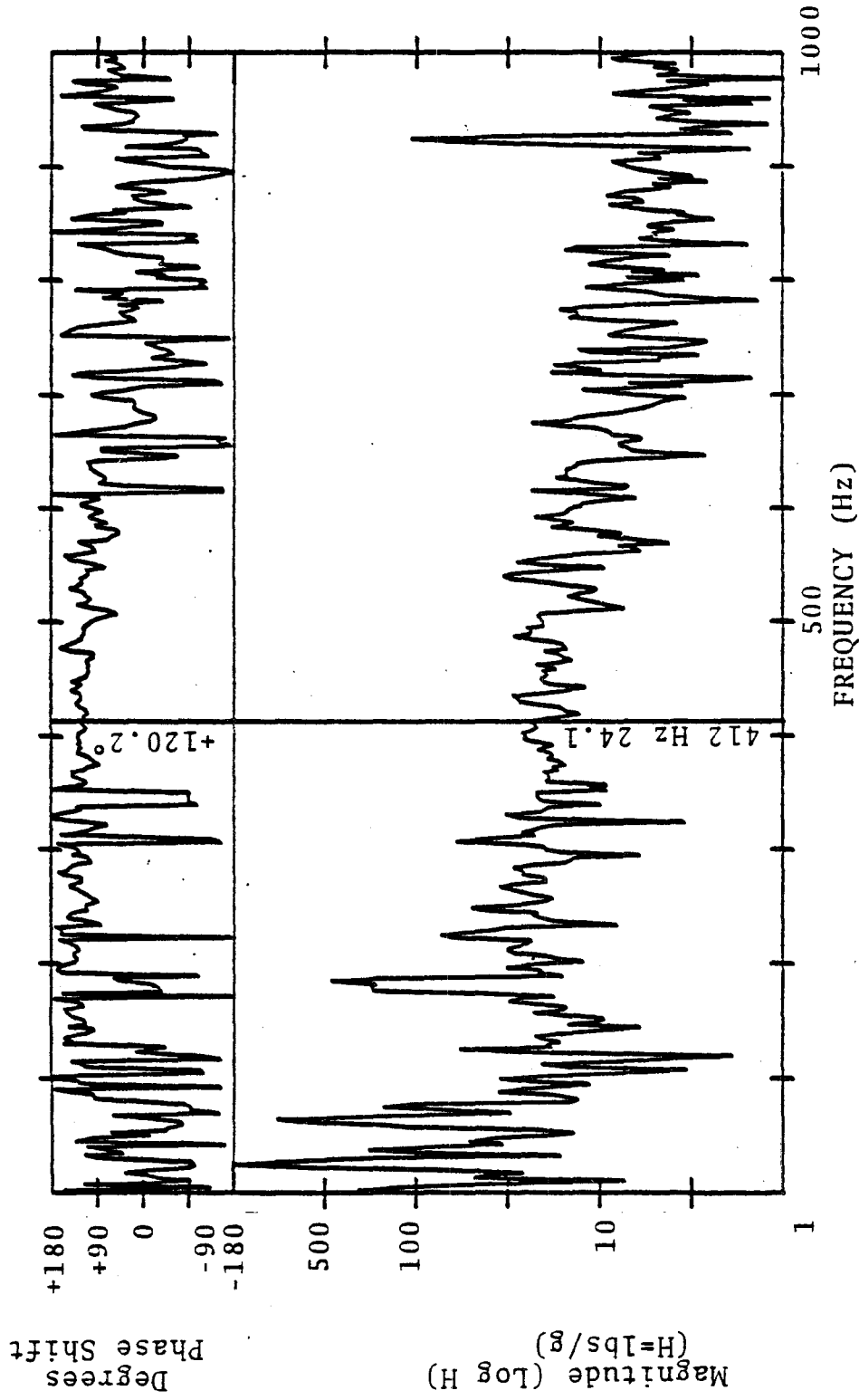


Figure 3-48. Transfer Function of Brake Disc Normal Force (SG₁-SG₂) To Lateral Axle Accelerations (L₁)

BOSTON RUN, TRENTON, NJ

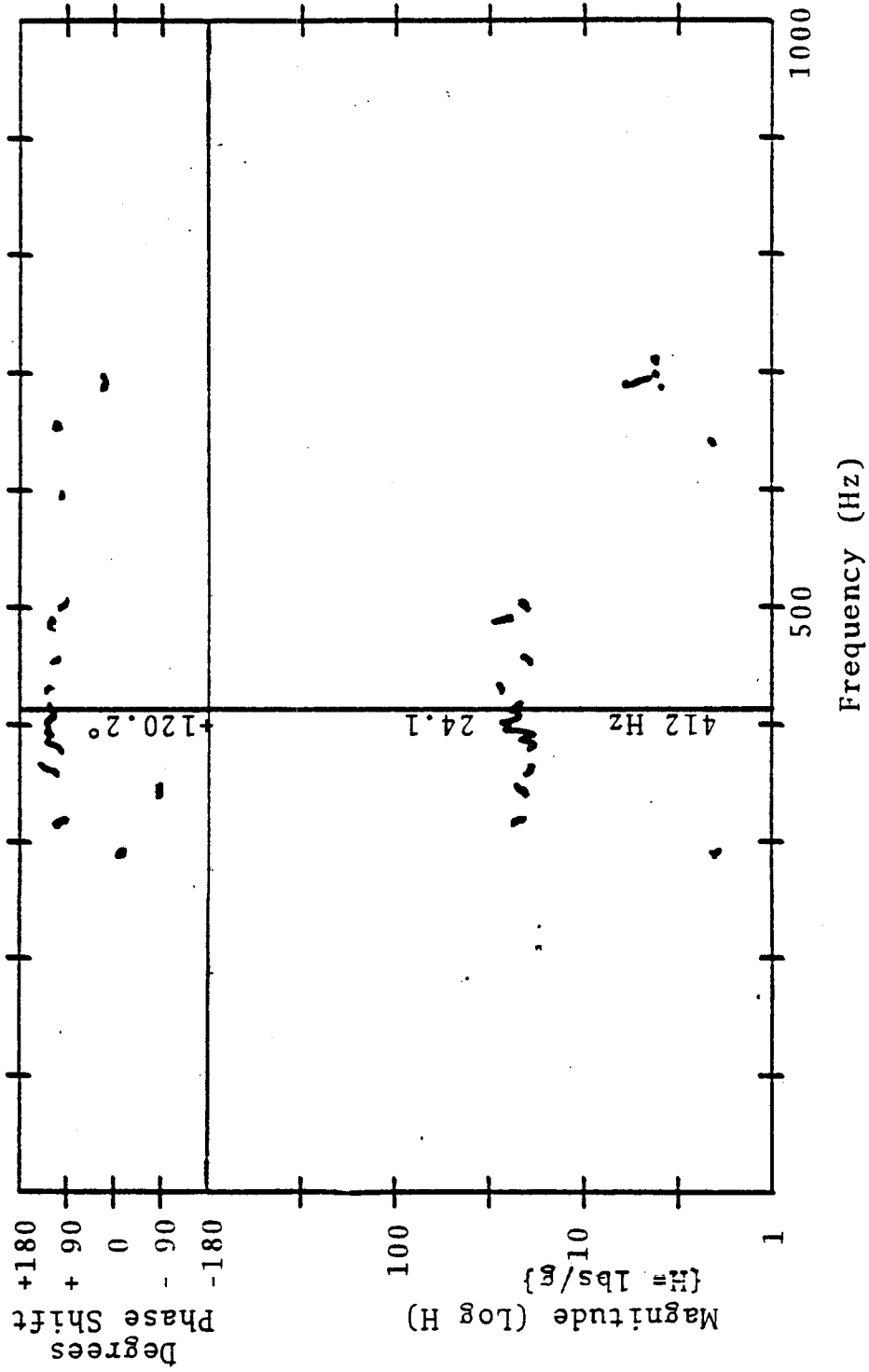


Figure 3-49. Transfer Function of Brake Disc Normal Force (SG_1-SG_2) To Lateral Axle Accelerations (L_1) With Coherence Blanking = 0.8

The significance of these cyclic loads was evaluated as described in Appendix B. The conclusion of this evaluation is that the loads from this input do not compare to the inertial loads.

4.0 LABORATORY SUBTEST

4.1 GENERAL REQUIREMENTS

The general requirements of this test were to utilize a complete Amcoach wheelset to perform tests on the Knorr disc-brake assembly under laboratory conditions.

4.1.1 GENERAL OBJECTIVES

The general objectives of this test were to determine how the pins which secure the disc to the hub are affected by shocks similar to those experienced in over-the-road operation. The tests examined pin-load responses that lead to fretting, corrosion or abrasion. In addition, the lateral resonance of the disc and wheelset were measured to try to understand the transfer mechanism of the inertial forces which cause pin loading.

4.1.2 TECHNICAL OBJECTIVES AND REQUIREMENTS

The technical objectives of this test were to gain an understanding of the stress-transfer characteristics of the Knorr brake resilient holding pin. The pin was subjected to loading similar to that encountered in the dynamic rail environment.

Technical objectives were subdivided into objectives related to disc-assembly static and dynamic loading.

Static loading was used to examine the stress response of the pin when it was subjected to loading similar to that observed using brake-rigging; strain gage instrumentation in the over-the-road testing conducted prior to this test. Static load testing also served as a calibration procedure. Dynamic loading was used to examine the stress response of the pin

when the wheelset was subjected to acceleration loads of similar magnitude to those observed using axle-bearing-housing accelerometers on the Over-the-Road tests.

4.2 STATIC LOADING REQUIREMENTS

Differential Torque Loading - force applied to the disc-brake rotor in a tangential direction while the disc-brake hub was held rigidly fixed (Figure 4-1). Parameters of interest are: tangential bending of pin and tangential reaction stress on hub hole.

Lateral Force Loading - force applied to the side of the disc-brake rotor parallel to the wheelset axis with the disc brake hub held fixed (Figure 4-1). Parameters of interest are: lateral bending of pin, lateral reaction stress on hub hole and pin-to-hub-hole micro-slip.

Diametric Force Loading of Disc - force applied diametrically across the disc and vertically to the wheelset axis (Figure 4-1). Parameter of interest: tangential bending of pin.

4.3 DYNAMIC LOADING REQUIREMENTS

Vertical Impulse Loading - impulse developed by raising one end of the wheelset and dropping it onto a rail section. The impulse loading on the disc-brake pins results when the disc, as part of the wheelset having been accelerated by gravity to some pre-impact velocity, undergoes a very high deceleration at the time of impact. Tangential bending forces will be experienced by the pins due to disc inertia and the clearance between the rotor and the hub. Parameters of interest are: tangential pin bending, and tangential reaction stress on the hub.

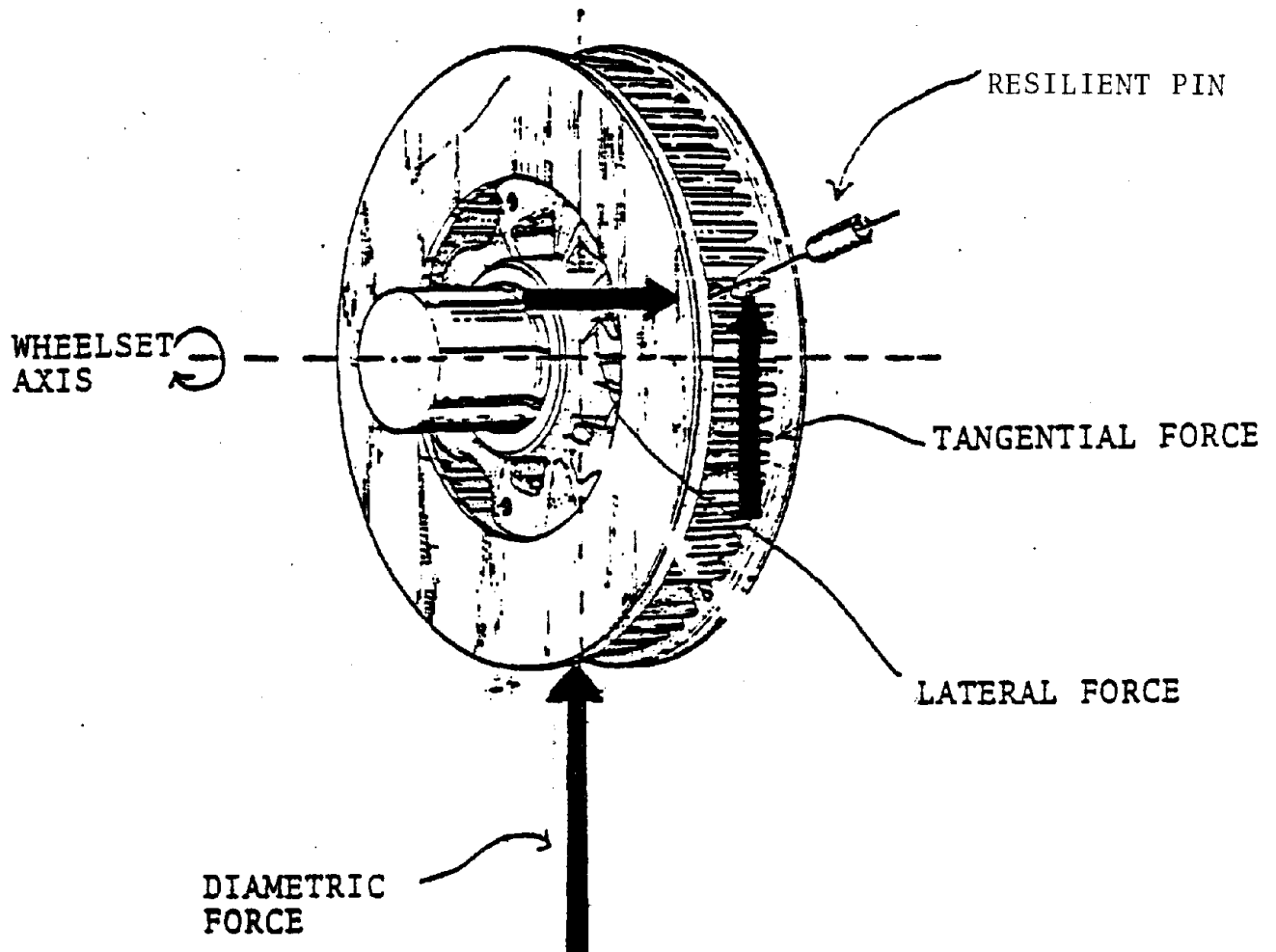


Figure 4-1. Knorr Disc Brake Assembly--Force Vectors are Indicated in Positive Direction

Lateral Impulse Loading - impulse loading was achieved by using gravity to accelerate a pendulous mass to some pre-impact velocity. By allowing the pendulous mass to strike the end of the axle, the disc as part of the wheelset is subjected to a high acceleration as the system attempts to conserve momentum. Lateral bending forces are experienced by the pins due to disc inertia. Parameters of interest are lateral bending of the pin, lateral reaction stress on the hub, and hub/pin micro-slip (Figure 4-2).

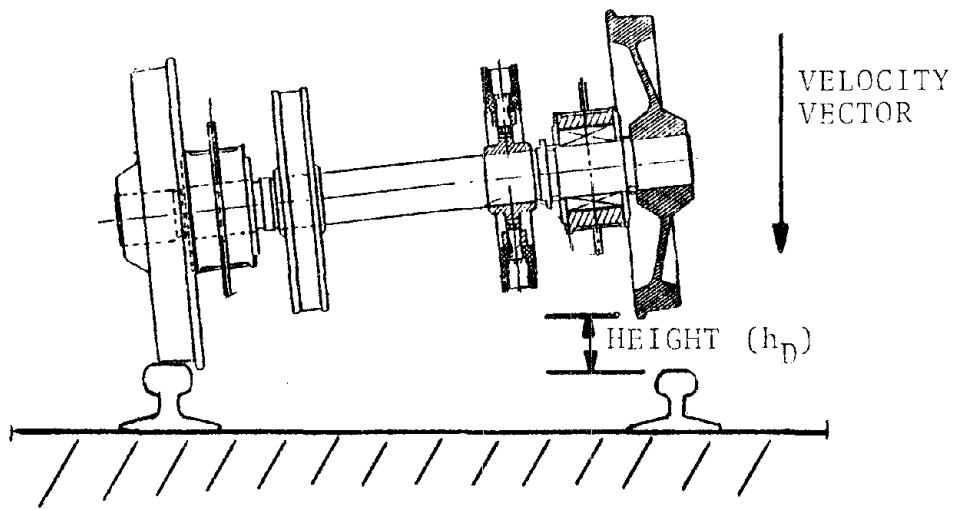


Figure 4-2(a). Drop Shock Testing Configuration

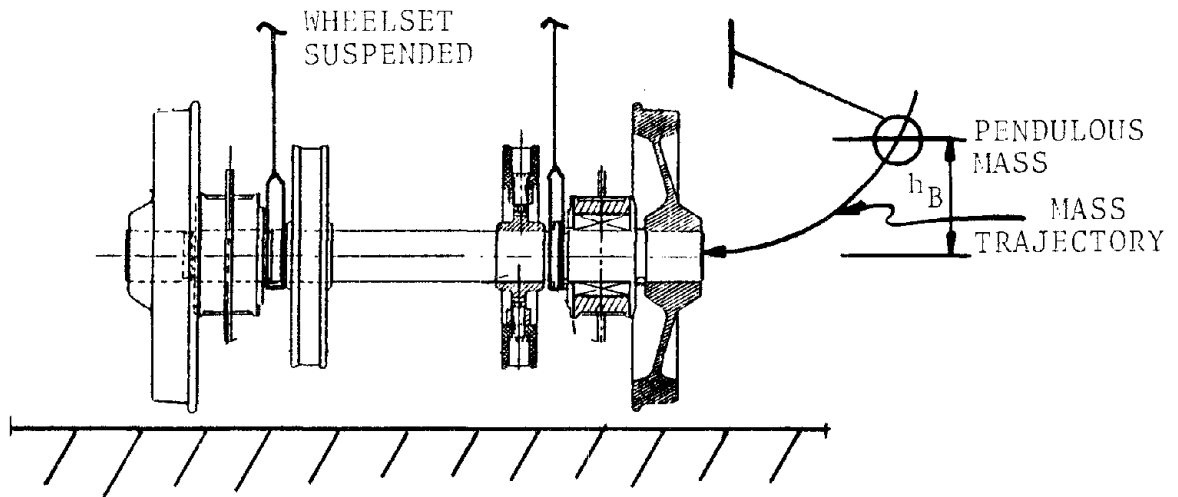


Figure 4-2(b). Pendulous Mass Used to Provide Lateral Impulse Loading on Disc Brake Assembly

4.4 INSTRUMENTATION AND DATA COLLECTION APPARATUS

The primary instrumentation and data collection apparatus included six channels of strain gage data, one channel of micro-slip data, and four channels of accelerometer data.

The seven channels of strain gage and micro-slip data were recorded by hand in test logs during static test. Data points were obtained using digital multimeter readings in millivolts, then appropriate conversion to engineering units was performed and the data were entered into the test logs.

All eleven channels of data were recorded during dynamic testing by photographing the time history data traces captured on a storage oscilloscope and simultaneously generating spectral data using a Nicolet Scientific UA-500 spectrum analyzer. Hardcopy was obtained by outputting UA-500 data to an X-Y plotter.

Data channels were designated as listed in Table 4-1.

Installation diagrams are shown in Figures 4-4 through 4-8. Additional instrumentation and data collection apparatus consisted of:

TABLE 4-1
DATA CHANNELS

System* Channel No.	Designator	Location	Measurement
8	TBS ₁	Instrumented Pin No. 1	Tangential Bending
7	LBS ₁	Instrumented Pin No. 1	Lateral Bending
6	TRS ₁	Instrumented Hub Hole Stress	Tangential Reaction
5	LRS ₁	Instrumented Hub Hole Stress	Lateral Reaction
4	MSDT ₁	Instrumented Pin No. 1	Micro-slip
10	TBS ₂	Instrumented Pin No. 2	Tangential Bending
9	LBS ₂	Instrumented Pin No. 2	Lateral Bending
11	LAA	Axle Bearing Housing	Vertical Axle Accelerometer
12	VAA	Axle Bearing Housing	Vertical Axle Accelerometer
13	LAR	Disc Brake Rotor	Lateral Rotor Accelerometer
14	VAR	Disc Brake Rotor	Vertical Rotor Accelerometer

*System Channels 1, 2 and 3 not used.

- A Nicolet Scientific UA-500 spectrum analyzer used in conjunction with an X-Y plotter to capture amplitude spectral data 1000 Hz on bandwidth.
- A storage oscilloscope, digital voltmeter, and function generator used to provide system calibration and alignment as well as real-time signal monitoring capabilities.

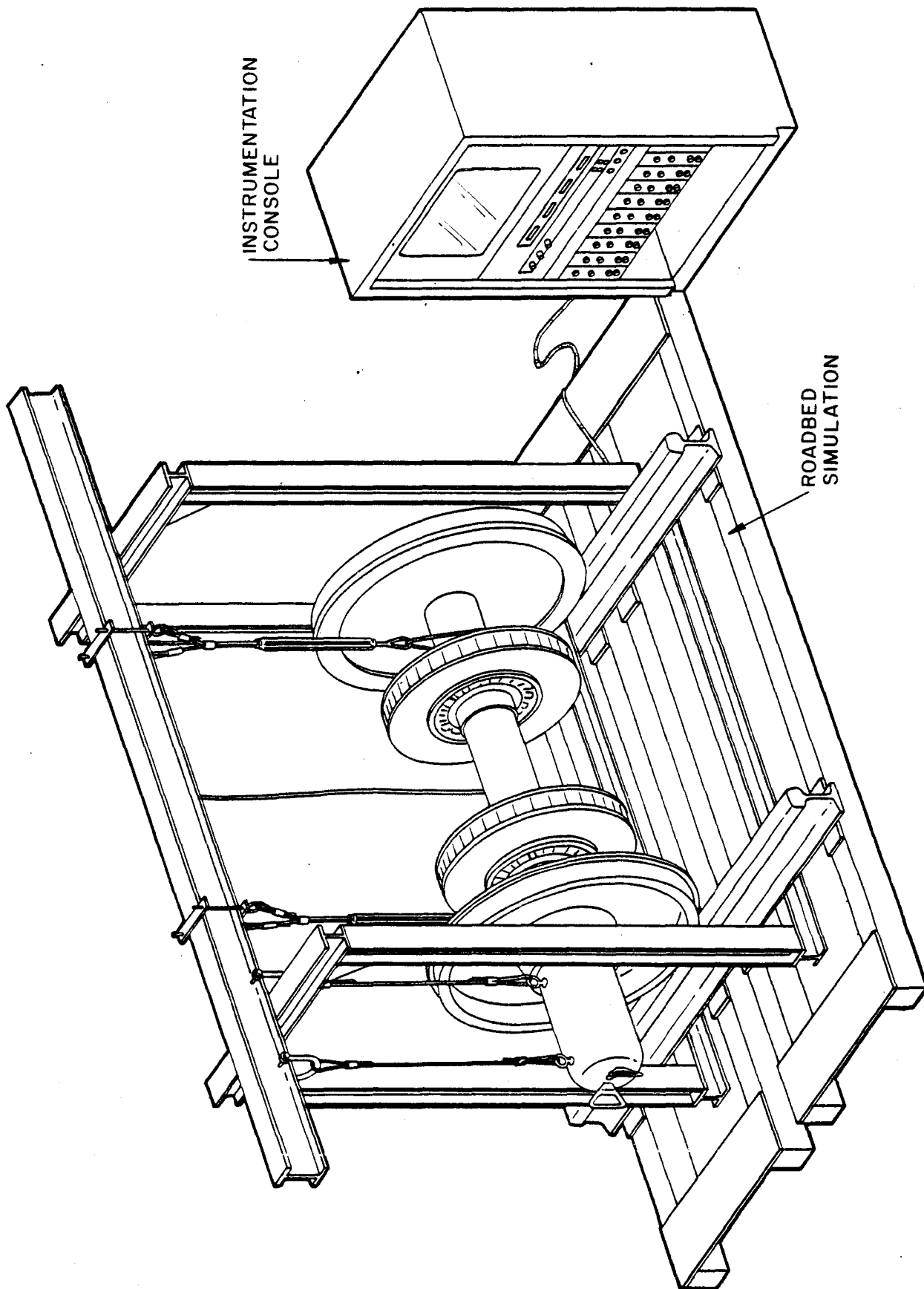
4.5 INSTRUMENTATION PROCEDURES

Amtrak provided a wheelset (No. 8M377D), two sections of track (each of which was approximately six feet long) and miscellaneous brake assembly hardware for use in testing. The Knorr disc-brake subassembly was instrumented with strain gages, a micro-slip detector (MSDT), and accelerometers described in Section 4.4. All work was performed at ENSCO's Farrington Avenue Facility in Alexandria, Virginia.

Four rail sections were integrated into a special rack constructed for handling the wheelset during testing. The test rack was constructed of steel I-beams and bolted together. The rack design is suitable for modification to enable handling of inboard-or-outboard-bearing wheelsets in the event of future test requirements (refer to Figure 4-3).

4.6 POST-TEST PROCEDURES

In the post-test period, the instrumentation was disassembled and returned to storage. The wheelset and any non-expendable purchased items procured with Amtrak funds were made available to Amtrak for disposition.



INSTRUMENTATION
CONSOLE

ROADBED
SIMULATION

Figure 4-3. Wheelset Handling Rack

TABLE 4-2
FUNCTIONS TO BE DETERMINED

Measurement	Type Load	Data Plot Coordinates
Tangential Pin Bending	Static	Force vs. Strain
	Dynamic	Peak Strain vs. Square Root of Impact Distance
Lateral Pin Bending	Static	Force vs. Strain
	Dynamic	Peak Strain vs. Square Root of Impact Distance
Tangential Hub Reaction	Static	Force vs. Strain
	Dynamic	Peak Strain vs. Square Root of Impact Distance
Lateral Hub Reaction	Static	Force vs. Strain
	Dynamic	Peak Strain vs. Square Root of Impact Distance
Hub/Pin Micro-Slip	Static	Force vs. Slip
	Dynamic	Peak Slip vs. Square Root of Impact Distance

4.7 MODIFICATIONS TO TEST PLAN

If any of the concerned parties (FRA/Amtrak/ENSCO) desired test plan modifications, the proposed modifications were discussed with the other parties involved and modifications were by mutual consent.

4.8 INSTRUMENTATION INSTALLATION

Instrumentation of the wheelset was accomplished as follows.

4.8.1 Strain Gaged Pins

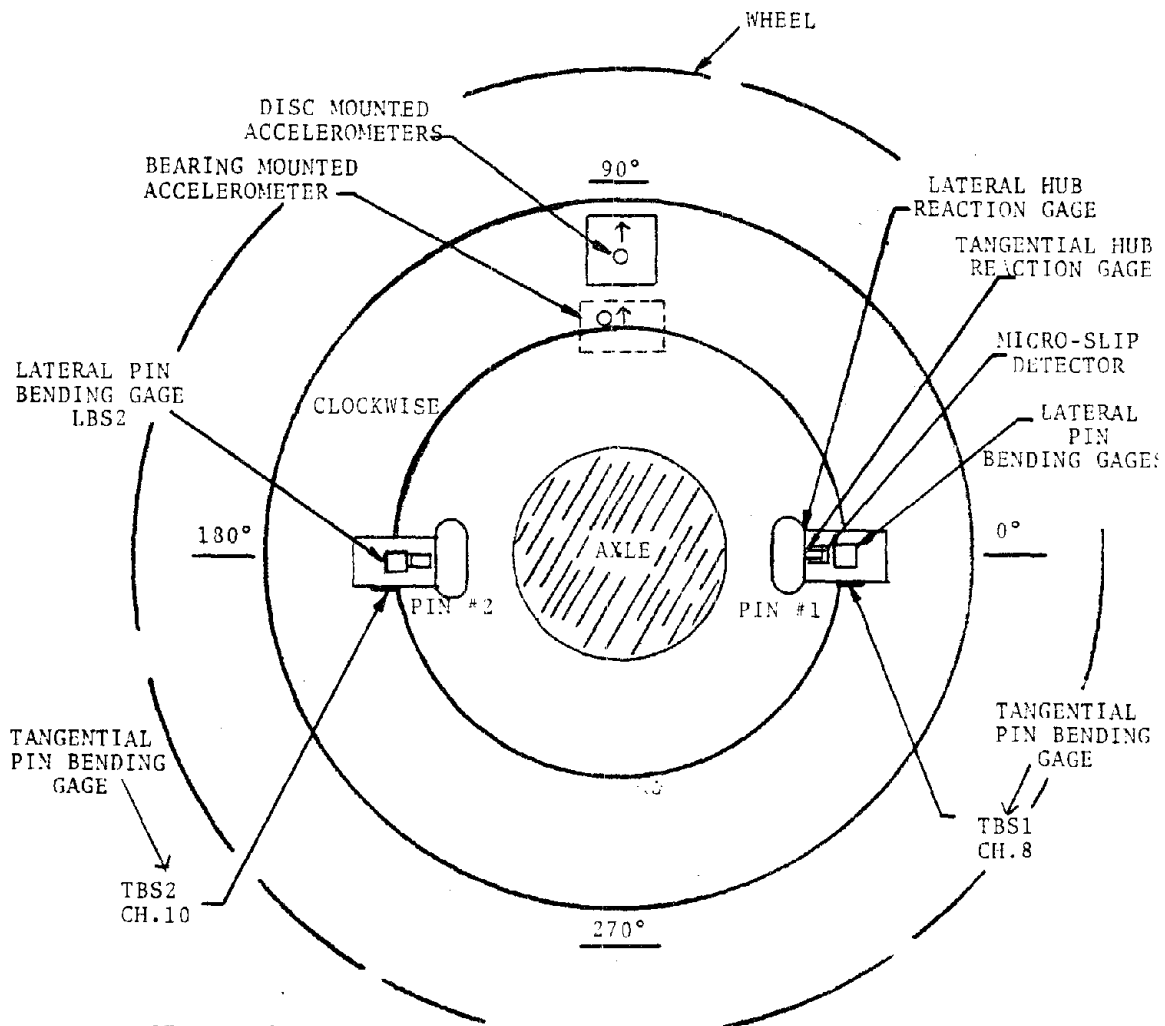
Two of the 34 millimeter, double-sleeve, resilient pins were removed from diametrically opposite positions in the disc brake assembly. One pin (hereafter designated Pin No. 1) was instrumented with two Micromasurement EA-06-062-AQ-350 strain gages located 90 degrees apart around the pin surface with sensitive axis aligned to measure pin bending strain (Figure 4-4). The disc brake hub socket from which pin No. 1 was removed, was also instrumented with two Micromasurement EA-06-062-AQ-350 strain gages positioned as shown in Figure 4-4. Pin No. 1 was then reinstalled in the disc assembly and aligned as shown in Figure 4-4.

The second pin (hereafter called Pin No. 2) was instrumented in a similar manner to pin No. 1 with the exceptions that the strain gages were Micromasurement WK-06-125BT-350 (a slightly larger gage than that used on pin No. 1) and the gage was positioned to sense lateral pin bending (Figure 4-4) and was located 180 degrees opposite its pin No. 1 counterpart. Pin No. 2 was then reinstalled in the disc brake assembly. The hub socket was not instrumented at pin No. 2.

4.8.2 Micro-Slip Detector

A strain-gaged feeler gage was incorporated in a micro-slip detection device as shown in Figures 4-7 and 4-8. The strain bridge was wired to make it insensitive to strain in the feeler gage other than bending strain. Following calibration of the micro-slip detector assembly, it was installed on the disc-brake assembly in a position to measure relative motion between pin No. 1 and the hub metal of the pin socket as shown in Figure 4-8. The micro-slip detector mounting fixture was bolted to the disc brake hub spoke.

The tip of the movement-sensitive arm was inserted in a shallow slot cut in the side of the pin. This slot allowed lateral



NOTE: Refer to Figure 4-5 for orientation of view

Figure 4-4. Instrumented Disc Coordinate System as Viewed from No. 5 Wheel Side of Brake Disc Assembly

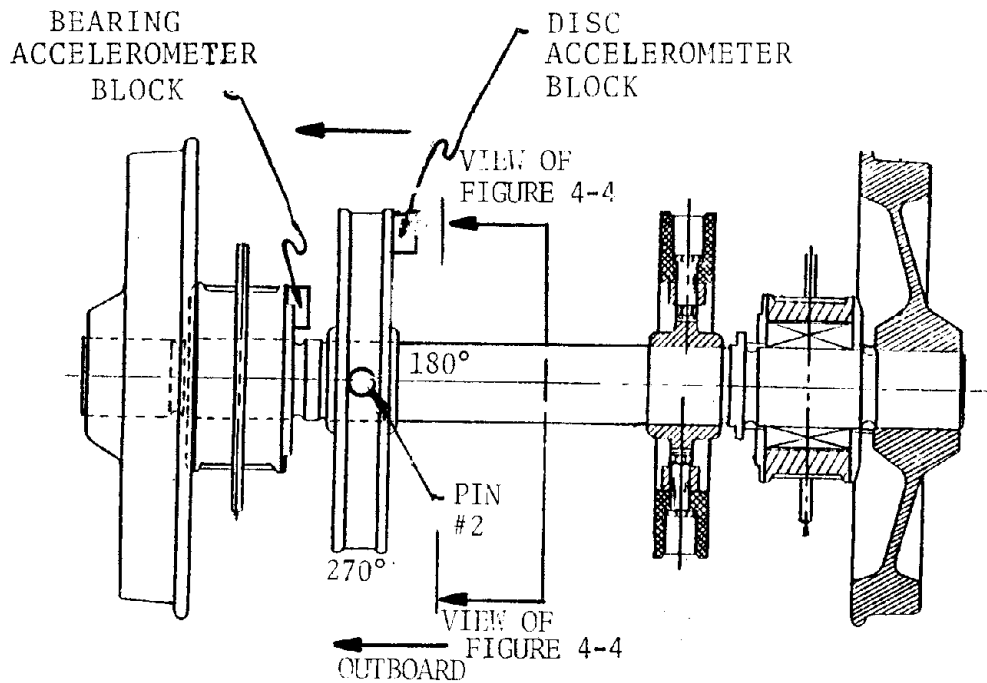


Figure 4-5. Side View of Instrumented Wheelset

movements of the pin to occur without affecting the micro-slip detector. Radial movements of the pin could, however, cause deflection of the movement-sensitive arm. The sensitive arm was adjusted to a 0.015-inch preloaded position in initial alignment to ensure continuous sensitivity to pin radial movements even though the lateral movement slot is wider than the 0.020-inch thick movement-sensitive arm.

4.8.3 Coordinate System

The disc brake assembly and the wheelset were assigned coordinates as shown in Figures 4-4 and 4-5.

4.8.4 Accelerometers

Four accelerometers were installed on the wheelset. Two were placed on the inboard side of the axle bearing housing and two were placed on the inboard side of the friction ring at the 90-degree position. At each location, one accelerometer was

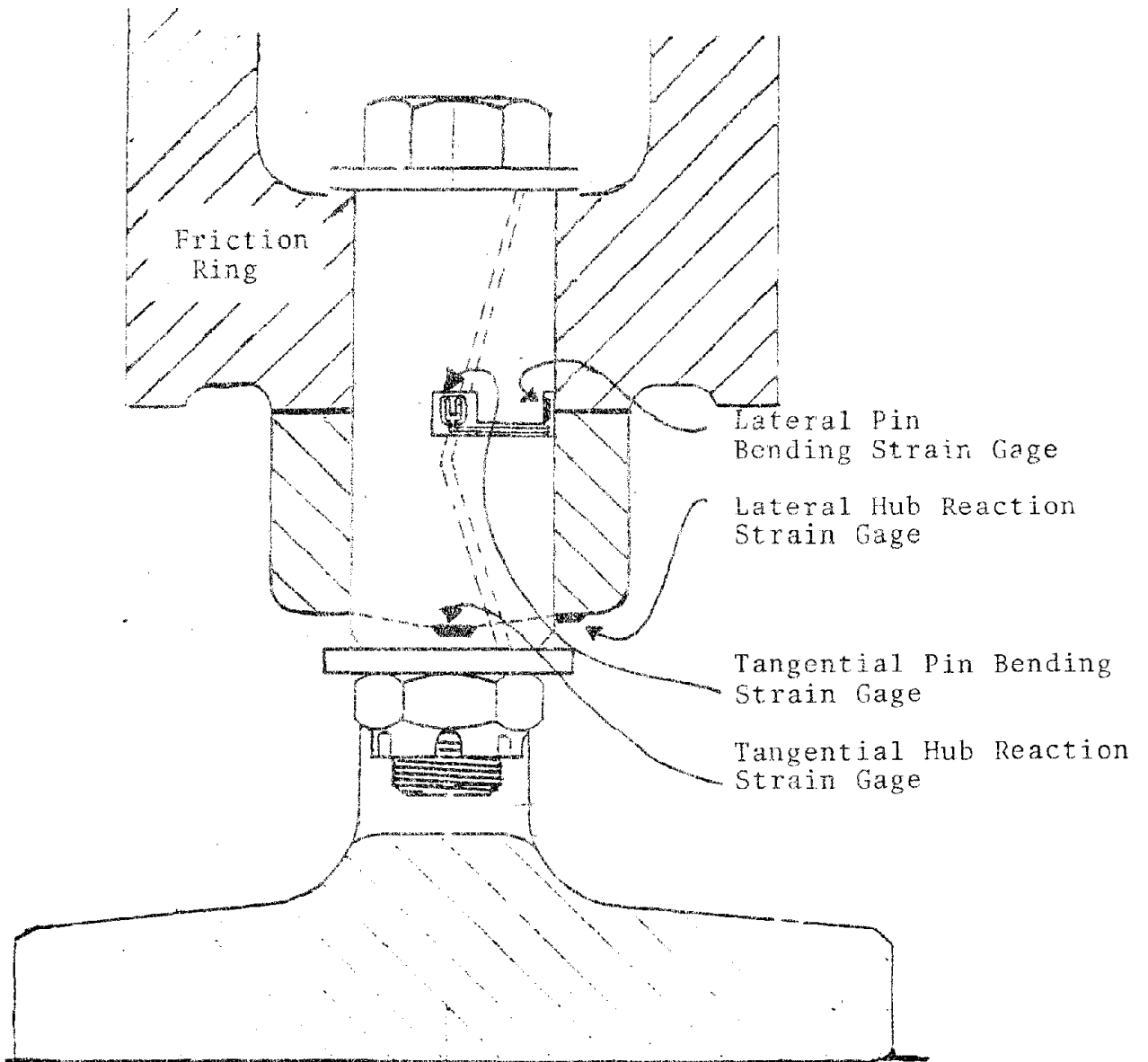
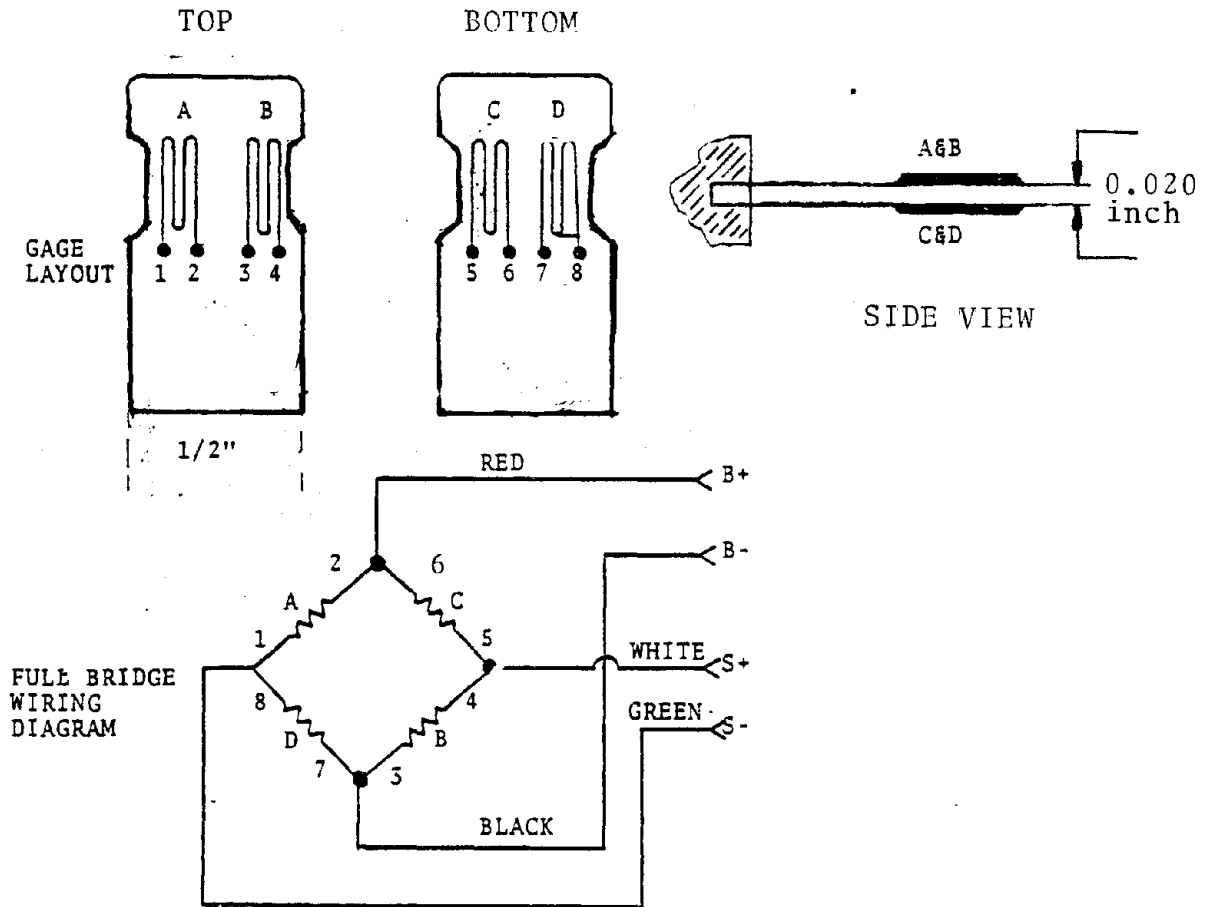


Figure 4-6. Cross Section of Disc Assembly Showing Strain Gaged Pin and Hub Socket. (Microslip detector not shown in this drawing.)



Gages A,B,C,D -- Micromasurement WK-06-125BT-350
 Gages: Gage Factor 2.04± 1.0%
 :k_t -2.3% :Lot #D-K06FD154
 applied with Micro-Measurements
 M-Bond-200 and environmentally
 protected with micromeasurements
 M-Coat A.

Figure 4-7. ENSCO Micro-slip Detector

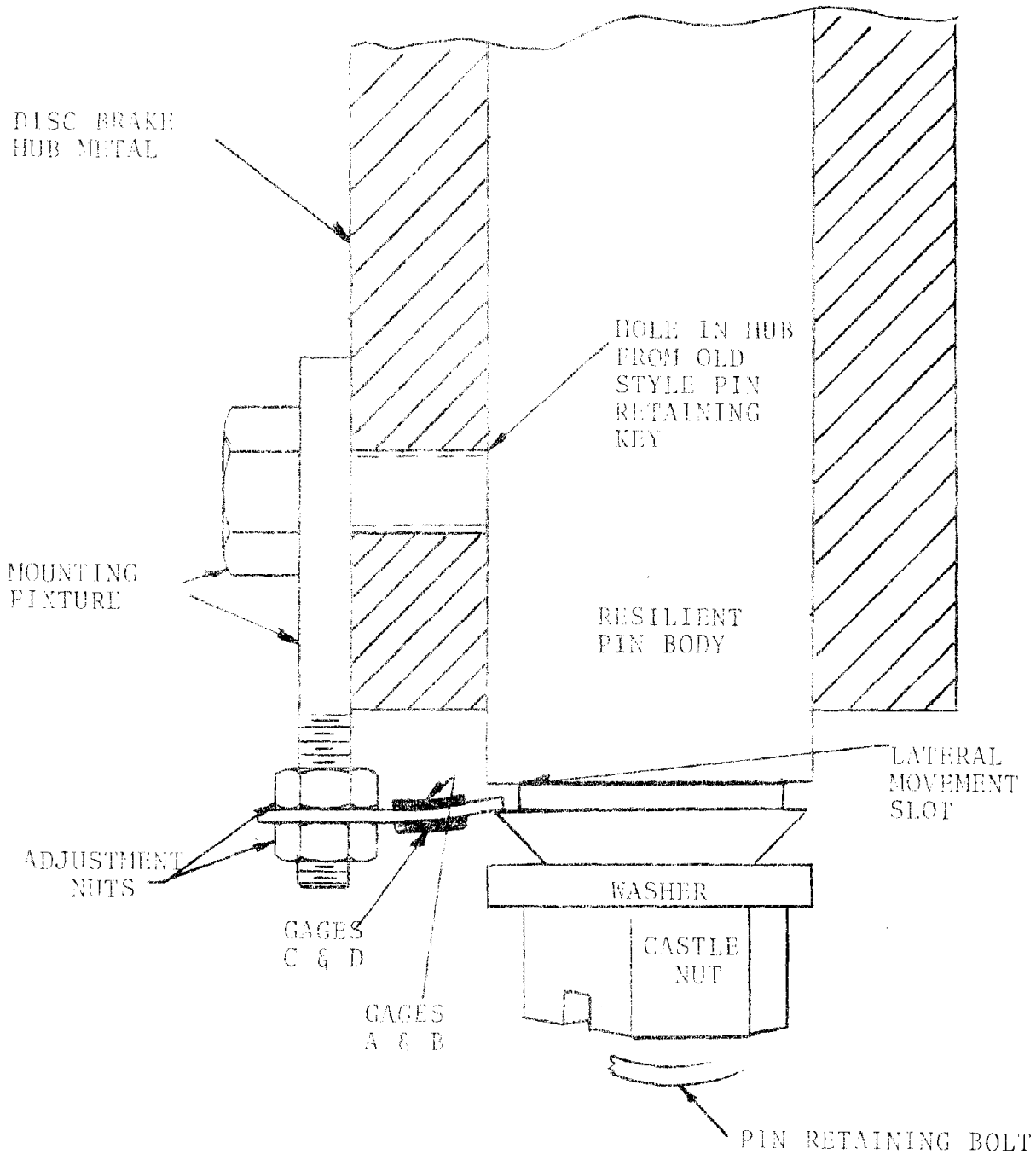


Figure 4-8. Micro-Slip Detector (MSDT) Installation Diagram

oriented to sense vertical accelerations, and the other was oriented to sense lateral accelerations. The bearing housing and brake disc were aligned to ensure zero angular displacement between the corresponding accelerometer's sensitive axis. The bearing housing was then fixed rigidly to the axle to maintain alignment and to ensure the bearing mounted accelerometers sensitivity to wheelset accelerations.

The accelerometers were mounted in phenolic blocks to decrease sensitivity to high frequency shock waves during testing.

The accelerometers mounted on the axle bearing were mounted identically to those used in the Over-the-Road testing so as to provide a reference for laboratory test acceleration levels sensed to those sensed in the Over-the-Road tests (OTR).

4.9 STATIC LOAD TESTING PROCEDURES AND RESULTS

Static load testing, as discussed in Section 4.1 was conducted to observe instrumented disc assembly behavior under the application of known static loads applied by using a 10,000-pound hydraulic jack. Three modes of disc assembly loading; tangential, lateral and diametric (as defined in Section 4.2) from zero to 5,000 pounds, were applied to the disc in six configurations (Table 4-3).

TABLE 4-3
LOAD CONFIGURATIONS

Mode	Angle (degrees)	Location Radius (inches)	Direction
Tangential	0	14.78	Clockwise
Tangential	180	14.78	Counter- clockwise
Lateral	0	10.78	Outboard
Lateral	180	10.78	Outboard
Diametric	0	13.78	N/A
Diametric	270	13.78	N/A

Figures 4-15 through 4-19 show the results of loading the disc in the six configurations described above. In all figures, tensile strain is given a positive sign and compressive strain is given a negative sign. Micro-slip data were assigned a positive sign convention to indicate outward radial motion of the pin towards the axle center. Solid lines are used to show data derived from controlled application of known static loads. Dashed lines are used to connect data points resulting from vibrational loads experienced by the wheelset/disc-brake assembly during testing. The results of the static load testing were as follows:

- Pin bending strain and micro-slip are essentially linear and proportioned to input loads up to 5,000 pounds.
- Hub hole reaction strain values were very small but reasonably close to values anticipated through calculation (Refer Appendix G)
- The static load testing showed that the relative rest positions of the three disc-brake components (friction ring, retaining pin, brake hub) are subject to change when the disc experiences even very low level shocks such as a light tap of a wrench or hammer.

Figures 4-9 through 4-13 illustrate this dynamic migration of the disc components. The micro-slip channel best illustrated this effect. Figure 4-14 shows a repeatable pattern to the dynamic migration produced by a hammer blow to the No. 6 wheelplate at 270 degrees followed by hitting the axle center at 180 degrees. The magnitude of the blow need only be slight (such as that produced by a No. 4 hammer allowed to fall under its own weight) to cause appreciable dynamic migration.

These graphs show that the disc easily moves around.

Figures 4-18 and Figure 4-19 further illustrate the effects of static and dynamic loading.

In summary, the results of this experiment indicate that the magnitude of pin slip resulting from small vibrational loads is much greater than pin slip which results from large static loads.

- The strain gaged pins were observed to incur approximately 13 $\mu\epsilon$ during temperature transitions from daytime at about 90 degrees to evening at about 75 degrees Fahrenheit.

4.10 DYNAMIC TEST PROCEDURES AND RESULTS

The primary purpose of the laboratory test was to examine the loads and the deflection of the instrumented pin resulting from non-rotating over-the-road testing. Dynamic testing employed two modes of wheelset dynamic loading. These were:

- Lateral impulse loads induced by hitting the suspended wheelset on the end of the axle (No. 6 wheelplate) with a 300-pound pendulum (bong) Figure 4-3.
- Vertical impulse loads were induced by placing the wheelset onto a simulated roadbed then lifting the No. 4 wheel end of the wheelset and letting it drop onto the rail section of the simulated roadbed (Figure 4-2).

During each mode of dynamic load testing, the bong height (h_B) or drop height (h_D) were selected to achieve the desired magnitude of wheelset accelerations as determined by the accelerometers located on the axle-bearing housing. Axle-bearing housing accelerations were monitored to observe peak acceleration data of approximately 10, 20, 40 and 80g for both dynamic loading modes. Sufficient test iterations were made at each reference g-level to allow photographing the real-time response of each of the eleven data channels via a four channel storage oscilloscope and a polaroid camera. Also, an amplitude spectral graph of each data channel was obtained at each reference g-level using a Nicolet Scientific UA-500 single-channel spectrum analyzer in conjunction with an x-y plotter. Spectral data were obtained from a 0.4-second data sample and analyzed for spectral data in a 0-1000 Hz bandwidth.

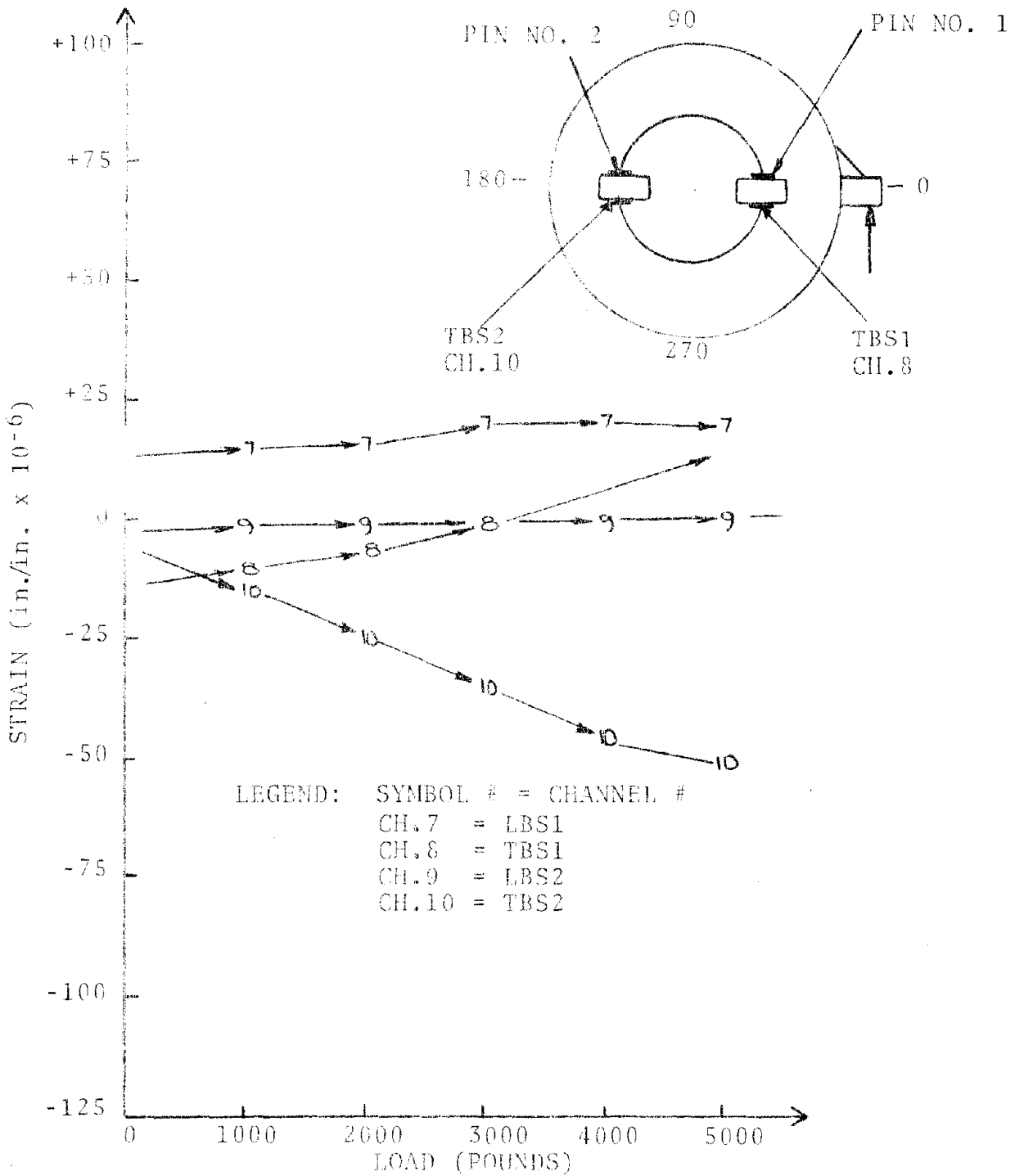


Figure 4-9. Clockwise Tangential Load Test at Zero Degrees (6-18-79)

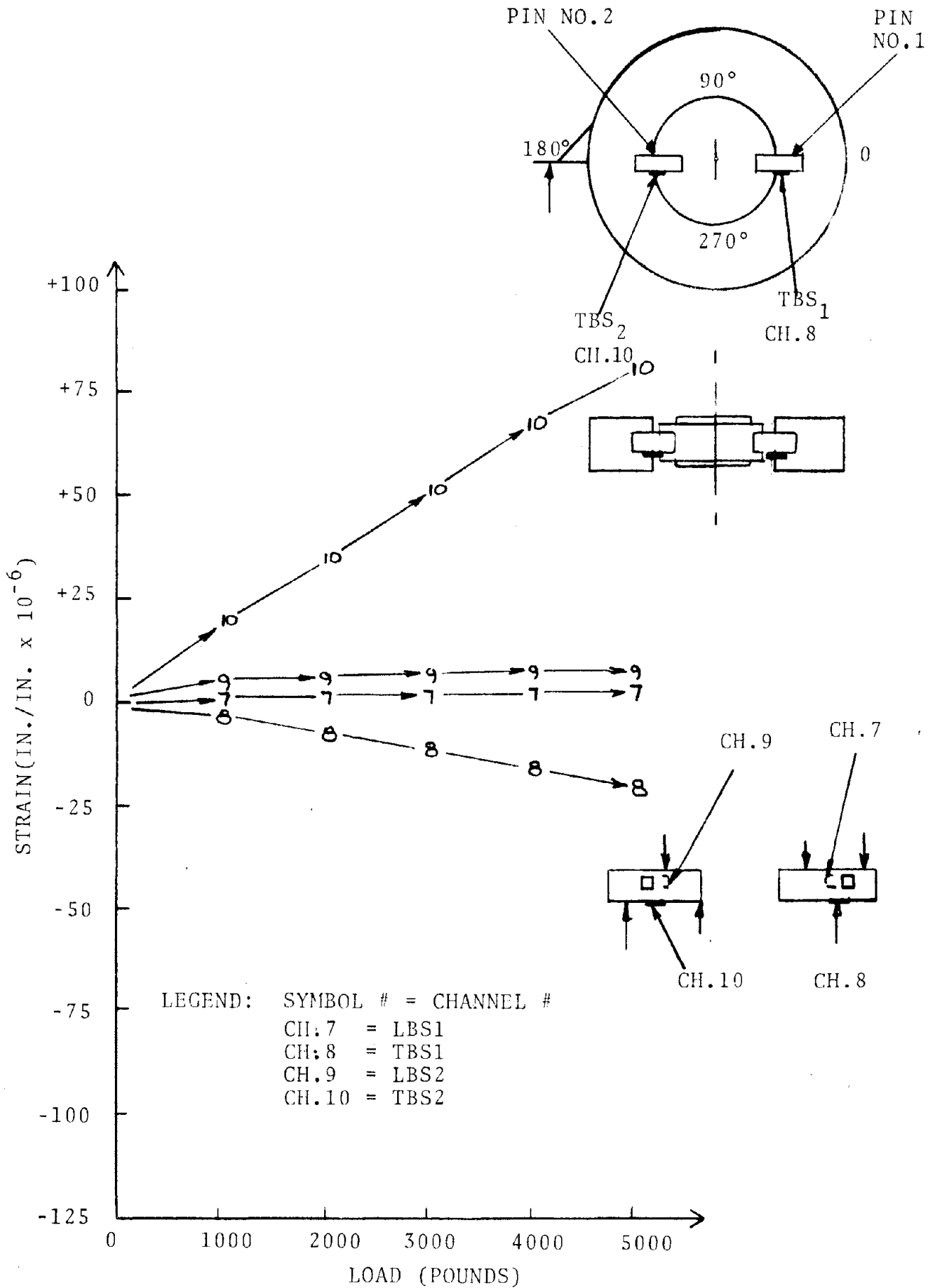


Figure 4-10. Counterclockwise Tangential Load Test at 180 Degrees (6-15-79)

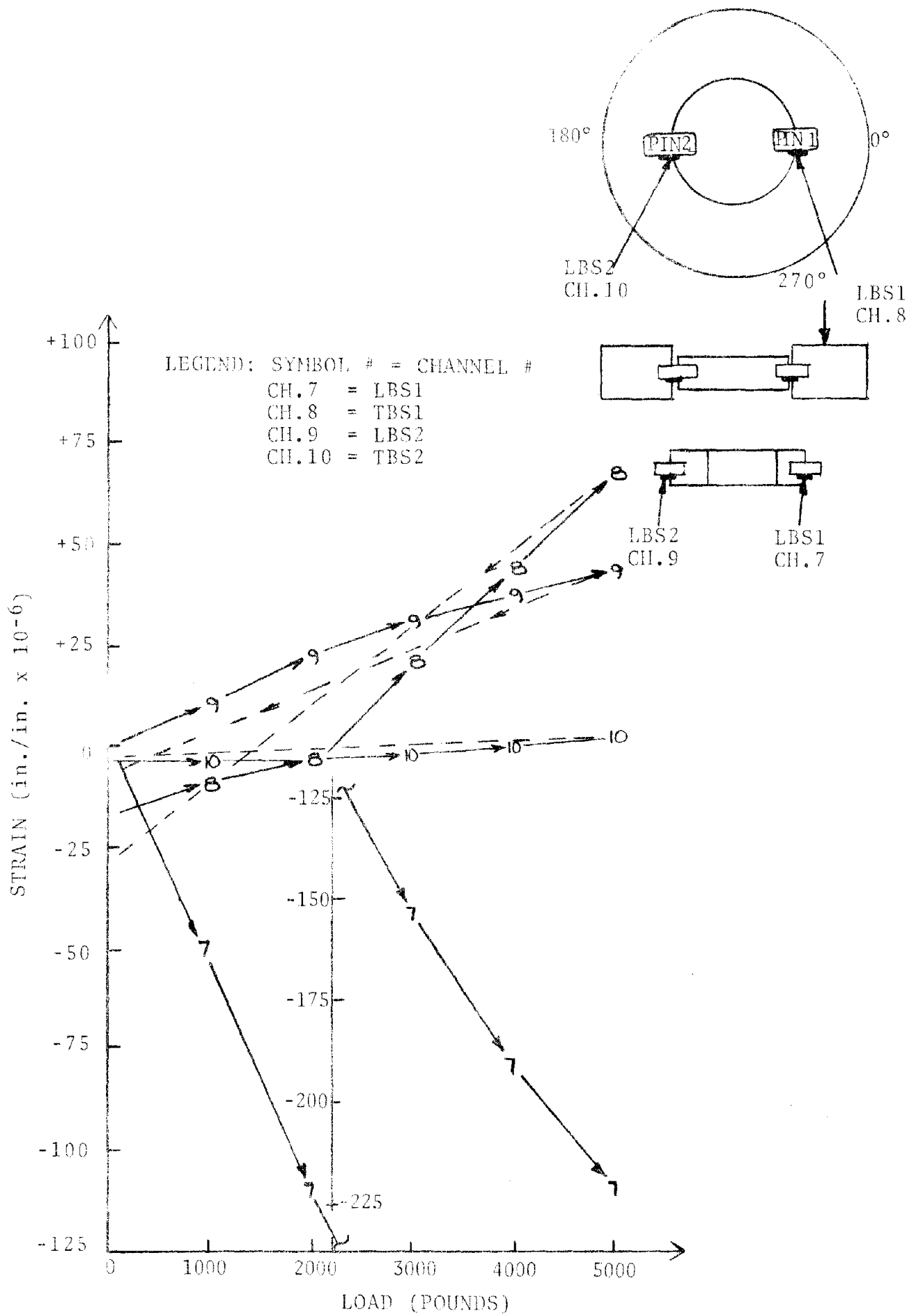


Figure 4-11. Outboard Lateral Load Test at Zero Degrees (6-18-79)

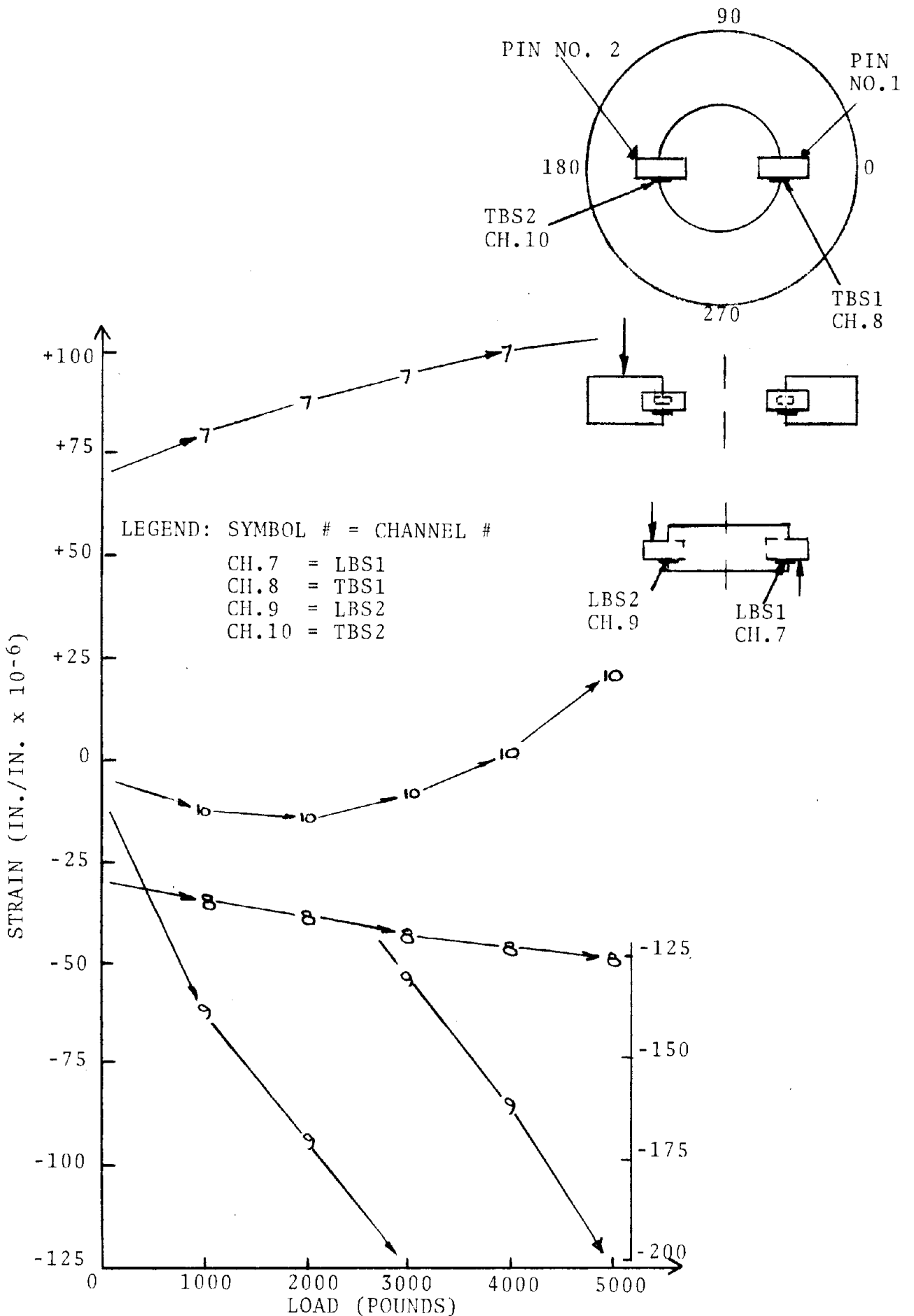


Figure 4-12. Outboard Lateral Load Test at 180 Degrees (6-18-79)

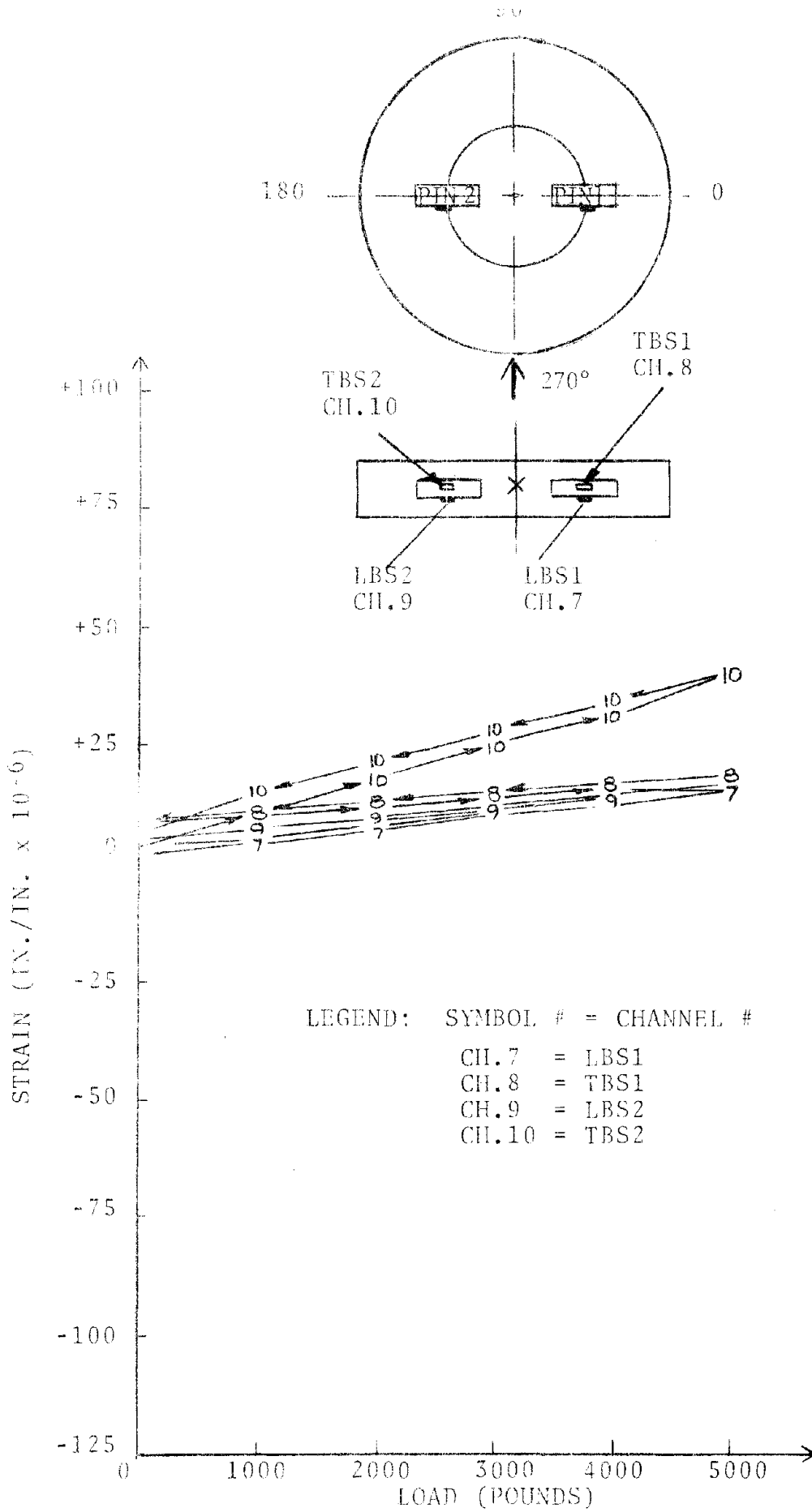


Figure 4-13. Diametric Load Test at 270 Degrees (6-19-79)

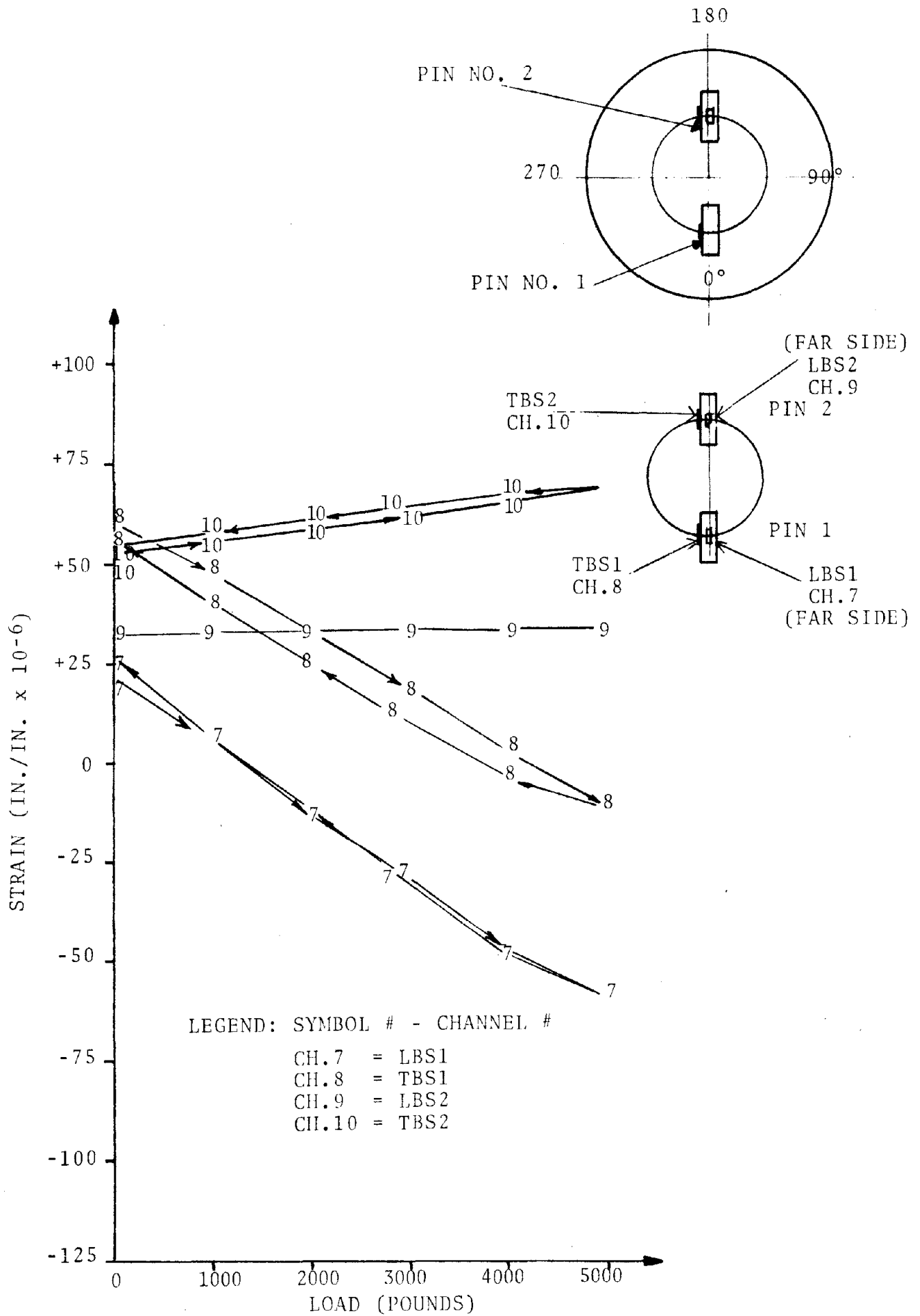


Figure 4-14. Diametric Load Test at Zero Degrees. (6-18-79)

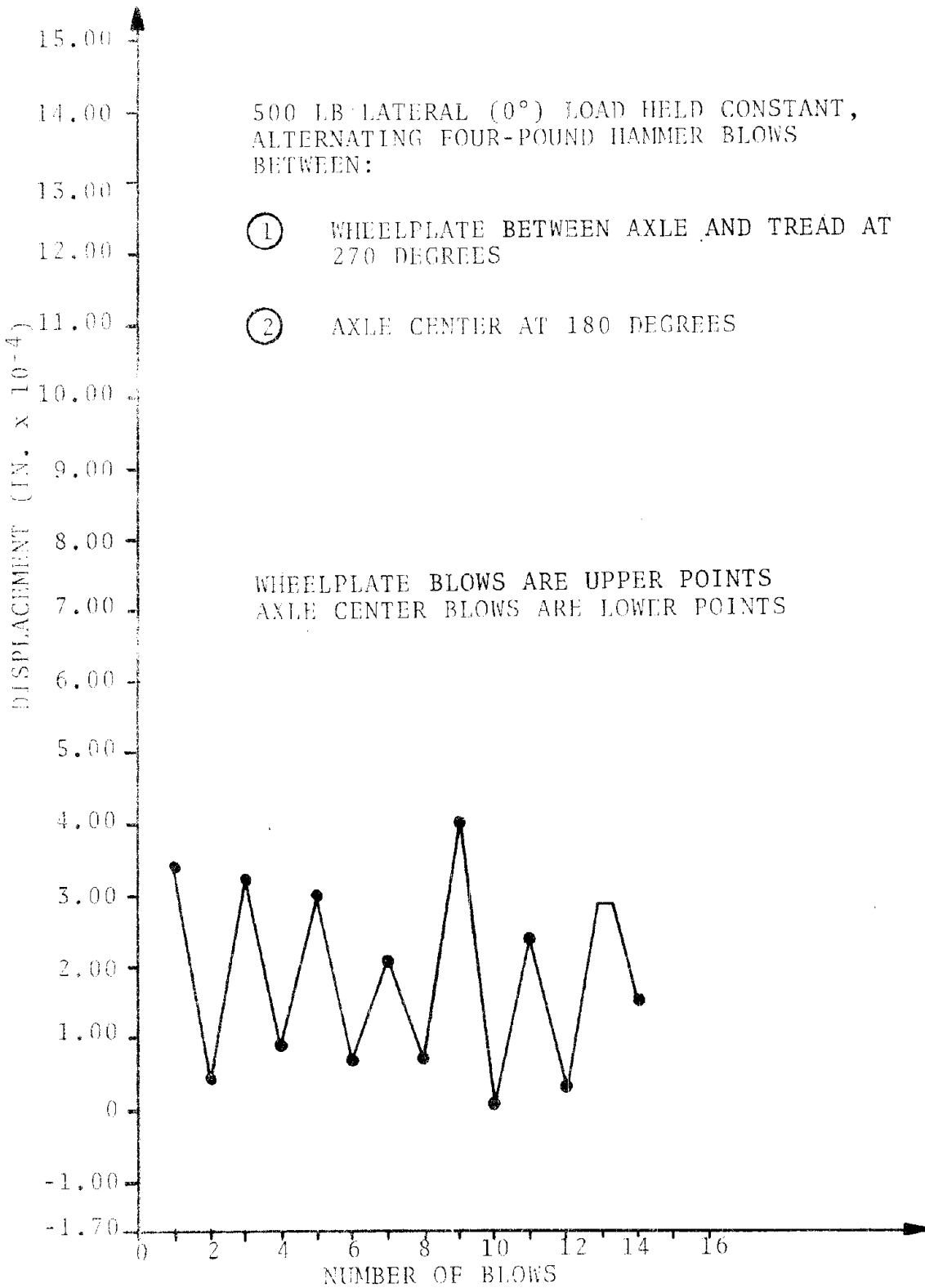


Figure 4-15. Micro-Slip of Pin with Lateral Loading

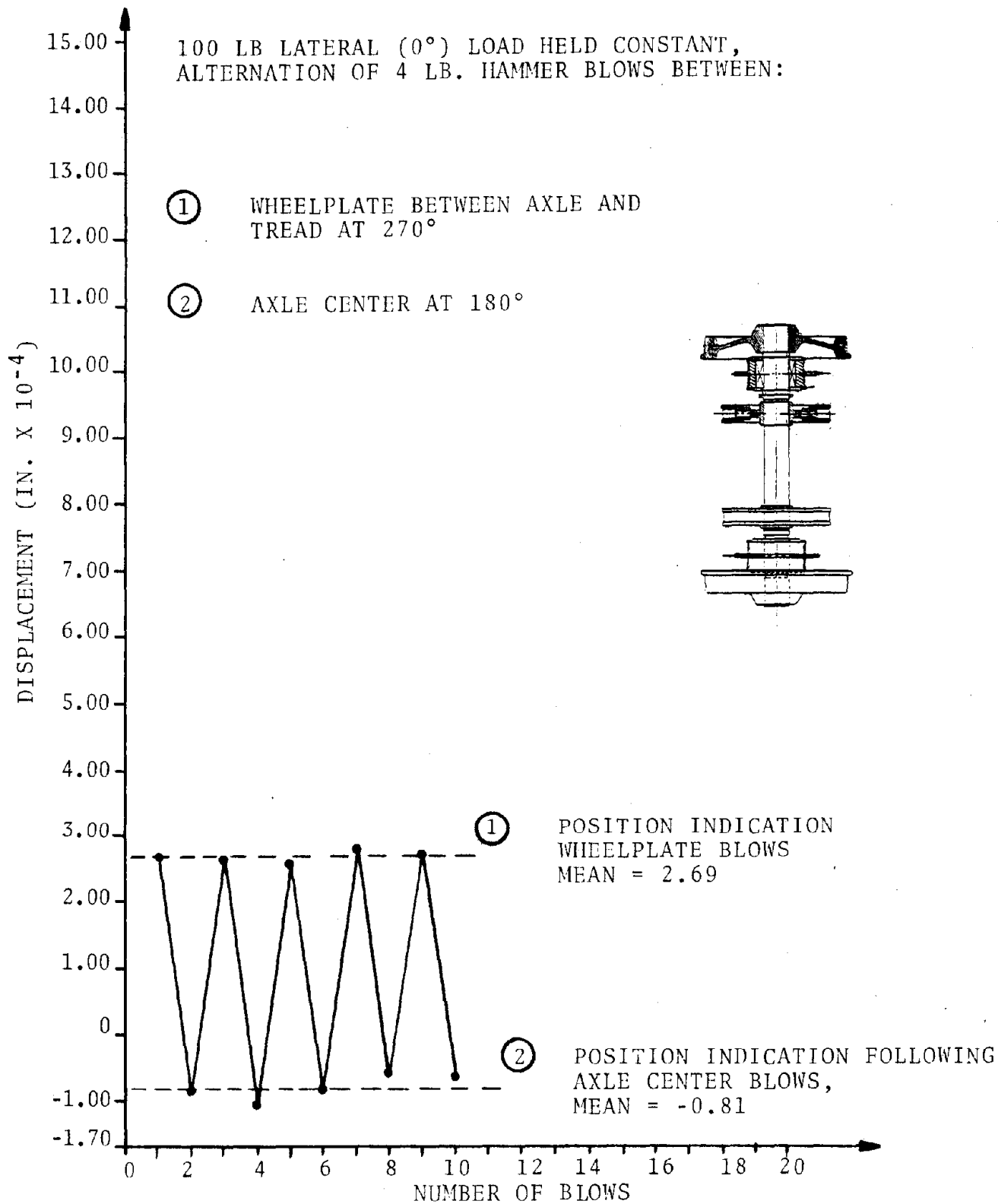


Figure 4-16. Micro-Slip of Pin with 100-Pound Lateral Load

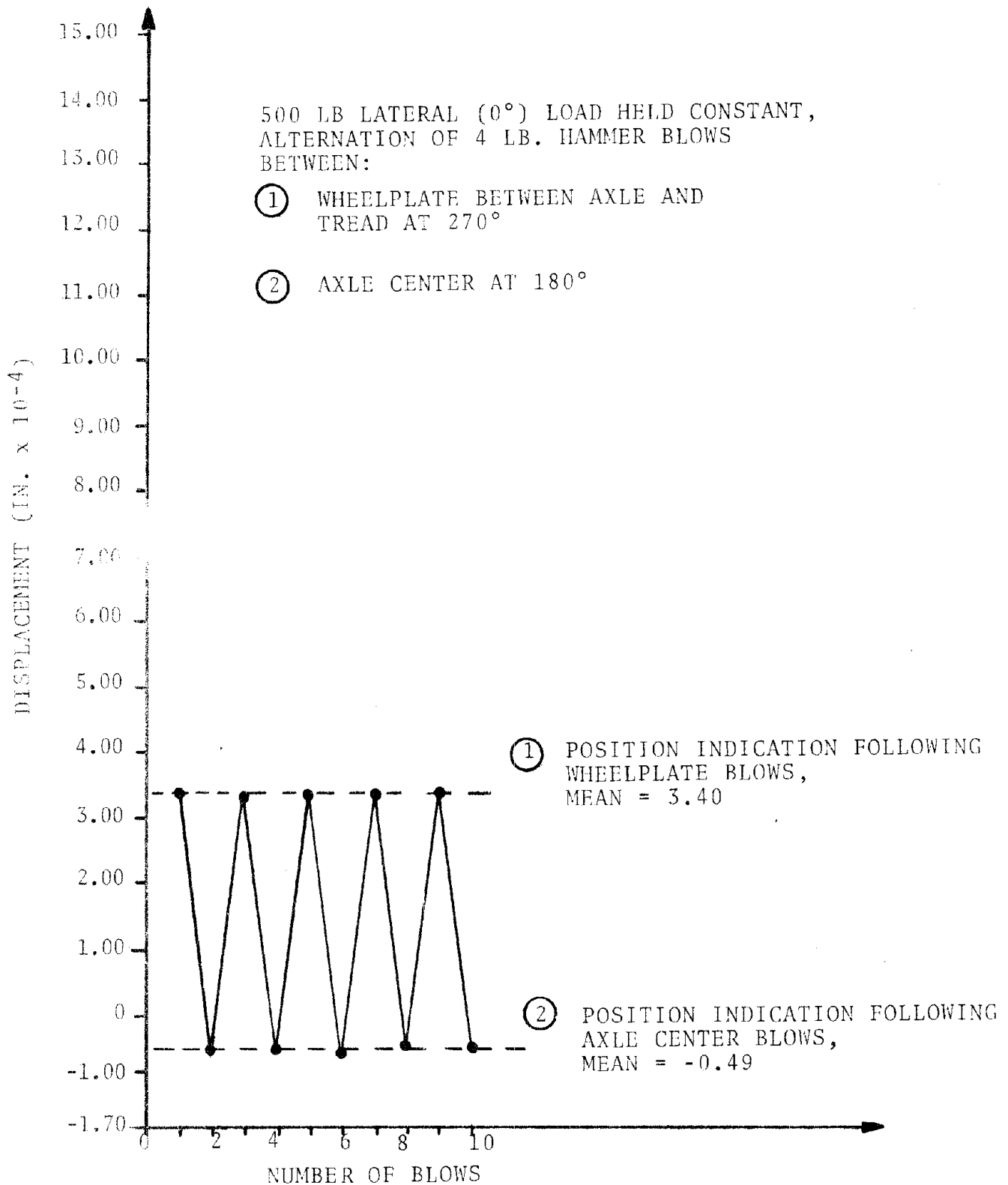


Figure 4-17. Pin Motion with 500-Pound Lateral Load

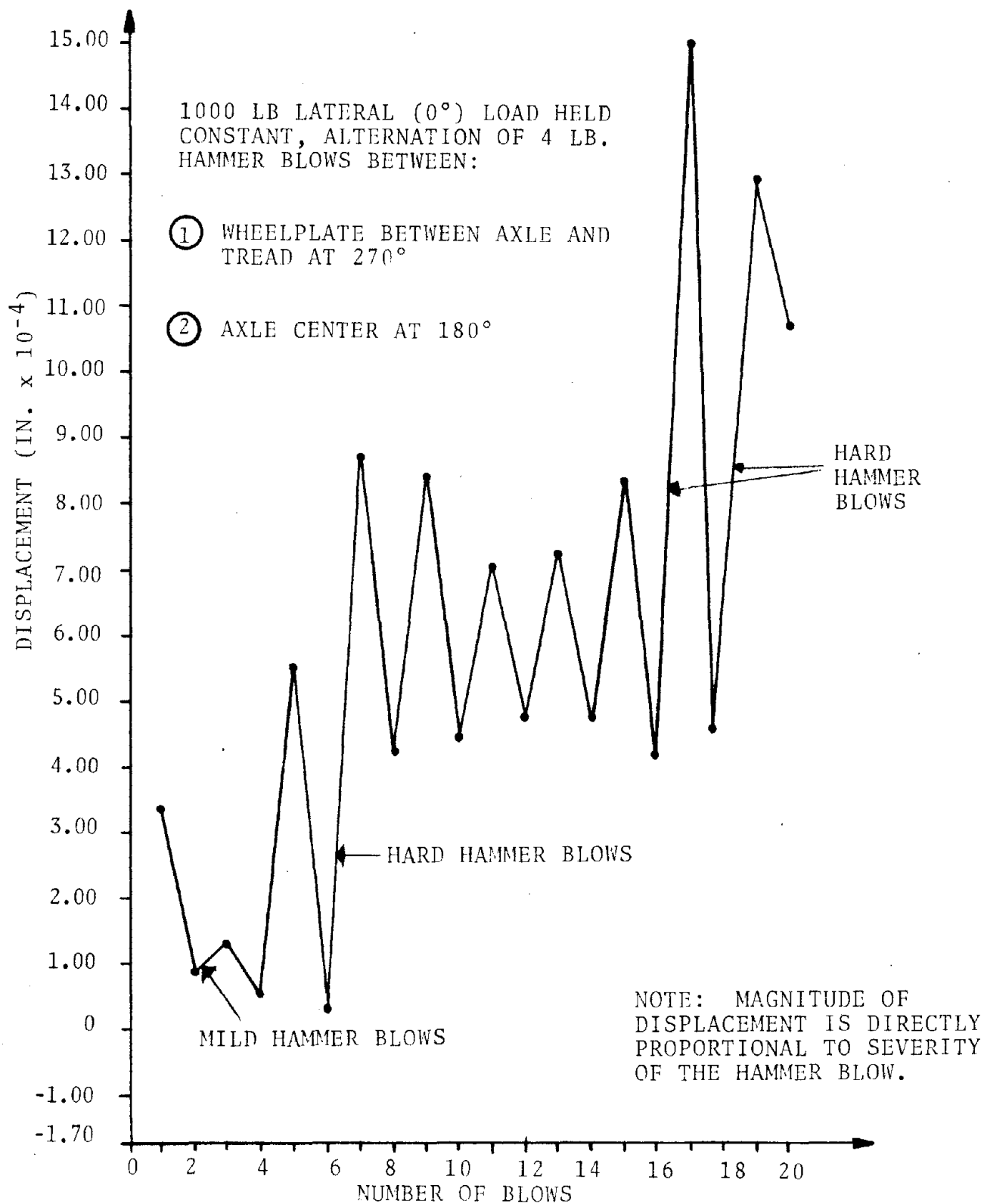


Figure 4-18. Pin Motion with Impulse Loading

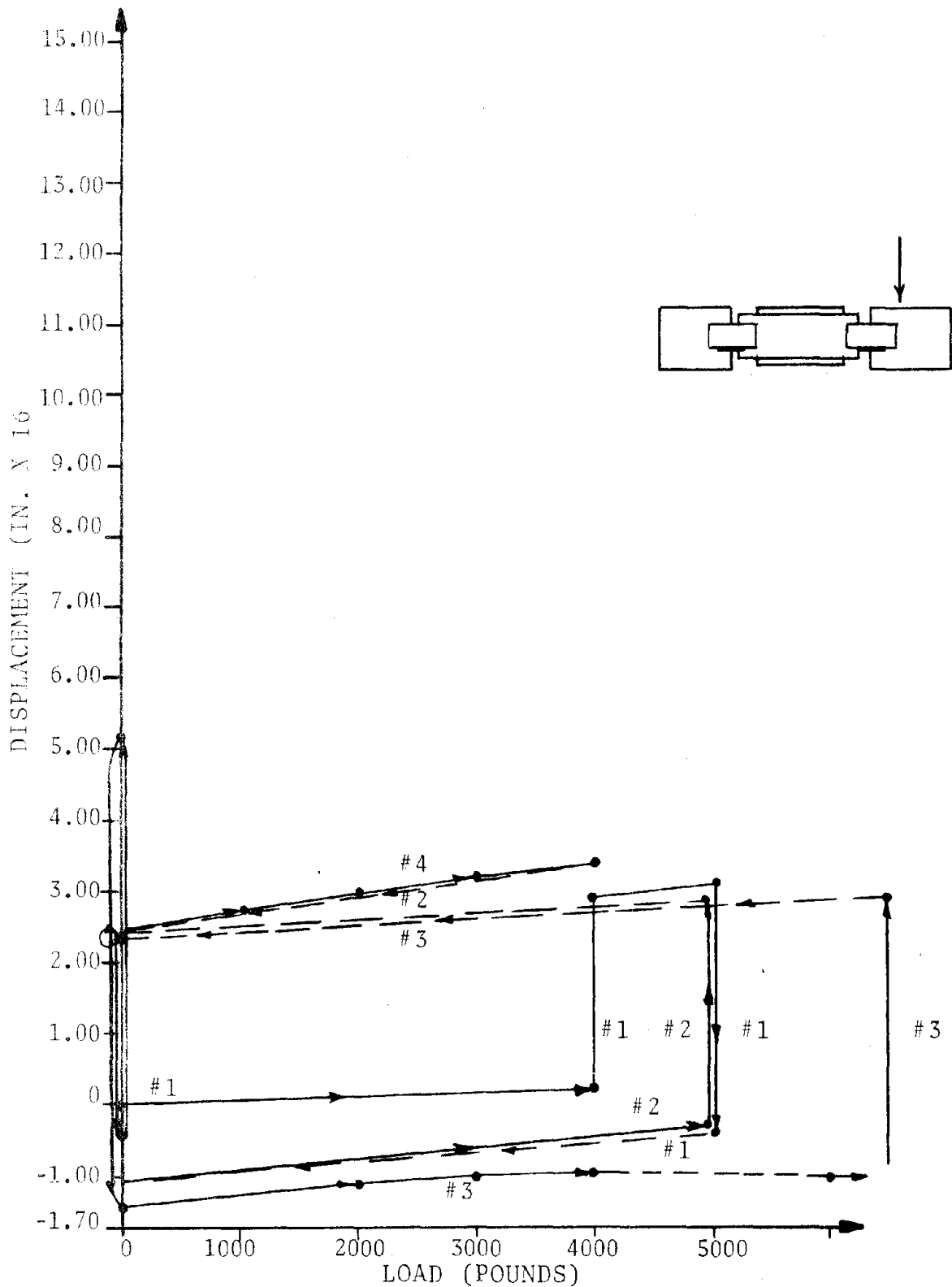


Figure 4-19. Pin Motion with Lateral Load

4.11 COMPARISON TO OVER-THE-ROAD DATA

The principle descriptor for OTR acceleration data was the rms g-level versus speed. In order to make a comparison of laboratory test data versus OTR data, it is necessary to develop a speed factor for the laboratory test data. The speed factor was developed as described in the following paragraphs.

A review of the OTR results showed that the acceleration data were dominated by wheelset, elastic-body motions excited by the impacting of minor defects (spalls) in the wheel tread surface on the rail surface when the wheelset was rolling. The time domain data from the OTR indicated that a major event occurred at least once during each half cycle of wheel revolution. For comparison purposes, the wheel-tread, surface-defect impact on the rail is analogous to the impact loading during laboratory testing. In each case the impact (hertzian contact) occurs in a few milliseconds then the wheelset vibrates in its fundamental modes for hundreds of milliseconds. Even minor defects in the wheels add energy to the vibrating system.

In the real world rolling environment, successive wheel rail impacts occur before the elastic body response has subsided. Because of this periodic excitation, the rms level of accelerations depends on the time between impacts determined by the rolling speed of the wheelset. At 80 mph with one major event per half cycle on a 36-inch diameter wheel, the time between significant events would be approximately 40 milliseconds.

For bong (pendulum) test data, the rms g-level for bearing accelerations was determined using the lateral accelerometer as a reference. The rms magnitude was approximated by combining the sinusoidal and triangular rms equation with the result that:

$$g_{rms} = A_{P_T} \div \sqrt{6} \quad (4.1)$$

where g_{rms} = RMS acceleration level

A_{P_T} = Peak acceleration level in T milli-seconds (T = 40 milliseconds for 80 mph)

For drop test data, the vertical bearing accelerometer was used as a reference. Drop test data exhibit a much higher damping rate to the high-frequency, high-g initial wheelset (elastic body) response to impact. The rms approximation was therefore divided into two regions. A combined sinusoidal/triangular approximation was used for the first 15 milliseconds and a pure sinusoidal rms value was used for the remaining 25 milliseconds of the 40-millisecond, 80-mph approximation. The result is:

$$g_{rms} = \frac{15}{T} (A_{P_{15}}) + \frac{T - 15}{T} (A_{P_{T-15}}) \quad (4.2)$$

g_{rms} = RMS acceleration level.

T = Basic period between impacts (40 milliseconds for 80 mph).

$A_{P_{15}}$ = Peak acceleration in the first 15 milliseconds after impact.

$A_{P_{T-15}}$ = Average peak acceleration in the interval after the first 15 milliseconds.

For 120-mph comparison, the rolling half period shortens to approximately 30 milliseconds. The drop test approximation (Equation 4.2) remains the same. The bong test approximation (Equation 4.1) becomes less accurate but still suitable to the purpose since the inaccuracy leads to a more conservative analysis.

Figure 4-20 summarizes the comparisons between the Laboratory Test, rms g-levels (based on the half-wheel-cycle approximation) and rms g-levels from the instrumented Non-Rotating Over-the-Road Test. Analysis of results from the Laboratory Test were based on the assumption that the wheel receives a hit each half-cycle; the resulting comparison is shown in Figure 4-20. The OTR, 120-mph predictions shown in Figure 4-21 are based on regression trend equations derived from the rms data graphs shown in Figures 3-7 and 3-8 from OTR test results (Section 3.5.1).

The results of this analysis indicate that sufficient impact magnitudes were used in both modes of laboratory testing to simulate 120-mph conditions in the rolling environment.

4.12 LATERAL IMPULSE LOADING TEST OBSERVATIONS

Figures 4-25 through 4-35 show the real time response of each of the eleven data channels on the instrumented wheelset. The data show real time response for 0.015, 0.105, 0.22, 0.27 and 0.45 inch bong heights which were collected photographically by two methods:

- First, the storage oscilloscope was triggered on impact, thereby using the first major positive gong event sensed by the lateral-axle accelerometer (LAA) to initiate data collection.
- Second, a microswitch was used to trigger data collection in advance of the impact, thus enabling the operator to view small signals at impact.

Both trigger methods proved to be unreliable in establishing synchronization between successive test iterations, but did provide some advantages in the way data were presented for viewing. Where advance triggering was allowed, observation of the full initial impact period including impact triggering, provided a longer period of observation after impact.

$$g_{rms} = \frac{15}{T} \left(\frac{A_{P15}}{\sqrt{6}} \right) + \frac{T-15}{T} \left(\frac{A_{P15-T}}{\sqrt{2}} \right)$$

g_{rms} VALUE WHERE FOR:

DROP:

$$g_{rms} = A_{P15} / \sqrt{6}$$

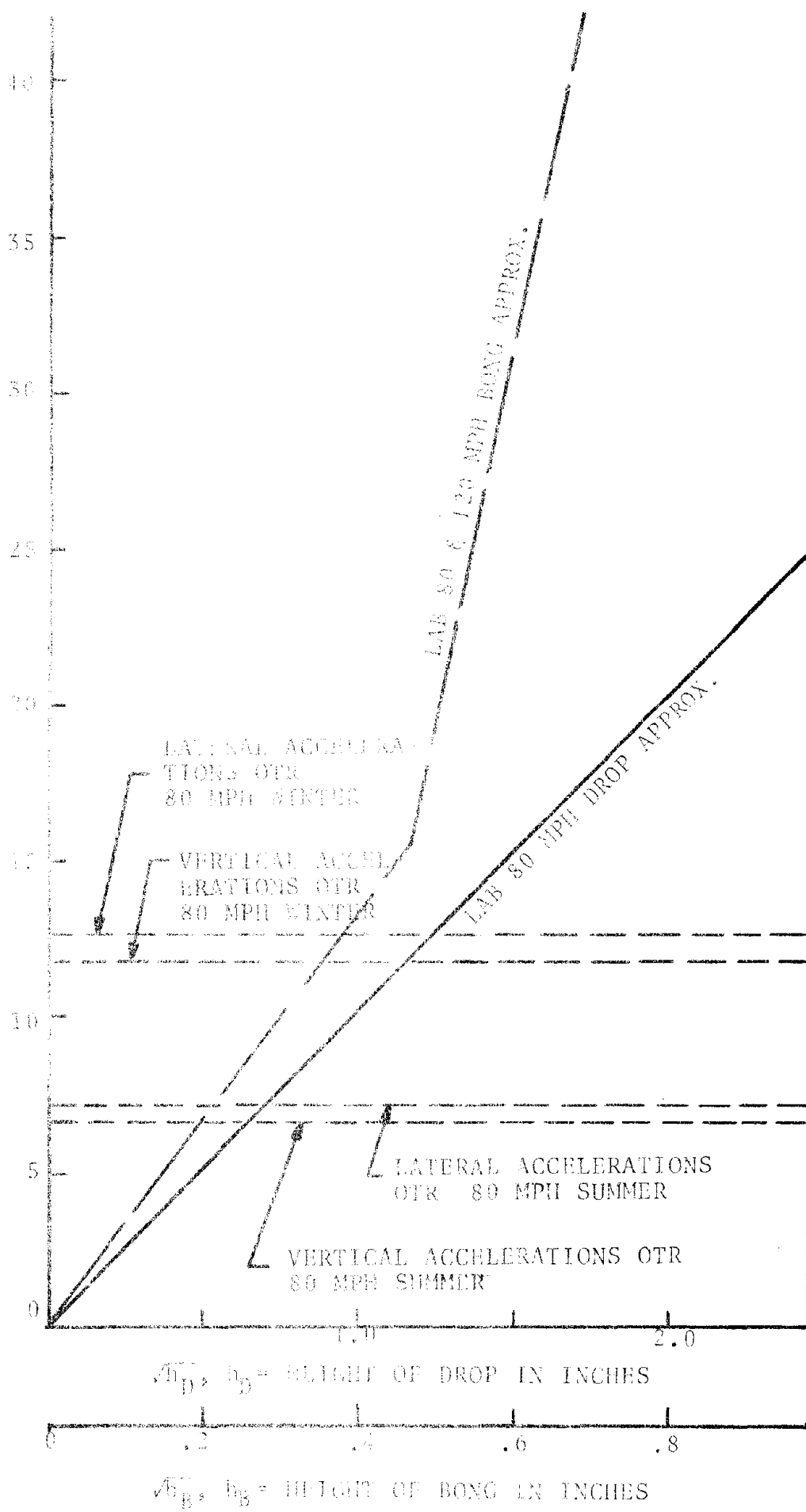


Figure 4-20. Comparison of 80 mph Over-The-Road Test (OTR) and Laboratory Test rms g-levels versus the Square Root of Bong and Drop Height

$$g_{rms} \text{ VALUE WHERE FOR: } \text{DROP: } g_{rms} = \frac{15}{T} \left(\frac{A P_{15}}{\sqrt{6}} \right) + \frac{T-15}{T} \left(\frac{P_{15-T}}{\sqrt{2}} \right)$$

$$\text{BONG: } g_{rms} = A p_T / \sqrt{6}$$

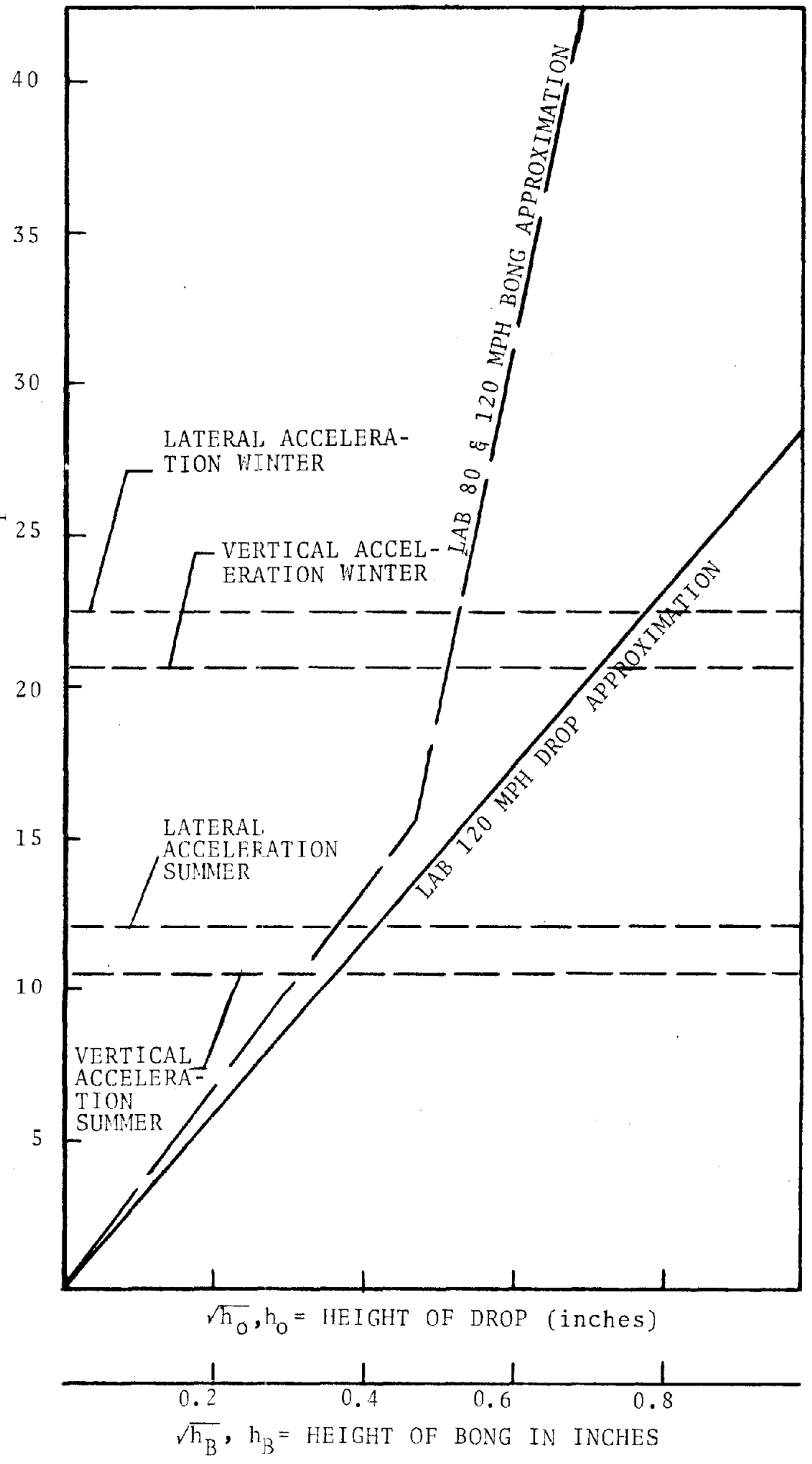


Figure 4-21. Comparison of Predicted 120 mph Over-the-Road to Laboratory Tests

The laboratory tests (Appendix E) contain an amplitude spectral graph for each of the time history data traces in the photographic presentation. The following observations were made from the real-time-data, photographic presentation of the bong tests:

- Lateral, pin-bending strain and lateral, rotor acceleration data due to micro-slip have similar characteristics. During the first 15 milliseconds after impact, the dominant frequency is approximately 560 Hz. The 560-Hz elastic-body motions of the friction ring subside rapidly in amplitude and are not readily observable 30 milliseconds after impact. At this point, 360 Hz is the dominant mode of disc vibration. The 360-Hz input decays slowly and is modulated in amplitude at a 72-Hz rate. This means that the friction ring is moving as a rigid body first inboard, then outboard at a 360-Hz rate, and that the eight pins connecting the friction ring to the hub experience a unidirectional 360-Hz bending (and corresponding slippage). At the same time, the entire disc assembly is being tilted about its axis at a 72-Hz rate as the axle bends at its fundamental rate.
- The lateral bending stress appears to ring out at 560 Hz initially and then continue to ring out at 360 Hz as shown in Figure 4-22.

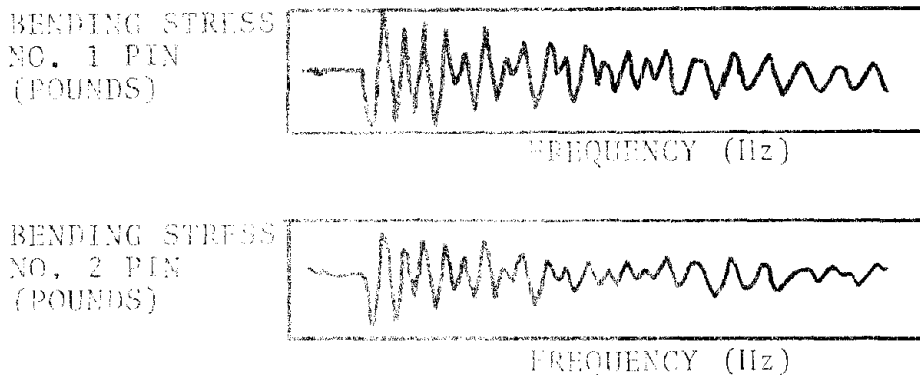


Figure 4-22. Lateral Bending Stress on Pins vs. Frequency

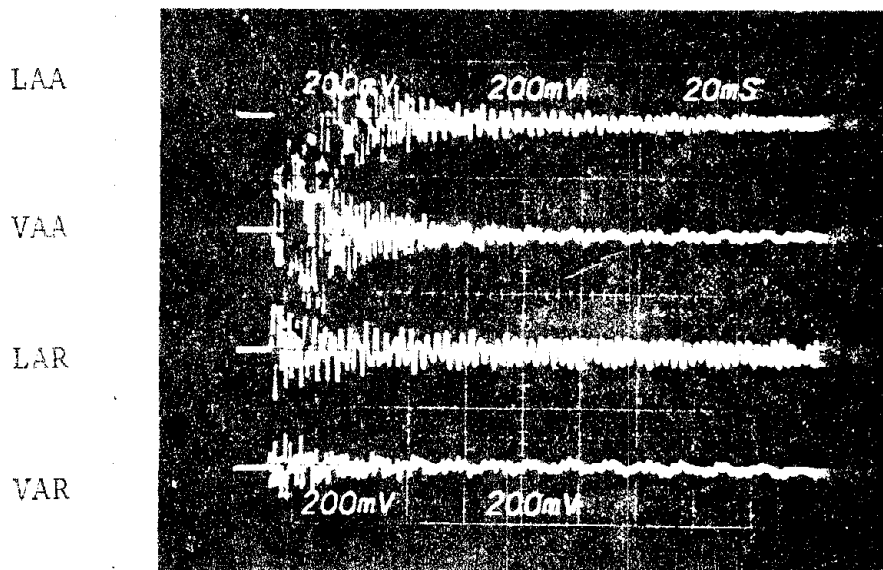
At the same time, the lateral acceleration measured at the top of the disc is 180 degrees out of phase with the bending signal. Since the acceleration signals are 180 degrees out of phase with the displacement signals, the disc is translating as a rigid body. Approximately 30 milliseconds after the initial impact, only the 330-Hz motion remains, and at this time the acceleration is still 180 degrees out of phase with the bending stress. Therefore, the disc appears to be still translating.

The micro-slip detector shows a similar initial ringing at 560 Hz which dies away within the first 20 milliseconds leaving a clear 330-Hz motion. The micro-slip appears to be in phase with the lateral acceleration signal and 180 degrees out of phase with the lateral bending.

- Tangential pin bending strain resembles vertical acceleration on the friction rotor; however, tangential strain on pin No. 1 tends to be 180 degrees out of phase with the tangential bending strain on pin No. 2. This signifies a rotary oscillation.
- Bearing accelerations are dominated initially by a 1012 Hz frequency which reaches a maximum amplitude at approximately 10 milliseconds after the instant of impact. The 1012-Hz signal decayed approximately 30 milliseconds after impact.

During the first 30 milliseconds, 1012-Hz bearing accelerations were approximately three times greater in amplitude than the 560-Hz disc accelerations; however, in the period greater than 30 milliseconds after impact, the data shows bearing and disc accelerations having very similar frequency characteristics (Bearing - 332 Hz, Disc - 360 Hz) with the amplitude of the disc acceleration approximately three times greater than the bearing acceleration (Figure 4-23).

- Micro-slip data were ac coupled, therefore, the effects of dynamic migration were not visible in dynamic testing. However, during demonstrations of the test apparatus, dc coupling was occasionally used to demonstrate that dynamic migration was significant with respect



* Amplitude = 4.0 g/division

Figure 4-23. Lateral Impulse Loading

to time-varying slip amplitude. In considering pin wear models, dynamic migration, while an interesting phenomenon relating to disc microscopic looseness, is probably not a significant factor.

4.13 CONCLUSIONS

The lateral impulse tests indicate that lateral shocks produce relative motion between the hub hole and the resilient pin of 10^{-4} inch. The magnitude of the slip-motion is directly proportional to the amplitude of accelerations measured at the axle bearing housing while its frequencies correspond to elastic body motions. The pin bending and hub hole reaction strains are in direct proportion to bearing housing accelerations and have the same frequency characteristics as observed by the OTR. The method of pin wear experienced in revenue service is microscopic abrasion

(fretting corrosion). Abrasion of this type is proportional to the normal force between two surfaces and the total relative slip between the two surfaces.

Wear slip distance x normal forces

where

$$\text{Slip distance} = 4 \times \frac{\text{peak amplitude}}{\text{cycles}} \times \frac{\text{cycles}}{\text{second}} \times \text{time}$$

Normal force pin bending strain.

The force caused by roll pin pre-load is not considered here since its relative magnitude is insignificant at high-pin-bending strains.

The wear equation becomes

Wear peak slip amplitude x pin bending strain

Both slip and strain are proportional to bearing acceleration amplitudes so the wear proportionality now becomes

$$\text{Wear (g-level of bearing)}^2$$

Figure 4-24 is a graphic presentation of the direct proportionality of both pin bending strain and micro-slip to lateral acceleration levels.

Wear (acceleration)

In winter, the acceleration is 2 to 4 times the acceleration experienced in summer. Therefore

$$\text{Wear}_{\text{winter}} = (2 \text{ to } 4)^2 \times \text{summer wear}$$

$$\text{Wear}_{\text{winter}} = 4 \text{ to } 16 \times \text{summer wear}$$

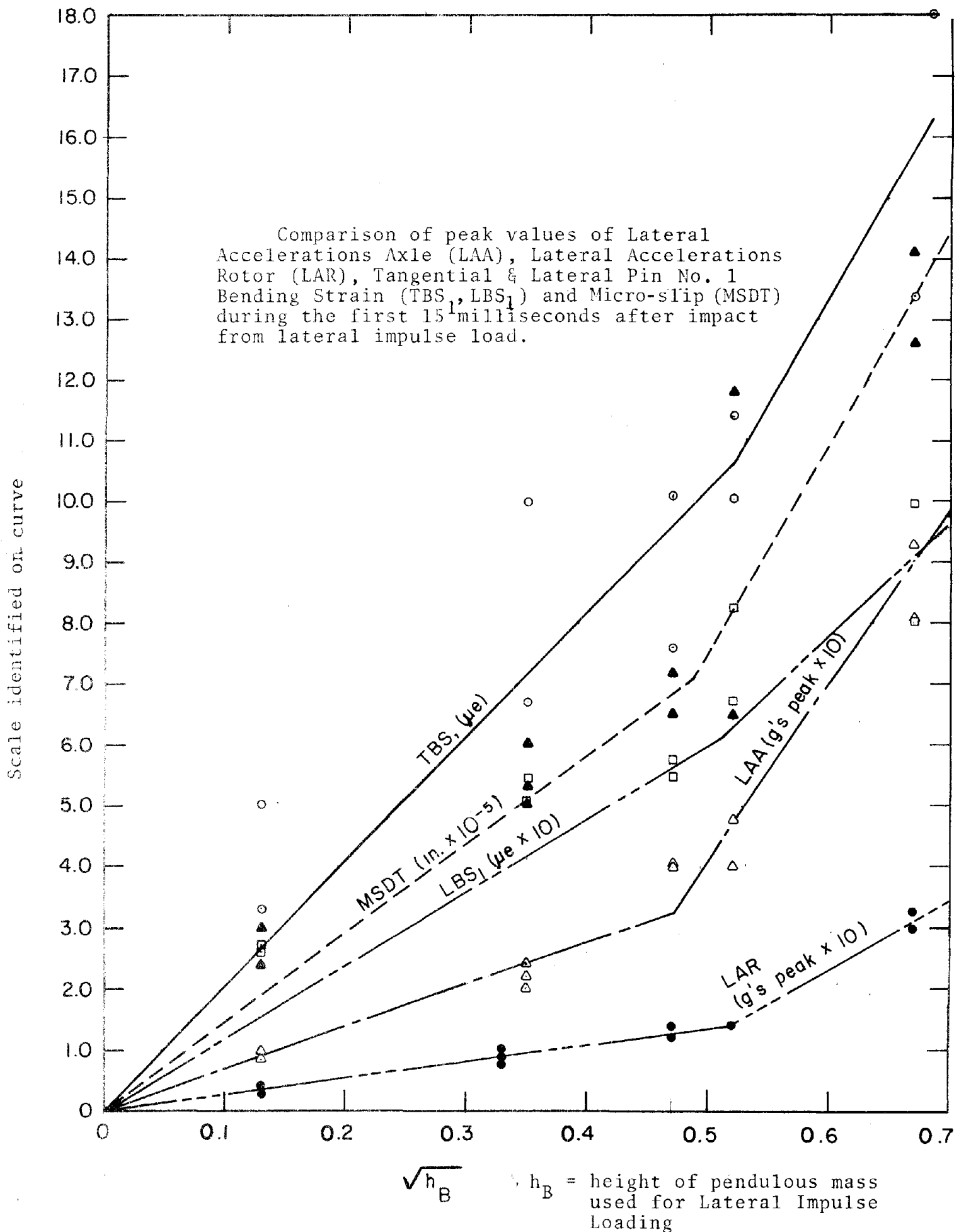


Figure 4-24. Comparison of Peak Values of LAA, LAR, TBS, LBS and MSDT












Height of Bong (in) .015 Observation Time Base (ms/div) 5
 Test Date 7/2/79

Description of Measurement	Signal Amp. (eng. units/div.)	Photograph of Observed Signal
Lateral Acceleration Axle (LAA)	10 g/div	
Vertical Acceleration Axle (VAA)	4 g/div	
Lateral Acceleration Rotor (LAR)	4 g/div	
Vertical Acceleration Rotor (VAR)	4 g/div	
Microslip (MSDT ₁)	1.18×10^{-4} in/div	
Lateral Reaction Strain (LRS ₁)	16.7 μ e/div	
Tangential Reaction Strain (TRS ₁)	16.7 μ e/div	
Lateral Bending Strain (LBS ₁)	16.7 μ e/div	
Tangential Bending Strain (TBS ₁)	16.7 μ e/div	
Lateral Bending Strain (LBS ₂)	16.7 μ e/div	
Tangential Bending Strain (TBS ₂)	16.7 μ e/div	

*Subscript 1 denotes instrumented pin No. 1
 2 denotes instrumented pin No. 2

Figure 4-25. Lateral Impulse Loading Data

Height of Bong (in) .015 Observation Time Base (ms/div) 5
 Test Date 7/2/79


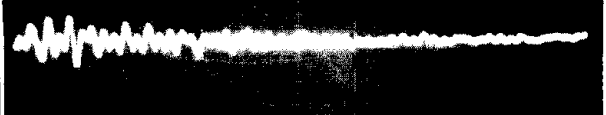

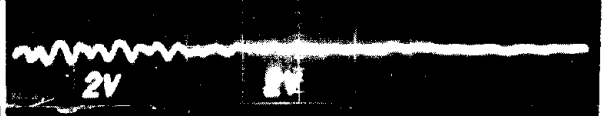


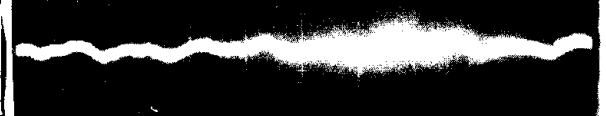




Description of Measurement	Signal Amp. (eng. units/div.)	Photograph of Observed Signal
Lateral Acceleration Axle (LAA)	10 g/div	
Vertical Acceleration Axle (VAA)	10 g/div	
Lateral Acceleration Rotor (LAR)	4 g/div	
Vertical Acceleration Rotor (VAR)	4 g/div	
Microslip (MSDT ₁)	1.18×10^{-4} in/div	
Lateral Reaction Strain (LRS ₁)	16.7 μ e/div	
Tangential Reaction Strain (TRS ₁)	16.7 μ e/div	
Lateral Bending Strain (LBS ₁)	16.7 μ e/div	
Tangential Bending Strain (TBS ₁)	16.7 μ e/div	
Lateral Bending Strain (LBS ₂)	16.7 μ e/div	
Tangential Bending Strain (TBS ₂)	16.7 μ e/div	

*Subscript 1 denotes instrumented pin No. 1
 2 denotes instrumented pin No. 2

Figure 4-26. Lateral Impulse Loading Data

Height of Bong (in) .105 Observation Time Base (ms/div) 5

Test Date 7/2/79

Description of Measurement	Signal Amp. (eng. units/div.)	Photograph of Observed Signal
Lateral Acceleration Axle (LAA)	40 g/div	
Vertical Acceleration Axle (VAA)	40 g/div	
Lateral Acceleration Rotor (LAR)	40 g/div	
Vertical Acceleration Rotor (VAR)	40 g/div	
Microslip (MSDT ₁)	1.18x10 ⁻⁴ in/div	
Lateral Reaction Strain (LRS ₁)	16.7 μe/div	
Tangential Reaction Strain (TRS ₁)	16.7 μe/div	
Lateral Bending Strain (LBS ₁)	67 μe/div	
Tangential Bending Strain (TBS ₁)	16.7 μe/div	
Lateral Bending Strain (LBS ₂)	67 μe/div	
Tangential Bending Strain (TBS ₂)	16.7 μe/div	

*Subscript 1 denotes instrumented pin No. 1
 2 denotes instrumented pin No. 2

Figure 4-27. Lateral Impulse Loading Data

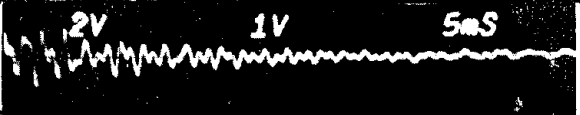










Height of Bong (in) .105 Observation Time Base (ms/div) 5
 Test Date 7/2/79

Description of Measurement	Signal Amp. (eng. units/div.)	Photograph of Observed Signal
Lateral Acceleration Axle (LAA)	40 g/div	
Vertical Acceleration Axle (VAA)	40 g/div	
Lateral Acceleration Rotor (LAR)	20 g/div	
Vertical Acceleration Rotor (VAR)	20 g/div	
Microslip (MSDT ₁)	1.18x10 ⁻⁴ in/div	
Lateral Reaction Strain (LRS ₁)	16.7 μe/div	
Tangential Reaction Strain (TRS ₁)	16.7 μe/div	
Lateral Bending Strain (LBS ₁)	67 μe/div	
Tangential Bending Strain (TBS ₁)	16.7 μe/div	
Lateral Bending Strain (LBS ₂)	67 μe/div	
Tangential Bending Strain (TBS ₂)	16.7 μe/div	

*Subscript 1 denotes instrumented pin No. 1
 2 denotes instrumented pin No. 2

Figure 4-28. Lateral Impulse Loading Data

Height of Bong (in) .105 Observation Time Base (ms/div) 5
 Test Date 7/2/79

Description of Measurement	Signal Amp. (eng. units/div.)	Photograph of Observed Signal
Lateral Acceleration Axle (LAA)	40 g/div	
Vertical Acceleration Axle (VAA)	40 g/div	
Lateral Acceleration Rotor (LAR)	20 g/div	
Vertical Acceleration Rotor (VAR)	20 g/div	
Microslip (MSDT ₁)	118×10^{-4} in/div	
Lateral Reaction Strain (LRS ₁)	16.7 μ e/div	
Tangential Reaction Strain (TRS ₁)	16.7 μ e/div	
Lateral Bending Strain (LBS ₁)	16.7 μ e/div	
Tangential Bending Strain (TBS ₁)	16.7 μ e/div	
Lateral Bending Strain (LBS ₂)	33 μ e/div	
Tangential Bending Strain (TBS ₂)	16.7 μ e/div	

*Subscript 1 denotes instrumented pin No. 1
 2 denotes instrumented pin No. 2

Figure 4-29. Lateral Impulse Loading Data

Height of Bong (in) .22 Observation Time Base (ms/div) 5
 Test Date 7/2/79

Description of Measurement	Signal Amp. (eng. units/div.)	Photograph of Observed Signal
Lateral Acceleration Axle (LAA)	40 g/div	
Vertical Acceleration Axle (VAA)	40 g/div	
Lateral Acceleration Rotor (LAR)	20 g/div	
Vertical Acceleration Rotor (VAR)	20 g/div	
Microslip (MSDT ₁)	118×10^{-4} in/div	
Lateral Reaction Strain (LRS ₁)	16.7 μ e/div	
Tangential Reaction Strain (TRS ₁)	16.7 μ e/div	
Lateral Bending Strain (LBS ₁)	67 μ e/div	
Tangential Bending Strain (TBS ₁)	67 μ e/div	
Lateral Bending Strain (LBS ₂)	67 μ e/div	
Tangential Bending Strain (TBS ₂)	67 μ e/div	

*Subscript 1 denotes instrumented pin No. 1
 2 denotes instrumented pin No. 2

Figure 4-30. Lateral Impulse Loading Data (Wheelset on Rails)












Height of Bong (in) .22 Observation Time Base (ms/div) 5
 Test Date 7/2/79

Description of Measurement	Signal Amp. (eng. units/div.)	Photograph of Observed Signal
Lateral Acceleration Axle (LAA)	40 g/div	
Vertical Acceleration Axle (VAA)	40 g/div	
Lateral Acceleration Rotor (LAR)	20 g/div	
Vertical Acceleration Rotor (VAR)	20 g/div	
Microslip (MSDT ₁)	1.18x10 ⁻⁴ in/div	
Lateral Reaction Strain (LRS ₁)	16.7 μe/div	
Tangential Reaction Strain (TRS ₁)	16.7 μe/div	
Lateral Bending Strain (LBS ₁)	67 μe/div	
Tangential Bending Strain (TBS ₁)	67 μe/div	
Lateral Bending Strain (LBS ₂)	67 μe/div	
Tangential Bending Strain (TBS ₂)	67 μe/div	

*Subscript 1 denotes instrumented pin No. 1
 2 denotes instrumented pin No. 2

Figure 4-31. Lateral Impulse Loading Data (Wheelset on Rails)

Height of Bong (in) .27 Observation Time Base (ms/div) 5
 Test Date 7/2/79

Description of Measurement	Signal Amp. (eng. units/div.)	Photograph of Observed Signal
Lateral Acceleration Axle (LAA)	40 g/div	
Vertical Acceleration Axle (VAA)	40 g/div	
Lateral Acceleration Rotor (LAR)	40 g/div	
Vertical Acceleration Rotor (VAR)	40 g/div	
Microslip (MSDT ₁)	118x10 ⁻⁴ in/div	
Lateral Reaction Strain (LRS ₁)	16.7 μe/div	
Tangential Reaction Strain (TRS ₁)	16.7 μe/div	
Lateral Bending Strain (LBS ₁)	67 μe/div	
Tangential Bending Strain (TBS ₁)	67 μe/div	
Lateral Bending Strain (LBS ₂)	67 μe/div	
Tangential Bending Strain (TBS ₂)	67 μe/div	

*Subscript 1 denotes instrumented pin No. 1
 2 denotes instrumented pin No. 2

Figure 4-32. Lateral Impulse Loading Data


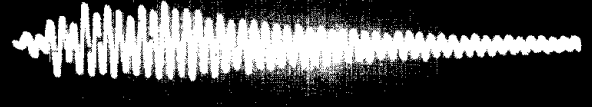
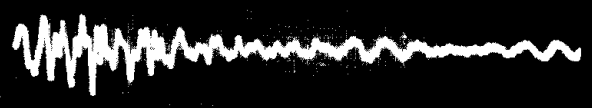








Height of Dong (in) .27 Observation Time Base (ms/div) 5
 Test Date 7/2/79

Description of Measurement	Signal Amp. (eng. units/div.)	Photograph of Observed Signal
Lateral Acceleration Axle (LAA)	40 g/div	
Vertical Acceleration Axle (VAA)	40 g/div	
Lateral Acceleration Rotor (LAR)	40 g/div	
Vertical Acceleration Rotor (VAR)	40 g/div	
Microslip (MSDT ₁)	118x10 ⁻⁴ in/div	
Lateral Reaction Strain (LRS ₁)	16.7 µe/div	
Tangential Reaction Strain (TRS ₁)	16.7 µe/div	
Lateral Bending Strain (LBS ₁)	67 µe/div	
Tangential Bending Strain (TBS ₁)	67 µe/div	
Lateral Bending Strain (LBS ₂)	67 µe/div	
Tangential Bending Strain (TBS ₂)	67 µe/div	

*Subscript 1 denotes instrumented pin No. 1
 2 denotes instrumented pin No. 2

Figure 4-33. Lateral Impulse Loading Data

Height of Bomb (in) .45 Observation Time Base (ms/div) 5
 Test Date 7/2/79

Description of Measurement	Signal Amp. (eng. units/div.)	Photograph of Observed Signal
Lateral Acceleration Axle (LAA)	100 g/div	
Vertical Acceleration Axle (VAA)	100 g/div	
Lateral Acceleration Rotor (LAR)	40 g/div	
Vertical Acceleration Rotor (VAR)	40 g/div	
Microslip (MSDT ₁)	2.35×10^{-4} in/div	
Lateral Reaction Strain (LRS ₁)	16.7 μ e/div	
Tangential Reaction Strain (TRS ₁)	67 μ e/div	
Lateral Bending Strain (LBS ₁)	33 μ e/div	
Tangential Bending Strain (TBS ₁)	33 μ e/div	
Lateral Bending Strain (LBS ₂)	67 μ e/div	
Tangential Bending Strain (TBS ₂)	33 μ e/div	

*Subscript 1 denotes instrumented pin No. 1
 2 denotes instrumented pin No. 2

Figure 4-34. Lateral Impulse Loading Data

Height of Bong (in) .45 Observation Time Base (ms/div) 5
 Test Date 7/2/79

Description of Measurement	Signal Amp. (eng. units/div.)	Photograph of Observed Signal
Lateral Acceleration Axle (LAA)	100 g/div	
Vertical Acceleration Axle (VAA)	100 g/div	
Lateral Acceleration Rotor (LAR)	40 g/div	
Vertical Acceleration Rotor (VAR)	40 g/div	
Microslip (MSDT ₁)	2.35×10^{-4} in/div	
Lateral Reaction Strain (LRS ₁)	16.7 μ e/div	
Tangential Reaction Strain (TRS ₁)	16.7 μ e/div	
Lateral Bending Strain (LBS ₁)	67 μ e/div	
Tangential Bending Strain (TBS ₁)	33 μ e/div	
Lateral Bending Strain (LBS ₂)	67 μ e/div	
Tangential Bending Strain (TBS ₂)	33 μ e/div	

*Subscript 1 denotes instrumented pin No. 1
 2 denotes instrumented pin No. 2

Figure 4-35. Lateral Impulse Loading Data

4.14 VERTICAL IMPULSE LOADING (DROP) TEST OBSERVATIONS

A photographic presentation of the real-time response of each of the eleven data channels is contained in Figures 4-36 through 4-45. All drop test data were recorded using the advance trigger technique so that data collection was started a few milliseconds prior to wheelset impact on the rails. Due to the high-level shocks, the trigger mechanism was repeatedly damaged. Therefore, the start time of successive tests is not synchronized. For the most part however, the initial impact can be observed from the time history data trace.

Drop testing was conducted at five wheelset heights. Real-time data were collected for a 50-millisecond and a 100-millisecond interval at each drop height. Drop heights were 0.25, 0.5, 1.0, 3.25 and 6.0 inches.

4.15 CONCLUSIONS

RMS g-levels were calculated for an 80-mph simulation as described in Section 4.12. The results are plotted versus the square root of drop height in Figure 4-46. The best fit curves indicate that the magnitude of accelerations due to wheelset elastic body motions are directly proportional to the wheelset velocity at the instant before impact.

Pin-bending and hub-hole reaction strains are plotted versus the square root of wheelset drop height in Figure 4-47. The strain data are linearly proportional to the square root of drop height and linearly proportional to the accelerations observed at the axle bearing housing. This result agrees with that observed in Section 4.12 describing bong test results.

Pin to hub-hole micro-slip is plotted versus the square root of drop height in Figure 4-47. The linear proportionality to bearing acceleration magnitudes are evident.

Drop test results support the wear proportionality expression of Section 4.16.

A study of the time history data traces of the photographs in Figures 4-36 through 4-45 resulted in the following observations:

- Initial impact (wheelset rigid body) acceleration magnitudes, as seen by the rotor accelerometers, are slightly smaller than accelerations seen by the bearing accelerometers which are in turn slightly smaller than the predicted impact accelerations for a three to four millisecond impact-duration. This observation is consistent with expectations since predicted accelerations are based on calculations for a point on the wheelset directly above the impact zone. Bearing accelerometers were located at a shorter radius with respect to the pivot point of the falling wheelset and therefore would be expected to sense only about 80 percent of the predicted impact accelerations. By the same logic, brake disk accelerometers sensed only about 60 percent of the predicted peak acceleration at impact.
- Drop-test, elastic-body-motion accelerations seen at the bearing housing were dominated by a 560-Hz input during the first 15 milliseconds after impact as opposed to 1012 Hz for the bong tests. Low amplitude, 1012-Hz accelerations are evident after approximately 15 to 20 milliseconds.
- Accelerations sensed at the disc brake rotor are initially 240 Hz decreasing in frequency to slightly less than 200 Hz approximately 60 milliseconds after impact. As drop height was increased to one inch and greater, 1600-Hz accelerations appear in the rotor accelerations. The 1600-Hz accelerations were recurrent at the 40-Hz rate.
- Drop test micro-slip data were consistent with rotor acceleration data and pin-bending-strain data. Although the micro-slip detector was designed to have its fundamental resonant

mode at 1600 Hz, the presence of a strong 1600-Hz variation in micro-slip data cannot be totally discounted as gage resonance, since a strong 1600-Hz variation is present in both rotor accelerometer and strain gage data.

- During the first 15 milliseconds after drop test impact, rotor accelerations are of similar magnitude to bearing accelerations, but have very little observable coherence with respect to time variance. In the period greater than 15 milliseconds after impact, rotor acceleration amplitudes are four to five times bearing acceleration amplitudes with similar time variant characteristics. This observation is considered significant with respect to pin wear potential in that pin wear is directly related to the dynamic behavior of the disc assembly. This observation may be restated as follows: wheelset elastic body responses (due to drop shock) decrease rapidly in magnitude at the bearing housing whereas elastic body responses of the disc assembly are sustained in amplitude for a much longer time. The associated micro-slip at the hub/pin interface is sustained as well. This sustained micro-slip occurs at approximately a 200-Hz rate. For a drop shock of one inch (Figure 4-42) the peak-to-peak micro-slip is approximately 1.5×10^{-4} inches, 80 milliseconds after impact.

4.16 SUMMARY OF LABORATORY TEST OBSERVATIONS

From the static tests, it was evident that the disc-brake assembly is subject to dynamic migration. That is, a condition of microscopic looseness exists, which when subjected to shock loading of relatively small magnitudes, causes disc components to change their relative positions in the assembly by small but measurable amounts (on the order of 10^{-4} inches). The amount of relative motion is a function of the magnitude of the dynamic loading. When subjected to a sustained vibrational input such as the operational rail environment, the potential for microscopic abrasion is inherent in this dynamic migration.

Height of Drop (in) 0.25 Observation Time Base (ms/div) 5
 Test Date 7/3/79

Description of Measurement	Signal Amp. (eng. units/div.)	Photograph of Observed Signal
Lateral Acceleration Axle (LAA)	20 g/div	
Vertical Acceleration Axle (VAA)	20 g/div	
Lateral Acceleration Rotor (LAR)	20 g/div	
Vertical Acceleration Rotor (VAR)	20 g/div	
Microslip (MSDT ₁)	1.18×10^{-4} in/div	
Lateral Reaction Strain (LRS ₁)	16.67 μ e/div	
Tangential Reaction Strain (TRS ₁)	16.67 μ e/div	
Lateral Bending Strain (LBS ₁)	33 μ e/div	
Tangential Bending Strain (TBS ₁)	33 μ e/div	
Lateral Bending Strain (LBS ₂)	33 μ e/div	
Tangential Bending Strain (TBS ₂)	33 μ e/div	

*Subscript 1 denotes instrumented pin No. 1
 2 denotes instrumented pin No. 2

Figure 4-36. Vertical Impulse Loading Data

Height of Drop (in) .25 Observation Time Base (ms/div) _____
 Test Date 7/3/79

Description of Measurement	Signal Amp. (eng. units/div.)	Photograph of Observed Signal
Lateral Acceleration Axle (LAA)	20 g/div	
Vertical Acceleration Axle (VAA)	20 g/div	
Lateral Acceleration Rotor (LAR)	20 g/div	
Vertical Acceleration Rotor (VAR)	20 g/div	
Microslip (MSDT ₁)	1.18×10^{-4} in/div	
Lateral Reaction Strain (LRS ₁)	16.67 μ e/div	
Tangential Reaction Strain (TRS ₁)	16.67 μ e/div	
Lateral Bending Strain (LBS ₁)	33 μ e/div	
Tangential Bending Strain (TBS ₁)	33 μ e/div	
Lateral Bending Strain (LBS ₂)	33 μ e/div	
Tangential Bending Strain (TBS ₂)	33 μ e/div	

*Subscript 1 denotes instrumented pin No. 1
 2 denotes instrumented pin No. 2

Figure 4-37. Vertical Impulse Loading Data

Height of Drop (in) .5 Observation Time Base (ms/div) 5
 Test Date 7/3/79

Description of Measurement	Signal Amp. (eng. units/div.)	Photograph of Observed Signal
Lateral Acceleration Axle (LAA)	40 g/div	
Vertical Acceleration Axle (VAA)	40 g/div	
Lateral Acceleration Rotor (LAR)	40 g/div	
Vertical Acceleration Rotor (VAR)	40 g/div	
Microslip (MSDT ₁)	1.18x10 ⁻⁴ in/div	
Lateral Reaction Strain (LRS ₁)	16.67 μe/div	
Tangential Reaction Strain (TRS ₁)	16.67 μe/div	
Lateral Bending Strain (LBS ₁)	33 μe/div	
Tangential Bending Strain (TBS ₁)	33 μe/div	
Lateral Bending Strain (LBS ₂)	33 μe/div	
Tangential Bending Strain (TBS ₂)	33 μe/div	

*Subscript 1 denotes instrumented pin No. 1
 2 denotes instrumented pin No. 2

Figure 4-38. Vertical Impulse Loading Data

Height of Drop (in) .5 Observation Time Base (ms/div) 10
 Test Date 7/3/79

Description of Measurement	Signal Amp. (eng. units/div.)	Photograph of Observed Signal
Lateral Acceleration Axle (LAA)	40 g/div	
Vertical Acceleration Axle (VAA)	40 g/div	
Lateral Acceleration Rotor (LAR)	40 g/div	
Vertical Acceleration Rotor (VAR)	40 g/div	
Microslip (MSDT ₁)	1.18x10 ⁻⁴ in/div	
Lateral Reaction Strain (LRS ₁)	16.67 μe/div	
Tangential Reaction Strain (TRS ₁)	16.67 μe/div	
Lateral Bending Strain (LBS ₁)	33 μe/div	
Tangential Bending Strain (TBS ₁)	33 μe/div	
Lateral Bending Strain (LBS ₂)	33 μe/div	
Tangential Bending Strain (TBS ₂)	33 μe/div	

*Subscript 1 denotes instrumented pin No. 1
 2 denotes instrumented pin No. 2

Figure 4-39. Vertical Impulse Loading Data

Height of Drop (in) 1.0 Observation Time Base (ms/div) 5
 Test Date 7/3/79



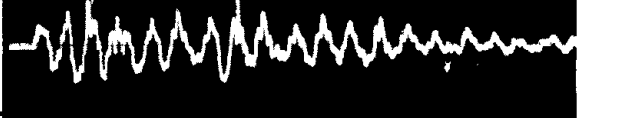





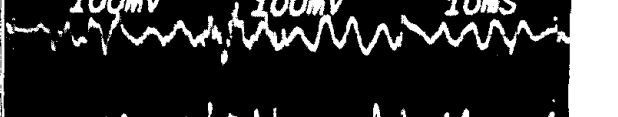
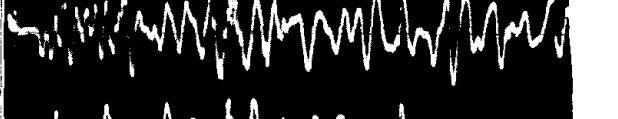

Description of Measurement	Signal Amp. (eng. units/div.)	Photograph of Observed Signal
Lateral Acceleration Axle (LAA)	40 g/div	
Vertical Acceleration Axle (VAA)	40 g/div	
Lateral Acceleration Rotor (LAR)	40 g/div	
Vertical Acceleration Rotor (VAR)	40 g/div	
Microslip (MSDT ₁)	1.18x10 ⁻⁴ in/div	
Lateral Reaction Strain (LRS ₁)	16.67 μe/div	
Tangential Reaction Strain (TRS ₁)	16.67 μe/div	
Lateral Bending Strain (LBS ₁)	33 μe/div	
Tangential Bending Strain (TBS ₁)	33 μe/div	
Lateral Bending Strain (LBS ₂)	33 μe/div	
Tangential Bending Strain (TBS ₂)	33 μe/div	

*Subscript 1 denotes instrumented pin No. 1
 2 denotes instrumented pin No. 2

Figure 4-40. Vertical Impulse Loading Data

Height of Drop (in) 1.0 Observation Time Base (ms/div) 10

Test Date 7/3/79










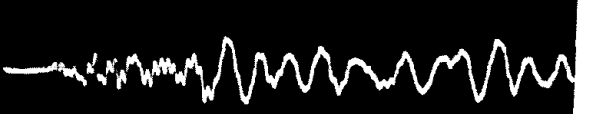

Description of Measurement	Signal Amp. (eng. units/div.)	Photograph of Observed Signal
Lateral Acceleration Axle (LAA)	40 g/div	
Vertical Acceleration Axle (VAA)	40 g/div	
Lateral Acceleration Rotor (LAR)	40 g/div	
Vertical Acceleration Rotor (VAR)	40 g/div	
Microslip (MSDT ₁)	1.18x10 ⁻⁴ in/div	
Lateral Reaction Strain (LRS ₁)	16.67 μe/div	
Tangential Reaction Strain (TRS ₁)	16.67 μe/div	
Lateral Bending Strain (LBS ₁)	33 μe/div	
Tangential Bending Strain (TBS ₁)	33 μe/div	
Lateral Bending Strain (LBS ₂)	33 μe/div	
Tangential Bending Strain (TBS ₂)	33 μe/div	

*Subscript 1 denotes instrumented pin No. 1
 2 denotes instrumented pin No. 2

Figure 4-41. Vertical Impulse Loading Data

Height of Drop (in) 3.25 Observation Time Base (ms/div) 5







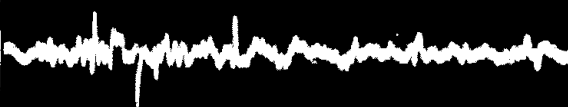




Test Date 7/3/70

Description of Measurement	Signal Amp. (eng. units/div.)	Photograph of Observed Signal
Lateral Acceleration Axle (LAA)	100 g/div	
Vertical Acceleration Axle (VAA)	100 g/div	
Lateral Acceleration Rotor (LAR)	100 g/div	
Vertical Acceleration Rotor (VAR)	100 g/div	
Microslip (MSDT ₁)	2.35x10 ⁻⁴ in/div	
Lateral Reaction Strain (LRS ₁)	16.67 μe/div	
Tangential Reaction Strain (TRS ₁)	16.67 μe/div	
Lateral Bending Strain (LBS ₁)	66.6 μe/div	
Tangential Bending Strain (TBS ₁)	66.6 μe/div	
Lateral Bending Strain (LBS ₂)	66.6 μe/div	
Tangential Bending Strain (TBS ₂)	66.6 μe/div	

*Subscript 1 denotes instrumented pin No. 1
 2 denotes instrumented pin No. 2

Figure 4-42. Vertical Impulse Loading Data

Height of Drop (in) 3.25 Observation Time Base (ms/div) 10
 Test Date 7/3/79

Description of Measurement	Signal Amp. (eng. units/div.)	Photograph of Observed Signal
Lateral Acceleration Axle (LAA)	100 g/div	
Vertical Acceleration Axle (VAA)	100 g/div	
Lateral Acceleration Rotor (LAR)	100 g/div	
Vertical Acceleration Rotor (VAR)	100 g/div	
Microslip (MSDT ₁)	2.35×10^{-4} in/div	
Lateral Reaction Strain (LRS ₁)	16.67 μ e/div	
Tangential Reaction Strain (TRS ₁)	16.67 μ e/div	
Lateral Bending Strain (LBS ₁)	66.6 μ e/div	
Tangential Bending Strain (TBS ₁)	66.6 μ e/div	
Lateral Bending Strain (LBS ₂)	66.6 μ e/div	
Tangential Bending Strain (TBS ₂)	66.6 μ e/div	

*Subscript 1 denotes instrumented pin No. 1
 2 denotes instrumented pin No. 2

Figure 4-43. Vertical Impulse Loading Data

Height of Drop (in) 6.0 Observation Time Base (ms/div) 5
 Test Date 7/3/79

Description of Measurement	Signal Amp. (eng. units/div.)	Photograph of Observed Signal
Lateral Acceleration Axle (LAA)	100 g/div	
Vertical Acceleration Axle (VAA)	100 g/div	
Lateral Acceleration Rotor (LAR)	100 g/div	
Vertical Acceleration Rotor (VAR)	100 g/div	
Microslip (MSDT ₁)	2.35x10 ⁻⁴ in/div	
Lateral Reaction Strain (LRS ₁)	16.67 μe/div	
Tangential Reaction Strain (TRS ₁)	16.67 μe/div	
Lateral Bending Strain (LBS ₁)	66.6 μe/div	
Tangential Bending Strain (TBS ₁)	66.6 μe/div	
Lateral Bending Strain (LBS ₂)	66.6 μe/div	
Tangential Bending Strain (TBS ₂)	66.6 μe/div	

*Subscript 1 denotes instrumented pin No. 1
 2 denotes instrumented pin No. 2

Figure 4-44. Vertical Impulse Loading Data

Height of Drop (in) 6.0 Observation Time Base (ms/div) 10
 Test Date 7/3/79

Description of Measurement	Signal Amp. (eng. units/div.)	Photograph of Observed Signal
Lateral Acceleration Axle (LAA)	100 g/div	
Vertical Acceleration Axle (VAA)	100 g/div	
Lateral Acceleration Rotor (LAR)	100 g/div	
Vertical Acceleration Rotor (VAR)	100 g/div	
Microslip (MSDT ₁)	2.35×10^{-4} in/div	
Lateral Reaction Strain (LRS ₁)	16.67 µe/div	
Tangential Reaction Strain (TRS ₁)	16.67 µe/div	
Lateral Bending Strain (LBS ₁)	66.6 µe/div	
Tangential Bending Strain (TBS ₁)	66.6 µe/div	
Lateral Bending Strain (LBS ₂)	66.6 µe/div	
Tangential Bending Strain (TBS ₂)	66.6 µe/div	

*Subscript 1 denotes instrumented pin No. 1
 2 denotes instrumented pin No. 2

Figure 4-45. Vertical Impulse Loading Data

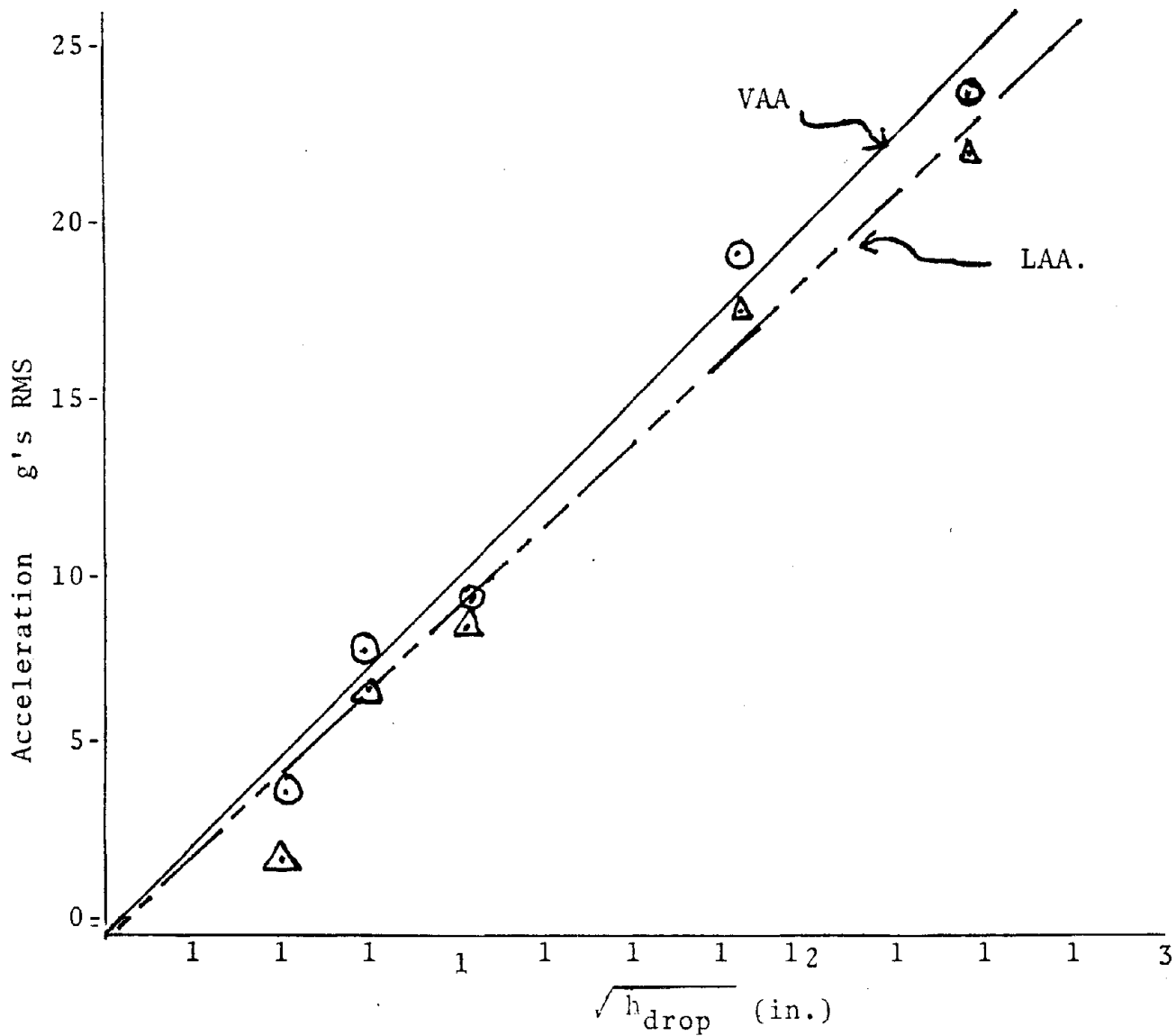


Figure 4-46. RMS Vertical Accelerations Axle (VAA) and rms Lateral Accelerations Axle (LAA) versus the Square Root of the Height of Wheelset Drop Distance (in.)

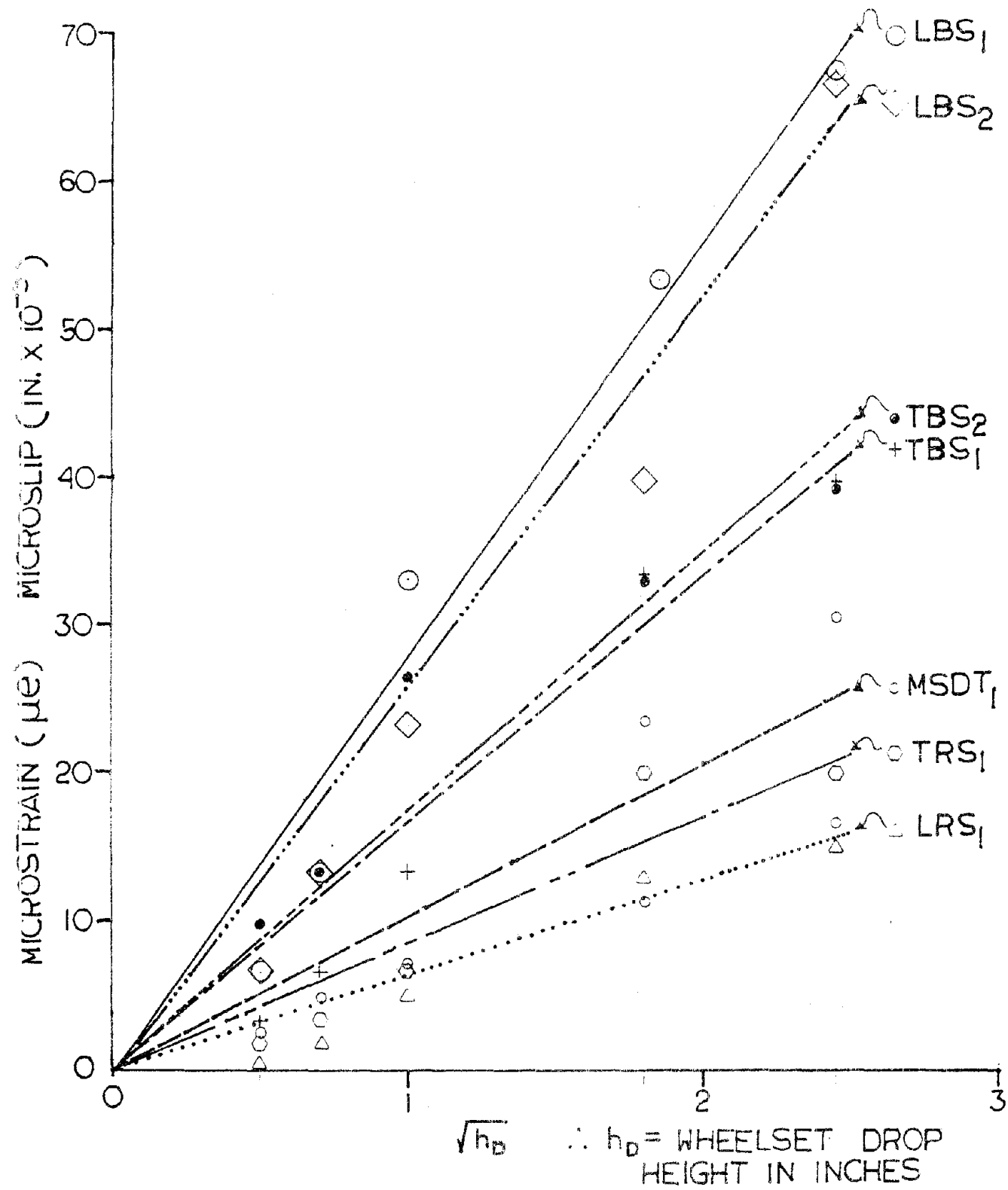


Figure 4-47. Pin Bending Strain, Hub Hole Reaction Strain and Pin-to-Hub Hole Micro-Slip Versus the Square Root of Wheelset Drop Distance

Since the vibrational environment of the roadbed is more severe in winter than in summer (as determined by the instrumented Non-Rotating Over-the-Road Test), then the microscopic abrasive action incurred by the pins will be more severe in a winter environment.

Observations from dynamic tests indicate that pin wear potential is proportional to the (g-level)² where the g-level is measured at the axle bearing housing. Two models which describe the ratio of pin wear potential of 26 February versus 16 March are shown in the following paragraphs.

4.17 RMS MODEL

Using the rms value of sinusoidally varying acceleration as a measure of g-level, these observations may be compared to Over-the-Road test results as follows:

$$\text{Pin Wear} \propto (G_{\text{rms}})^2$$

$$G_{\text{rms}}(2/26/79) \approx 2 G_{\text{rms}}(3/10/79)$$

From this relationship, we see that leaving out the intermediate terms:

$$\begin{aligned} \text{Pin Wear}(2/26/79) &\propto (G_{\text{rms}}(2/26/79))^2 \\ &\propto (2G_{\text{rms}}(3/10/79))^2 \\ &\propto (4 G_{\text{rms}}(3/10/79))^2 \\ &\propto 4 \times \text{Pin Wear}(3/10/79) \end{aligned}$$

In summary, pin wear potential due to acceleration levels on 26 February was four times the pin wear potential due to acceleration levels measured on 10 March. It should be emphasized that proportionality and not equality is essential

for this comparison. Other factors, of which pin surface condition is a major consideration (beyond the scope of this experiment), substantially affect the wear rate of the surfaces under examination.

4.18 PERCENT TIME EXCEEDENCE MODEL

A second wear model comparison between Over-the-Road tests of 26 February and 10 March uses the percent time exceedence.

Again:

Pin Wear potential \propto (G-level)²

G-level exceeded 10 percent of the time at 80 mph on 2/26/79 was \approx 40 g.

G-level exceeded 10 percent of the time at 80 mph on 3/10/79 was \approx 13 g.

Comparing g-levels gives:

G-level (2/16/79) \approx 3 times G-level (3/10/79)

From this, we see that for 10 percent of the time:

Pin wear potential on 26 February was nine times the pin wear potential on 10 March.

4.19 SPECTRAL GRAPHS

The complete set of spectral graphs obtained in the laboratory tests are included in Appendices E and F. Appendix E includes the spectral graphs obtained in the bong test where the wheel was struck by a lead weight suspended as a pendulum. These graphs were taken with the wheelset resting on the rails, and with the wheelset suspended by cables. Appendix F includes the graphs obtained during the drop tests. The signals from the strain gaged pins (which secure the disc friction ring to the hub) are particularly interesting because these signals confirm that pin motion and stress occur at the same resonant frequency as observed on the Over-the-Road Tests. This

shows that the winter factor is, in fact, related to pin motion stress and, therefore, to the pin-wear problem. The output from the micro-slip detector shows that the major motion occurs at 330 and 360 Hz. The micro-slip detector and the lateral pin-bending signals show that bending stress and micro-slip also occur at 580 Hz in agreement with the Over-the-Road Tests. The signature of the response at 580 Hz is not as well defined as the response at 330 and 360 Hz. A mechanical system normally has a well defined resonance frequency which shows on a spectral graph as a single line. The spreading of the response at 580 Hz indicates that the response frequency of the structure varies with time (variable damping indicated) so that the entire frequency actually varied over the period of time used for the test. Figures 4-48 and 4-49 show typical data obtained from the bong test with the wheels resting on the rails. The tests were repeated with the pendulum pulled back different distances. The velocity at impact depends on the height to which the ball is raised; the distance the ball was raised was measured each time and used to control the experiment. The data, shown in Figure 4-48, resulted from dropping the pendulum from a height of 0.22 inches. With the wheel resting on the rail, the primary response at the journal bearing was at 385 and 580 Hz. The friction ring resonated at these frequencies and at 330 Hz. The lateral accelerometers on the friction ring and the journal bearing housing show strong response at 580 Hz.

In addition to the frequencies observed on the vertical channels, the lateral accelerometers on the friction ring and the journal bearing housing show strong responses at 580 Hz. Figure 4-50 shows the corresponding data from the micro-slip detector and the instrumented strain gages. This graph shows that the predominant slip frequencies are 330, 385 and 580 Hz. Both tangential and lateral stress show resonance peaks at 330, 385 and 580 Hz. When the bong test was performed

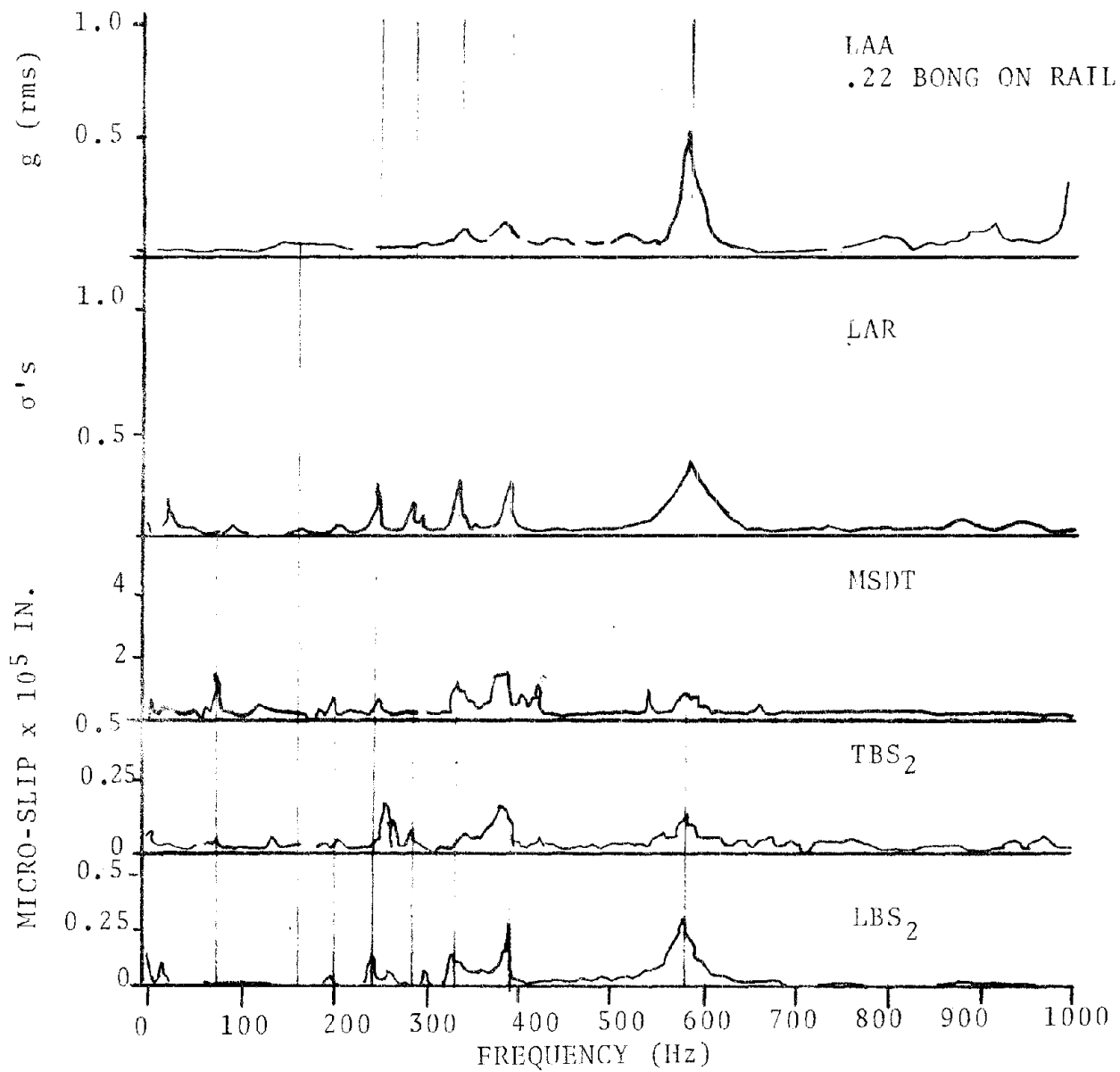


Figure 4-48. Typical Spectral Graph (Bong Test, Wheel on Rails)

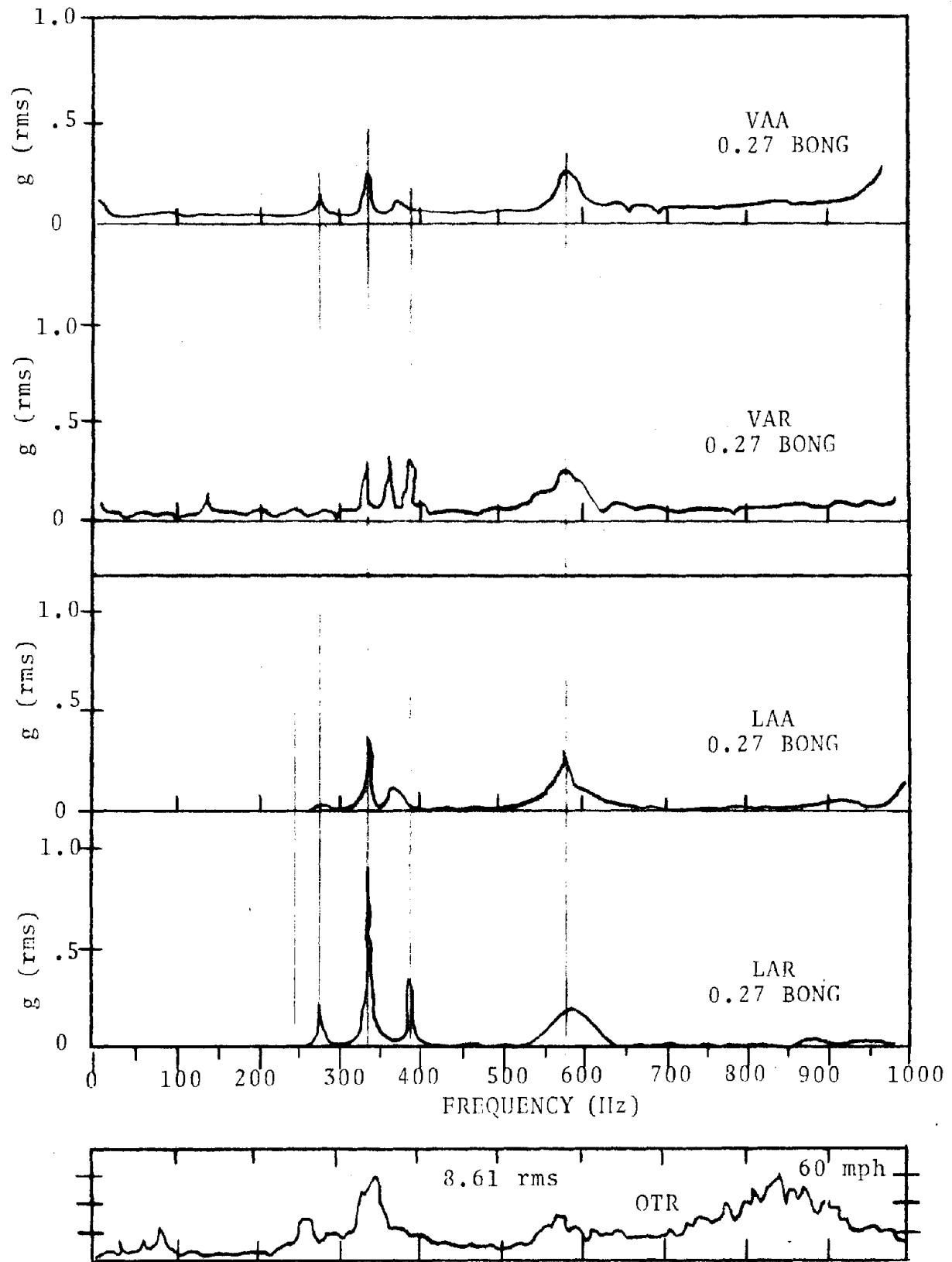


Figure 4-49. Typical Spectral Graph (Bong Test, Wheels on Rails)

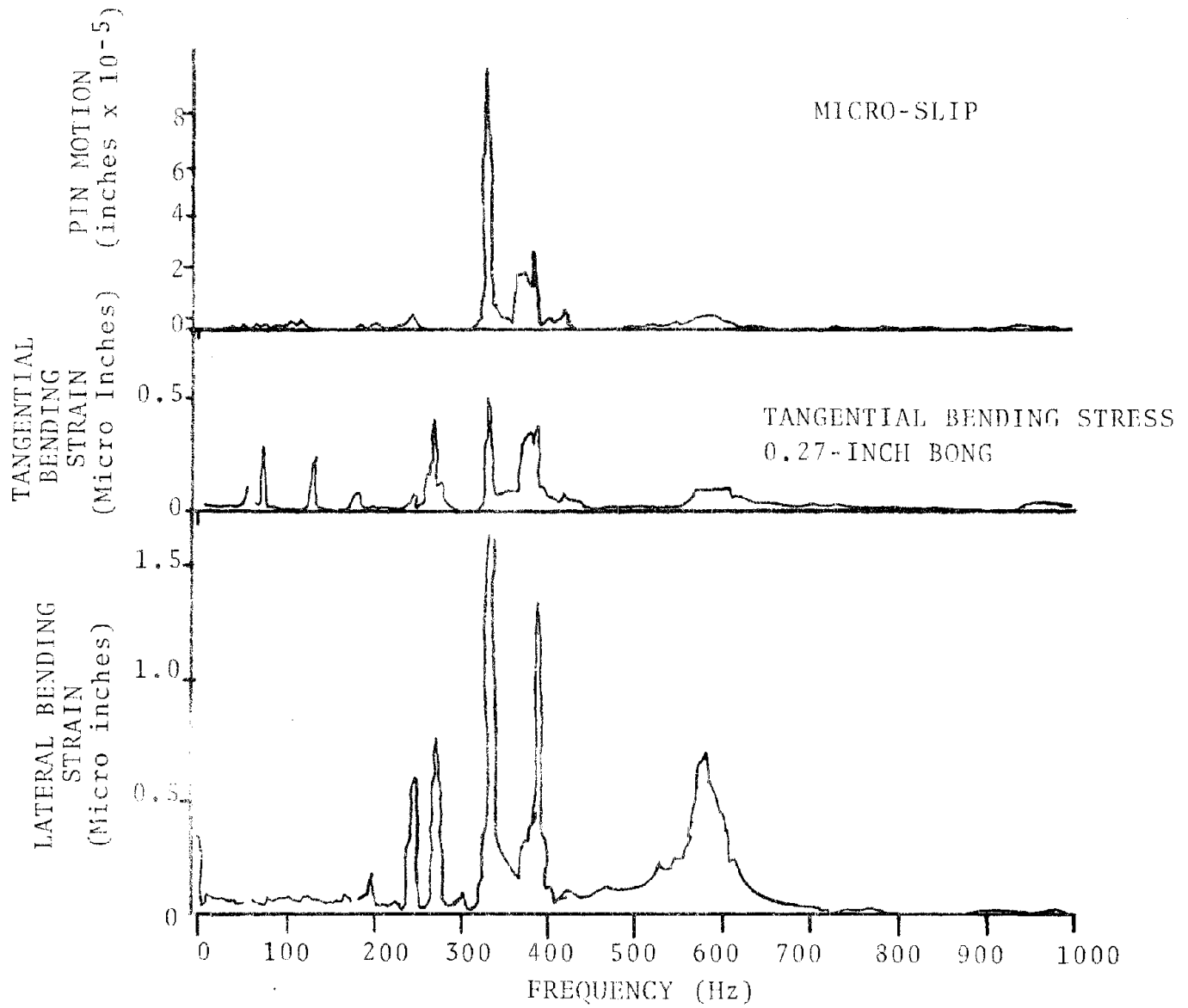
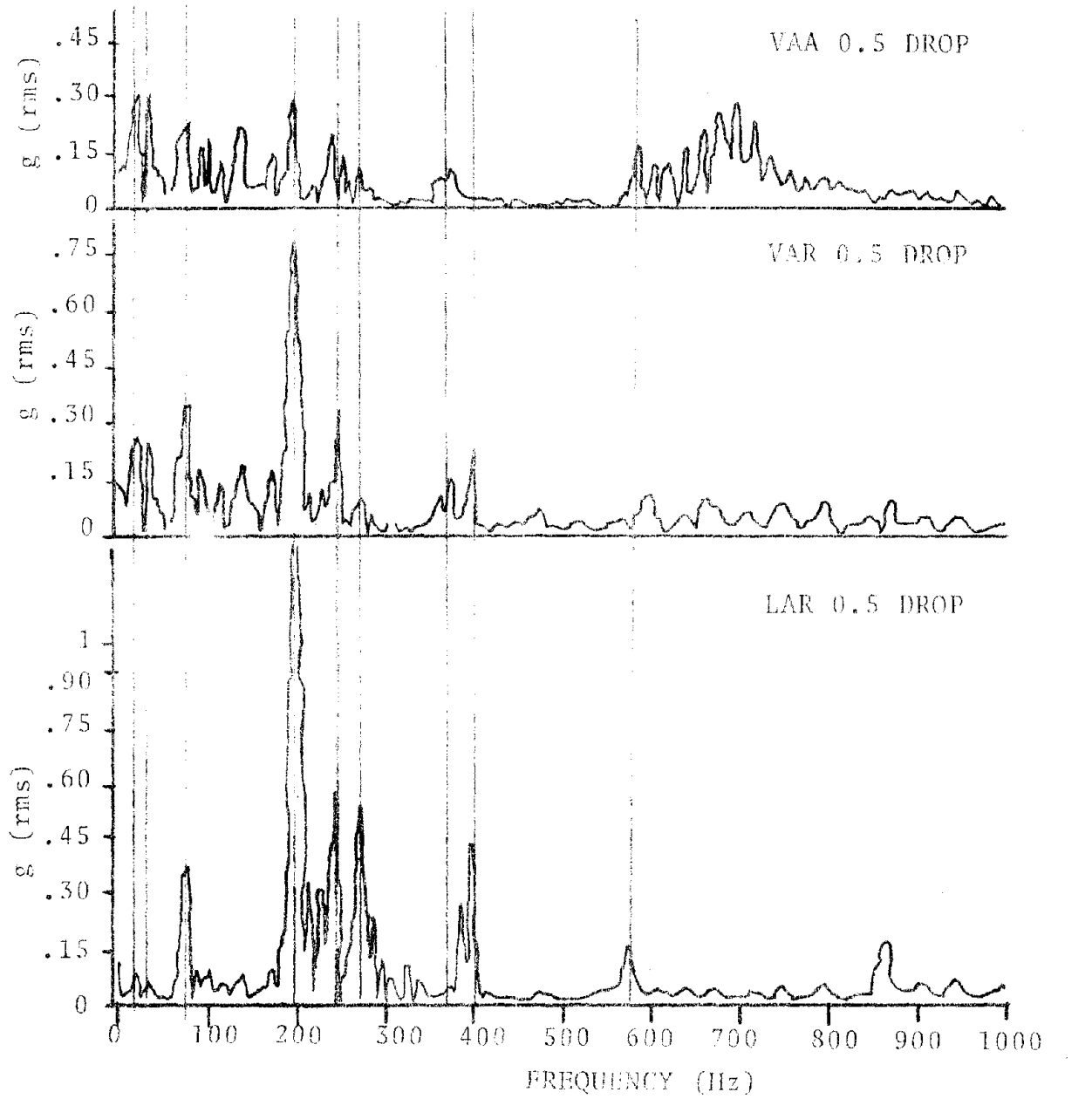


Figure 4-50. Corresponding Data from the Micro-Slip Detector and the Instrumented Strain Gages

with the wheel assembly suspended above the rails, similar results were obtained. Typical bong-test results are shown in Figure 4-52 and the complete results are included in Appendix E. The suspended-above-the-rail bong test results show much stronger resonance at 330 Hz in all channels. The vertical accelerometers on the journal bearing and the friction ring also display the 580-Hz resonance seen only in the lateral channels when the wheel was resting on the rail. The micro-slip measurement indicates motion at the same frequencies with the predominant response at 330 Hz. The tangential bending stresses are similar but dominant-response spectral lines appear at 75, 126 and 275 Hz in addition to the normal response at 330, 385, and 580 Hz. The lateral bending response is significantly different in that the bending stresses were much higher and the stress at 330 Hz exceeded three microstrain. The lateral bending stress also shows resonance at 240 and 275 Hz.

For reference, this group of spectral graphs includes the 60-mph results from one of the Over-the-Road Tests. This comparison shows that the response resulting from the bong test agrees very well with the journal bearing response from the Over-the-Road Test.

Figure 4-51 shows a typical set of spectral results obtained from the drop test. The complete set of drop test graphs is included in Appendix F. The results, shown in Figure 4-51, correspond to dropping the wheelset from a height of 0.5 inches onto the simulated rail. The drop test results are similar to the bong test except that the drop test shows many more resonances at lower frequencies. The predominant frequencies are 20, 30, 75, 192, 245, 380, 400 and 580 Hz. The low frequency responses are very weak as recorded on the lateral accelerometer mounted on the friction ring. They may be a



VAA (0.5-Inch Drop)
 VAR (0.5-Inch Drop)
 LAR (0.5-Inch Drop)

Figure 4-51. Typical Spectral Results (Drop Test)

bounce frequency introduced by the test fixture. The vertical and lateral accelerometer channels show a strong resonance at 75 Hz similar to that found in the bong test and the Over-the-Road Test. This probably corresponds to one of the axle bending modes. The next dominant frequency occurs at about 195 Hz. This is very strong in the drop test series but does not appear in the bong test. Therefore, it must be excited by the vertical impact. Some of the spectral plots from the Over-the-Road Tests show a trace of this resonance but it is never as dominant as indicated by the laboratory test series. The response at 195 Hz might be disregarded except that it is a dominant response in the pin stress and micro-slip indicators. The disc was dropped with the instrumented pins aligned horizontally. Therefore, the output from the lateral pins is excited by disc mutation of pure lateral motion.

The next dominant response was at 245 and 275 Hz. These frequencies occur on both the bong test and the Over-the-Road Test and are certainly characteristic resonances of the wheelset system.

The drop test does not appear to excite the 330 or 380 Hz modes as strongly as the bong and the Over-the-Road Tests. This may be an interesting result since one of the two frequencies is clearly associated with wheelplate ringing which is easily excited by the bong and is a dominant signal in the winter on frozen track as recorded in the Over-the-Road Tests. However, it appears to be significantly reduced in warm weather.

Apparently, the drop test does not excite wheelplate ringing. The associated response at 385 Hz appears to be a disc resonance mode which may be excited by wheelplate ringing. The absence of both frequencies suggests that the disc resonance is strongly

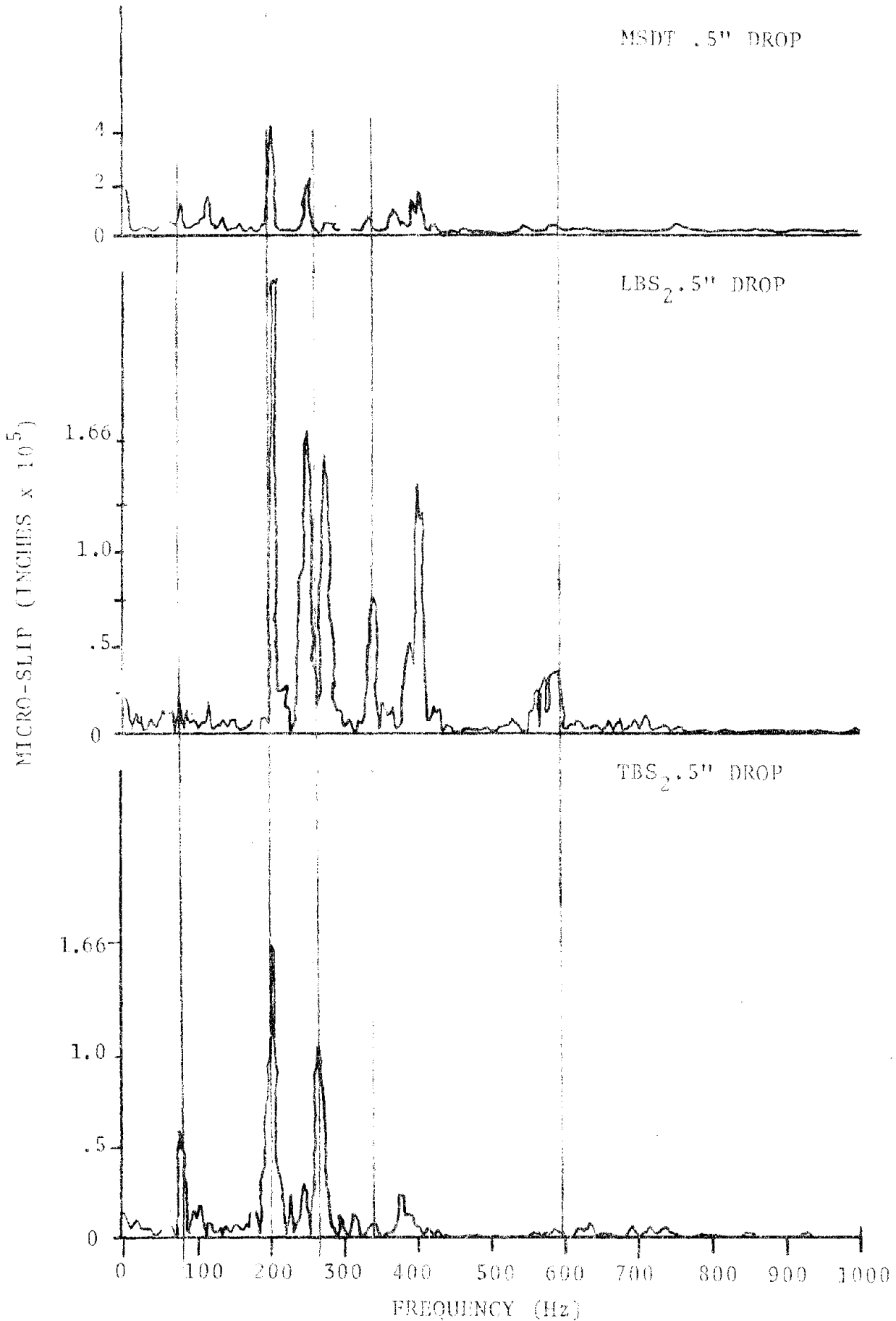


Figure 4-52. Typical Spectral Results (Drop Test)

forced by wheel response which might be a major magnifying factor in the real world. The winter factor appears to operate on the 330-Hz mode causing the wheel to resonate violently at this frequency, which in turn drives the disc to cause slip and stress to occur at 330, 385 and 580 Hz. This, in turn, produces the extreme wear due to fretting corrosion in the pin joints.

The spectral graphs obtained in the laboratory test show that the axle assembly has multiple modes which are easily excited by impulsive inputs. When excited, the system rings at the natural frequencies associated with the various modes of the system. In some cases, time histories captured by the storage oscilloscope clearly show that the system rings at distinct frequencies. At other times, the response is made up of such a complex combination of frequencies that no single component is clearly discernible.

The spectrum analyzer is a very useful tool which displays the components which are contained in these complex waveforms. The spectral graph of the various accelerometer, strain gage, and micro-slip measurements show that the dominant modes of the wheelset are at 330, 380 and 580 Hz. The spectral graph also provides information about wear because when excited by an impulse, an element which is lightly damped will ring differently than elements which are rubbing together and have heavy nonlinear damping. A lightly damped part of the system will ring at a constant frequency like a tuning fork. This produces a single sharply defined spectral line on a spectral graph.

The spectral graph from a lightly damped system tends to look like the graph at point A on Figure 4-53. The mode which produces the response at point C is clearly different. This mode was produced by a system which has a lot of damping and

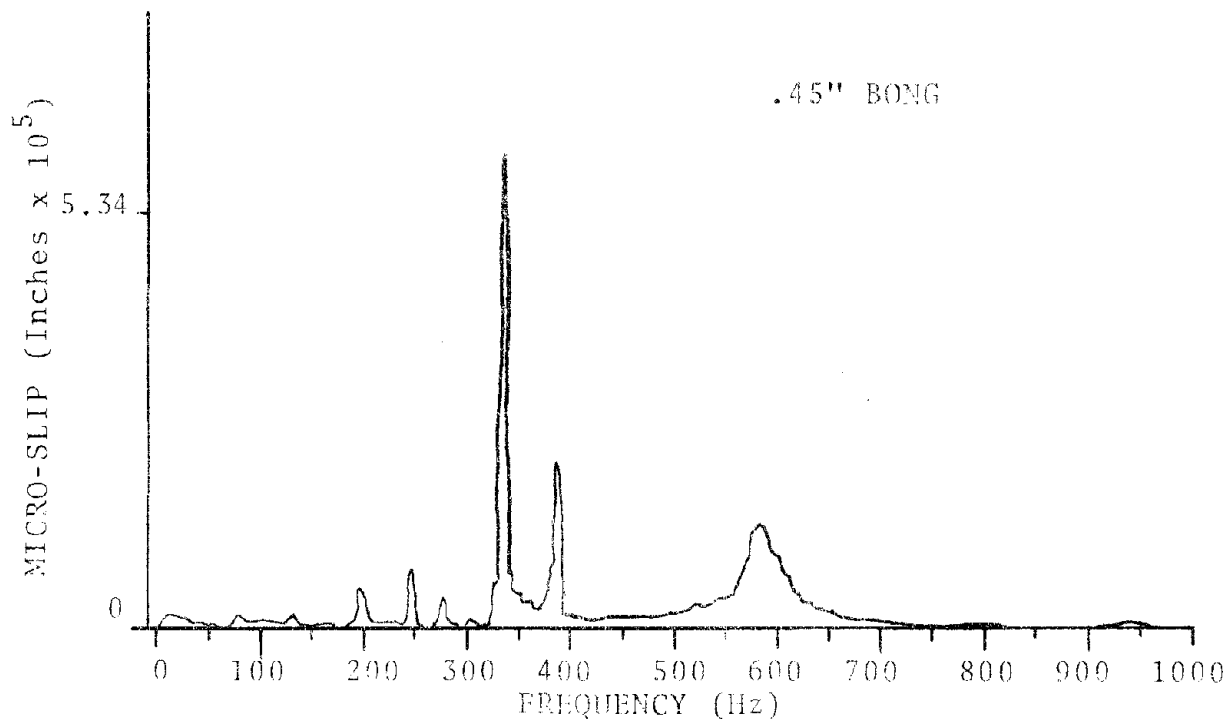


Figure 4-53. Micro-Slip vs. Frequency

is likely to be wearing because the response shows that the frequency was not constant. The mass and stiffness of the system do not change. The variation in frequency results from nonlinearity in damping. This type of response is characteristic of a system which has a lot of friction damping produced by elements which slide over each other and, therefore, have heavy wear tendencies. The spectral graph of the wheelset shows that the response at 330 Hz is lightly damped and the system rings at a very constant frequency.

At 580 Hz, the system is very heavily damped and the response is always spread indicating that this response is generated by a nonlinear mode. The response at 360 Hz is often a combination because at lower amplitudes the frequency is spread but not as much as in the 580 Hz mode.

The spectral response from the wheelset indicates that the mode which produces the 580-Hz response is probably associated with pin wear.

The time history response data in the oscilloscope photographs show that the 580-Hz mode is a major resonance of the disc for the first 30 milliseconds. This mode dies away quickly and the system continues to ring at less damped modes. In actual service, however, the input will occur every 40 to 80 milliseconds or sooner. Therefore, even though heavily damped the system will continue to have large response amplitudes at 580 Hz. With repeated inputs, the element which responds at 580 Hz is likely to wear.

5.0 RESULTS AND CONCLUSIONS

5.1 SUMMARY OF OBSERVATIONS

This section provides a summary of the findings discussed more extensively in Sections 2.0, 3.0 and 4.0, and the conclusions and recommendations resulting from those findings.

In Section 2.0, the revenue service test (see Figures 5-1 and 5-2) indicates that the Knorr resilient pins experience a dramatic increase in wear during the winter and that this increased wear can be related to the local average temperature.

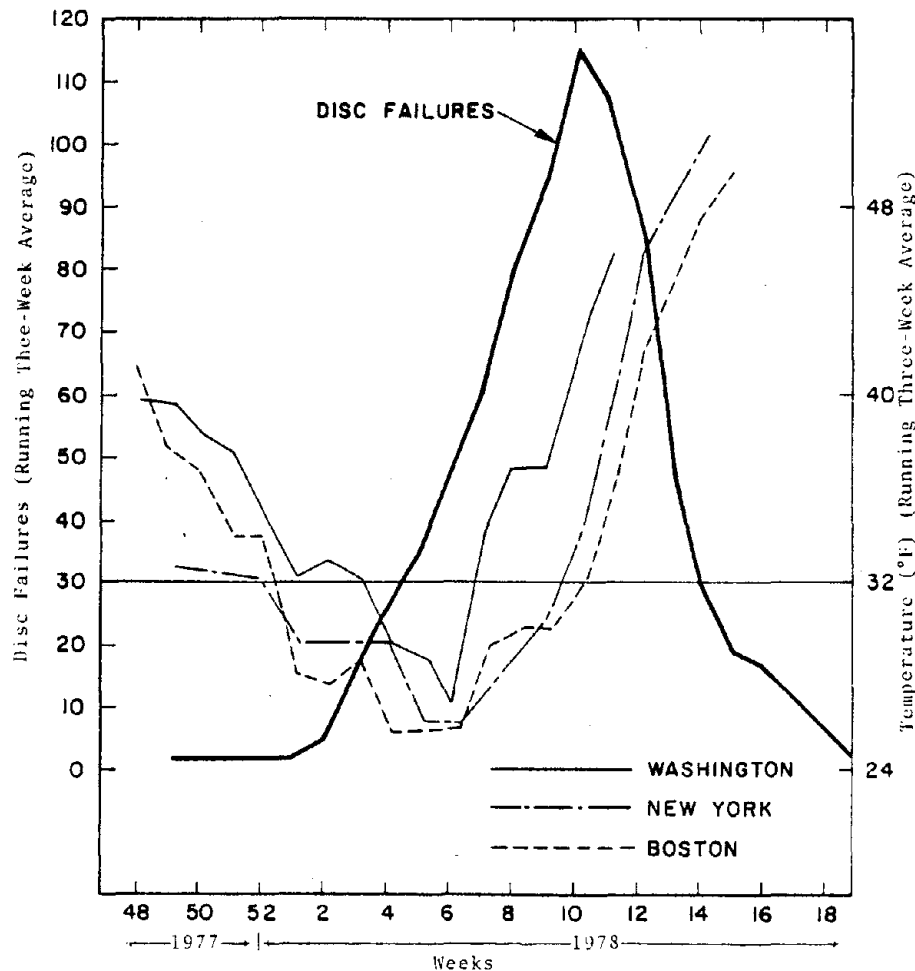


Figure 5-1. Amfleet Disc-Brake Failures During the Winter of 1977/1978

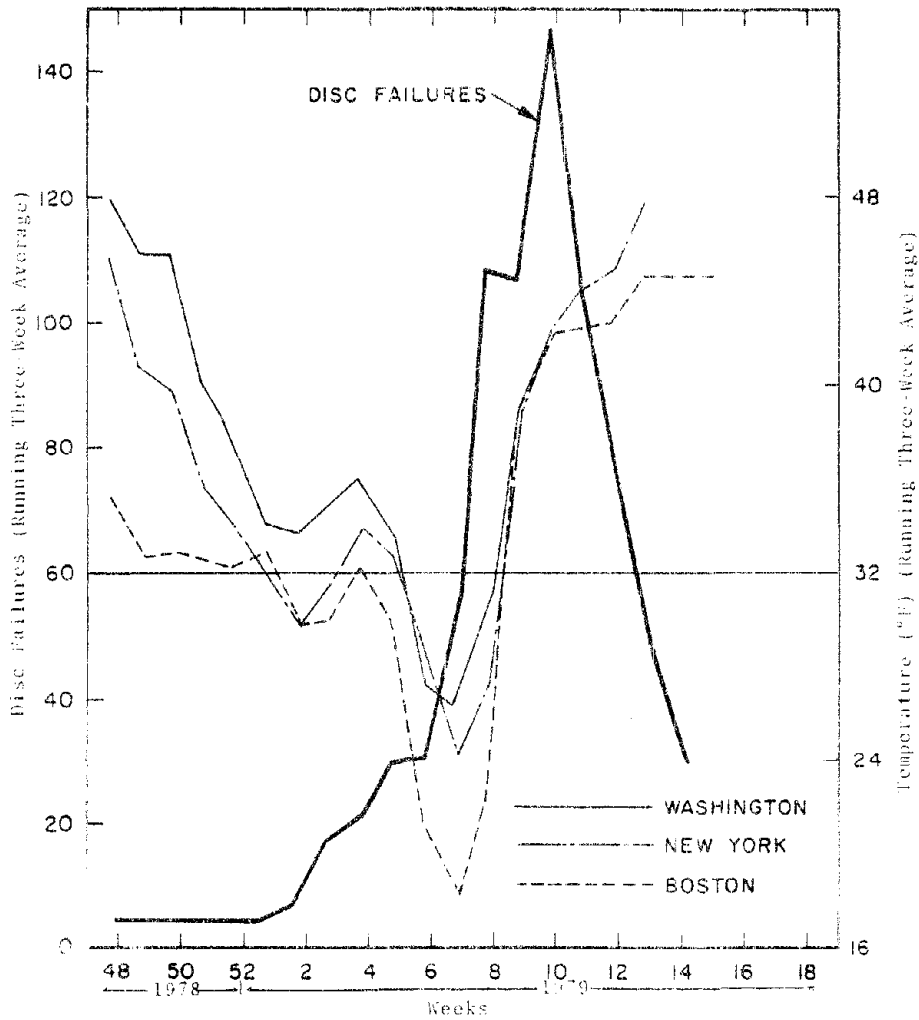


Figure 5-2. Amfleet Disc-Brake Failures During the Winter of 1978/1979

The data indicate that the failures increase significantly when the average temperatures are below 32 degrees Fahrenheit. The failures do not correlate to any other apparent environmental factors.

Section 3.0 describes the investigation of the dynamic environment of the wheelset using non-rotating instrumentation located on the bearing journal housing, the truck frame, and the brake rigging. The results of the Over-the-Road test show that the rms value of wheelset accelerations decreased significantly

(more than two to one) as the toadbed went from a partially frozen (local ambient temperature 35° Fahrenheit) to an unfrozen condition (local ambient temperature 50° Fahrenheit) (Figures 5-3 and 5-4). This effect is described as the "winter factor".

The engineering checkout run indicated that when the track is very cold, the wheelset resonant acceleration levels are even higher than recorded during the test when the roadbed was partially frozen.

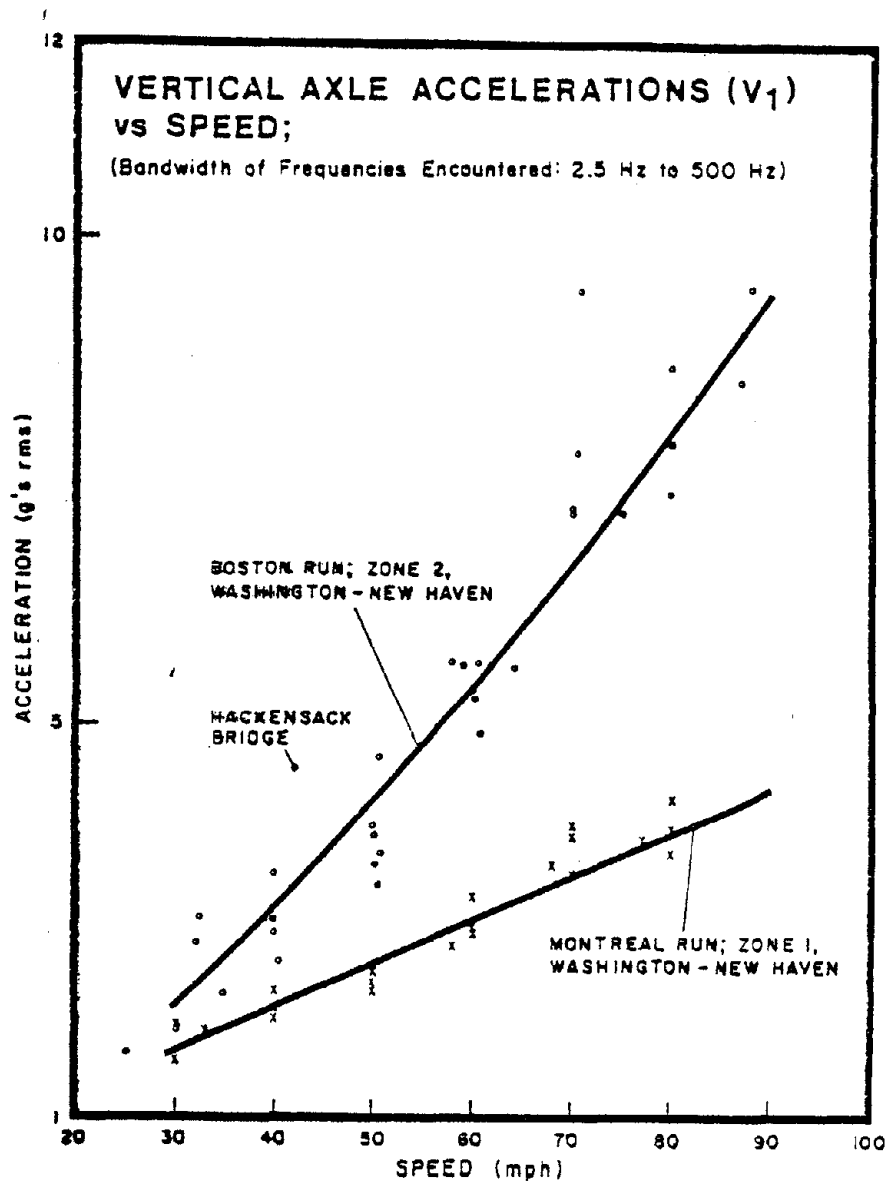


Figure 5-3. Vertical Axle Accelerations (V_1) vs Speed (Bandwidth 2.5 to 500 Hz)

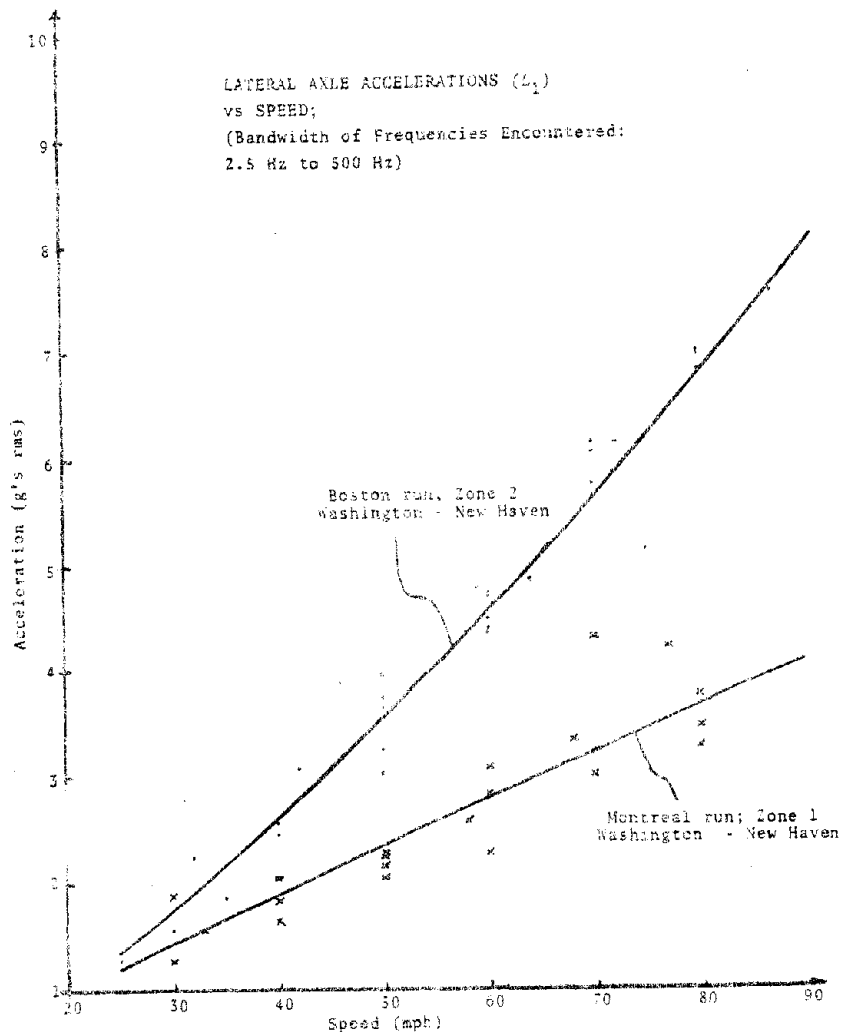


Figure 5-4. Lateral Axle Accelerations (L_1) vs Speed (Bandwidth 2.5 to 500 Hz)

As shown in Figure 5-5, the data from the Over-the-Road test indicate that the dominant wheelset responses occur at 70, 260, 330, 360, 580 and 750 to 900 hertz. The test data indicates that the major change in rms acceleration levels was that the wheelset vibrated more violently at these particular frequencies during the colder test run.

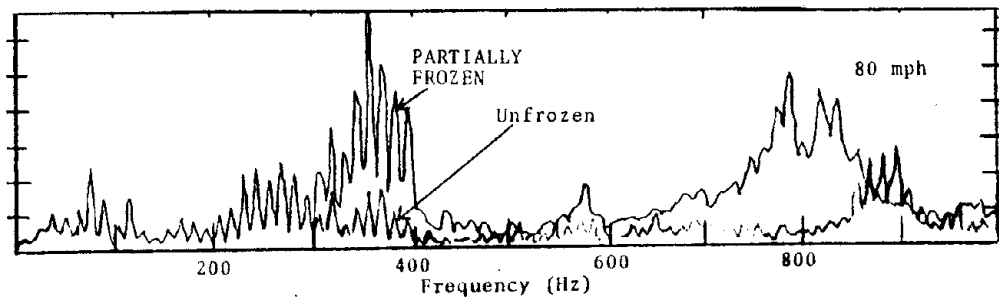


Figure 5-5. Comparison of Frozen and Unfrozen Vertical Axle Accelerations

The test showed that the forces developed by the disc brake calipers were not responsible for the pin wear problems. The "winter factor" comes from the variation in system internal resonant response to wheel/rail impacts. The results also show that the trend is slightly more pronounced when the analysis is restricted to a 500-hertz bandwidth instead of including all acceleration information from 0 to 1000 hertz. This shows that the "winter factor" can be related to acceleration frequencies which are most likely to have significant displacements with respect to abrasive wear analysis.

Section 5.0 of the report also shows that the Pioneer-III truck primary shock ring is not an effective vibrational isolator at frequencies below 400 hertz (as shown in Figure 5-6). This means that the shock ring provides virtually no protection to truck mounted components from vibrations of the wheelset initiated by impacts at the wheel/rail interface.

Statistical analysis was used to develop a prediction tool called percent time exceedance. This tool allows the prediction of the number of high-level acceleration events that might be encountered based on operating speed and distance. The data were developed as shown in Figure 5-7.

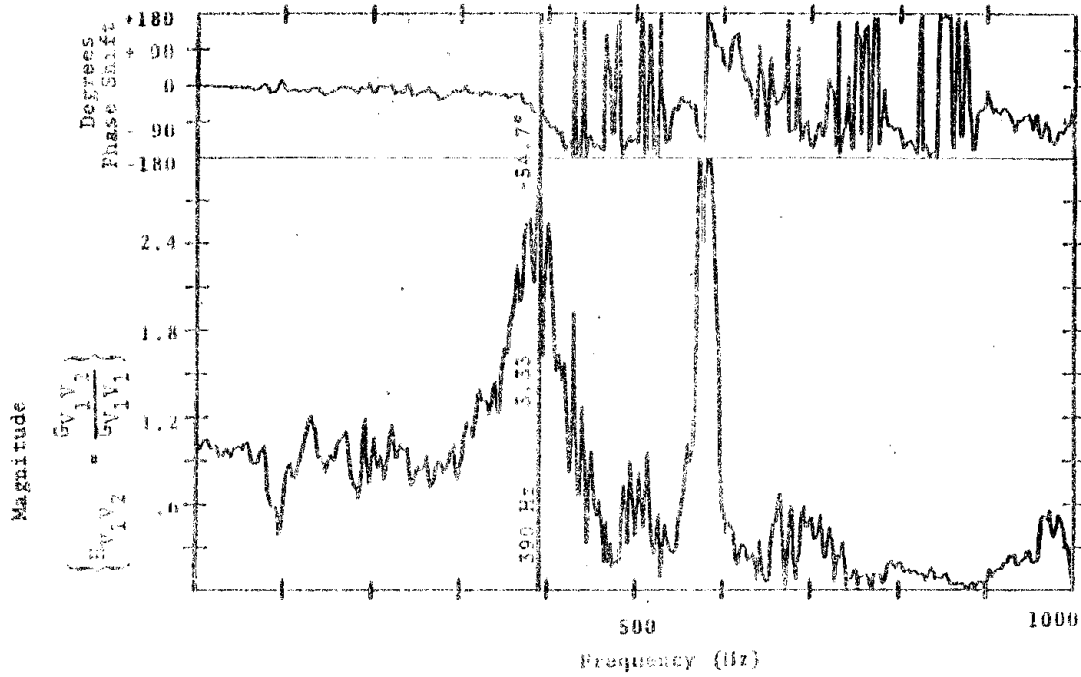


Figure 5-6. Transfer Function of Vertical Accelerations (V_2) to Vertical Axle Accelerations (V_1)

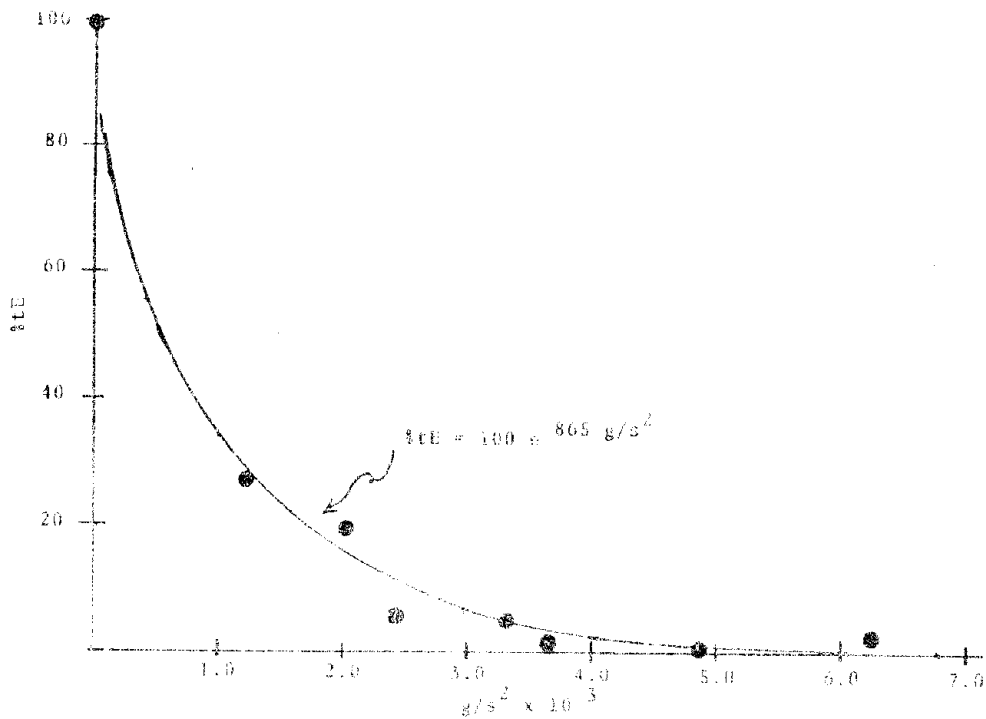


Figure 5-7. Percent Time Exceedance (%E) as a Function of Acceleration (g) Exceedance Level and Train Speed (s)

The percent-time-exceedance tool was one method used to predict the acceleration levels which may result from running at 120 miles per hour. At these speeds, acceleration levels in warm weather are predicted to be equivalent to those measured during cold weather testing as shown in Figure 5-8.

Section 4.0 described how the laboratory test was used to tie the testing project together by relating the wheelset acceleration observations to pin motion and pin stress. The drop test and the lateral bong test caused the wheelset to vibrate at its characteristic resonant frequencies and these in fact were the same frequencies observed by the accelerometers mounted on the bearing journal housing during the over-the-road tests.

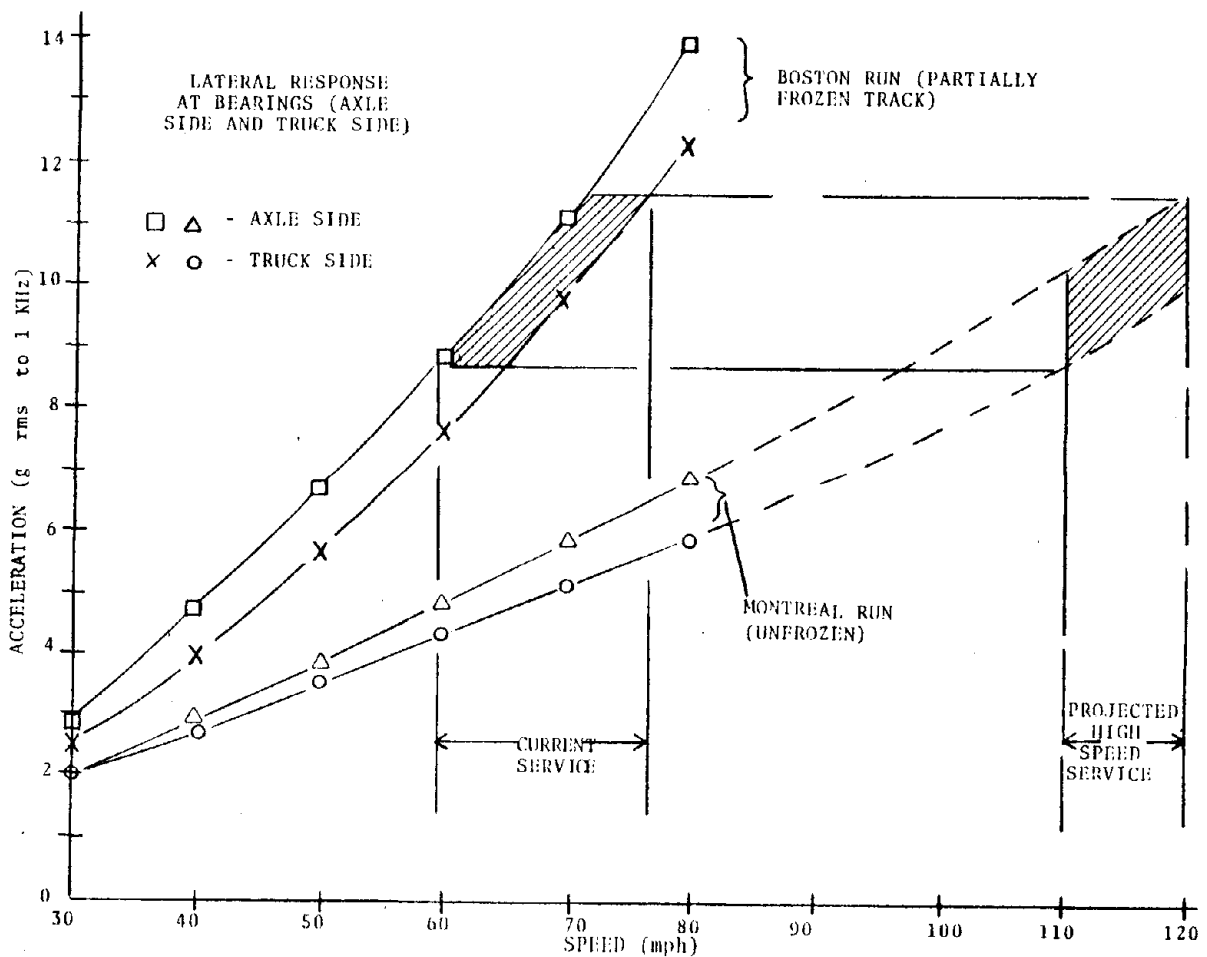


Figure 5-8. Lateral Response at Bearings (Axle Side and Truck Side)

Data from the instrumented pins revealed that pin slip and strain were direct responses to wheelset resonant accelerations.

The principal pin-slip mode for the first 15 to 20 milliseconds is the 580-hertz resonance of the friction rotor. This vibration is very heavily damped and is probably associated with pin wear. The spectral graphs show the 580-hertz resonance to be a dominant mode, but since the resonance dies away so quickly, the significance of this mode is even greater than suggested by the spectral graphs.

5.2 CONCLUSIONS

This report indicates that the key to the pin wear problem is associated with the change which occurs in the damping provided by the rail or the way that the vibrational energy is absorbed or not absorbed by the rail system. In warm weather, much of the vibrational energy generated by the wheel rolling over the rail, and defects in the wheel and rail surfaces is absorbed by the rail. In the winter, when water freezes in and around the rail components or the tension in the rail is higher, the rail does not dissipate the vibrational energy as rapidly so the wheel system is forced to vibrate at higher energy levels in order to dissipate the energy acquired from the inputs. Wheel and rail defects are the major source of the impacts but the way the system dissipates the vibrational energy is the "message" which caused the "winter factor".

The most dominant slip frequency of the pin (leading to wear) is believed to be approximately 580 hertz. This frequency appears to be related to one of the higher order resonant modes of the friction ring. The pin/hub bore interface is a direct link in the primary energy dissipation path for the disc in a free rolling situation. Spectral data, collected in both the laboratory and the over-the-road tests, show a

spreading of the spectral data about this 580-hertz frequency. This spreading is characteristic of damped resonant systems. Lower frequencies seen in the pin spectral data are suspected to be of a less destructive nature in relation to pin wear since the critical event is the breaking of the friction lock and thus the number of cycles per unit time is the dominant factor. The lower frequencies may interact in the wear phenomena by helping develop displacement during changes in the relative position between the pin and hub-bore walls during the low coefficient of friction portion of the slip cycle.

5.3 RECOMMENDATIONS

The results of the test show how and why the Knorr-pin design is not capable of surviving the NEC environment. When viewed collectively with the deterioration of other components (brake rigging, cabling and conduit fittings), the bearing adapter, the wheel tread, and pin loosening are evidently only symptoms of the overall problem. Field reports indicate that trucks operating in West Coast service do not have this problem. From this the NEC problem appears to be system damping that is not adequate to suppress the vibrational behavior of system components.

The approach to solving the problem should be a multi-directional program which can be outlined as follows:

- COMPLETE REVENUE SERVICE EVALUATION TESTS
ON CANDIDATE REPLACEMENTS FOR PRESENT KNORR
DISCS

The best approach to the brake problem is to design taper lock hardware which will survive in spite of the severe environment. The WABCO and Knorr taper-lock design provide a means for implementing maintenance procedures where the mechanic could simply tighten the bolts on any disc if bolts were found to

be loose during routine inspections. The car would not need to be removed from service beyond the normal time required for inspection.

- CONDUCT MODAL RESPONSE EVALUATION OF CANDIDATE DISC BRAKES AS PART OF A WHEELSET ASSEMBLY

This will produce a data base that can be used to assess the potential susceptibility to fretting and fatigue in a candidate disc brake that might result from the resonant behavior of a wheelset.

- DEVELOP A BETTER PRIMARY SUSPENSION

Truck mounted components, such as brake rigging can be protected significantly by improving the truck primary suspension. A softer primary suspension would eliminate high-level vibrations from the truck frame, and the brake rigging would only be exposed to the vibrational inputs when the brakes are applied. The conduit and other truck mounted components would also benefit from a reduction in the vibrational energy transmitted to the truck frame through the primary suspension. The test showed that the primary suspension on the Pioneer Three truck is effective in eliminating frequencies above 400 hertz but provides no attenuation below these frequencies.

- ENCOURAGE DEVELOPMENT OF A SOLID DISC

Advanced metallurgical techniques look promising in offering a disc that would not only be virtually immune to vibrational loads but also be able to withstand the cycling thermal loads to which a solid disc is most vulnerable. The interference fit technique of the KNORR KN design may be capable of providing the benefits of both the solid design and the component

design. Both of these should be given strong consideration for use in dual braking systems or reduced brake rate methods.

- CONDUCT A SHORT STUDY ON THE NEC TO INVESTIGATE THE EFFECT OF HIGH LEVEL VIBRATION ON WHEEL-TO-RAIL ADHESION

The problem of wheel tread damage is suspected to be related to the adverse effects of high level vibrations on adhesion between the wheel and rail. On trucks equipped with dual brakes, the tread brake may be readily adaptable as a damping mechanism.

An additional benefit of this study would be to determine the change in the rms amplitude of wheelset vibration associated with a specific wheel tread defect.

- INITIATE A STUDY OF THE MECHANISM OF VIBRATIONAL DAMPING BY THE RAIL AND RAIL SUBSTRATE

The system damping problem will require additional investigation of the damping mechanism to determine the cause of the change associated with decreasing temperatures (i.e., the "winter factor").

One approach to the solution of this problem is to ensure that the rail system does not undergo this change. If the "winter factor" is related to the freezing of water in and around the tie and rail fastener components, changes already in the implementation or in the planning stages may be effective at reducing the severity of this problem. Other changes which may be economically feasible might solve the problem; if the problem centers on rail tension or the basic rail hardware, correction techniques will involve improving the ability of the truck hardware to survive even with high-level vibrations.

